

Unified Informational Theory: Time, Relativity, Force, Gauge Structure, Matter, Thermodynamics, and Cosmology

Yaniv Riz

Independent Researcher

Contact: yanivriz@gmail.com

Previous publications: C. I. Garfinkel, V. Silverman, N. Harnik, C. Haspel, and Y. Riz
(2015). Stratospheric response to intraseasonal changes in incoming solar radiation. Journal of
Geophysical Research: Atmospheres. <https://doi.org/10.1002/2015JD023244>

Abstract

What is time?

Unified Informational Theory develops an information-registration framework in which physical time is defined through the writing of distinguishable information relative to the entropic cost of that writing. The manuscript begins from three informational sectors: potential information, distinguished information, and dispersed information. These sectors are represented geometrically by a two-sphere informational model: an outer sphere of potential information, an inner sphere of realized information represented by the distinct-plus-dispersed sector $I_{\text{dist}} + I_{\text{disp}}$, and a present realization boundary between them.

The outer sphere represents unrealized distinctions, possible configurations, coherent phase structure, and future-oriented informational capacity. The inner sphere represents realized information in its decomposed form: distinct records I_{dist} together with dispersed thermodynamic cost I_{disp} , giving the already written structure of physical records, causal order, and measurable spacetime history. The boundary of the realized three-dimensional informational sphere is a two-dimensional spherical interface. This interface is mathematically the Riemann sphere,

$$\Sigma_{\text{now}} = \partial S_R^3 \simeq S^2 \simeq \hat{\mathbb{C}}.$$

The present therefore carries a complex phase geometry by construction. Quantum physics describes potential information on the complex phase side of this interface, while relativistic physics describes information that has been registered into realized records and causal spacetime structure. Forward time is the growth of the realized sphere into the potential sphere: information is written from potential into reality, while dispersed information records the thermodynamic cost of that writing.

Their ratio defines the dimensionless informational time variable

$$dt^* = \frac{dI_{\text{dist}}}{dI_{\text{disp}}} = (k_B \ln 2) \frac{dI_{\text{dist}}}{dS}.$$

In the physical clock projection, this dimensionless ratio is read as the local clock-rate capacity,

$$dt^* \text{ to } \chi = \frac{d\tau}{dt}, \quad d\tau = \chi dt.$$

The same capacity law is then used to reinterpret the relativistic sectors. Information describing motion consumes part of a finite informational bandwidth, and the residual capacity available for writing time gives the Lorentz factor. Mass-related informational consumption is radial, and the residual capacity available for writing time gives the Schwarzschild clock-rate structure. In this reading of spacetime, temporal geometry is expressed as reduced registration capacity, while spatial geometry is expressed as the available configuration capacity for writing distinguishable information. In the two-sphere geometry, these are complementary projections of the same realization process.

The framework is extended by completing the clock-rate field with internal phase,

$$\Xi = \chi e^{-i\phi}.$$

The physical force law is then written as the gradient of this complex phase-time field,

$$\mathbf{F}_\phi = -E_{\text{scale}} \nabla \Xi,$$

where E_{scale} is the relevant energy scale of the physical branch. Substituting $\Xi = \chi e^{-i\phi}$ gives the two fundamental gradient components,

$$\mathbf{F}_\phi = -E_{\text{scale}} e^{-i\phi} \nabla \chi + i E_{\text{scale}} \chi e^{-i\phi} \nabla \phi.$$

The first term is the real clock-rate branch. The second term is the phase-gradient branch. Linear time is therefore the realized projection of a deeper phase-time structure, while the familiar interaction branches are represented as gradients of that phase-time structure under different projections.

Since the present interface is a Riemann-sphere phase surface, this complex phase-time field lives naturally on the boundary where potential information becomes realized record. Physical interactions are then organized through gradients, connections, curvatures, rewrite events, and closure conditions associated with Ξ .

The real clock-rate gradient,

$$\nabla \chi,$$

gives the inertial, gravitational, thermodynamic, and diffusion-like branch: forces arise from spatial variation in realized time-writing capacity.

The phase gradient,

$$\nabla \phi,$$

gives the gauge branch: local phase-time transport on the complex present interface defines the electromagnetic connection, and the curvature of that connection gives the electromagnetic field strength. In this form, electromagnetism is introduced as the curvature of coherent phase transport on the realization interface inside the same field Ξ .

Later sections apply the same principle to the non-Abelian sectors. The weak interaction is developed as a local rewrite mechanism on the realization boundary. The parent distinct-plus-dispersed record can be locally unwritten and returned to the potential sector; the system then rejoins the forward-time branch by rewriting stable daughter-product information as new $I_{\text{dist}} + I_{\text{disp}}$ structure. This local erase-and-rewrite geometry supplies the phase-time basis for weak transitions and the electroweak rewrite scale.

The strong interaction is read as internal phase-time closure: color corresponds to confined internal phase-time orientations, and the strong restoring response arises from gradients of broken closure in the internal phase-time configuration. Matter is developed through a closed spherical Compton phase-time structure in which Compton recurrence, spinorial orientation, charge projection, and mass-energy are carried by closed internal geometry. Flavor is interpreted as a stable Compton phase-time writing resonance structure inside the closed phase-time architecture.

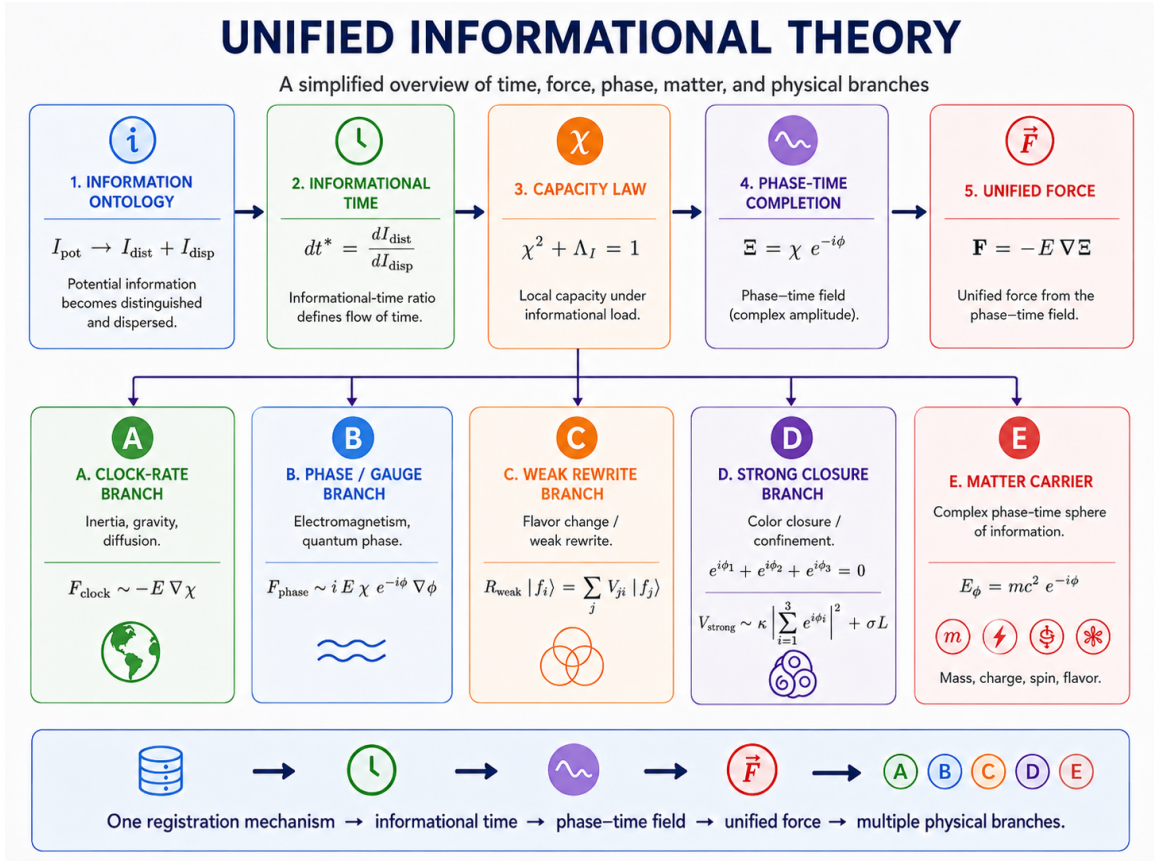
The cosmological sections apply the same informational time action to inflation, horizons, dark energy, and large-scale metric opening. In the two-sphere picture, cosmology is the large-scale behavior of the same registration process: the realized sphere expands through the conversion of

potential informational capacity into distinct records and dispersed thermodynamic cost, while entropy controls the cost, rate, and limits of registration.

The empirical section identifies a testable signature in driven coherent transport above the equilibrium critical temperature, an effect reported in several driven coherent-material systems, and interprets it within a single mechanism: external driving can temporarily increase coherent phase-writing capacity while suppressing dissipative spectral weight.

The central proposal is therefore that the familiar physical sectors are projections of one deeper process: the realization of physical information through phase-time and entropy. In compact form, the sectors are different projections of gradients, connections, curvatures, rewrite events, and closure conditions of the unified phase-time field

$$\Xi = \chi e^{-i\phi}.$$



Contents

1	Informational Ontology and Emergent Time	7
1.1	The Definition of Physical Information	7
1.2	The Energetic Taxonomy of Information	8
1.3	Physical Channels of Distinguished Information	8
1.4	Mass-Information: Compton Writing Rate	9
1.5	Motion-Information: Planck-Normalized Spatial Updating	10
1.6	Time-Information: Temporal Registration	12
1.7	Potential Information, Measurement, and Realized Record	12
2	Thermodynamic Derivation of Time via Power	13
2.1	From Power Cancellation to the Pure Informational Time Equation	13
2.2	Thermodynamic Registration Efficiency and Inefficiency	15
2.3	The Two-Spheres Geometry and the Riemann-Surface Present	16
2.4	The Arrow of Time and Human Memory	18
3	Informational Special Relativity	20
3.1	Informational Special Relativity: Planck-Normalized Spatial Resolution and the Kinematic Load	20
3.2	Kinematic Capacity Load and the Lorentz Factor	22
3.3	Thermodynamic Writing Cost of the Lorentz Factor	23
3.4	Longitudinal Spatial Capacity and Length Contraction	24
3.5	Invariant Mass and Observed Inertial Energy	25
3.6	Kinetic Energy as Relative Time-Load	27
3.7	Inertial Force from the Same Temporal Mismatch	27
3.8	Relativistic Diffusion at Non-Relativistic Velocities	29
4	Informational General Relativity	32
4.1	Schwarzschild-Compton Writing Length	33
4.2	Radial Information Flux and the Exterior Gravitational Load	33
4.3	Gravitational Clock-Rate Factor and Proper Time	34
4.4	Radial Spatial Capacity and the Schwarzschild Metric	36
4.5	Horizon Writing Capacity, Dispersed Information, and Saturation	39
4.6	Special and General Relativity as One Capacity Geometry	44
4.7	Free Fall and the Equivalence Principle: Temporal and Radial Spatial Matching	46
4.8	The Meaning of the Gravitational Constant G	48
4.9	The Empty-Time Limit and the Physical Closure of Registration	51
5	Metric and Tensor Completion and the Informational Graviton	54
5.1	Tensor Completion of the Informational Metric	54
5.2	Ricci Scalar and the Variational Field Equation	56
5.3	Informational Stress-Energy Tensor	57
5.4	Directional Information Flux and the Mixed Time-Angular Metric Component	59
5.5	Metric Capacity Updates and Gravitational Waves	62
5.6	Unified Force Mechanism: Massive Matter and the Compton Writing Scale	63
5.7	Massless Signals and Photon Energy as the Invariant Scale	65
6	Unified Phase-Time Force and Electromagnetism	67
6.1	The Coherent Phase-Time Branch	67

6.2	From Compton Phase-Time to the Unified Time-Load Field	69
6.3	The Complex Time-Load Field	71
6.4	Kinematic Phase-Time Closure	72
6.5	Clock-Rate Branch and Phase Branch of the Force	73
6.6	Relativity as the Hermitian Metric Projection of the Unified Phase-Time Field.	74
6.7	Local Phase-Time Fiber, Gauge Transport, and Metric Form	76
6.8	Electromagnetic Curvature	77
6.9	Maxwell Equations from Phase-Time Curvature	78
6.10	Charge and Current as Phase-Writing Sources	79
6.11	The U(1) Phase Fiber on the Two-Sphere Interface	79
6.12	Metric Re-Derivation of the Electromagnetic Connection	81
7	The Weak Interaction Sector	84
7.1	Phase-Time Form of the Second Law	85
7.2	Local Weak Rewrite Rate in Compton Time	87
7.3	Integral Rewrite Barrier and Bit Suppression	88
7.4	The Rewrite Mechanism	89
7.5	The Neutrino as Residual Phase-Time Closure	90
7.6	Rewrite Barriers, Half-Life Scaling, and Environmental Shifts	93
7.7	SU(2), U(1), and Electroweak Decomposition of the Two-Sphere Interface	96
7.8	Weak Rewrite Scale, Electroweak Boson Masses, and the Metric Weinberg Angle	98
7.9	Metric Form of the Electroweak Interface	103
7.10	The Temporal Bit and the Symmetric Weak Doublet	105
7.11	CP Bias and the Weak Rewrite Force from Reverse Realized-Time Orientation	106
8	The Strong Interaction Sector: Confined Phase-Time Circulation and SU(3)	109
8.1	Three-State Phase-Time Closure: Mesons and Baryons	110
8.2	Strong Load and Restoring Force	111
8.3	Stable Baryonic Closure and Emergent SU(3)	114
8.4	Color Exchange and Internal Phase-Vector Closure	115
8.5	Electric Charge Holonomy and the Strong Commutation Structure	118
8.6	Flavor as a Closed Compton Phase-Time Resonance	120
8.7	Weak Rewrite and CKM-Like Flavor Mixing	122
8.8	Generations as Stable Flavor-Resonance Bands	123
8.9	Color Singlets, Gluon Self-Coupling, and the QCD Limit	126
8.10	Phase-Time Bridge and Metric Form of Strong Phase Closure	129
9	What Is Mass?	133
9.1	Mass as a Closed Complex Spherical Phase-Time Mode	134
9.2	Internal Phase Closure and Radial Lorentzian Distortion	135
9.3	Compton Writing Rate and the Closed Mass-Information Channel	138
9.4	Fast Compton Carrier, Slow Envelope, and Free Schrödinger Dynamics	139
9.5	Planck Closure, Compton Scale, and Gravitational Radius	140
9.6	Spinorial Orientation on the Spherical Phase Boundary	141
9.7	Dirac Spinor as the Relativistic Completion of the Temporal Spinor Doublet	142
9.8	Mass, Electromagnetic Phase, Fine Structure, and Observed Electron Mass	145
9.9	CPT Orientation and Horizon Closure of the Closed Spherical Phase State	148
9.10	The Higgs Excitation and the Information Fraction	149
10	Quantum Records and Schrödinger Dynamics	151
10.1	Quantum Records and Phase-Time Potential Information	151

10.2	Informational Wormhole Interpretation	152
10.3	Black-Hole Information Paradox and White-Hole Projection	153
10.4	Informational Diffusion and Schrödinger Dynamics from the Clock-Rate Force Branch	153
10.5	Phase-Time Diffusion and Complex Schrödinger Transport	156
11	Unified Action, Cosmology, and Metric Residues	159
11.1	The Unified Informational Action	159
11.2	Metric Fiber Form of the Unified Action	164
11.3	Cosmic Inflation, Self-Braking, and Dark Energy from the Time Action	167
11.4	Osmosis as the Membrane Limit of Local Capacity Opening	170
11.5	Dark Matter as Metric Residue: Realized Time as the Linear Projection of Phase-Time	170
11.6	Quadratic Gravity and the Fourth-Order Electromagnetic Residue	171
11.7	Effective Dark-Matter Clock-Rate Residue and Structural Significance	174
12	Empirical Test: Driven Coherent Transport Above the Critical Temperature	177
12.1	General Registration Law for Coherent Transport	177
12.2	Empirical Transport Arena and Complex Force Projections	178
12.3	Dissipative Projection and Effective Resistance	179
12.4	Criterion for Coherent Dissipationless Transport	180
12.5	Cooper-Pair Phase-Time Closure and the Vanishing Real Projection	181
12.6	Driven Coherent Transport Above the Equilibrium Critical Temperature	184
12.7	Minimal Driven-Phase Toy Model	185
12.8	Microscopic Phonon Closure of the Driven-Phase Criterion	186
12.9	Observable Optical and Transport Signatures	188
12.10	Integral Spectral-Weight Test of Coherent Transport	189
12.11	Thermodynamic Phase Driving: Chemical Potential, Phase-Time, and Coherent Registration	191
12.12	Nernst Response as Thermal Phase-Time Registration	194
12.13	Pressure, Phonon Phase-Time, and Isotope Tuning of Coherent Registration	196
12.14	Existing Experiments and the Final Empirical Prediction	199
13	Final Structural Map of the Theory	202
	References	204

1 Informational Ontology and Emergent Time

This section establishes the informational ontology used throughout the manuscript. It defines physical distinguishability, separates potential, distinguished, and dispersed information, and derives emergent time as thermodynamic registration.

1.1 The Definition of Physical Information

The foundational primitive of this framework is physical distinguishability. Information denotes the physical content by which one state, configuration, event, record, or phase relation can be distinguished from another, with algorithmic information theory providing the complementary notion of finite description length [1] [2] [3]. This usage begins from Shannon's formal measure of distinguishable alternatives [4] and the modern information-theoretic formulation of discrete distinguishability [5], carries thermodynamic content through Brillouin's reading of information and entropy [6], and connects to the physical-information programs of Wheeler [7], Zeilinger [8], and Landauer [9].

Let Δ denote the distinguishability content of a system. Total physical information is represented as a strict monotone of this content,

$$I = F(\Delta), \quad \frac{dF}{d\Delta} > 0.$$

The monotonicity condition states that increasing the number or sharpness of physical distinctions increases the informational content. A single bit is the elementary distinction between two physically distinguishable alternatives. At the elementary level this distinction is binary: an alternative is unregistered or registered, 0 or 1. Continuous physical fields in later sections describe registration capacity, phase, load, and event density associated with bit-events; the elementary distinction itself supplies the unit capacity used in the one-bit closure law. A system is therefore represented by the collection of distinctions that specify its state, configuration, records, and allowed transformations. In discrete and continuum forms,

$$I_{\text{sys}} = \sum_k \delta I_k, \quad I_{\text{sys}} = \int dI.$$

Evolution is then described as a transformation of distinguishability. If a system evolves from $s(t_1)$ to $s(t_2)$, the corresponding informational map is

$$T : I_{\text{in}} \text{ to } I_{\text{out}},$$

with total informational change

$$\Delta I = I_{\text{out}} - I_{\text{in}}.$$

This notation gives the common language used throughout the manuscript. Communication-theoretic distinguishability [4], statistical-mechanical information [10], and finite physical information processing [11] and constructor-theoretic distinguishability [12] are treated as mutually compatible expressions of physical distinguishability. A physical quantity is read as a channel through which distinguishability is stored, updated, transported, or dispersed.

1.2 The Energetic Taxonomy of Information

The energetic taxonomy follows the connection between measurement and entropy introduced by Szilard [13], Landauer's analysis of physical information costs [14] [9], and the later statistical and bounded-information readings of physical systems [10] [15]. The taxonomy separates information according to its physical role in realization and energetic availability.

The total informational content is decomposed into three sectors:

1. Potential information I_{pot} is the domain of physically possible distinctions before registration into a stable record or realized configuration.
2. Distinguished information I_{dist} is realized, work-coupled structure. It includes configurations, records, mass-energy content, motion state, and clock-rate state. Its variation is coupled to available physical work,

$$\left| \frac{dE_{\text{avail}}}{dI_{\text{dist}}} \right| = \mu_{\text{dist}} > 0.$$

3. Dispersed information I_{disp} is entropic information. It measures the dispersive cost associated with realization, registration, and loss of usable structural organization,

$$\frac{dE_{\text{avail}}}{dI_{\text{disp}}} = 0.$$

The realized bookkeeping used in the following sections is

$$I_{\text{tot}} = I_{\text{dist}} + I_{\text{disp}},$$

with energetic conditions

$$\left| \frac{\partial E_{\text{avail}}}{\partial I_{\text{dist}}} \right| > 0, \quad \frac{\partial E_{\text{avail}}}{\partial I_{\text{disp}}} = 0.$$

Potential information supplies the domain of possible distinctions. Distinguished information is the portion written into physical structure. Dispersed information is the entropic cost of that writing. This three-sector taxonomy is the basis for the later time equation, because linear time will be defined as the rate at which distinguishable structure is written relative to the dispersive cost paid for that writing.

1.3 Physical Channels of Distinguished Information

Distinguished physical information appears through three physical writing channels:

$$\boxed{I_{\text{dist}} = I_m + I_{\text{mot}} + I_\tau} \tag{1}$$

This equation identifies the physical carriers of realized distinguishability. I_m is the mass-information channel. I_{mot} is the motion-information channel. I_τ is the temporal-registration channel.

Each channel has its own physical dimensional form. The relativistic closure laws are developed after these channels are defined.

Physical interactions express their realized effect through these channels. Forces change momentum,

$$\sum_a \mathbf{F}_a = \frac{d\mathbf{p}}{dt}, \quad (2)$$

where \mathbf{F}_a is the force contribution from interaction a , \mathbf{p} is momentum, and t is coordinate time. Energetic interactions change internal energy, binding energy, field energy, or rest-energy content. Temporal effects change the rate at which physical change is registered into ordered sequence.

The relativistic energy-momentum relation displays the mass and motion channels in Einstein's special relativity [16] and Minkowski's spacetime formulation [17]:

$$E^2 = p^2 c^2 + m^2 c^4. \quad (3)$$

Here E is total energy, $p = |\mathbf{p}|$ is momentum magnitude, c is the invariant propagation speed, and m is invariant mass. The term

$$m^2 c^4 \quad (4)$$

is the invariant mass-energy contribution. The term

$$p^2 c^2 \quad (5)$$

is the motion contribution. The temporal channel is the ordering channel through which physical change is registered.

Thus physical change projects into

$$dI_{\text{physical}} \text{ to } dI_m + dI_{\text{mot}} + dI_\tau. \quad (6)$$

The three channels are now defined as the elementary channels through which all interactions in nature can be expressed.

1.4 Mass-Information: Compton Writing Rate

Mass-information I_m is the internal Compton writing channel of a massive system.

The Compton angular frequency follows the matter-wave scale introduced by de Broglie [18] and the Compton energy scale [19]:

$$\omega_C = \frac{mc^2}{\hbar}. \quad (7)$$

Here m is mass, c is the invariant propagation speed, and \hbar is the reduced Planck constant. The units are

$$[\omega_C] = \frac{\text{J}}{\text{J s}} = \text{s}^{-1}. \quad (8)$$

The ordinary Compton frequency is

$$f_C = \frac{\omega_C}{2\pi} = \frac{mc^2}{h}, \quad (9)$$

where $h = 2\pi\hbar$. Its units are

$$[f_C] = \text{Hz} = \text{s}^{-1}. \quad (10)$$

A bit is dimensionless. The mass-writing channel is normalized operationally by defining one completed Compton tick as one elementary physical distinction update. This is the unit choice for the mass-information channel. Therefore,

$$1 \text{ Compton tick} = 1 \text{ bit.} \quad (11)$$

The mass-information writing rate is

$$\dot{I}_m = \frac{dI_m}{dt} = f_C = \frac{mc^2}{h}. \quad (12)$$

Its units are

$$[\dot{I}_m] = \frac{\text{bit}}{\text{s}} = \text{s}^{-1}. \quad (13)$$

Thus,

$$\dot{I}_m = \frac{mc^2}{h} \text{ bits/s.} \quad (14)$$

The corresponding Compton time per tick is

$$\tau_C = \frac{1}{f_C} = \frac{h}{mc^2}. \quad (15)$$

The associated Compton wavelength is

$$\lambda_C = \frac{h}{mc}. \quad (16)$$

In angular notation,

$$\tau_C^{(\omega)} = \frac{1}{\omega_C} = \frac{\hbar}{mc^2}, \quad \bar{\lambda}_C = \frac{\hbar}{mc}. \quad (17)$$

For the informational construction, this is the operational mass-channel equation.

1.5 Motion-Information: Planck-Normalized Spatial Updating

Motion-information I_{mot} is spatial updating expressed in minimal physical distinguishability units.

The elementary spatial distinction is the Planck length, [20]

$$\ell_P = \sqrt{\frac{\hbar G}{c^3}}. \quad (18)$$

The elementary temporal update is the Planck time [20].

$$t_P = \sqrt{\frac{\hbar G}{c^5}}. \quad (19)$$

Their ratio is

$$\frac{\ell_P}{t_P} = \frac{\sqrt{\hbar G/c^3}}{\sqrt{\hbar G/c^5}} = \sqrt{c^2} = c. \quad (20)$$

Thus,

$$c = \frac{\ell_P}{t_P}. \quad (21)$$

This gives the maximal physical information-update speed as one elementary spatial distinction per one elementary temporal update.

Define the spatial distinguishability increment

$$dI_x = \frac{dx}{\ell_P}. \quad (22)$$

Since dx and ℓ_P both have units of length,

$$[dI_x] = \frac{\text{m}}{\text{m}} = 1 = \text{bits}. \quad (23)$$

Define the temporal update increment

$$dI_t = \frac{dt}{t_P}. \quad (24)$$

Since dt and t_P both have units of time,

$$[dI_t] = \frac{\text{s}}{\text{s}} = 1 = \text{ticks}. \quad (25)$$

The normalized spatial-update rate is

$$\frac{dI_x}{dI_t} = \frac{dx/\ell_P}{dt/t_P}. \quad (26)$$

Rearrange:

$$\frac{dI_x}{dI_t} = \frac{dx}{dt} \frac{t_P}{\ell_P}. \quad (27)$$

Since

$$\frac{dx}{dt} = v, \quad \frac{\ell_P}{t_P} = c, \quad (28)$$

we have

$$\frac{t_P}{\ell_P} = \frac{1}{c}. \quad (29)$$

Therefore,

$$\boxed{\frac{dI_x}{dI_t} = \frac{v}{c}}. \quad (30)$$

This is the Planck-normalized spatial-update rate of the motion channel. A moving system carries distinguishability about position together with distinguishability about the rate at which position is updated. The motion channel therefore contributes as the product of spatial distinction and spatial-update distinction. After normalization by the invariant update speed c , the dimensionless kinematic load is the squared update fraction,

$$\beta^2 = \left(\frac{dI_x}{dI_t} \right)^2 = \frac{v^2}{c^2}. \quad (31)$$

This explains why the special-relativistic load is quadratic: v/c is the normalized spatial-update amplitude, and v^2/c^2 is the corresponding informational load in the conserved writing budget. The inertial closure law is developed later from this ratio. The symbol I_t in this subsection denotes the Planck-normalized update counter used to normalize motion. It is distinct from I_τ , introduced below, which denotes the realized temporal-registration channel.

1.6 Time-Information: Temporal Registration

Time-information I_τ is the temporal-registration channel: the writing of physical change into ordered realized sequence, consistent with thermodynamic accounts of time in generally covariant settings [21].

At the channel level,

$$[I_\tau] = \text{bits}. \quad (32)$$

The temporal-registration rate is

$$\frac{dI_\tau}{dt}, \quad (33)$$

with units

$$\left[\frac{dI_\tau}{dt} \right] = \frac{\text{bits}}{\text{s}}. \quad (34)$$

The temporal channel remains explicit during the geometric development. The thermodynamic closure section derives the registration efficiency relative to dispersive cost and defines the inverse quantity as the thermodynamic inefficiency factor.

$$dt^* = \frac{dI_{\text{dist}}}{dI_{\text{disp}}}. \quad (35)$$

The temporal-registration channel I_τ remains one physical channel inside the realized distinguished sector,

$$I_{\text{dist}} = I_m + I_{\text{mot}} + I_\tau. \quad (36)$$

The dimensionless informational-time ratio is defined at the level of the full realized registration balance,

$$dt^* = \frac{dI_{\text{dist}}}{dI_{\text{disp}}}, \quad (37)$$

where I_{disp} is the dispersed informational cost of record formation.

1.7 Potential Information, Measurement, and Realized Record

Before one derives a time equation, one must specify what kind of information is being written into physics. The present framework therefore distinguishes a third informational sector in addition to the distinct and dispersed sectors already defined above. That sector is potential information,

$$I_{\text{pot}}.$$

Potential information is the informational domain of unrealized physical possibilities. In the present framework, this is the sector described by the wave function before record formation. It is not yet written into causal history. It is not yet part of realized, distinguishable record. It is the domain of what can be realized but has not yet been written.

Measurement is a physical record-forming interaction, in line with von Neumann's measurement formulation [22], decoherence and einselection [23] [24] [25], relational quantum mechanics [26], and

information-based quantum foundations [8]. Any physical interaction that writes one previously potential distinction into realized record counts as measurement in the present framework. When such a record-forming event occurs, one option leaves the potential sector and is written into the realized branch. The realized part splits into distinct record and dispersed thermodynamic cost. The elementary informational bookkeeping is therefore

$$-dI_{\text{pot}} = dI_{\text{dist}} + dI_{\text{disp}}.$$

This equation refers only to the particular potential distinction that becomes realized; all other unrealized possibilities remain in the potential sector. One potential option leaves the potential sector and becomes dI_{dist} , while the corresponding thermodynamic payment appears as dI_{disp} .

This point is necessary because Landauer’s principle acts on realized record formation [27], and because logical reversibility [28] and thermodynamic computation [29] distinguish reversible information handling from irreversible record production. The relevant informational increment in the thermodynamic bridge is the distinct increment created when one previously potential distinction is written into realized history. In the present framework, time is generated precisely by this transfer from the potential sector into the realized branch, together with its dispersed thermodynamic payment.

2 Thermodynamic Derivation of Time via Power

To derive the nature of time, we analyze the system through Power (P), the rate of energy transfer.

From classical thermodynamics, with Clausius’ entropy principle [30], Gibbs’ statistical thermodynamics [31], Boltzmann’s statistical mechanics [32], and Jaynes’ statistical reading of entropy [10] and Prigogine’s irreversible-process framework [33], dissipated power is, in the standard thermodynamic notation used by Callen and statistical-mechanics treatments [34] [35] [36]:

$$P_{\text{diss}} = T \left(\frac{dS}{dt} \right)$$

From Landauer’s principle [27], refined through the thermodynamics of reversible and irreversible computation [28] [29], the minimum power required to inscribe distinct information (dI_{dist}) is:

$$P_{\text{dist}} = k_B T \ln(2) \left(\frac{dI_{\text{dist}}}{dt} \right)$$

2.1 From Power Cancellation to the Pure Informational Time Equation

We define the dimensionless physical time increment, dt^* , as the ratio of distinct-information power to dissipated power:

$$dt^* = \frac{P_{\text{dist}}}{P_{\text{diss}}}$$

Substituting the equations:

$$dt^* = \frac{k_B T \ln(2) \left(\frac{dI_{\text{dist}}}{dt} \right)}{T \left(\frac{dS}{dt} \right)}$$

The temperature (T) and the coordinate time increment (dt) cancel out entirely, leaving the informational ratio as the physical time parameter [27]:

$$dt^* = k_B \ln(2) \left(\frac{dI_{\text{dist}}}{dS} \right)$$

The primary time postulate of UiT identifies dimensionless linear physical time with the thermodynamic registration ratio between distinguished information and dispersed information. The power construction motivates and constrains this identification by showing that the same ratio is isolated when temperature and an external time parameter cancel from the registration and dissipation powers.

By substituting entropy with its informational equivalent, using Landauer's bit cost [27], Jaynes' entropy-information relation [10], and Brillouin's negentropy reading [6],

$$dt^* = \frac{k_B \ln(2) dI_{\text{dist}}}{k_B \ln(2) dI_{\text{disp}}}$$

The constants cancel, leaving the thermodynamic-information definition supported by Landauer's physical bit principle [27] and Jaynes' statistical mechanics of information [10]:

$$dt^* = \frac{dI_{\text{dist}}}{dI_{\text{disp}}}$$

One must now define time in the present framework. Linear time is introduced as the informational registration ratio of the theory. The relevant written sector is the structured distinct information that is registered as ordered sequence, record, or measurable history. Denote this written sector by

$$I_{\text{dist}}.$$

If the distinct structural sector is represented as a set of distinguishable informational elements,

$$I_{\text{dist}} = \{i_\alpha\},$$

then the written distinct sector may be represented as the ordered set

$$I_{\text{dist}} = \{i_n\}_{n=1}^N, \quad i_n \prec i_{n+1},$$

where \prec denotes ordered registration within the distinct sector of the realized domain.

Time is then defined by the ratio between distinct informational change and dispersed informational change. In the notation used throughout the manuscript, the elementary informational time equation is

$$dt^* = \frac{dI_{\text{dist}}}{dI_{\text{disp}}}.$$

Using the entropy-bit conversion only as notation for dispersed information,

$$dI_{\text{disp}} \equiv \frac{dS}{k_B \ln 2},$$

time is generated by the relation between distinguished information and dispersed information, with entropy entering through the dispersed-information denominator. One may write the same relation as

$$dt^* = (k_B \ln 2) \frac{dI_{\text{dist}}}{dS}.$$

This equation is the correct starting point for everything that follows. It defines linear time as an informational ratio [21]. At this stage it is still dimensionless.

2.2 Thermodynamic Registration Efficiency and Inefficiency

Real processes are dissipative in the irreversible thermodynamic sense [33], meaning $dI_{\text{disp}} \geq dI_{\text{dist}}$. The thermodynamic registration efficiency is the dimensionless ratio

$$\eta_{\text{th}} = \frac{dI_{\text{dist}}}{dI_{\text{disp}}}, \quad 0 < \eta_{\text{th}} \leq 1.$$

The inverse quantity is the thermodynamic inefficiency factor

$$\gamma_{\text{th}} = \frac{1}{\eta_{\text{th}}} = \frac{dI_{\text{disp}}}{dI_{\text{dist}}}, \quad \gamma_{\text{th}} \geq 1.$$

The ideal Landauer-saturating limit [27] is $\eta_{\text{th}} = 1$ and $\gamma_{\text{th}} = 1$. Any nonideal dissipative process has $0 < \eta_{\text{th}} < 1$ and $\gamma_{\text{th}} > 1$.

Equivalently,

$$dI_{\text{disp}} = \gamma_{\text{th}} dI_{\text{dist}}.$$

Substituting this into the time equation gives

$$dt^* = \frac{dI_{\text{dist}}}{\gamma_{\text{th}} dI_{\text{dist}}} = \frac{1}{\gamma_{\text{th}}} = \eta_{\text{th}}.$$

The same dimensionless registration ratio therefore has three equivalent readings:

$$dt^* = \eta_{\text{th}} = \frac{1}{\gamma_{\text{th}}}.$$

Here dt^* is the informational-time reading of the ratio, η_{th} is its thermodynamic-efficiency reading, and $1/\gamma_{\text{th}}$ is the remaining registration efficiency, or clock-rate capacity. The quantity γ_{th} itself is the thermodynamic load or inefficiency factor.

At this stage dt^* remains the dimensionless informational-time ratio. Its physical Compton-scaled phase-time completion is introduced later, after the coherent phase variable and the phase-time field have been constructed.

2.3 The Two-Spheres Geometry and the Riemann-Surface Present

1. The Outer Sphere (Potential Realm): Represents I_{pot} , the domain of unrealized physical distinguishability in the spirit of information-based foundations [7].
2. The Inner Sphere (Realized Realm): Represents $I_{\text{dist}} + I_{\text{disp}}$.

$$-dI_{\text{pot}} = dI_{\text{dist}} + dI_{\text{disp}}$$

Once the informational content of physics has been separated into potential, distinct, and dispersed sectors, the same structure can be expressed geometrically. Consider a finite outer sphere that represents the full domain of potential information that can exist in the universe. Within it, a second sphere grows from the center and represents the information that has already been written into realized history through physical interaction and thermodynamic payment.

In this picture, the outer sphere is the potential realm. The inner sphere is the realized realm. As the realized sphere grows, it does so at the expense of the potential sphere. That growth is the physical meaning of time in the present framework. Time is therefore not introduced as a primitive background parameter. It is the ordered transfer of information from the potential sector into realized record, with the corresponding thermodynamic cost required by Landauer's principle.

This picture gives a direct geometric interpretation of the later division between quantum theory and relativity. Quantum theory describes the potential sphere, because the quantum state belongs to the domain of unrealized possibilities before record formation. Relativity describes the realized sphere, because relativity governs the structure of already written, causal, measured history. The two descriptions meet at the two-dimensional interface between the spheres. That interface is the present.

The boundary is a Riemann Sphere (S^2), anchored in the classical theory of Riemann surfaces [37] [38] [39]. Its information-theoretic motivation follows Wheeler's information program [7], while its boundary reading is aligned with the holographic tradition of 't Hooft [40], Susskind [41],

and Maldacena [42]. Updates on this boundary are described using complex numbers and the differential-geometric language used in modern geometry and physics [43] [44]:

$$z = r e^{i\phi}$$

The Riemann-sphere language is used here in its geometric role: it compactifies the complex plane into a closed two-dimensional surface,

$$\hat{\mathbb{C}} = \mathbb{C} \cup \{\infty\} \simeq S^2.$$

Thus the complex coordinate is not only an algebraic notation for amplitude and phase. It is also a geometric coordinate on the present interface. In this sense, the Riemann construction supplies the global surface language of the theory: coherent phase is written locally in the complex plane, while the present interface is represented globally as a compact geometric boundary.

The present surface is represented here as a Riemann sphere. Since the Riemann sphere is naturally represented in the complex plane, the model also supplies a geometric motivation for why coherent quantum evolution is written in a complex form. In this framework, the complex plane is not a formal trick added afterwards. It is the natural language of the interface where potential information is written as distinct information with dispersed thermodynamic cost.

This geometric model supplies the entry point for the derivations that follow, connecting relational quantum structure [26] with information-based quantum foundations [8]. It shows why relativity and quantum theory appear different, what informational domain each one describes, where they meet, and why the transition from one to the other requires a thermodynamic price. In the present framework, that price is the cost of writing a potential distinction into realized history.

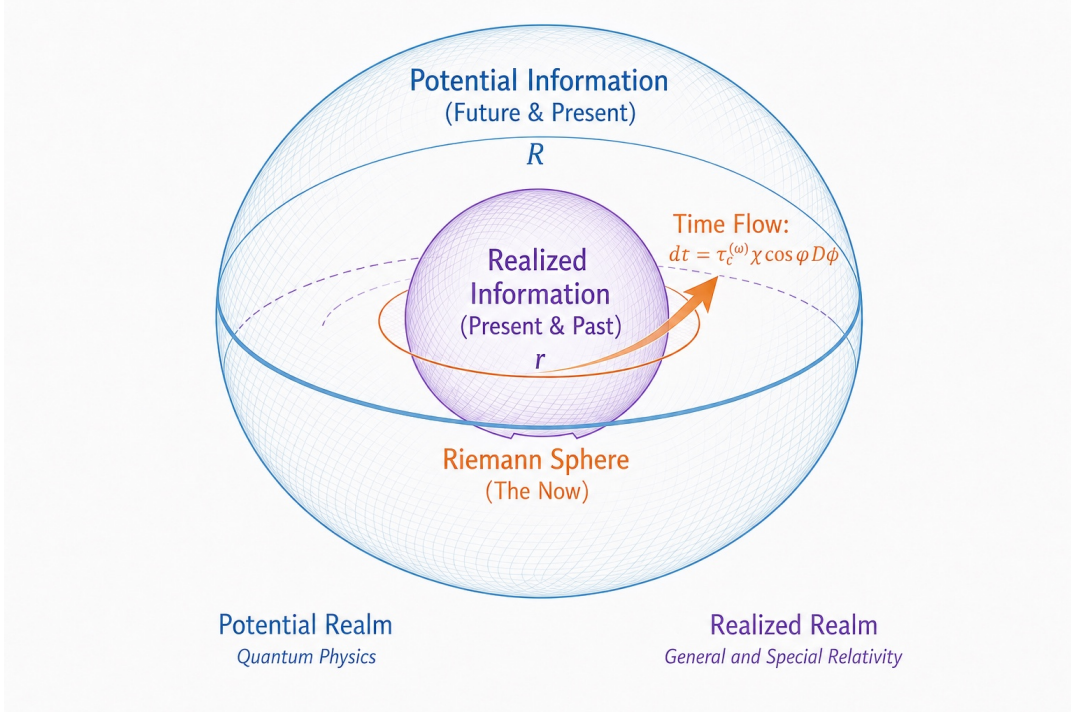


Figure 1: Geometric two-spheres model of informational reality. The outer sphere represents the domain of potential information. The inner sphere represents realized information in its decomposed form, $I_{\text{dist}} + I_{\text{disp}}$. Their two-dimensional interface is the present surface. In this picture, quantum theory describes the potential realm, relativity describes the realized realm, and time is the growth of the distinct-plus-dispersed realized sector at the expense of potential information. Because the Riemann sphere is represented on the complex plane, the temporal structure already has a phase form; the full phase-time development is introduced in the later coherent-branch sections.

2.4 The Arrow of Time and Human Memory

The two-spheres construction already places temporal registration on a complex Riemann interface. Schematically, an elementary phase-time orientation on that interface may be represented by the unit complex vector

$$\hat{t}_\phi(\phi) = e^{-i\phi} = \cos \phi - i \sin \phi. \quad (38)$$

Its realized linear projection is therefore the real component,

$$\hat{t}_{\text{lin}}(\phi) = \text{Re}[\hat{t}_\phi(\phi)] = \cos \phi. \quad (39)$$

This schematic projection is used here as the geometric motivation for the question: if the realized temporal projection has positive and negative real orientations, how does an observer experience a single arrow of time? The full phase-time equation is developed in the later coherent-branch sections.

The following thought experiment illustrates how records and memory generate the experienced direction of time. The ordinary conviction that time moves from past to future rests on four simple claims.

First, I remember the past.

Second, I experience the present.

Third, I do not remember the future.

Fourth, entropy increases on average around me.

These four claims are the basis on which we infer a preferred temporal direction, a theme central to statistical accounts of the arrow of time [32]. One must therefore test what happens to all four if time is reversed completely, like a film running in rewind.

Consider a theoretical case in which a person dies, is buried, and then the entire temporal order reverses. The person rises out of the grave and becomes younger and younger while moving toward what, from our ordinary description, would be called the past. One may now examine the four claims one by one.

The first claim still holds. The moment the person rises from the grave, that person already emerges with the memories of the life that has been lived. In other words, the person remembers the past, or more precisely, remembers what is already written for that observer.

The second claim also still holds. The person continues to experience the present. Even in a reversed world, there is always a lived present.

The third claim now becomes the decisive point. As the person proceeds in the reversed direction, the memories of what, from our ordinary point of view, would be called the future begin to disappear. The reason is simple. Writing memory is a physical act. It is a physical operation, not a human label or psychological metaphor. To write memory, one must invest energy, organize information, and expel heat into the environment, as in the thermodynamics of irreversible information processing [27] [29].

$$dW_{\min} \geq k_B T \ln 2 dI_{\text{bit}}, \quad dS_{\text{env}} \geq k_B \ln 2 dI_{\text{bit}}. \quad (40)$$

It is a physical operation in exactly the same sense that throwing a ball to the left is a physical operation.

Therefore, if the entire film is run backward, the writing of memory must also reverse. Just as a ball thrown to the left returns to the right under total reversal, so too the heat and energy expelled to the environment return into the system. The memory is erased, and the energy invested in writing it is released back. The entropy of the environment truly decreases, exactly as a reversed world requires. Therefore the person necessarily loses the memory of what, for us, would be called the future while moving in that direction. The third condition is therefore also satisfied.

The fourth claim is then no less important. In such a world, things really do become more ordered. Entropy decreases. Broken things become whole. One may imagine a broken egg on the floor that rises and becomes whole again on the table. That is indeed what happens in such a world. But here a crucial point enters. By the time the egg is once again whole on the table, the observer has already lost the memory that it ever fell and broke. So even though entropy decreases, the memory state is still perfectly consistent with the experienced temporal direction. The fourth condition is therefore satisfied as well.

The conclusion is that all four of the conditions from which we usually infer that time moves from past to future remain valid even if time were running in the opposite direction, consistent with time-symmetric microscopic dynamics and record-based asymmetry [45] [46] [47]. The arrow of time as we experience it is generated by memory and by the direction in which records are written. Physics may be time-symmetric, while the experienced arrow is determined by the direction in which records are written and retained.

In this sense, memory is our sense of time. Like every other sense, it is limited. Vision does not capture the whole electromagnetic spectrum. Hearing does not capture all frequencies. In the same way, our sense of time is also limited. It depends on physical records, and it is limited by their erasure. We see only half of the dynamical reality. Therefore, opposite temporal orientations can be physically indistinguishable from inside a memory-based record structure. The observer experiences a coherent temporal direction because the accessible record sequence is the only operational basis for temporal awareness.

If one now returns to the two-spheres model, the same point becomes even clearer. The inner sphere, which contains the distinct-plus-dispersed realized sector, can grow and shrink. It has no preferred direction in itself. At the deeper level, the process is a zero-sum structure. Time does not intrinsically prefer one side of the story. What creates the one-directional narrative of experience is memory, which records measured outcomes and builds a sequence out of what it can preserve.

This also resolves the intuitive paradox of the past. If past and future are, first of all, informational structures, then returning to the past means re-entering a prior record structure within the total informational state. The past is not a place in that sense. Past and future exist equally within the total informational structure. What turns one side into a lived narrative is memory.

3 Informational Special Relativity

This section develops the relativistic capacity geometry. Special relativity is treated through directional motion load, general relativity through radial gravitational load, and both limits are then collected into one capacity law.

3.1 Informational Special Relativity: Planck-Normalized Spatial Resolution and the Kinematic Load

The special-relativistic sector is the motion-only projection of the informational capacity law. For this reason the Planck-normalized spatial-update relation is restated here, where it does the work of producing the Lorentz load.

The elementary spatial distinction is the Planck length [20].

$$\ell_P = \sqrt{\frac{\hbar G}{c^3}}. \quad (41)$$

The elementary temporal update is the Planck time,

$$t_P = \sqrt{\frac{\hbar G}{c^5}}. \quad (42)$$

Their ratio is

$$\frac{\ell_P}{t_P} = \frac{\sqrt{\hbar G/c^3}}{\sqrt{\hbar G/c^5}} = \sqrt{c^2} = c, \quad (43)$$

so

$$\boxed{c = \frac{\ell_P}{t_P}}. \quad (44)$$

Thus the invariant speed is the maximal update rate of distinguishable physical change: one elementary spatial distinction per one elementary temporal update. This connects the capacity construction to the standard invariant-speed structure of special relativity [48] and to the spacetime-clock formulation of relativistic kinematics [49].

Define the spatial distinguishability increment

$$dI_x = \frac{dx}{\ell_P}, \quad (45)$$

and the temporal update increment

$$dI_t = \frac{dt}{t_P}. \quad (46)$$

Both are dimensionless counts of elementary distinctions or ticks:

$$[dI_x] = \frac{\text{m}}{\text{m}} = 1, \quad [dI_t] = \frac{\text{s}}{\text{s}} = 1. \quad (47)$$

The normalized spatial-update rate is therefore

$$\frac{dI_x}{dI_t} = \frac{dx/\ell_P}{dt/t_P}. \quad (48)$$

Rearranging gives

$$\frac{dI_x}{dI_t} = \frac{dx}{dt} \frac{t_P}{\ell_P}. \quad (49)$$

Since

$$\frac{dx}{dt} = v, \quad \frac{\ell_P}{t_P} = c, \quad (50)$$

one has

$$\boxed{\frac{dI_x}{dI_t} = \frac{v}{c}}. \quad (51)$$

This is the Planck-normalized spatial-update amplitude of the motion channel. The corresponding dimensionless kinematic load is the squared update fraction,

$$\boxed{\Lambda_{I,v} = \left(\frac{dI_x}{dI_t}\right)^2 = \frac{v^2}{c^2}}. \quad (52)$$

The square appears because the conserved writing budget is a norm. The amplitude v/c measures the spatial-update fraction, while v^2/c^2 is the motion load that competes with the surviving temporal writing fraction in the one-bit closure law.

3.2 Kinematic Capacity Load and the Lorentz Factor

The inertial case is developed first as the purely motional projection of the general capacity law, with gravitational load set to zero:

$$\frac{r_s}{r} = 0. \quad (53)$$

Then

$$\chi_g = 1. \quad (54)$$

The active channel is motion-information. From the Planck-normalized spatial-update relation developed above,

$$\frac{dI_x}{dI_t} = \frac{v}{c}. \quad (55)$$

The dimensionless motion load is the squared normalized spatial-update rate:

$$\Lambda_{I,v} = \left(\frac{dI_x}{dI_t} \right)^2 = \frac{v^2}{c^2}. \quad (56)$$

Equivalently, set

$$\beta = \frac{v}{c}. \quad (57)$$

The realized temporal fraction and the spatial-update fraction form the normalized informational amplitude

$$\chi_v + i\beta. \quad (58)$$

Conservation of the writing norm on the present interface gives

$$|\chi_v + i\beta|^2 = 1. \quad (59)$$

Expanding the norm gives

$$\chi_v^2 + \beta^2 = 1. \quad (60)$$

Since $\beta^2 = v^2/c^2$, this is the same one-bit closure law used below. The unit on the right-hand side is the normalized capacity of one elementary registered distinction; χ_v^2 and v^2/c^2 allocate that capacity between temporal availability and motional load.

The units are dimensionless:

$$[\Lambda_{I,v}] = \left[\frac{v^2}{c^2} \right] = \frac{\text{m}^2/\text{s}^2}{\text{m}^2/\text{s}^2} = 1. \quad (61)$$

The temporal writing factor for the kinematic case is

$$\chi_v = \frac{d\tau}{dt}. \quad (62)$$

The closure law is

$$\chi_v^2 + \Lambda_{I,v} = 1. \quad (63)$$

Substitute the motion load:

$$\chi_v^2 + \frac{v^2}{c^2} = 1. \quad (64)$$

Then

$$\chi_v^2 = 1 - \frac{v^2}{c^2}, \quad (65)$$

so

$$\chi_v(v) = \sqrt{1 - \frac{v^2}{c^2}}. \quad (66)$$

Since

$$\chi_v = \frac{d\tau}{dt}, \quad (67)$$

the proper-time relation is

$$d\tau = \sqrt{1 - \frac{v^2}{c^2}} dt. \quad (68)$$

The gamma factor is the inverse temporal writing factor, matching the standard Lorentz kinematic factor [16] [48] [49]:

$$\gamma_I = \frac{1}{\chi_v} = \frac{1}{\sqrt{1 - \frac{v^2}{c^2}}}. \quad (69)$$

All quantities in the closure law are dimensionless:

$$[\chi_v] = 1, \quad \left[\frac{v^2}{c^2} \right] = 1, \quad [\gamma_I] = 1. \quad (70)$$

Motion-information consumes part of the local writing capacity through the normalized load v^2/c^2 , leaving the temporal fraction χ_v .

3.3 Thermodynamic Writing Cost of the Lorentz Factor

The thermodynamic construction above identified physical time as the registration of distinct information relative to the dispersed cost paid in making that registration, using the physical-information reading of irreversible writing cost [27]. In that language, the efficiency of writing distinct structure from the potential domain into realized record is

$$\eta_{\text{th}} = \frac{dI_{\text{dist}}}{dI_{\text{disp}}}, \quad 0 < \eta_{\text{th}} \leq 1, \quad (71)$$

and the inverse cost factor is

$$\gamma_{\text{th}} = \frac{dI_{\text{disp}}}{dI_{\text{dist}}} = \frac{1}{\eta_{\text{th}}}, \quad \gamma_{\text{th}} \geq 1. \quad (72)$$

The kinematic reconstruction has now supplied the corresponding temporal-writing fraction under pure motion,

$$\chi_v = \frac{d\tau}{dt} = \sqrt{1 - \frac{v^2}{c^2}}, \quad \gamma_I = \frac{1}{\chi_v}. \quad (73)$$

For a pure kinematic load, these are the same physical ratio expressed in thermodynamic and relativistic languages; the reversible-computation background fixes the interpretation of thermodynamic cost without adding a new relativistic factor [29]. The thermodynamic registration efficiency is the surviving Lorentz clock-rate fraction:

$$\eta_{\text{th}}^{(v)} = \chi_v. \quad (74)$$

The thermodynamic writing-cost factor is the Lorentz factor [16]:

$$\gamma_{\text{th}}^{(v)} = \gamma_I = \frac{1}{\sqrt{1 - \frac{v^2}{c^2}}}. \quad (75)$$

Equivalently,

$$\frac{dI_{\text{dist}}}{dI_{\text{disp}}} = \frac{d\tau}{dt} = \sqrt{1 - \frac{v^2}{c^2}} \quad (76)$$

and, using

$$dI_{\text{disp}} = \frac{dS}{k_B \ln 2}, \quad (77)$$

the Lorentz clock factor can be written in entropy-registration form as

$$(k_B \ln 2) \frac{dI_{\text{dist}}}{dS} = \sqrt{1 - \frac{v^2}{c^2}}. \quad (78)$$

The inverse thermodynamic cost factor is

$$\frac{1}{k_B \ln 2} \frac{dS}{dI_{\text{dist}}} = \frac{1}{\sqrt{1 - \frac{v^2}{c^2}}} = \gamma_I. \quad (79)$$

Thus

$$\gamma_{\text{th}}^{(v)} = \gamma_I. \quad (80)$$

The tested proper-time law remains

$$d\tau = \sqrt{1 - \frac{v^2}{c^2}} dt = \frac{dt}{\gamma_I}. \quad (81)$$

This reconstruction gives the Lorentz factor an informational-thermodynamic meaning while preserving the empirical content of special relativity.

3.4 Longitudinal Spatial Capacity and Length Contraction

The same motion load reduces distinguishable spatial writing capacity along the direction of motion.

Let

$$\Omega_{\parallel, \text{write}}(v) \quad (82)$$

denote the distinguishable spatial writing capacity along the direction of motion. Define longitudinal spatial distinguishability as

$$I_{x_{\parallel}}(v) = \log_2 \Omega_{\parallel, \text{write}}(v). \quad (83)$$

Since $\Omega_{\parallel, \text{write}}$ counts possible distinguishable configurations,

$$[I_{x_{\parallel}}] = \text{bits}. \quad (84)$$

Equivalently, the normalized logarithmic configuration capacity along the direction of motion is

$$\mathcal{C}_{\parallel}(v) = \frac{\log_2 \Omega_{\parallel, \text{write}}(v)}{\log_2 \Omega_{\parallel, \text{write}}(0)}. \quad (85)$$

The surviving longitudinal writing capacity is

$$\boxed{\mathcal{C}_{\parallel}(v) = \chi_v, \quad I_{x_{\parallel}}(v) = \chi_v I_{x_{\parallel}}(0).} \quad (86)$$

In terms of the underlying number of available configurations, this is

$$\boxed{\Omega_{\parallel, \text{write}}(v) = \Omega_{\parallel, \text{write}}(0)^{\chi_v}.} \quad (87)$$

Using

$$\chi_v = \sqrt{1 - \frac{v^2}{c^2}}, \quad (88)$$

this becomes

$$\boxed{I_{x_{\parallel}}(v) = \sqrt{1 - \frac{v^2}{c^2}} I_{x_{\parallel}}(0).} \quad (89)$$

The geometric length expression is the spatial reading of the same capacity reduction. [50] [51] Let L_0 be the proper longitudinal spatial capacity. The surviving longitudinal length is

$$L_{\parallel} = \chi_v L_0. \quad (90)$$

Substitute χ_v :

$$\boxed{L_{\parallel} = L_0 \sqrt{1 - \frac{v^2}{c^2}}.} \quad (91)$$

Using

$$\gamma_I = \frac{1}{\chi_v}, \quad (92)$$

the same relation is

$$\boxed{L_{\parallel} = \frac{L_0}{\gamma_I}.} \quad (93)$$

The units are

$$[L_{\parallel}] = [L_0] = \text{m}, \quad [\chi_v] = [\gamma_I] = 1. \quad (94)$$

3.5 Invariant Mass and Observed Inertial Energy

The internal Compton process of a massive mode and the externally measured energy of that mode must still be distinguished.

The observed internal clock rate is read through the surviving realized temporal fraction,

$$\omega_{\text{clock, obs}} = \omega_C \chi_v = \omega_C \sqrt{1 - \frac{v^2}{c^2}}. \quad (95)$$

Thus the internal clock slows as motion increases the dispersive load.

The observed inertial energy, however, is obtained from the action. For a free massive mode, [52] [48]

$$S = -mc^2 \int d\tau. \quad (96)$$

Using

$$d\tau = \chi_v dt, \quad (97)$$

the action becomes

$$S = -mc^2 \int \chi_v dt, \quad (98)$$

so the Lagrangian is

$$L = -mc^2 \chi_v = -mc^2 \sqrt{1 - \frac{v^2}{c^2}}. \quad (99)$$

The canonical momentum is

$$p = \frac{\partial L}{\partial v}. \quad (100)$$

Since

$$\chi_v = \sqrt{1 - \frac{v^2}{c^2}}, \quad (101)$$

one has

$$\frac{\partial \chi_v}{\partial v} = -\frac{v}{c^2 \chi_v}. \quad (102)$$

Therefore

$$p = -mc^2 \frac{\partial \chi_v}{\partial v} = \frac{mv}{\chi_v} = \gamma_I mv. \quad (103)$$

The Hamiltonian energy is

$$E = v \frac{\partial L}{\partial v} - L, \quad (104)$$

hence

$$E = v \frac{mv}{\chi_v} + mc^2 \chi_v = \frac{mv^2}{\chi_v} + mc^2 \chi_v. \quad (105)$$

Using

$$\chi_v^2 = 1 - \frac{v^2}{c^2}, \quad (106)$$

this becomes

$$E = \frac{m}{\chi_v} \left(v^2 + c^2 \chi_v^2 \right) = \frac{m}{\chi_v} \left(v^2 + c^2 \left(1 - \frac{v^2}{c^2} \right) \right) = \frac{mc^2}{\chi_v} = \gamma_I mc^2. \quad (107)$$

Thus the observed inertial energy increases as

$$E = \gamma_I mc^2, \quad (108)$$

while the observed clock rate decreases according to

$$\omega_{\text{clock,obs}} = \omega_C \chi_v = \frac{\omega_C}{\gamma_I} = \omega_C \sqrt{1 - \frac{v^2}{c^2}}. \quad (109)$$

The invariant mass channel remains

$$E_m = mc^2, \quad \omega_C = \frac{mc^2}{\hbar}, \quad \dot{I}_m = \frac{mc^2}{h}. \quad (110)$$

The factor γ_I belongs to the external dynamical state and to the dispersive cost of writing that state into realized history. It multiplies the observed inertial energy, while the internal Compton mass-information remains the same invariant channel.

The two readings are complementary. The internal realized writing rate slows because motion depletes temporal bandwidth, while the externally measured energy increases because the same moving mode occupies a more costly dynamical state in the conserved informational geometry.

As $v \rightarrow c$, one has

$$\beta \rightarrow 1, \quad \chi_v \rightarrow 0, \quad \gamma_I \rightarrow \infty. \quad (111)$$

The surviving realized temporal fraction collapses to zero. This is the informational meaning of the light-speed barrier.

3.6 Kinetic Energy as Relative Time-Load

The same clock-rate factor also gives the usual relativistic kinetic-energy expression [48]. The total relativistic energy is

$$E = \gamma mc^2,$$

while the rest energy is

$$E_0 = mc^2.$$

The kinetic energy is therefore [52]

$$K = E - E_0 = (\gamma - 1)mc^2.$$

Since $\gamma = 1/\chi_v$, this can be written as

$$K = mc^2 \left(\frac{1}{\chi_v} - 1 \right) = mc^2 \left(\frac{1 - \chi_v}{\chi_v} \right).$$

Thus kinetic energy is the energetic cost of relative time-load. Motion reduces the available local clock-rate fraction χ_v , and the observed kinetic energy measures the corresponding increase in the inverse load factor.

3.7 Inertial Force from the Same Temporal Mismatch

The inertial case also uses the invariant Compton writing rate,

$$\dot{I}_m = \frac{mc^2}{h}, \quad (112)$$

with invariant energy scale

$$E_m = mc^2. \quad (113)$$

The Lorentzian temporal factor is

$$\chi_v(v) = \sqrt{1 - \frac{v^2}{c^2}}. \quad (114)$$

Motion changes the temporal channel available to the invariant internal writing rate. The corresponding embedding energy is

$$E_{\text{embed}}(v) = mc^2 \chi_v(v). \quad (115)$$

The associated mismatch magnitude is

$$E_T(v) = mc^2 (1 - \chi_v(v)), \quad (116)$$

while the dynamical action is generated by the relativistic free-particle Lagrangian

$$\boxed{L = -mc^2 \chi_v = -mc^2 \sqrt{1 - \frac{v^2}{c^2}}.} \quad (117)$$

Thus $mc^2(1 - \chi_v)$ quantifies temporal mismatch, while $L = -mc^2 \chi_v$ gives the correct momentum response of the invariant mass channel under changing velocity.

The canonical momentum is obtained from the Lagrangian:

$$p = \frac{\partial L}{\partial v}. \quad (118)$$

Using

$$\frac{\partial \chi_v}{\partial v} = -\frac{v}{c^2 \chi_v}, \quad (119)$$

one obtains

$$p = -mc^2 \frac{\partial \chi_v}{\partial v} = \frac{mv}{\chi_v} = \gamma_I mv. \quad (120)$$

For the free particle alone the Euler–Lagrange equation gives $dp/dt = 0$. When an external longitudinal generalized force is applied to change the velocity state, [53] the generalized force is the rate of change of canonical momentum:

$$\boxed{Q_{\parallel} = F_{\parallel} = \frac{dp}{dt} = \frac{d}{dt} (\gamma_I mv).} \quad (121)$$

For one-dimensional longitudinal acceleration,

$$a = \frac{dv}{dt}. \quad (122)$$

Therefore

$$F_{\parallel} = m \left(\frac{d\gamma_I}{dt} v + \gamma_I a \right). \quad (123)$$

The time derivative of the Lorentz factor is

$$\frac{d\gamma_I}{dt} = \frac{d}{dt} \left(1 - \frac{v^2}{c^2} \right)^{-1/2}. \quad (124)$$

Hence

$$\frac{d\gamma_I}{dt} = \gamma_I^3 \frac{v}{c^2} a. \quad (125)$$

Substitute this into the longitudinal force expression:

$$F_{\parallel} = m \left(\gamma_I^3 \frac{v^2}{c^2} a + \gamma_I a \right). \quad (126)$$

Factor out $m\gamma_I a$:

$$F_{\parallel} = m\gamma_I a \left(\gamma_I^2 \frac{v^2}{c^2} + 1 \right). \quad (127)$$

Since

$$\gamma_I^2 = \frac{1}{1 - \frac{v^2}{c^2}}, \quad (128)$$

one has

$$\gamma_I^2 \frac{v^2}{c^2} + 1 = \frac{\frac{v^2}{c^2}}{1 - \frac{v^2}{c^2}} + 1 = \frac{1}{1 - \frac{v^2}{c^2}} = \gamma_I^2. \quad (129)$$

Therefore the longitudinal inertial force is

$$\boxed{F_{\parallel} = \gamma_I^3 m a.} \quad (130)$$

The low-velocity limit is recovered immediately:

$$v \ll c, \quad \gamma_I \approx 1, \quad \boxed{F_{\parallel} \approx m a.} \quad (131)$$

This section supplies the analytic-mechanics form of the same temporal-mismatch mechanism. The invariant Compton channel remains mc^2 , the temporal writing fraction is χ_v , the canonical momentum is $p = \gamma_I m v$, and the longitudinal resistance to changing the velocity state is $F_{\parallel} = \gamma_I^3 m a$.

3.8 Relativistic Diffusion at Non-Relativistic Velocities

The preceding derivation can now be sharpened. The theory has already identified the thermodynamic inefficiency factor with the Lorentz factor,

$$\gamma_{\text{th}} = \gamma_I, \quad (132)$$

or equivalently,

$$\chi_{\text{th}} = \chi_v. \quad (133)$$

Therefore diffusion should not be formulated as if a new conversion factor were being invented between thermodynamics and relativity. The factor is the same factor. What changes is the physical source of the load.

In special relativity,

$$\gamma_I = \frac{1}{\sqrt{1 - v^2/c^2}}. \quad (134)$$

In the thermodynamic sector of UiT,

$$\gamma_{\text{th}} = \frac{dI_{\text{disp}}}{dI_{\text{dist}}}. \quad (135)$$

The identification is

$$\boxed{\gamma_{\text{th}} = \gamma_I.} \quad (136)$$

Thus,

$$\boxed{\frac{dI_{\text{disp}}}{dI_{\text{dist}}} = \frac{1}{\sqrt{1 - v^2/c^2}}.} \quad (137)$$

Equivalently,

$$\boxed{\frac{dI_{\text{dist}}}{dI_{\text{disp}}} = \sqrt{1 - v^2/c^2}.} \quad (138)$$

When the theory is applied to diffusion, no separate object such as a new γ_{diff} is required. The same Lorentz-informational factor becomes a local spatial field because the dispersive cost and the registration ratio depend on concentration:

$$\gamma(x) = \frac{dI_{\text{disp}}(x)}{dI_{\text{dist}}(x)}. \quad (139)$$

By the existing identification,

$$\gamma(x) = \gamma_I(x), \quad (140)$$

where $\gamma_I(x)$ is the Lorentzian equivalent of the local time-load factor. It is not introduced as the Lorentz factor of an aircraft or a macroscopic high-speed body. It is the same time-capacity factor evaluated locally, in the thermodynamic limit where the load is produced by concentration and dispersive cost.

The clean connection to chemical potential is obtained by writing the local Lorentz load as a local thermodynamic driving term, in continuity with standard non-equilibrium thermodynamics [84].

$$mc^2[\gamma(x) - 1] = \Delta\mu_{\text{load}}(x), \quad \Delta\mu_{\text{load}}(x) \geq 0. \quad (141)$$

Here $\gamma(x) = 1/\chi(x)$ is the local thermodynamic load or inefficiency factor already defined in the power derivation, while $\chi(x)$ is the remaining registration efficiency or clock-rate capacity. A higher concentration increases the local dispersive load, so

$$C \text{ increases} \implies \chi \text{ decreases} \implies \gamma \text{ increases}. \quad (142)$$

For an ideal solution, the chemical-potential gradient is [84]

$$\nabla\mu = k_B T \nabla \ln n, \quad (143)$$

where $n(x)$ is the local number concentration. The reference value of μ fixes the zero of chemical potential, while $\Delta\mu_{\text{load}}$ denotes the positive load branch represented by $mc^2(\gamma - 1)$.

This is the standard relativistic energy rule,

$$\Delta E = mc^2(\gamma - 1), \quad (144)$$

read as a local dispersive-load energy. Therefore,

$$\boxed{\gamma(x) = 1 + \frac{\Delta\mu_{\text{load}}(x)}{mc^2}.} \quad (145)$$

This writes the same γ through the local thermodynamic load.

The corresponding force is

$$\mathbf{F} = -\nabla[mc^2(\gamma - 1)]. \quad (146)$$

Therefore,

$$\mathbf{F} = -mc^2 \nabla \gamma. \quad (147)$$

Using the ideal-solution gradient gives

$$\mathbf{F} = -\nabla \Delta \mu_{\text{load}} = -\nabla \mu, \quad (148)$$

and therefore

$$\boxed{\mathbf{F} = -k_B T \nabla \ln n.} \quad (149)$$

This is the ordinary thermodynamic force obtained from the gradient of chemical potential. In the χ representation the same direction is

$$\mathbf{F} = -mc^2 \nabla \gamma = +mc^2 \frac{1}{\chi^2} \nabla \chi, \quad (150)$$

which agrees with the dissipative projection $+mc^2 \nabla \chi$ in the weak-load limit $\chi \approx 1$.

Introducing the mobility M , the drift velocity is the linear-response transport step associated with Onsager reciprocity [85] [86]:

$$\mathbf{v}_{\text{drift}} = M \mathbf{F}. \quad (151)$$

The flux is then

$$\mathbf{J} = n \mathbf{v}_{\text{drift}} = M n \mathbf{F}. \quad (152)$$

Substitution gives

$$\mathbf{J} = -M n k_B T \nabla \ln n. \quad (153)$$

Since

$$n \nabla \ln n = \nabla n, \quad (154)$$

one obtains Fick's law [132]

$$\boxed{\mathbf{J} = -D \nabla n,} \quad (155)$$

where the Einstein mobility-diffusion relation gives [133]

$$D = M k_B T. \quad (156)$$

Together with matter conservation,

$$\frac{\partial n}{\partial t} + \nabla \cdot \mathbf{J} = 0, \quad (157)$$

this gives

$$\frac{\partial n}{\partial t} = \nabla \cdot (D \nabla n). \quad (158)$$

For constant D ,

$$\boxed{\frac{\partial n}{\partial t} = D \nabla^2 n.} \quad (159)$$

This is the diffusion equation.

The result shows that diffusion is relativistic also at non-relativistic velocities. The Lorentzian structure remains present when $v \ll c$; its kinematic contribution is simply small. Ordinary mechanical energy is already the low-velocity projection of the Lorentz time-cost factor. For one kilogram moving at one meter per second, the relative clock-rate change is extremely small, but when multiplied by mc^2 it gives the ordinary kinetic energy,

$$mc^2(\gamma - 1) \approx \frac{1}{2}mv^2. \quad (160)$$

The same structure operates in diffusion. The dominant load is the local dispersive-information cost encoded in the chemical potential.

Thus the recovery of Fick's law and the diffusion equation gives an internal consistency proof of the identification already made in the theory:

$$\gamma_{\text{th}} = \gamma_I. \quad (161)$$

If this identification were artificial, it would not naturally return the standard diffusion law. Instead, the chain closes:

$$n(x) \text{ to } \nabla\mu = k_B T \nabla \ln n, \quad (162)$$

$$\Delta\mu_{\text{load}}(x) = mc^2[\gamma(x) - 1], \quad (163)$$

$$\mathbf{F} = -mc^2 \nabla \gamma, \quad (164)$$

$$\mathbf{J} = Mn\mathbf{F}, \quad (165)$$

$$\mathbf{J} = -D\nabla n, \quad (166)$$

$$\frac{\partial n}{\partial t} = D\nabla^2 n. \quad (167)$$

Diffusion follows when the already-identified equality $\gamma_{\text{th}} = \gamma_I$ is applied locally, with $mc^2(\gamma - 1)$ written as the local dispersive-load energy and the ideal chemical-potential gradient supplying $\nabla\mu = k_B T \nabla \ln n$. In this form, diffusion is the non-relativistic-velocity thermodynamic projection of the same Lorentz time-capacity structure.

4 Informational General Relativity

The gravitational case is developed next as the static radial sector of the information-flux reconstruction. In this sector the source is a stationary concentration of mass-information and the motion channel is set to zero. The standard Schwarzschild length is recovered here as the gravitational length associated with the same Compton mass-writing channel. [54] In the static gravitational sector,

$$v = 0, \quad (168)$$

so the motion channel is set to zero:

$$I_{\text{mot}} = 0. \quad (169)$$

The distinguished sector becomes

$$I_{\text{dist}} = I_m + I_r. \quad (170)$$

4.1 Schwarzschild-Compton Writing Length

Let M be the source mass. Its mass-information writing rate is

$$\dot{I}_M = \frac{Mc^2}{h} \quad (\text{bits/s}). \quad (171)$$

Equivalently, the source has the Compton angular writing rate

$$\omega_C = \frac{Mc^2}{\hbar}, \quad (172)$$

so that

$$M = \frac{\hbar\omega_C}{c^2}. \quad (173)$$

Coupling this invariant mass-writing rate to the gravitational conversion constant G defines the associated gravitational saturation length, in continuity with the Schwarzschild radius of a compact mass source [54].

$$r_s = \frac{2GM}{c^2} = \frac{2G\hbar\omega_C}{c^4}. \quad (174)$$

Thus r_s is the radial length at which the Compton mass-writing of the source saturates the static radial writing channel. The units are

$$[r_s] = \frac{(\text{m}^3 \text{kg}^{-1} \text{s}^{-2})(\text{kg})}{\text{m}^2 \text{s}^{-2}} = \text{m}. \quad (175)$$

The reduced Compton wavelength of the same source is the Compton length scale associated with the invariant mass-writing rate [19].

$$\bar{\lambda}_C = \frac{\hbar}{Mc}. \quad (176)$$

The Compton and Schwarzschild lengths obey

$$r_s \bar{\lambda}_C = \frac{2GM}{c^2} \frac{\hbar}{Mc} = 2 \frac{\hbar G}{c^3} = 2\ell_P^2. \quad (177)$$

At the Planck mass, $\bar{\lambda}_C = \ell_P$. The gravitational radius $r_g = GM/c^2$ is then $r_g = \ell_P$, while the Schwarzschild radius is $r_s = 2r_g = 2\ell_P$. Thus the Schwarzschild radius equals the reduced-Compton diameter [20]. This gives the gravitational load a direct information-channel meaning: it is the concentration of Compton mass-writing over the radial writing capacity available at r .

4.2 Radial Information Flux and the Exterior Gravitational Load

The radial dependence follows from the information-flux continuity principle, the spherical analogue of conserved inverse-square flux [83]. Outside the compact source there is no local production of distinguished information, so the radial information flux is conserved through every two-sphere enclosing the source:

$$\nabla \cdot \mathbf{J}_I = 0, \quad r > r_s. \quad (178)$$

For a static spherically symmetric source this gives

$$4\pi r^2 J_I^r(r) = \mathcal{F}_I = \text{constant}, \quad (179)$$

where \mathcal{F}_I is the total outward bookkeeping flux associated with the source mass-writing channel. Thus the local flux density falls as

$$J_I^r(r) = \frac{\mathcal{F}_I}{4\pi r^2}. \quad (180)$$

The dimensionless gravitational load is the radial saturation potential whose gradient measures this conserved spherical dilution of writing capacity. Its exterior vacuum form is the scalar potential limit of the Schwarzschild geometry [67]. In the exterior vacuum sector it therefore satisfies the Laplace equation for the source-free radial field [68].

$$\nabla^2 \Lambda_{I,g} = 0, \quad r > r_s, \quad (181)$$

or, explicitly,

$$\frac{1}{r^2} \frac{d}{dr} \left(r^2 \frac{d\Lambda_{I,g}}{dr} \right) = 0. \quad (182)$$

Integrating once gives

$$r^2 \frac{d\Lambda_{I,g}}{dr} = -A, \quad (183)$$

and integrating again gives

$$\Lambda_{I,g}(r) = \frac{A}{r} + B. \quad (184)$$

The exterior writing load vanishes at infinity,

$$\Lambda_{I,g}(\infty) = 0, \quad (185)$$

so $B = 0$. The saturation boundary is defined by the Schwarzschild-Compton writing length: at $r = r_s$ the temporal writing capacity closes, so the dimensionless load reaches unity,

$$\Lambda_{I,g}(r_s) = 1. \quad (186)$$

Therefore $A = r_s$, and the exterior load is fixed as

$$\boxed{\Lambda_{I,g}(r) = \frac{r_s}{r} = \frac{2G\hbar\omega_C}{c^4 r}}. \quad (187)$$

The factor $1/r$ is the integrated potential associated with a conserved $1/r^2$ spherical information flux. It is the unique static spherical exterior solution with vanishing load at infinity and saturation at r_s .

The load $\Lambda_{I,g}$ is dimensionless because r_s and r are both lengths:

$$[\Lambda_{I,g}] = \frac{\text{m}}{\text{m}} = 1. \quad (188)$$

4.3 Gravitational Clock-Rate Factor and Proper Time

The temporal writing factor in the gravitational field is introduced here as the standard gravitational proper-time clock factor [55] [56] [57] [58]

$$\chi_g(r) = \frac{d\tau}{dt}. \quad (189)$$

The closure law is

$$\chi_g^2 + \Lambda_{I,g} = 1. \quad (190)$$

Substitute the gravitational load:

$$\chi_g^2 + \frac{r_s}{r} = 1. \quad (191)$$

Then

$$\chi_g^2 = 1 - \frac{r_s}{r}, \quad (192)$$

and therefore

$$\boxed{\chi_g(r) = \sqrt{1 - \frac{r_s}{r}}.} \quad (193)$$

This is the radial gravitational projection of the same one-bit closure law. The elementary event carries one registered distinction; the radial load r_s/r and the surviving temporal availability χ_g^2 allocate the normalized capacity of that bit-event. Using

$$r_s = \frac{2GM}{c^2}, \quad (194)$$

this becomes

$$\boxed{\chi_g(r) = \sqrt{1 - \frac{2GM_{\text{obs}}}{rc^2}}.} \quad (195)$$

Since

$$\chi_g(r) = \frac{d\tau}{dt}, \quad (196)$$

the gravitational proper-time relation is

$$\boxed{d\tau = \sqrt{1 - \frac{r_s}{r}} dt} \quad (197)$$

or

$$\boxed{d\tau = \sqrt{1 - \frac{2GM_{\text{obs}}}{rc^2}} dt.} \quad (198)$$

The sectorial thermodynamic identification gives

$$\boxed{\eta_{\text{th}}^{(g)} = \chi_g(r) = \frac{d\tau}{dt}.} \quad (199)$$

Therefore

$$\boxed{\eta_{\text{th}}^{(g)} = \sqrt{1 - \frac{r_s}{r}} = \sqrt{1 - \frac{2GM_{\text{obs}}}{rc^2}}.} \quad (200)$$

Using $dI_{\text{disp}} = dS/(k_B \ln 2)$, this same local clock factor has the entropy-registration form

$$\boxed{(k_B \ln 2) \frac{dI_{\text{dist}}}{dS} = \sqrt{1 - \frac{r_s}{r}} = \sqrt{1 - \frac{2GM_{\text{obs}}}{rc^2}}.} \quad (201)$$

The inverse cost factor is

$$\gamma_{\text{th}}^{(g)} = \frac{1}{\eta_{\text{th}}^{(g)}} = \frac{dt}{d\tau} = \frac{1}{\sqrt{1 - \frac{r_s}{r}}}. \quad (202)$$

The Schwarzschild clock factor is recovered exactly as the thermodynamic registration efficiency of the static radial gravitational sector. The entropy expression is the thermodynamic reading of the same proper-time factor obtained from the Schwarzschild geometry.

At the Schwarzschild radius,

$$r = r_s, \quad (203)$$

the temporal factor becomes

$$\chi_g(r_s) = 0. \quad (204)$$

The temporal writing channel reaches closure at the Schwarzschild scale. At this boundary the radial load $\Lambda_{I,g} = 1$ saturates the one-bit registration capacity of the static radial sector. The realized branch has no remaining ordinary capacity for radial distinguishable-configuration writing at this boundary.

Since

$$\frac{1}{k_B \ln 2} \frac{dS}{dI_{\text{dist}}} = \frac{1}{\sqrt{1 - \frac{r_s}{r}}}, \quad (205)$$

the horizon limit gives

$$r \rightarrow r_s \quad \text{implies} \quad \eta_{\text{th}}^{(g)} \rightarrow 0, \quad \frac{dS}{dI_{\text{dist}}} \rightarrow \infty. \quad (206)$$

From the exterior realized-time description, ordinary temporal writing capacity vanishes at the Schwarzschild horizon, while the entropy cost of externally continuing distinguishable temporal registration diverges.

4.4 Radial Spatial Capacity and the Schwarzschild Metric

The temporal factor χ_g measures the surviving temporal writing fraction. In the present theory the metric is an informational object: it measures the bit-writing capacity and bit-registration cost of physical distinction. Each component of $g_{\mu\nu}^{(I)}$ gives the local cost density for writing distinguishable physical increments along the corresponding direction of the writing map.

The constant c fixes the conversion between temporal writing and spatial writing. It is the maximal propagation and update rate of distinguishable physical change, so the temporal component of the bit-capacity map is

$$g_{tt} = -c^2 \chi_g^2. \quad (207)$$

The radial component is fixed by conservation of the elementary bit-area in the local (t, r) writing plane. In the static, spherically symmetric sector, a mass concentration loads the radial direction singled out by the gradient of $\Lambda_{I,g}(r)$. The temporal channel and the radial continuation channel then form a two-channel registration cell for one completed physical event. The temporal capacity factor is

$$-\frac{g_{tt}}{c^2} = \chi_g^2, \quad (208)$$

and the radial registration cost is g_{rr} .

The normalization is fixed by the elementary distinction introduced at the foundation of the theory: one bit is the minimal invariant unit of registered physical distinction. A complete event in the local (t, r) writing plane must preserve this elementary registration unit. Therefore the product of temporal capacity and radial cost is the conserved bit-area of one elementary event,

$$\left(-\frac{g_{tt}}{c^2}\right) g_{rr} = 1. \quad (209)$$

This is the informational closure of the radial sector. When mass concentration reduces temporal writing capacity, radial continuation becomes more costly by the reciprocal factor, preserving the one-bit event-registration cell.

Substituting $g_{tt} = -c^2 \chi_g^2$ gives

$$g_{rr} = \chi_g^{-2}. \quad (210)$$

Thus the radial metric component is the reciprocal bit-registration cost required by conservation of the local one-bit writing budget in the radial sector. Together,

$$g_{tt} = -c^2 \chi_g^2, \quad g_{rr} = \chi_g^{-2}. \quad (211)$$

Because

$$\chi_g(r) = (k_B \ln 2) \frac{dI_{\text{dist}}}{dS}, \quad (212)$$

the same metric coefficients can be written directly in entropy-registration form:

$$\boxed{g_{tt} = -c^2 \left[(k_B \ln 2) \frac{dI_{\text{dist}}}{dS} \right]^2, \quad g_{rr} = \left[(k_B \ln 2) \frac{dI_{\text{dist}}}{dS} \right]^{-2}.} \quad (213)$$

The Schwarzschild substitution

$$(k_B \ln 2) \frac{dI_{\text{dist}}}{dS} = \sqrt{1 - \frac{r_s}{r}} \quad (214)$$

gives

$$g_{tt} = -c^2 \left(1 - \frac{r_s}{r}\right), \quad g_{rr} = \left(1 - \frac{r_s}{r}\right)^{-1}. \quad (215)$$

The Schwarzschild metric coefficients are therefore two geometric projections of the same entropy-registration ratio. The temporal component measures the surviving realized writing rate, while the radial component measures the reciprocal spatial/configuration cost required by the same informational closure.

The line element is

$$ds^2 = -c^2 \chi_g(r)^2 dt^2 + \chi_g(r)^{-2} dr^2 + r^2 d\Omega^2. \quad (216)$$

Here

$$d\Omega^2 = d\theta^2 + \sin^2 \theta d\phi^2 \quad (217)$$

is the angular line element on the two-sphere.

Substitute

$$\chi_g^2 = 1 - \frac{r_s}{r}. \quad (218)$$

Then

$$-c^2 \chi_g^2 dt^2 = -\left(1 - \frac{r_s}{r}\right) c^2 dt^2, \quad (219)$$

and

$$\chi_g^{-2} dr^2 = \left(1 - \frac{r_s}{r}\right)^{-1} dr^2. \quad (220)$$

Therefore,

$$\boxed{ds^2 = -\left(1 - \frac{r_s}{r}\right) c^2 dt^2 + \left(1 - \frac{r_s}{r}\right)^{-1} dr^2 + r^2 d\Omega^2.} \quad (221)$$

The units are consistent:

$$[c^2 dt^2] = \frac{\text{m}^2}{\text{s}^2} \text{s}^2 = \text{m}^2, \quad (222)$$

$$[dr^2] = \text{m}^2, \quad (223)$$

$$[r^2 d\Omega^2] = \text{m}^2, \quad (224)$$

because $d\Omega^2$ is dimensionless. Thus every term in ds^2 has units of length squared.

Let

$$\Omega_{\text{write}}(r) \quad (225)$$

denote distinguishable spatial writing capacity around the source. Define spatial distinguishability schematically as

$$I_x(r) = \log_2 \Omega_{\text{write}}(r). \quad (226)$$

Since the logarithm of a count of possible states is dimensionless,

$$[I_x] = \text{bits}. \quad (227)$$

As the temporal writing factor decreases,

$$\chi_g \text{ decreases}, \quad (228)$$

the radial spatial cost increases,

$$g_{rr} = \chi_g^{-2} \text{ increases}. \quad (229)$$

Radial curvature is the geometric expression of increased informational cost per distinguishable radial step.

At the horizon,

$$r \rightarrow r_s, \quad \Lambda_{I,g} \rightarrow 1, \quad \chi_g \rightarrow 0, \quad g_{rr} \rightarrow \infty. \quad (230)$$

The informational reading is that the radial load saturates the one-bit registration cell. The event horizon is the surface on which the normalized load reaches the full capacity of one elementary bit-event, leaving no surviving ordinary temporal-writing fraction in this effective spacetime description. The horizon is therefore the writing-capacity boundary of the realized radial geometry, consistent with gravitational-collapse horizons [59], black-hole thermodynamics [60], and horizon-temperature physics [61] and quantum fields in curved spacetime [62].

4.5 Horizon Writing Capacity, Dispersed Information, and Saturation

The preceding reconstruction identifies the Schwarzschild horizon as a writing-capacity boundary: the radius at which ordinary radial continuation in the effective spacetime description reaches saturation. This interpretation connects directly with the standard Bekenstein–Hawking entropy-area law, according to which the entropy of a stationary black hole is proportional to the area of its horizon, in direct contact with the black-hole entropy tradition of Bekenstein [63] and Hawking. [64]

The local registration law gives the clock-rate mechanism:

$$\boxed{\frac{d\tau}{dt} = \chi_g(r) = (k_B \ln 2) \frac{dI_{\text{dist}}}{dS} = \sqrt{1 - \frac{r_s}{r}}.} \quad (231)$$

This is the local radial writing-rate level. At the horizon,

$$\boxed{\chi_g(r_s) = \eta_{\text{th}}^{(g)}(r_s) = 0,} \quad (232)$$

so the Schwarzschild surface acts as a registration boundary in the exterior realized-time description. The Bekenstein–Hawking formula gives the total boundary capacity of that surface.

For a horizon area A , the Bekenstein–Hawking entropy is

$$S_{\text{BH}} = \frac{k_B A}{4\ell_P^2}, \quad \ell_P^2 = \frac{\hbar G}{c^3}. \quad (233)$$

Equivalently, the associated horizon information in bits is

$$I_{\text{BH}} = \frac{S_{\text{BH}}}{k_B \ln 2} = \frac{A}{4\ell_P^2 \ln 2}. \quad (234)$$

For a Schwarzschild black hole,

$$A = 4\pi r_s^2, \quad r_s = \frac{2GM}{c^2}. \quad (235)$$

Therefore,

$$S_{\text{BH}} = \frac{k_B \pi r_s^2}{\ell_P^2} = \frac{4\pi k_B G M^2}{\hbar c}, \quad (236)$$

and

$$I_{\text{BH}} = \frac{4\pi G M^2}{\hbar c \ln 2}. \quad (237)$$

In the language of the present paper, the horizon is the limiting surface on which distinguishable internal configurations are counted as boundary information. At the black-hole limit, maximal information capacity follows horizon-area scaling. This places the result within the holographic line of thought initiated by 't Hooft [40] and Susskind, [41] and reviewed by Bousso. [65]

The same conclusion is consistent with the Bekenstein entropy bound, [15]

$$S \leq \frac{2\pi k_B R E}{\hbar c}. \quad (238)$$

For a Schwarzschild black hole, $R = r_s$ and $E = M c^2$, giving

$$S \leq \frac{2\pi k_B r_s M c^2}{\hbar c} = \frac{4\pi k_B G M^2}{\hbar c} = S_{\text{BH}}. \quad (239)$$

Thus the Schwarzschild horizon saturates the entropy bound. In the present reconstruction, this saturation has a direct informational reading: once radial writing capacity reaches the horizon boundary, the maximal distinguishable content of the system is encoded by the boundary area.

The thermodynamic time law gives the local registration mechanism that drives the Schwarzschild horizon to become an entropy-bearing boundary. The Bekenstein–Hawking formula gives the total area capacity of that boundary.

The preceding subsection identified the Schwarzschild horizon as a writing-capacity boundary and connected that boundary to the Bekenstein–Hawking entropy-area law. The present subsection makes the informational limiting statement explicit.

The gravitational clock-rate factor is

$$\chi_g(r) = \frac{d\tau}{dt} = \sqrt{1 - \frac{r_s}{r}}. \quad (240)$$

The thermodynamic registration law gives the same factor as

$$\chi_g(r) = \eta_{\text{th}}^{(g)}(r) = \frac{dI_{\text{dist}}}{dI_{\text{disp}}} = (k_B \ln 2) \frac{dI_{\text{dist}}}{dS}. \quad (241)$$

At the Schwarzschild horizon,

$$r = r_s, \quad (242)$$

so

$$\chi_g(r_s) = 0. \quad (243)$$

Therefore,

$$\frac{dI_{\text{dist}}}{dI_{\text{disp}}} \rightarrow 0. \quad (244)$$

This is the central informational meaning of the horizon. In the exterior realized-time description, the ability to write further distinguishable temporal information vanishes at the horizon. The horizon is the surface at which the exterior channel for writing distinguishable information into realized time closes.

The total realized informational bookkeeping used throughout this paper is

$$I_{\text{tot}} = I_{\text{dist}} + I_{\text{disp}}. \quad (245)$$

At the horizon, the exterior distinguishable-writing channel reaches the limiting condition

$$I_{\text{dist}}^{\text{horizon}} \rightarrow 0 \quad (246)$$

as a continuing exterior temporal-registration channel. Therefore the remaining accessible information attributed to the horizon must be represented in the dispersed, entropy-bearing sector:

$$I_{\text{tot}}^{\text{horizon}} = I_{\text{disp}}^{\text{horizon}}. \quad (247)$$

Equivalently,

$$\boxed{\chi_g(r_s) = 0 \quad \text{implies} \quad I_{\text{dist}}^{\text{horizon}} \rightarrow 0 \quad \text{implies} \quad I_{\text{tot}}^{\text{horizon}} = I_{\text{disp}}^{\text{horizon}}.} \quad (248)$$

This is the dispersed-information reading of black-hole entropy. The horizon is the limiting surface where externally distinguishable temporal writing disappears, so the remaining accessible information is necessarily boundary entropy.

Using the entropy-bit relation,

$$I_{\text{disp}} = \frac{S}{k_B \ln 2}, \quad (249)$$

the horizon dispersed information is

$$I_{\text{disp}}^{\text{horizon}} = \frac{S_{\text{BH}}}{k_B \ln 2}. \quad (250)$$

With the Bekenstein–Hawking entropy,

$$S_{\text{BH}} = \frac{k_B A}{4\ell_P^2}, \quad (251)$$

one obtains

$$I_{\text{disp}}^{\text{horizon}} = \frac{1}{k_B \ln 2} \frac{k_B A}{4\ell_P^2}. \quad (252)$$

Thus,

$$\boxed{I_{\text{disp}}^{\text{horizon}} = \frac{A}{4\ell_P^2 \ln 2}.} \quad (253)$$

For a Schwarzschild black hole,

$$A = 4\pi r_s^2, \quad r_s = \frac{2GM}{c^2}. \quad (254)$$

Therefore,

$$I_{\text{disp}}^{\text{horizon}} = \frac{4\pi r_s^2}{4\ell_P^2 \ln 2} = \frac{\pi r_s^2}{\ell_P^2 \ln 2}. \quad (255)$$

Substituting

$$r_s = \frac{2GM}{c^2} \quad (256)$$

gives

$$I_{\text{disp}}^{\text{horizon}} = \frac{\pi}{\ell_P^2 \ln 2} \left(\frac{2GM}{c^2} \right)^2. \quad (257)$$

Using

$$\ell_P^2 = \frac{\hbar G}{c^3}, \quad (258)$$

one obtains

$$I_{\text{disp}}^{\text{horizon}} = \frac{4\pi G^2 M^2}{c^4} \frac{c^3}{\hbar G \ln 2}. \quad (259)$$

Hence,

$$\boxed{I_{\text{disp}}^{\text{horizon}} = \frac{4\pi G M^2}{\hbar c \ln 2}}. \quad (260)$$

This is the same bit count already obtained from the Bekenstein–Hawking area law, but now its role is explicit: it is the dispersed-information limit of gravitational time-writing collapse.

The corresponding entropy statement is

$$S_{\text{horizon}} = k_B \ln 2 I_{\text{disp}}^{\text{horizon}}. \quad (261)$$

Substituting the horizon bit count gives

$$S_{\text{horizon}} = k_B \ln 2 \frac{A}{4\ell_P^2 \ln 2} = \frac{k_B A}{4\ell_P^2} = S_{\text{BH}}. \quad (262)$$

Thus,

$$\boxed{S_{\text{horizon}} = S_{\text{BH}}} \quad (263)$$

because the horizon is the limit in which the exterior distinguishable-writing channel vanishes and all accessible boundary information is represented as dispersed information.

The same result can be written directly from the registration equation. Since

$$\chi_g = (k_B \ln 2) \frac{dI_{\text{dist}}}{dS}, \quad (264)$$

the horizon condition gives

$$0 = (k_B \ln 2) \frac{dI_{\text{dist}}}{dS} \quad (265)$$

at

$$r = r_s. \quad (266)$$

For finite boundary entropy,

$$dS_{\text{horizon}} \neq 0, \quad (267)$$

this requires

$$dI_{\text{dist}}^{\text{exterior}} \text{ to } 0. \quad (268)$$

The entropy remains finite because the horizon does not contain zero information. It contains information no longer available as ordinary exterior distinguishable time-writing. That information is counted as boundary entropy:

$$dI_{\text{horizon}} = dI_{\text{disp}}^{\text{horizon}} = \frac{dS_{\text{BH}}}{k_B \ln 2}. \quad (269)$$

This also clarifies why the entropy scales with area. Once

$$\chi_g(r_s) = 0, \quad (270)$$

the exterior radial continuation of ordinary distinguishable configuration-writing closes. The remaining information is encoded on the saturation boundary. Therefore the accessible information is counted by the horizon area,

$$A = 4\pi r_s^2, \quad (271)$$

not by an interior spatial volume.

The final horizon limit can therefore be summarized as

$$\boxed{\chi_g \text{ to } 0 \quad \text{implies} \quad dI_{\text{dist}}^{\text{exterior}} \text{ to } 0 \quad \text{implies} \quad dI_{\text{horizon}} = dI_{\text{disp}}^{\text{horizon}} \quad \text{implies} \quad S_{\text{horizon}} = S_{\text{BH}}.} \quad (272)$$

In words, black-hole entropy is the dispersed-information limit of gravitational time-writing collapse. The event horizon is the surface where externally distinguishable temporal registration vanishes, and the remaining accessible information becomes boundary entropy.

This interpretation supplies the registration mechanism behind the Bekenstein–Hawking area law. The Bekenstein–Hawking formula gives the total boundary capacity. The UiT time law explains why that capacity is thermodynamic: at the horizon, the distinguishable writing channel closes, so the information accessible to the exterior description is necessarily dispersed horizon information.

At the Schwarzschild radius,

$$r = r_s, \quad \chi(r_s) = 0.$$

The local realized temporal fraction vanishes there. In the present framework this means that the realized sector has exhausted its available capacity for further distinct temporal writing and radial configurational continuation.

This gives the physical interpretation of the horizon. The horizon is the saturation boundary of realized informational capacity in the effective spacetime description.

Since spatial geometry is the realized projection of configurational distinguishability, the vanishing of χ means that ordinary radial configuration-writing has reached its limit. The same realized-space description cannot be continued inward as if ordinary configuration capacity still remained available.

In this sense, the classical singularity is displaced by the saturation of realized writing capacity at the horizon. The effective configurational description reaches closure at the saturation surface. Once $\chi = 0$, the realized sector has exhausted its bandwidth for ordinary continuation of the same geometric narrative.

Phase-Time Extension.

The horizon saturation derived here belongs to the realized metric branch. The phase-time extension of this horizon saturation, including the reverse projection and the white-hole reading, is developed later after the complex phase-time field has been introduced.

4.6 Special and General Relativity as One Capacity Geometry

The preceding reconstruction shows that special and general relativity are two projections of the same writing-capacity geometry. The kinematic projection follows the Lorentz-Minkowski structure [16] [17], while the static radial projection follows the Schwarzschild sector of general relativity [54]. In special relativity, the active constrained direction is the direction of motion, \hat{v} . In the static gravitational sector, the active constrained direction is radial, \hat{r} . The mathematical role of the capacity factor is the same in both cases.

In UiT, space is the available capacity to register distinguishable configurations. In special relativity, motion consumes this capacity along the direction of motion, producing Lorentz contraction. In gravitation, mass consumes this capacity radially around the source, producing the Schwarzschild radial structure. These are the same informational effect expressed along different axes.

For inertial motion,

$$\chi_v = \sqrt{1 - \frac{v^2}{c^2}}, \quad (273)$$

and the normalized configuration capacity available for writing distinguishable longitudinal structure is

$$\mathcal{C}_{\parallel}(v) = \frac{\log_2 \Omega_{\parallel, \text{write}}(v)}{\log_2 \Omega_{\parallel, \text{write}}(0)} = \chi_v. \quad (274)$$

The observed length contraction is the geometric reading of this reduced longitudinal writing capacity:

$$L_{\parallel} = \chi_v L_0. \quad (275)$$

For the static gravitational sector,

$$\chi_g(r) = \sqrt{1 - \frac{r_s}{r}} = \sqrt{1 - \frac{2GM_{\text{obs}}}{rc^2}}. \quad (276)$$

Define the corresponding normalized radial configuration capacity by

$$\mathcal{C}_r(r) = \frac{\log_2 \Omega_{r, \text{write}}(r)}{\log_2 \Omega_{r, \text{write}}(\infty)}. \quad (277)$$

Then the radial gravitational sector has the same capacity form,

$$\mathcal{C}_r(r) = \chi_g(r). \quad (278)$$

Thus the two reductions differ by the direction singled out by the physical load:

$$\boxed{\mathcal{C}_{\parallel}(v) = \chi_v \quad \text{along } \hat{v}, \quad \mathcal{C}_r(r) = \chi_g(r) \quad \text{along } \hat{r}.} \quad (279)$$

The standard relativistic classification is preserved inside this capacity reading. The special-relativistic sector is flat Minkowski spacetime with a directional kinematic capacity reduction along \hat{v} . The gravitational sector is curved spacetime with a radial source-centered capacity reduction along \hat{r} . The common UiT content is the writing-capacity law: motion and gravitation select different axes for the same loss of available configuration states.

The common law is

$$\chi^2 + \Lambda_I = 1.$$

Therefore

$$\boxed{\chi = \sqrt{1 - \Lambda_I}.} \quad (280)$$

The sectorial thermodynamic identification is

$$\boxed{\eta_{\text{th}}^{(\text{sector})} = \chi_{\text{sector}} = \frac{d\tau}{dt}, \quad \gamma_{\text{th}}^{(\text{sector})} = \frac{1}{\eta_{\text{th}}^{(\text{sector})}} = \frac{dt}{d\tau}.} \quad (281)$$

Thus the unified entropy-registration law is

$$\boxed{\eta_{\text{th}} = \chi = \sqrt{1 - \Lambda_I},} \quad (282)$$

or equivalently

$$\boxed{(k_B \ln 2) \frac{dI_{\text{dist}}}{dS} = \sqrt{1 - \Lambda_I}.} \quad (283)$$

The inverse cost factor is

$$\boxed{\gamma_{\text{th}} = \frac{1}{\eta_{\text{th}}} = \frac{1}{\sqrt{1 - \Lambda_I}} = \frac{1}{k_B \ln 2} \frac{dS}{dI_{\text{dist}}}.} \quad (284)$$

In the special-relativistic projection, the load is directional,

$$\Lambda_{I,v} = \frac{v^2}{c^2}.$$

In the Schwarzschild projection, the load is radial,

$$\Lambda_{I,g} = \frac{r_s}{r}.$$

For the special-relativistic load,

$$\Lambda_I = \Lambda_{I,v} = \frac{v^2}{c^2}, \quad (285)$$

so

$$\boxed{\gamma_{\text{th}}^{(v)} = \frac{1}{\sqrt{1 - \frac{v^2}{c^2}}} = \gamma_I.} \quad (286)$$

For the Schwarzschild load,

$$\Lambda_I = \Lambda_{I,g} = \frac{r_s}{r}, \quad (287)$$

so

$$\boxed{\gamma_{\text{th}}^{(g)} = \frac{1}{\sqrt{1 - \frac{r_s}{r}}}.} \quad (288)$$

Special relativity and the static Schwarzschild sector of general relativity are recovered as two load choices of the same thermodynamic registration law. The same entropy-registration ratio becomes the Lorentz clock factor in the kinematic projection and the Schwarzschild clock factor in the radial gravitational projection.

Thus Lorentz contraction and Schwarzschild radial curvature express the same loss of distinguishable configuration-writing capacity along different axes.

The temporal part remains the Einsteinian time-dilation structure: clocks run according to the surviving temporal-writing fraction χ . The spatial part receives an informational reading: spatial geometry measures the available configuration capacity for writing distinguishable physical states. In motion, reduced writing capacity gives longitudinal contraction along \hat{v} . In gravity, reduced writing capacity is organized radially around the mass source and appears as radial spatial cost and curvature. The reciprocal metric coefficient is then the cost representation of the same reduction. In the radial gravitational sector,

$$\mathcal{C}_r(r) = \chi_g(r), \quad \boxed{g_{rr} = \mathcal{C}_r(r)^{-2} = \chi_g(r)^{-2}}. \quad (289)$$

In the longitudinal inertial sector,

$$\mathcal{C}_{\parallel}(v) = \chi_v, \quad \boxed{L_{\parallel} = \mathcal{C}_{\parallel}(v)L_0 = \chi_v L_0}. \quad (290)$$

This is the bridge between the scalar relativistic reconstruction and the metric construction that follows: SR is the directional, kinematic capacity reduction along the velocity axis; GR is the radial, source-generated capacity reduction around mass. Both express the same loss of available configuration states for writing distinguishable information.

4.7 Free Fall and the Equivalence Principle: Temporal and Radial Spatial Matching

The preceding subsections have built the two relativistic capacity factors separately from the standard Lorentz and Schwarzschild structures. In the kinematic sector, motion selects the direction of motion and gives

$$\chi_v = \sqrt{1 - \frac{v^2}{c^2}}, \quad \gamma_v = \frac{1}{\chi_v}.$$

In the static Schwarzschild sector, mass selects the radial direction and gives

$$\chi_g(r) = \sqrt{1 - \frac{r_s}{r}}, \quad \sqrt{g_{rr}(r)} = \frac{1}{\sqrt{1 - r_s/r}}.$$

The equivalence principle can now be read directly in the clean radial case of a body falling from rest at infinity, in continuity with the standard theoretical and experimental literature on equivalence-principle tests [73] [74] [75]. At every radius r along this trajectory, the locally measured velocity satisfies

$$\frac{v(r)^2}{c^2} = \frac{2GM_{\text{obs}}}{rc^2} = \frac{r_s}{r}, \quad r_s = \frac{2GM}{c^2}.$$

In UiT language this is the equality of the inertial and gravitational load projections,

$$\Lambda_{I,v} = \frac{v(r)^2}{c^2}, \quad \Lambda_{I,g} = \frac{r_s}{r}, \quad \Lambda_{I,v} = \Lambda_{I,g}.$$

Both are projections of the same scalar capacity closure,

$$\chi^2 + \Lambda_I = 1.$$

The gravitational and inertial sectors therefore share the same available clock-rate factor once the free-fall condition is imposed.

Temporal matching. The Lorentz clock-rate factor of the falling body is

$$\chi_v(r) = \sqrt{1 - \frac{v(r)^2}{c^2}}.$$

Using the free-fall relation,

$$\frac{v(r)^2}{c^2} = \frac{r_s}{r},$$

one obtains

$$\chi_v(r) = \sqrt{1 - \frac{r_s}{r}}.$$

But the Schwarzschild gravitational clock-rate factor at the same radius is

$$\chi_g(r) = \sqrt{1 - \frac{r_s}{r}} = \sqrt{1 - \frac{2GM_{\text{obs}}}{rc^2}}.$$

Therefore, along the entire radial free-fall trajectory,

$$\chi_v(r) = \chi_g(r),$$

or explicitly,

$$\sqrt{1 - \frac{v(r)^2}{c^2}} = \sqrt{1 - \frac{2GM_{\text{obs}}}{rc^2}}.$$

The falling body acquires exactly the velocity whose Lorentz clock factor matches the gravitational clock factor of the radius it has reached. Free fall is therefore the dynamical process by which the body remains time-matched to the local gravitational field.

Radial spatial matching. The same free-fall relation also matches the longitudinal spatial factor of special relativity to the radial spatial factor of Schwarzschild geometry. In special relativity, the longitudinal length contraction is

$$L_{\parallel} = \chi_v L_0,$$

so the reciprocal spatial cost factor in the direction of motion is

$$\gamma_v(r) = \frac{1}{\chi_v(r)} = \frac{1}{\sqrt{1 - v(r)^2/c^2}}.$$

In the Schwarzschild radial sector, the physical radial distance element is

$$d\ell_r = \frac{dr}{\sqrt{1 - r_s/r}},$$

so

$$\sqrt{g_{rr}(r)} = \frac{1}{\sqrt{1 - r_s/r}}.$$

Using again

$$\frac{v(r)^2}{c^2} = \frac{r_s}{r},$$

one obtains

$$\gamma_v(r) = \sqrt{g_{rr}(r)},$$

or explicitly,

$$\frac{1}{\sqrt{1 - v(r)^2/c^2}} = \frac{1}{\sqrt{1 - r_s/r}}.$$

Thus the motion-generated longitudinal spatial cost factor reproduces the radial spatial cost factor of the gravitational field.

Together, the temporal and radial spatial equalities give

$$\chi_v(r) = \chi_g(r), \quad \gamma_v(r) = \sqrt{g_{rr}(r)}.$$

This is the radial Schwarzschild-sector proof of the equivalence principle in the present reconstruction: in free fall from rest at infinity, the Lorentz temporal and longitudinal spatial factors acquired by motion exactly reproduce the Schwarzschild temporal and radial spatial factors of the gravitational field.

Equivalently, free fall is the dynamical process by which the Lorentz factors of motion become identical to the local Schwarzschild factors of the gravitational field. The body converts the gravitational time and radial-space structure of the field into the temporal and longitudinal spatial factors of its own motion. This is why the freely falling frame is locally inertial: locally, the kinematic factors generated by motion and the geometric factors generated by the gravitational field are the same factors.

4.8 The Meaning of the Gravitational Constant G

The equivalence relation derived above gives the local free-fall matching between Newtonian escape-speed structure and Schwarzschild clock-rate structure [83] [54].

$$\frac{v(r)^2}{c^2} = \frac{r_s}{r} = \frac{2GM_{\text{obs}}}{rc^2}.$$

Thus the gravitational constant appears as the scale that connects source mass, radial distance, and the free-fall velocity required to match the local Schwarzschild factors. Solving for G gives

$$G = \frac{rv(r)^2}{2M}.$$

This expression should not be read as a new definition of G ; it is the standard gravitational constant read inside the equivalence-principle matching structure tested in modern relativity experiments [74]. It is a physical reading of the same constant inside the free-fall equivalence relation. The constant G fixes how strongly a mass M sets the radial load

$$\Lambda_{I,g} = \frac{r_s}{r} = \frac{2GM_{\text{obs}}}{rc^2},$$

and therefore how much velocity a freely falling body must acquire in order for its Lorentz factors to match the local Schwarzschild factors.

In this sense, G sets the scale of gravitational time-depth and radial spatial cost produced by mass. The free-fall condition then converts that gravitational load into the kinematic load

$$\Lambda_{I,v} = \frac{v(r)^2}{c^2}.$$

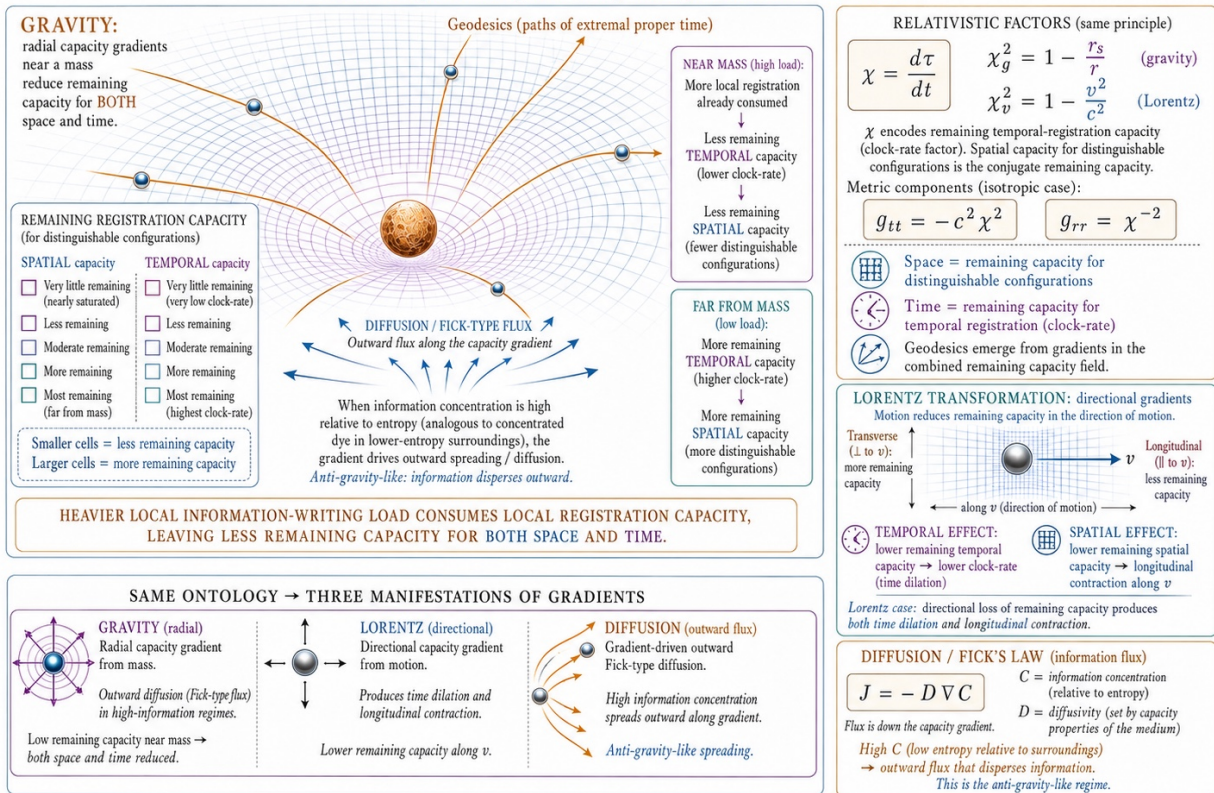
The equality

$$\Lambda_{I,v} = \Lambda_{I,g}$$

shows that G fixes the conversion scale between the gravitational field's radial load and the motion required for local equivalence. The temporal and radial spatial matching derived above are the geometric expression of this conversion.

GEODESICS AS GRADIENTS IN INFORMATION-REGISTRATION CAPACITY

→ *UIT reinterpretation of Einstein geometry and Lorentz contraction* ←



SAME RELATIVISTIC FACTORS • SAME GEODESICS • SAME DIFFUSION LAW – ONE INFORMATIONAL ONTOLOGY

4.9 The Empty-Time Limit and the Physical Closure of Registration

The preceding sections developed the informational structure of spacetime in terms of three sectors,

$$I_{\text{pot}}, \quad I_{\text{dist}}, \quad I_{\text{disp}}, \quad (291)$$

together with the local realized clock-rate factor

$$\chi = \frac{dt_{\text{phys}}}{dt_{\text{coord}}}. \quad (292)$$

Within this structure, space is associated with available distinguishability capacity, while physical time is associated with the realized registration of distinguishable information. The purpose of the present section is to state the corresponding logical closure in its sharpest form.

The question is whether a physically meaningful interval of time can exist when no distinguishable information changes.

The operational content of the question is simple. If all informational change is halted, no observer inside the system can experience the passage of time, since experience itself requires changing informational states. No memory of an interval can be formed, since memory is a physical record, and record formation carries the thermodynamic writing logic of physical information [27]. No before-and-after relation can be established, since such a relation requires distinguishable records. Thus one second, one year, and one million years become physically indistinguishable within the frozen-information limit.

A defender of independent time may still introduce an external coordinate parameter. Reversible-computation arguments clarify why a formal parameter can be separated from irreversible record creation [28]. This preserves a formal label and leaves the physical issue open. It divides the word “time” into two different notions: a physical time associated with clocks, records, entropy, phase evolution, and distinguishable change; and an empty coordinate label that advances without any physical distinction. The latter is a mathematical or metaphysical extension external to operational physical time. The empty-time limit therefore forces the conclusion that physical time obtains its content from informational change, in the same record-based sense emphasized by decoherence and arrow-of-time analyses [25] [45].

Consider an interval between two coordinate labels t_1 and t_2 , with

$$\Delta t_{\text{coord}} = t_2 - t_1 > 0. \quad (293)$$

Suppose that throughout this interval no distinguishable physical information is registered:

$$\Delta I_{\text{dist}} = 0. \quad (294)$$

Since I_{dist} is the sector of realized, physically distinguishable information, this condition means that no physical distinction changes. No record is written, no state becomes distinguishable from another, no clock process registers a tick, and no physical configuration acquires a new distinguishable relation.

The realized temporal interval is defined through the local clock-rate factor,

$$dt_{\text{phys}} = \chi dt_{\text{coord}}. \quad (295)$$

The clock-rate factor is the sectoral realization of the informational registration ratio,

$$\chi_{\text{sector}} = \eta_{\text{th}}^{(\text{sector})} = \frac{dI_{\text{dist}}}{dI_{\text{disp}}}, \quad (296)$$

For the local channel under discussion, χ_{sector} is written simply as χ , with

$$dI_{\text{disp}} = \frac{dS}{k_B \ln 2}. \quad (297)$$

Equivalently, the dimensionless temporal-registration ratio is

$$dt^* = \frac{dI_{\text{dist}}}{dI_{\text{disp}}} = \frac{k_B \ln 2 dI_{\text{dist}}}{dS}. \quad (298)$$

Therefore, in the empty-time limit,

$$dI_{\text{dist}} = 0, \quad (299)$$

one obtains

$$dt^* = 0, \quad (300)$$

and hence

$$\chi = 0. \quad (301)$$

Substitution into the physical-time relation gives

$$dt_{\text{phys}} = \chi dt_{\text{coord}} = 0 \cdot dt_{\text{coord}} = 0. \quad (302)$$

Thus,

$$\boxed{dI_{\text{dist}} = 0 \quad \text{implies} \quad dt_{\text{phys}} = 0.} \quad (303)$$

This is the empty-time closure.

It states that coordinate advancement without distinguishable registration carries no realized temporal content. The parameter t_{coord} remains a label; the physical interval vanishes.

In finite form,

$$\Delta I_{\text{dist}} = 0 \quad \text{implies} \quad \Delta t^* = 0, \quad (304)$$

$$\Delta t_{\text{phys}} = \int_{t_1}^{t_2} \chi dt_{\text{coord}} = 0. \quad (305)$$

Therefore two coordinate labels separated by $\Delta t_{\text{coord}} > 0$ but carrying no change in I_{dist} correspond to the same realized physical state:

$$I_{\text{dist}}(t_2) = I_{\text{dist}}(t_1), \quad I_{\text{disp}}(t_2) = I_{\text{disp}}(t_1), \quad \chi(t) = 0, \quad (306)$$

and so

$$\Delta t_{\text{phys}} = 0. \quad (307)$$

The apparent interval is therefore a coordinate redundancy: it labels an interval that no physical process can experience, record, measure, or distinguish.

This gives the logical core of the argument:

$$\boxed{\Delta t_{\text{phys}} > 0 \quad \text{implies} \quad \Delta I_{\text{dist}} > 0.} \quad (308)$$

and equivalently,

$$\boxed{\Delta I_{\text{dist}} = 0 \quad \text{implies} \quad \Delta t_{\text{phys}} = 0.} \quad (309)$$

The result is not an additional postulate. It follows from the previously defined identification of physical time with realized registration.

The contrast with spatial extension is immediate in the existing notation. A spatial region may be empty of realized events while still carrying potential distinguishability capacity:

$$I_{\text{pot}}^{\text{space}} > 0. \quad (310)$$

A point or region of space can therefore remain physically meaningful as available registration capacity, even before a particular event is realized there.

Time has a different operational role in the theory. Physical time is the realized progression of registration. Hence, in the absence of realized distinction,

$$\Delta I_{\text{dist}} = 0, \quad (311)$$

there is no corresponding realized temporal interval.

This gives the compact informational distinction:

$$\boxed{\text{space: } I_{\text{pot}}} \quad (312)$$

$$\boxed{\text{time: } dI_{\text{dist}}} \quad (313)$$

or, in the language already developed earlier,

$$\boxed{\text{spatial extension corresponds to capacity for distinguishability,}} \quad (314)$$

$$\boxed{\text{physical time corresponds to realized distinguishability.}} \quad (315)$$

The empty-time limit also clarifies the relativistic meaning of χ . In ordinary relativistic language, physical clock time is proper time along a physical process. In the present notation,

$$d\tau = \chi dt. \quad (316)$$

For the Schwarzschild case developed earlier,

$$\chi_g(r) = \sqrt{1 - \frac{r_s}{r}}. \quad (317)$$

At the horizon,

$$r = r_s, \quad (318)$$

so

$$\chi_g(r_s) = 0. \quad (319)$$

Therefore,

$$d\tau = 0. \quad (320)$$

In the informational interpretation, the horizon is the limiting surface at which external temporal registration capacity vanishes. This is the physical interpretation of what the relativistic metric is measuring: the collapse of realized clock-rate capacity in a particular registration channel.

The same structure appears in the general empty-time argument. Whenever the realized registration factor vanishes,

$$\chi = 0, \quad (321)$$

the physical temporal interval vanishes:

$$dt_{\text{phys}} = 0. \quad (322)$$

Thus the “flow of empty time” is not a physical degree of freedom. It is the continuation of a coordinate label after the registration content has disappeared.

The final closure can be written as:

$$\boxed{dt_{\text{phys}} = \chi dt_{\text{coord}}, \quad \chi_{\text{sector}} = \eta_{\text{th}}^{(\text{sector})} = \frac{dI_{\text{dist}}}{dI_{\text{disp}}}, \quad dI_{\text{disp}} = \frac{dS}{k_B \ln 2}} \quad (323)$$

so that

$$\boxed{dI_{\text{dist}} = 0 \quad \text{implies} \quad \chi = 0 \quad \text{implies} \quad dt_{\text{phys}} = 0.} \quad (324)$$

This is the physical closure of the empty-time paradox.

A coordinate interval without distinguishable registration can be written mathematically. A physical temporal interval is realized only through the writing of distinguishable information.

5 Metric and Tensor Completion and the Informational Graviton

This section lifts the scalar clock-rate factor into the tensorial metric structure. It then develops the informational field equation, the shared time-factor reading of equivalence, angular information flux, and capacity-update quanta.

5.1 Tensor Completion of the Informational Metric

The preceding construction was written in the static radial sector, where the informational writing factor reduces to the scalar field $\chi_g(r)$. This scalar presentation is the radial projection of a tensorial structure. The tensorial form follows from two principles already introduced: invariance

of distinguished information and local continuity of information flux, expressed with the standard geometric machinery of tetrads and metric fields [66] [67] [68].

The number of distinguished bits written into realized physical structure is a scalar quantity. It expresses physical registration itself and therefore has the same value in every coordinate description. Let the dimensionless informational writing interval be defined by

$$dI_{\text{dist}}^2 = \eta_{ab}^{(I)} dI^a dI^b, \quad \eta_{ab}^{(I)} = \text{diag}(-1, 1, 1, 1), \quad (325)$$

where dI^a are the elementary writing-channel increments, including temporal and spatial registration. A coordinate transformation may relabel the increments, while the total distinguished writing interval remains fixed.

Mass-information modifies this invariant writing space by changing the local registration cost. A concentration of mass-information I_m loads the temporal channel and also changes the spatial writing capacity available to neighboring increments. In general this cost is direction-dependent. The local writing capacity Ω_{write} therefore becomes anisotropic, so temporal, radial, angular, and dynamical increments can carry different registration costs.

Maintaining the scalar invariance of dI_{dist} under this direction-dependent writing cost requires a local transformation from the flat writing basis to a curved writing basis. This transformation is represented by informational writing tetrads $e^a{}_\mu$. Each tetrad component represents the locally available writing power along the corresponding physical direction. The natural covariant object is therefore an effective informational metric,

$$ds^2 = g_{\mu\nu}^{(I)}(x) dx^\mu dx^\nu, \quad (326)$$

where $g_{\mu\nu}^{(I)}$ is the capacity map of spacetime writing. The informational interval dI_{dist} is the normalized writing interval measured in elementary distinctions, while ds^2 is its physical geometric representation after the writing tetrads convert coordinate increments into cost-weighted spacetime intervals. Thus the metric coefficients act as bit-capacity conversion factors, while the line element retains the ordinary physical units of spacetime geometry.

The physical metric is obtained from the writing tetrads by

$$g_{\mu\nu}^{(I)} = \eta_{ab}^{(\text{phys})} e^a{}_\mu e^b{}_\nu, \quad (327)$$

with

$$\eta_{ab}^{(\text{phys})} = \text{diag}(-c^2, 1, 1, 1). \quad (328)$$

The static radial sector derived above is recovered by choosing

$$e^0{}_t = \chi_g, \quad e^1{}_r = \chi_g^{-1}, \quad e^2{}_\theta = r, \quad e^3{}_\phi = r \sin \theta. \quad (329)$$

These writing tetrads give

$$g_{tt}^{(I)} = -c^2 \chi_g^2, \quad g_{rr}^{(I)} = \chi_g^{-2}, \quad (330)$$

together with the ordinary angular sector $r^2 d\Omega^2$. Thus the radial result is the diagonal static projection of the informational metric. The scalar χ_g is the temporal writing component of a covariant writing structure, and the reciprocal radial component is the corresponding radial writing cost required by static flux continuity.

5.2 Ricci Scalar and the Variational Field Equation

The next step is fixed by information-flux continuity. The noncovariant continuity law,

$$\frac{\partial \rho_I}{\partial t} + \nabla \cdot \mathbf{J}_I = 0, \quad (331)$$

becomes, in covariant form for the local source sector,

$$\nabla_\mu T_{(I)}^{\mu\nu} = 0. \quad (332)$$

When the homogeneous temporal-writing term is dynamical, the conserved object is the total source defined below. The field equation must therefore equate the informational source, including any homogeneous vacuum-writing component, to a conserved tensor built from the capacity map $g_{\mu\nu}^{(I)}$.

This can be obtained variationally from the invariant four-volume element of the writing map. The invariant four-volume element of the writing map is

$$d\Omega_I = d^4x \sqrt{-g^{(I)}}. \quad (333)$$

The lowest-order local scalar that measures nonuniformity of this capacity map is the Ricci scalar $R[g^{(I)}]$. This is the minimal covariant choice: it is local, scalar, second-order in the metric through curvature, and leads to second-order field equations with a covariantly conserved variational response. Higher-curvature scalars such as R^2 or $R_{\mu\nu}R^{\mu\nu}$ represent higher-order response terms beyond the minimal reconstruction. Hence the minimal curvature action for the informational capacity field is

$$\mathcal{A}_{\text{cap}} = \frac{c^3}{16\pi G} \int d^4x \sqrt{-g^{(I)}} \left(R[g^{(I)}] - 2\Lambda_\tau \right). \quad (334)$$

Here Λ_τ denotes the homogeneous temporal-writing contribution to the capacity action. The notation distinguishes it from the local dimensionless load Λ_I used in the scalar closure law. The measure is written in the same convention used throughout the paper, with $x^0 = t$ and g_{tt} carrying the required factor of c^2 ; equivalently one may pass to $x^0 = ct$, where the standard Einstein-Hilbert normalization is recovered.

The informational source action is denoted by $\mathcal{A}_{\text{src}}^{(I)}$. In the $x^0 = t$ convention used here, the metric variation defines the informational stress-energy tensor by

$$T_{\mu\nu}^{(I)} = - \frac{2c}{\sqrt{-g^{(I)}}} \frac{\delta \mathcal{A}_{\text{src}}^{(I)}}{\delta g_{(I)}^{\mu\nu}}. \quad (335)$$

Equivalently, if the invariant measure is written with $x^0 = ct$, the factor of c is absorbed into the four-volume element and the standard definition is recovered. This convention keeps the final coupling in the usual form $8\pi G/c^4$. Stationarity of the total informational action,

$$\delta \left(\mathcal{A}_{\text{cap}} + \mathcal{A}_{\text{src}}^{(I)} \right) = 0, \quad (336)$$

gives

$$\delta \mathcal{A}_{\text{cap}} = \frac{c^3}{16\pi G} \int d^4x \sqrt{-g^{(I)}} \left(G_{\mu\nu}[g^{(I)}] + \Lambda_\tau g_{\mu\nu}^{(I)} \right) \delta g_{(I)}^{\mu\nu}, \quad (337)$$

and

$$\delta \mathcal{A}_{\text{src}}^{(I)} = -\frac{1}{2c} \int d^4x \sqrt{-g^{(I)}} T_{\mu\nu}^{(I)} \delta g_{(I)}^{\mu\nu}. \quad (338)$$

Because the variation $\delta g_{(I)}^{\mu\nu}$ is arbitrary, the equilibrium equation is

$$\boxed{G_{\mu\nu}[g^{(I)}] + \Lambda_\tau g_{\mu\nu}^{(I)} = \frac{8\pi G}{c^4} T_{\mu\nu}^{(I)}}. \quad (339)$$

For a constant homogeneous term this equation is compatible with the separate covariant conservation of $T_{\mu\nu}^{(I)}$. If the temporal-writing background is allowed to vary, the Bianchi identity requires conservation of the total information source, matter plus vacuum-writing contribution:

$$\boxed{\nabla^\mu \left(T_{\mu\nu}^{(I)} - \frac{c^4}{8\pi G} \Lambda_\tau g_{\mu\nu}^{(I)} \right) = 0}. \quad (340)$$

Equivalently,

$$\nabla^\mu T_{\mu\nu}^{(I)} = \frac{c^4}{8\pi G} \partial_\nu \Lambda_\tau. \quad (341)$$

Thus a time-dependent Λ_τ is not added as an independent violation of conservation; it represents exchange between the ordinary informational source and the homogeneous temporal-writing sector.

In this derivation, the Einstein tensor is the variational response of the minimal scalar action for the writing-capacity map. Lovelock's theorem supplies the uniqueness statement [69]: in four dimensions, for a symmetric rank-two tensor built locally from the metric and its first two derivatives, with second-order field equations and covariant conservation, the Einstein tensor plus a cosmological term is the unique completion, matching Einstein's field-equation structure [70].

The curvature tensors are constructed from $g_{\mu\nu}^{(I)}$ in the usual covariant way [71], as in standard treatments by Misner, Thorne, and Wheeler [67] and Wald. [68] The connection is

$$\Gamma^\rho{}_{\mu\nu} = \frac{1}{2} g^{\rho\sigma} (\partial_\mu g_{\nu\sigma} + \partial_\nu g_{\mu\sigma} - \partial_\sigma g_{\mu\nu}), \quad (342)$$

and the curvature is

$$R^\rho{}_{\sigma\mu\nu} = \partial_\mu \Gamma^\rho{}_{\nu\sigma} - \partial_\nu \Gamma^\rho{}_{\mu\sigma} + \Gamma^\rho{}_{\mu\lambda} \Gamma^\lambda{}_{\nu\sigma} - \Gamma^\rho{}_{\nu\lambda} \Gamma^\lambda{}_{\mu\sigma}. \quad (343)$$

The Einstein tensor built from the informational metric is

$$G_{\mu\nu}[g^{(I)}] = R_{\mu\nu} - \frac{1}{2} R g_{\mu\nu}^{(I)}. \quad (344)$$

It measures covariant nonuniformity in writing capacity.

5.3 Informational Stress-Energy Tensor

The corresponding source tensor is the covariant compilation of the writing channels defined above, written in the standard role played by stress-energy as the source of spacetime geometry [70]. In a local proper volume dV_0 , define the mass-writing-rate density, temporal-registration density, and dispersive-information density by

$$\mathcal{R}_m = \frac{dI_m}{d\tau dV_0}, \quad \mathcal{N}_\tau = \frac{dI_\tau}{dV_0}, \quad \mathcal{N}_{\text{disp}} = \frac{dI_{\text{disp}}}{dV_0}. \quad (345)$$

The volume element dV_0 is the local proper coarse-graining volume. It is assumed to contain many elementary information-update cells while remaining small compared with the macroscopic curvature, clock-rate, and thermodynamic-gradient scales. The continuum tensor below is therefore the hydrodynamic limit of discrete writing updates, not an additional microscopic postulate. We introduce the constitutive informational energy density carried by the mass-information and temporal-registration channels,

$$\varepsilon_I = h\mathcal{R}_m + k_B T \ln 2\mathcal{N}_\tau. \quad (346)$$

Here T denotes the local effective temperature of the dispersive registration reservoir. The density \mathcal{R}_m has units $\text{m}^{-3}\text{s}^{-1}$, so $h\mathcal{R}_m$ has units J m^{-3} ; \mathcal{N}_τ has units m^{-3} , so $k_B T \ln 2\mathcal{N}_\tau$ also has units J m^{-3} . The Landauer-based thermodynamic closure that motivates this term was developed in the thermodynamic time section above. The units close directly:

$$[h\mathcal{R}_m] = \frac{\text{J}}{\text{m}^3}, \quad [k_B T \ln 2\mathcal{N}_\tau] = \frac{\text{J}}{\text{m}^3}. \quad (347)$$

Thus the local energy-density component is a constitutive expression of the same mass and temporal-writing channels already introduced in the physical writing-channel section.

The motion-information channel enters through the four-velocity

$$u^\mu = \frac{dx^\mu}{d\tau}, \quad g_{\mu\nu}^{(I)} u^\mu u^\nu = -c^2. \quad (348)$$

It is the covariant form of the normalized updating rate $dI_x/dI_t = v/c$. In a local orthonormal frame, the coherent transported part of the source tensor is

$$T_{\text{coh}}^{\hat{a}\hat{b}} = \frac{\varepsilon_I}{c^2} u^{\hat{a}} u^{\hat{b}}, \quad (349)$$

so that motion-information supplies the momentum and energy-flux components as well as the transported spatial momentum flux.

The dispersive channel supplies entropy density,

$$s_I = k_B \ln 2\mathcal{N}_{\text{disp}}, \quad (350)$$

and therefore pressure and stress through the response of dispersive free energy to changes in spatial configuration capacity. In spatial form this response is

$$p_I = - \left(\frac{\partial F_{\text{disp}}}{\partial V} \right)_{T,I}, \quad (351)$$

with the anisotropic stress given by the metric variation of the dispersive free energy,

$$\sigma_{ij}^{(I)} = - \frac{2}{\sqrt{\gamma}} \frac{\delta F_{\text{disp}}}{\delta \gamma^{ij}}. \quad (352)$$

Here γ_{ij} is the induced spatial metric. In the isotropic limit $\sigma_{ij}^{(I)} = p_I \gamma_{ij}$; direction-dependent configuration loss contributes anisotropic stress.

Following the usual covariant fluid decomposition of stress-energy [68], the full informational stress-energy tensor is therefore

$$T_{\mu\nu}^{(I)} = \frac{\varepsilon_I}{c^2} u_\mu u_\nu + \frac{1}{c^2} \left(u_\mu q_\nu^{(I)} + u_\nu q_\mu^{(I)} \right) + p_I h_{\mu\nu} + \pi_{\mu\nu}^{(I)}, \quad (353)$$

where

$$h_{\mu\nu} = g_{\mu\nu}^{(I)} + \frac{u_\mu u_\nu}{c^2}. \quad (354)$$

The spatial energy flux $q_\mu^{(I)}$ and the anisotropic stress $\pi_{\mu\nu}^{(I)}$ obey

$$u^\mu q_\mu^{(I)} = 0, \quad u^\mu \pi_{\mu\nu}^{(I)} = 0, \quad \pi^\mu{}_\mu = 0. \quad (355)$$

In the perfect informational-fluid limit, where directional heat flux and anisotropic stress vanish,

$$q_\mu^{(I)} = 0, \quad \pi_{\mu\nu}^{(I)} = 0, \quad (356)$$

the source reduces to

$$T_{\mu\nu}^{(I)} = \frac{\varepsilon_I + p_I}{c^2} u_\mu u_\nu + p_I g_{\mu\nu}^{(I)}. \quad (357)$$

The equilibrium field equation for a conserved information flux is therefore

$$\boxed{G_{\mu\nu}[g^{(I)}] + \Lambda_\tau g_{\mu\nu}^{(I)} = \frac{8\pi G}{c^4} T_{\mu\nu}^{(I)}}. \quad (358)$$

The additional homogeneous term is allowed by Lovelock's theorem and by the contracted Bianchi identity. In the present reconstruction it is retained as an informational term: Λ_τ is the homogeneous background component of the temporal-writing capacity of the vacuum. Local sources enter through $T_{\mu\nu}^{(I)}$, while the term $\Lambda_\tau g_{\mu\nu}^{(I)}$ represents the isotropic background writing pressure of the metric itself. The coupling $8\pi G/c^4$ is fixed by the weak-field limit of the Compton–Schwarzschild load. In that limit, the temporal capacity factor satisfies $g_{tt} = -c^2(1 - r_s/r)$, and the temporal-gradient force recovers Newtonian gravity. The same constant therefore relates information-energy density to writing-capacity curvature in the covariant theory.

This is the tensorial completion of the scalar closure relation. The scalar law $\chi^2 + \Lambda_I = 1$ is the single-axis projection of the finite writing budget, while the tensor equation distributes that same budget across energy density, momentum flux, pressure, and anisotropic stress. The static Schwarzschild sector is the spherically symmetric projection of this covariant informational balance.

In this reading, the curvature tensor is the differential bookkeeping of writing-capacity variation. Neighboring events with different local writing power define a nonzero connection; closed comparisons of writing directions define curvature. The Einstein tensor $G_{\mu\nu}[g^{(I)}]$ measures covariant erosion, redistribution, or imbalance of writing capacity across neighboring regions. The tensorial structure is the covariant completion of the same conservation principle that first appeared as the scalar relation $\chi^2 + \Lambda_I = 1$.

5.4 Directional Information Flux and the Mixed Time-Angular Metric Component

A rotating source carries mass-writing density together with angular information flux. In the static spherical case the exterior information flux is purely radial. In the rotating case the source has angular momentum

$$J = Mac, \quad (359)$$

where $a = J/(Mc)$ is the usual rotational length parameter. The information flux therefore has an azimuthal component,

$$J_I^\phi \neq 0. \quad (360)$$

A nonzero angular information flux means that temporal registration and azimuthal registration are no longer independent writing directions. The elementary writing interval must include a mixed time-angular term,

$$ds_{t\phi}^2 = g_{tt}^{(I)} dt^2 + 2g_{t\phi}^{(I)} dt d\phi + g_{\phi\phi}^{(I)} d\phi^2. \quad (361)$$

Since dt has units of seconds and $d\phi$ is dimensionless in this convention, the mixed coefficient must have units

$$[g_{t\phi}^{(I)}] = \text{m}^2/\text{s}. \quad (362)$$

The mixed term is determined by the weak-field angular flux load. This load follows from a stationary axial flux equation. Let $\Omega_I(r)$ denote the angular writing-drag rate produced by the rotating source. In the vacuum exterior there is no local torque-source of angular information, so the radial flux of angular writing moment is conserved. In the slow-rotation, weak-field sector this gives the axial capacity equation

$$\frac{d}{dr} \left(r^4 \frac{d\Omega_I}{dr} \right) = 0, \quad r > r_s. \quad (363)$$

The factor r^4 is the axial-flux measure of rotational registration. One factor r^2 is the spherical area through which the angular-writing flux is transported; the second factor r^2 is the areal angular moment arm associated with rotational writing. Thus the conserved quantity is a flux of angular writing moment.

The first integration gives

$$r^4 \frac{d\Omega_I}{dr} = -3C_J, \quad (364)$$

and the second gives

$$\Omega_I(r) = \frac{C_J}{r^3} + \Omega_\infty. \quad (365)$$

The exterior angular writing drag must vanish at infinity, so $\Omega_\infty = 0$. The integration constant is fixed by the two source lengths that characterize a rotating mass: the gravitational saturation length r_s and the rotational length $a = J/(Mc)$. Dimensional closure requires

$$[C_J] = \text{m}^3/\text{s}, \quad C_J = cr_s a, \quad (366)$$

so that

$$\boxed{\Omega_I(r) = \frac{cr_s a}{r^3}.} \quad (367)$$

This is the informational analogue of the weak-field frame-dragging angular rate generated by a conserved axial angular-momentum flux. The angular capacity load is the dimensionless fraction of angular writing dragged during one areal angular step. Since the physical angular arc is $r d\phi$ and regular axial rotation vanishes on the symmetry axis, the leading axial projection is $\sin^2 \theta$:

$$\boxed{\Lambda_{I,J}(r, \theta) = \frac{r}{c} \Omega_I(r) \sin^2 \theta = \frac{r_s a}{r^2} \sin^2 \theta.} \quad (368)$$

Thus the r^{-2} rotational load is not an independent multiplication rule. It is the dimensionless angular-writing load generated by a vacuum axial drag rate $\Omega_I \propto r^{-3}$ and by the areal angular conversion factor r/c .

The corresponding time-angular capacity coefficient must convert this dimensionless load into the units of $g_{t\phi}$, which are supplied by cr in the areal angular direction. Therefore

$$g_{t\phi}^{(I)} \simeq -cr \Lambda_{I,J}(r, \theta) = -c \frac{r_s a}{r} \sin^2 \theta. \quad (369)$$

Using

$$r_s = \frac{2GM}{c^2}, \quad a = \frac{J}{Mc}, \quad (370)$$

this becomes

$$\boxed{g_{t\phi}^{(I)} \simeq -\frac{2GJ}{c^2 r} \sin^2 \theta.} \quad (371)$$

The dimensions close directly:

$$\left[\frac{GJ}{c^2 r} \right] = \frac{\text{m}^3 \text{kg}^{-1} \text{s}^{-2} \text{kg m}^2 \text{s}^{-1}}{\text{m}^2 \text{s}^{-2} \text{m}} = \text{m}^2/\text{s}. \quad (372)$$

Thus the leading off-diagonal, frame-dragging component is recovered as the capacity-map expression of angular information flux. The result is the weak-field rotating limit of the Kerr time-angular structure [76] and the Lense–Thirring dragging effect [77].

With the energy-writing channels now defined, the common configuration-gradient force law is written as

$$\boxed{\mathbf{F} = -E_{\text{inv}} \nabla \chi.} \quad (373)$$

For massive matter,

$$E_{\text{inv}} = mc^2, \quad (374)$$

so the massive limit is

$$\boxed{\mathbf{F} = -mc^2 \nabla \chi.} \quad (375)$$

For light,

$$E_{\text{inv}} = E_\gamma = h\nu = pc. \quad (376)$$

In gravitation, $\chi = \chi_g(r)$. In inertia, $\chi = \chi_v(v)$. The common variable is the temporal writing field χ . The common dynamical scale is the appropriate invariant energy scale E_{inv} . The common force structure is the gradient or effective gradient of temporal writing capacity.

This supplies the informational form of the equivalence principle:

$$\boxed{\text{gravity and inertia are responses to gradients or changes in the same temporal writing field } \chi. \text{ [72]}}$$

5.5 Metric Capacity Updates and Gravitational Waves

The preceding tensor equation also clarifies the status of the graviton within the present reconstruction. In the standard particle picture, force carriers such as photons or gluons are bosonic excitations propagating on an already defined spacetime background. Perturbative and effective-field-theory treatments of quantum gravity describe low-energy gravitons as spin-2 metric excitations in this sense. [78] [79] [80] They are contents written on the capacity map. In the present reconstruction, gravitation is the response of the capacity map itself to finite information writing. The gravitational quantum is therefore not introduced as a standard matter-like exchange particle propagating on a fixed background. It is interpreted as the elementary update of the writing-capacity field.

The reason is direct. Physical information is written in elementary distinguishability units, and the maximal update of spatial distinction is Planck-normalized:

$$\ell_P = \sqrt{\frac{\hbar G}{c^3}}, \quad t_P = \sqrt{\frac{\hbar G}{c^5}}, \quad c = \frac{\ell_P}{t_P}. \quad (377)$$

Hence a change in gravitational capacity cannot be an arbitrarily divisible classical deformation. It must be built from discrete updates of the information-writing map. Let the local capacity state be represented schematically by $g_{\mu\nu}^{(I)}$. An elementary gravitational update is then

$$\delta g_{\mu\nu}^{(I)}|_{\text{elem}}, \quad (378)$$

the smallest distinguishable change in the local registration capacity consistent with the Planck writing cell. The corresponding update rate is

$$\dot{g}_{\mu\nu}^{(I)} = \frac{\delta g_{\mu\nu}^{(I)}|_{\text{elem}}}{t_P}. \quad (379)$$

In this sense, the informational graviton is the quantum of capacity update: the elementary bit of change by which the metric writing map adjusts to a change in mass-information, motion-information, temporal-registration cost, or angular information flux.

A gravitational wave is then a propagating ripple of capacity updates, described macroscopically in the metric-perturbation language of general relativity and gravitational-wave theory [67] [81] [82]. Its macroscopic description is a wave in the metric perturbation $h_{\mu\nu}$, where

$$g_{\mu\nu}^{(I)} = \eta_{\mu\nu} + h_{\mu\nu}. \quad (380)$$

The informational reading is

$$h_{\mu\nu} = \text{coarse-grained propagation of elementary capacity updates.} \quad (381)$$

Thus the graviton expected by this theory is the discrete update quantum of spacetime writing capacity. The quantized object is the update rule of the page, the capacity rule through which metric writing proceeds.

This preserves quantum gravity inside the theory as the quantum-informational character of the capacity map. Since gravity is the dynamics of information-writing capacity, and the writing capacity is defined at finite Planck resolution, the gravitational field is quantum at the level of its elementary updates. The missing graviton is therefore read as the missing capacity-update quantum of the metric-writing rule.

5.6 Unified Force Mechanism: Massive Matter and the Compton Writing Scale

Mass-information is carried by the invariant Compton writing rate

$$\dot{I}_m = \frac{mc^2}{h}. \quad (382)$$

The associated invariant energy scale is

$$E_m = mc^2. \quad (383)$$

A gravitational field changes the local temporal writing factor,

$$\chi_g(r) = \frac{d\tau}{dt}. \quad (384)$$

The internal mass-writing rate remains invariant, while the local temporal field varies with position. The energy associated with embedding the invariant mass channel in the local temporal writing field is therefore

$$E_{\text{embed}}(r) = mc^2 \chi_g(r). \quad (385)$$

Here

$$[mc^2] = \text{J}, \quad [\chi_g] = 1, \quad (386)$$

so

$$[E_{\text{embed}}] = \text{J}. \quad (387)$$

The complementary mismatch magnitude is

$$E_T(r) = mc^2 (1 - \chi_g(r)). \quad (388)$$

This quantity measures the departure from the undistorted temporal field: $E_T = 0$ when $\chi_g = 1$, and E_T grows as the available temporal writing fraction decreases. The force-producing potential is the realized embedding energy

$$U(r) = mc^2 \chi_g(r). \quad (389)$$

The distinction fixes the sign. Since

$$\nabla(1 - \chi_g) = -\nabla\chi_g, \quad (390)$$

deriving the attractive branch from the mismatch magnitude would reverse the direction. The physical force branch is generated by the negative gradient of the realized embedding potential U .

A spatial gradient in this embedding energy produces force:

$$F_r = -\frac{dE_{\text{embed}}}{dr}. \quad (391)$$

Thus,

$$F_r = -\frac{d}{dr} (mc^2 \chi_g(r)). \quad (392)$$

For constant test mass m ,

$$F_r = -mc^2 \frac{d\chi_g}{dr}. \quad (393)$$

Now use

$$\chi_g(r) = \sqrt{1 - \frac{r_s}{r}}. \quad (394)$$

Differentiate:

$$\frac{d\chi_g}{dr} = \frac{1}{2} \left(1 - \frac{r_s}{r}\right)^{-1/2} \frac{d}{dr} \left(1 - \frac{r_s}{r}\right). \quad (395)$$

Because

$$\frac{d}{dr} \left(1 - \frac{r_s}{r}\right) = \frac{r_s}{r^2}, \quad (396)$$

we obtain

$$\frac{d\chi_g}{dr} = \frac{1}{2} \left(1 - \frac{r_s}{r}\right)^{-1/2} \frac{r_s}{r^2}. \quad (397)$$

Therefore,

$$F_r = -mc^2 \frac{1}{2} \left(1 - \frac{r_s}{r}\right)^{-1/2} \frac{r_s}{r^2}. \quad (398)$$

So

$$F_r = -\frac{mc^2 r_s}{2r^2} \frac{1}{\sqrt{1 - \frac{r_s}{r}}}. \quad (399)$$

For a source mass M ,

$$r_s = \frac{2GM}{c^2}. \quad (400)$$

Substitute this into the force:

$$F_r = -\frac{mc^2}{2r^2} \frac{2GM}{c^2} \frac{1}{\sqrt{1 - \frac{r_s}{r}}}. \quad (401)$$

Cancel c^2 :

$$\boxed{F_r = -\frac{GMm}{r^2} \frac{1}{\sqrt{1 - \frac{r_s}{r}}}.} \quad (402)$$

In the weak-field limit of general relativity [68],

$$r \gg r_s, \quad (403)$$

so

$$\frac{r_s}{r} \ll 1, \quad (404)$$

and

$$\sqrt{1 - \frac{r_s}{r}} \approx 1. \quad (405)$$

Thus,

$$\boxed{F_r \approx -\frac{GMm}{r^2}.} \quad (406)$$

The units are

$$\left[\frac{GMm}{r^2} \right] = \frac{(\text{m}^3 \text{kg}^{-1} \text{s}^{-2})(\text{kg})(\text{kg})}{\text{m}^2} = \text{kg m s}^{-2} = \text{N}. \quad (407)$$

Newtonian gravity is recovered as the weak-field limit of the temporal writing gradient. [83]

The force law obtained here is

$$\boxed{\mathbf{F} = -mc^2 \nabla \chi.} \quad (408)$$

In the gravitational case,

$$\chi = \chi_g(r). \quad (409)$$

The force law expresses the energetic mismatch between invariant internal mass-writing and a spatially varying temporal writing field. Gravitation is the spatial gradient of that mismatch. A massive body carries an internal Compton writing rate; in a nonuniform χ -field, the local capacity for realizing that rate changes with position. Gravitational fall is the dynamical response of this internal Compton register to a gradient in temporal registration capacity. In the present reconstruction, $\mathbf{F}_\chi = -mc^2 \nabla \chi$ gives the static configuration-gradient force associated with holding or comparing a massive body across neighboring values of the temporal writing field. In the conventional geometric language of general relativity, free motion is represented as geodesic motion in an effective metric. The two descriptions are therefore different representations of the same gravitational dynamics: the temporal-gradient expression is the configuration-gradient representation, while the Einsteinian geodesic is the metric representation.

5.7 Massless Signals and Photon Energy as the Invariant Scale

The same temporal-gradient mechanism also applies to light once the energy scale is written in the correct channel. For a massive body the relevant invariant energy scale is the rest energy,

$$E_m = mc^2. \quad (410)$$

For a photon or massless signal the corresponding invariant energy scale is the photon energy,

$$E_\gamma = h\nu = \hbar\omega = pc. \quad (411)$$

Here E_γ denotes the transported photon-energy scale associated with the stationary external time parameter, equivalently the conserved Killing energy E_∞ in the static description and the reference energy measured at infinity in the weak-field scattering setup. It is not the locally redshifted energy assigned by each static observer along the ray. [57] With this convention, E_γ is held fixed when taking the spatial gradient of the temporal field.

The coupling of a photon to the same temporal writing field follows from the energy-information channel. Any coherent energy carrier of energy E carries a phase-writing rate

$$\dot{I}_E = \frac{E}{h}, \quad (412)$$

because one period of phase writing corresponds to one elementary cycle of distinguishable update. For massive matter at rest this gives

$$\dot{I}_E = \frac{mc^2}{h} = \dot{I}_m, \quad (413)$$

which is the Compton mass-writing channel already used above. For a photon the same energy-writing rule gives

$$\dot{I}_\gamma = \frac{E_\gamma}{h} = \nu, \quad (414)$$

with

$$E_\gamma = h\nu = \hbar\omega = pc. \quad (415)$$

Thus the photon has no rest-mass Compton channel, but it does have an energy-frequency writing channel. The invariant quantity that couples to the temporal capacity factor is therefore the conserved transported energy of the carrier:

$$E_{\text{inv}} = \begin{cases} mc^2, & \text{massive rest-energy channel,} \\ E_\gamma, & \text{photon energy-frequency channel.} \end{cases} \quad (416)$$

This is the same energy-to-writing-rate relation applied to two different channels. Massive matter carries internal Compton writing, while light carries transported phase writing. Both consume temporal registration capacity through their conserved energy scale.

The realized embedding energy of a photon in the local gravitational temporal field is

$$U_\gamma(r) = E_\gamma \chi_g(r). \quad (417)$$

Here

$$[E_\gamma] = \text{J}, \quad [\chi_g] = 1, \quad (418)$$

so

$$[U_\gamma] = \text{J}. \quad (419)$$

Taking the negative spatial gradient gives the force-like momentum-change law for the photon,

$$\boxed{\mathbf{F}_\gamma = -\nabla U_\gamma = -\nabla(E_\gamma \chi_g).} \quad (420)$$

With the photon energy treated as the transported invariant energy scale along the ray, this becomes the effective momentum-gradient law

$$\boxed{\mathbf{F}_\gamma = -E_\gamma \nabla \chi_g.} \quad (421)$$

This is a force-like law for the rate and direction of photon momentum change in the temporal gradient, not a rest-mass force acting on a massive particle. The units close directly:

$$[E_\gamma \nabla \chi_g] = \text{J m}^{-1} = \text{N}. \quad (422)$$

Equivalently, the photon carries the effective gravitational energy scale

$$\frac{E_\gamma}{c^2} \quad (423)$$

in the same temporal-gradient law,

$$\mathbf{F}_\gamma = -\frac{E_\gamma}{c^2} c^2 \nabla \chi_g = -E_\gamma \nabla \chi_g. \quad (424)$$

Thus light responds to the gravitational temporal gradient through its photon energy. The massive expression and the massless expression are the same rule written with the appropriate invariant energy scale:

$$\boxed{\mathbf{F} = -E_{\text{inv}} \nabla \chi,} \quad (425)$$

with

$$E_{\text{inv}} = mc^2 \quad (426)$$

for massive matter and

$$E_{\text{inv}} = E_\gamma = h\nu = pc \quad (427)$$

for light. This is the compact reason that the same informational gravitational field affects both massive bodies and photons.

The complete weak-field bending angle is recovered when this photon energy response is combined with the effective Schwarzschild metric derived above. For a null ray written with $u = 1/r$ and impact parameter b , the weak-field null-geodesic equation is

$$\frac{d^2u}{d\phi^2} + u = \frac{3GM}{c^2}u^2. \quad (428)$$

Using the zeroth-order path $u_0 = \sin \phi/b$ and retaining the first gravitational correction gives the standard leading deflection [89]

$$\boxed{\Delta\phi = \frac{4GM}{bc^2}}. \quad (429)$$

Thus the photon section supplies the energy-channel reason why light enters the same temporal-gradient field, while the effective metric supplies the spatial part required for the full light-bending angle. Both descriptions express the same bending mechanism. The null trajectory is determined by the null-geodesic condition of the informational metric, $ds^2 = 0$; the temporal-gradient force is the local energy-channel reading of the same metric structure.

6 Unified Phase-Time Force and Electromagnetism

This section develops the force mechanism from invariant Compton writing in a varying temporal field and then extends the same structure into coherent phase-time transport. The phase branch supplies the electromagnetic connection, curvature, and Maxwell structure.

6.1 The Coherent Phase-Time Branch

The preceding sections used the real clock-rate factor χ to reconstruct inertial and gravitational capacity geometry. The complex completion of the same time-load structure contains the coherent phase-time orientation $e^{-i\phi}$. Electromagnetism is developed here as the local transport and curvature dynamics of that coherent phase branch.

In the coherent branch, the process sits at the ideal thermodynamic limit $\gamma_{\text{th}} = 1$, meaning that no excess thermodynamic cost is paid beyond the minimal saturated relation. Irreversible linear historical writing belongs to the dispersive branch, where $\gamma_{\text{th}} > 1$. On the interface of the Present (the Riemann Sphere), continuous, reversible informational evolution is represented geometrically as a continuous phase rotation:

$$\psi = \psi_0 e^{-i\phi}$$

The next question is what this informational time equation implies for coherent quantum evolution. The guiding point is that the unitary Schrödinger equation [90] omits explicit entropic inscription. For an energy eigenstate one has

$$i\hbar \frac{\partial \psi}{\partial t} = H\psi, \quad \psi(t) = \psi_0 e^{-iEt/\hbar}.$$

The changing quantity in the coherent solution is the phase,

$$\phi(t) = \frac{Et}{\hbar}, \quad \psi(t) = \psi_0 e^{-i\phi(t)}.$$

The informational time equation now clarifies the interpretation. In the coherent branch, phase evolves coherently, but no irreversible registration into linear history has yet occurred. Therefore the dispersed-information sector is absent there as an active dynamical inscription variable. The coherent branch is thus the branch in which the changing quantity is informational change itself. In that branch one first writes the normalized coherent relation,

$$dt_q^* \propto dI_q.$$

Choosing the coherent informational normalization gives the simplest compact form,

$$dt_q^* = dI_q.$$

Passing from the normalized coherent parameter to physical time requires the Compton time scale,

$$dt_q = \tau_C^{(\omega)} dt_q^* = \tau_C^{(\omega)} dI_q.$$

Returning to the Schrödinger phase,

$$d\phi = \frac{E}{\hbar} dt_q,$$

one immediately obtains

$$d\phi = \frac{E}{\hbar} \tau_C^{(\omega)} dI_q, \quad E = \frac{\hbar}{\tau_C^{(\omega)}} \frac{d\phi}{dI_q}.$$

For a rest mode, where $E_0 = mc^2$ and $\tau_C^{(\omega)} = \hbar/(mc^2)$, this reduces to

$$d\phi = dI_q.$$

Equivalently, in the coherent branch the phase coordinate itself is the coordinate of coherent informational change:

$$dI_\phi \equiv d\phi.$$

Thus a local phase field $\phi(x)$ is also a local coherent-information field.

This is the central statement of the coherent branch: the normalized coherent time is informational change, while the physical phase-time scale is set by the Compton time. For a rest mode,

$$E_0 = mc^2, \quad \omega_C = \frac{mc^2}{\hbar}, \quad \psi(t) = \psi_0 e^{-i\omega_C t}.$$

The rest mode is therefore carried by a Compton phase factor [19]. This motivates the phase completion of rest energy:

$$E_\phi = mc^2 e^{-i\phi}$$

Expanding the phase-completed energy gives

$$E_\phi = mc^2 (\cos \phi - i \sin \phi).$$

Hence the two sectors are

$$\Re(E_\phi) = mc^2 \cos \phi, \quad \Im(E_\phi) = -mc^2 \sin \phi.$$

The real sector is the branch that couples to the linear-time field and therefore underlies inertia, gravitation, and diffusion. The imaginary sector is the coherent phase branch.

In this form the realized linear branch is the cosine projection of the phase structure. The linear time that appears in experience is the realized projection of the full phase object. In that sense, the appearance of the cosine is not a technical artifact. It is the mathematical signature that linear time is a projection of a deeper phase-time structure.

6.2 From Compton Phase-Time to the Unified Time-Load Field

Two ingredients are now joined into one object.

The first ingredient is the local clock-rate factor,

$$\chi(x),$$

which measures the realized time-writing capacity left after informational load. In the inertial and gravitational sectors, this factor determines how much linear temporal registration remains available under motion or mass loading.

The second ingredient is the Compton phase-time increment of a massive carrier,

$$dt_\phi^{(0)} = \tau_C^{(\omega)} e^{-i\phi} d\phi,$$

with

$$\tau_C^{(\omega)} = \frac{\hbar}{mc^2}.$$

Here $\tau_C^{(\omega)}$ is the angular Compton time. It supplies the intrinsic physical time scale of the massive carrier. The factor $e^{-i\phi}$ gives the coherent phase-time orientation. The superscript (0) denotes the unloaded coherent Compton mode.

This gives the ideal phase-time increment of a massive mode before local informational loading is included.

The general thermodynamic phase-time form is therefore

$$dt_{\phi,\text{gen}} = \tau_C^{(\omega)} dt^* e^{-i\phi} d\phi,$$

with

$$dt^* = \frac{dI_{\text{dist}}}{dI_{\text{disp}}}, \quad \tau_C^{(\omega)} = \frac{\hbar}{mc^2}.$$

This is the Compton-scaled completion of the dimensionless informational-time ratio introduced earlier.

When the same carrier is embedded in a realized informational geometry, its available temporal writing capacity is no longer unity. It is weighted by the local clock-rate factor $\chi(x)$. The embedded phase-time increment therefore becomes

$$dt_{\phi} = \tau_C^{(\omega)} \chi(x) e^{-i\phi(x)} d\phi.$$

This equation is the missing bridge between the clock-rate-amplitude branch and the coherent phase branch.

The Compton factor

$$\tau_C^{(\omega)}$$

sets the physical time scale.

The clock-rate factor

$$\chi(x)$$

sets the local realized writing amplitude.

The phase factor

$$e^{-i\phi(x)}$$

sets the coherent phase-time orientation.

Therefore the product

$$\chi(x) e^{-i\phi(x)}$$

is the natural complex completion of the real clock-rate factor. This motivates the definition of the unified time-load field,

$$\Xi(x) = \chi(x)e^{-i\phi(x)}.$$

With this definition, the embedded phase-time increment can be written compactly as

$$dt_\phi = \tau_C^{(\omega)} \Xi(x) d\phi.$$

Thus $\Xi(x)$ is the phase-completed form of the already defined clock-rate factor $\chi(x)$. The amplitude χ supplies the local clock-rate loading, while the realized linear projection of the complex field is

$$\text{Re } \Xi = \chi \cos \phi. \quad (430)$$

The complementary phase projection carries the coherent phase-transport branch.

Using Euler's identity,

$$e^{-i\phi} = \cos \phi - i \sin \phi,$$

the field can be expanded as

$$\Xi(x) = \chi(x) \cos \phi(x) - i\chi(x) \sin \phi(x).$$

Accordingly, the embedded phase-time increment becomes

$$dt_\phi = \tau_C^{(\omega)} \chi(x) [\cos \phi(x) - i \sin \phi(x)] d\phi.$$

The realized linear-time projection is the real component,

$$d\tau = \text{Re}(dt_\phi) = \tau_C^{(\omega)} \chi(x) \cos \phi(x) d\phi.$$

The coherent phase projection is the imaginary component,

$$\text{Im}(dt_\phi) = -\tau_C^{(\omega)} \chi(x) \sin \phi(x) d\phi.$$

The theory uses one phase-time rotation whose real projection appears as realized linear time and whose imaginary projection carries coherent phase structure.

The unified field

$$\Xi(x) = \chi(x)e^{-i\phi(x)}$$

therefore collects both branches in one object: the clock-rate amplitude χ and the coherent phase-time orientation $e^{-i\phi}$. Its realized linear projection is $\text{Re } \Xi = \chi \cos \phi$, while its complementary phase projection carries coherent phase structure. This is why the same field can later generate both the gravitational/inertial clock-rate branch and the electromagnetic/gauge phase branch.

6.3 The Complex Time-Load Field

The real clock-rate factor χ and the phase-time orientation $e^{-i\phi}$ form one compact geometric object,

$$\boxed{\Xi(x) = \chi(x)e^{-i\phi(x)}}.$$

The factor χ is the local realized writing amplitude. The phase factor $e^{-i\phi}$ is the coherent orientation of the same temporal writing process. Their product is the complex time-load field. Its amplitude supplies clock-rate loading, its realized linear projection is

$$\text{Re } \Xi = \chi \cos \phi, \quad (431)$$

and its complementary phase projection supplies coherent transport.

For sectors written as capacity potentials, the phase-completed potential is

$$U_\phi = E_0 \Xi,$$

and the corresponding force law is

$$\boxed{\mathbf{F}_\phi = -E_0 \nabla \Xi.}$$

For closure-cost or dissipative-load sectors, the physical potential is

$$u_\phi = E_0(1 - \Xi),$$

and therefore

$$\boxed{\mathbf{F}_\phi = -\nabla u_\phi = E_0 \nabla \Xi.}$$

For massive matter $E_0 = mc^2$. For a photon $E_0 = \hbar\omega$. This compact structure explains why the same gradient principle can appear in inertial, gravitational, electromagnetic, internal, and coherent-transport sectors while each branch uses the physical potential appropriate to its capacity or closure-cost form.

6.4 Kinematic Phase-Time Closure

The kinematic branch now has a compact phase-time representation. Since the Lorentz clock-rate fraction is the thermodynamic registration efficiency for pure motion,

$$\chi_v = \eta_{\text{th}}^{(v)} = \frac{1}{\gamma_I}, \quad (432)$$

the complex time-load field on the kinematic branch is

$$\Xi_v = \chi_v e^{-i\phi}. \quad (433)$$

Substitution gives

$$\boxed{\Xi_v = \eta_{\text{th}}^{(v)} e^{-i\phi} = \frac{e^{-i\phi}}{\gamma_I}.} \quad (434)$$

The factor $e^{-i\phi}$ is the Euler phase factor,

$$e^{-i\phi} = \cos \phi - i \sin \phi.$$

It supplies the local complex phase structure of the theory. The real projection carries the registered linear-time component, while the orthogonal imaginary projection carries the coherent phase component. Thus the complex time-load field combines a real registration amplitude χ with an Euler phase-time orientation.

Thus the same object carries the two readings of the moving state. Its amplitude is the surviving thermodynamic writing efficiency of the realized branch, and its phase factor is the coherent temporal orientation of that branch. The realized linear projection is $\text{Re } \Xi_v = \chi_v \cos \phi$. In the kinematic sector, the complex time-load field is the Lorentz writing-efficiency amplitude completed by phase-time orientation.

6.5 Clock-Rate Branch and Phase Branch of the Force

Using the complex time-load field $\Xi(x) = \chi(x)e^{-i\phi(x)}$, the massive-particle potential is $U_\phi(x) = mc^2\Xi(x)$. The force law $F = -\nabla U_\phi$ yields a strict decomposition whose phase branch connects naturally to fiber-bundle gauge geometry [91]:

$$F = -m c^2 e^{-i\phi} \nabla(\chi) + i m c^2 \chi e^{-i\phi} \nabla(\phi).$$

Substituting the complex potential gives

$$F = -\nabla(mc^2\chi e^{-i\phi}) = -mc^2\nabla(\chi e^{-i\phi}).$$

Using the product rule,

$$\nabla(\chi e^{-i\phi}) = e^{-i\phi} \nabla\chi - i\chi e^{-i\phi} \nabla\phi,$$

and therefore

$$F = -mc^2 e^{-i\phi} \nabla\chi + imc^2 \chi e^{-i\phi} \nabla\phi.$$

The first term is controlled by the gradient of the clock-rate amplitude χ and gives the clock-rate branch,

$$\mathbf{F}_\chi = -mc^2 \nabla\chi.$$

The second term is controlled by coherent phase transport and gives the phase branch,

$$\mathbf{F}_{\text{phase}} = imc^2 \chi e^{-i\phi} \nabla\phi.$$

The exact real and imaginary projections of the full complex force are

$$\begin{aligned} \Re(\mathbf{F}_\phi) &= -mc^2 \cos \phi \nabla\chi + mc^2 \chi \sin \phi \nabla\phi, \\ \Im(\mathbf{F}_\phi) &= mc^2 \sin \phi \nabla\chi + mc^2 \chi \cos \phi \nabla\phi. \end{aligned}$$

The $\nabla\chi$ branch was used above for inertial and gravitational capacity geometry. The $\nabla\phi$ branch now requires a local transport law for coherent informational phase.

6.6 Relativity as the Hermitian Metric Projection of the Unified Phase-Time Field.

The relativistic sector was first written in terms of the real clock-rate factor

$$\chi(x) = \frac{d\tau}{dt}.$$

In this form, the local clock-rate gradient gives the inertial and gravitational response,

$$\mathbf{F}_\chi = -mc^2 \nabla \chi,$$

and the static spherical metric is written as

$$ds^2 = -c^2 \chi^2 dt^2 + \chi^{-2} dr^2 + r^2 d\Omega^2.$$

This is the real clock-rate form of the theory. However, once the clock-rate field is completed by phase, the more general object is the unified phase-time field

$$\Xi(x) = \chi(x) e^{-i\phi(x)}.$$

The relativistic metric uses the Hermitian product of the phase-time field with its conjugate. A physical metric measures squared interval, and a squared physical interval is obtained from that product:

$$\Xi^* \Xi = (\chi e^{+i\phi}) (\chi e^{-i\phi}) = \chi^2.$$

Thus the relativistic clock-rate factor can be written as the Hermitian norm of the unified field,

$$\chi^2 = \Xi^* \Xi.$$

The metric form of the relativistic sector may therefore be rewritten as

$$ds^2 = -c^2 \Xi^* \Xi dt^2 + (\Xi^* \Xi)^{-1} dr^2 + r^2 d\Omega^2.$$

Substituting $\Xi^* \Xi = \chi^2$ immediately returns the usual clock-rate metric,

$$ds^2 = -c^2 \chi^2 dt^2 + \chi^{-2} dr^2 + r^2 d\Omega^2.$$

For the Schwarzschild exterior,

$$\chi_g(r) = \sqrt{1 - \frac{r_s}{r}},$$

so

$$\Xi_g(r) = \sqrt{1 - \frac{r_s}{r}} e^{-i\phi_0}.$$

When the phase is constant,

$$\nabla \phi = 0,$$

there is no active phase-gradient branch. The Hermitian product gives

$$\Xi_g^* \Xi_g = 1 - \frac{r_s}{r},$$

and the metric becomes

$$ds^2 = -c^2 \left(1 - \frac{r_s}{r}\right) dt^2 + \left(1 - \frac{r_s}{r}\right)^{-1} dr^2 + r^2 d\Omega^2,$$

which is the Schwarzschild exterior line element.

The force law may be written in the same unified language. Starting from

$$\mathbf{F}_\Xi = -mc^2 \nabla \Xi,$$

one obtains

$$\mathbf{F}_\Xi = -mc^2 e^{-i\phi} \nabla \chi + imc^2 \chi e^{-i\phi} \nabla \phi.$$

The first term is the clock-rate branch. The second term is the phase-gradient branch. In the purely relativistic sector,

$$\nabla \phi = 0,$$

so the force reduces to

$$\mathbf{F}_\Xi = -mc^2 e^{-i\phi_0} \nabla \chi.$$

Taking the physical real projection, for $\phi_0 = 0$, gives

$$\text{Re}(\mathbf{F}_\Xi) = -mc^2 \nabla \chi.$$

Thus the relativistic force law is recovered as the real clock-rate projection of the unified phase-time gradient.

Relativity is therefore not separate from the unified field. It is the Hermitian metric projection of

$$\Xi = \chi e^{-i\phi}.$$

The metric sector depends on the norm

$$\Xi^* \Xi,$$

while the gauge sector appears when the phase gradient

$$\nabla \phi$$

is active. In this form, gravity and inertia are the real clock-rate projection of the same phase-time field whose phase-gradient projection supplies the gauge branch.

6.7 Local Phase-Time Fiber, Gauge Transport, and Metric Form

Since $dI_\phi = d\phi$ and ϕ is compact, the local coherent-information coordinate is naturally represented by a circle fiber S_ϕ^1 over spacetime in the standard gauge-bundle language [92]. Each spacetime point therefore carries its own internal coherent-information phase.

The phase variable ϕ is read as an internal compact phase-time coordinate on a local fiber. Each spacetime point carries an internal circle fiber S_ϕ^1 , and the physical spacetime manifold M is equipped with a $U(1)$ phase-time bundle,

$$M \text{ from } P(M, S_\phi^1) \text{ to } S_\phi^1, \quad \phi \in S_\phi^1.$$

Once ϕ is local, a physical comparison of phase values at neighboring spacetime points requires a transport rule between coherent-information fibers.

This is the point at which the local Euler phase becomes a geometric object. Euler's formula supplies the internal phase rotation at each point, while the fiber connection supplies the rule for comparing that rotation between neighboring points of the spacetime manifold. The connection is therefore the bridge between the local complex phase structure and the geometric field structure.

The ordinary phase increment is lifted to the gauge-covariant fiber increment, as in standard Abelian gauge theory [93],

$$D\phi = d\phi - \frac{q}{\hbar}A,$$

or, in components,

$$D\phi = \left(\partial_\mu \phi - \frac{q}{\hbar} A_\mu \right) dx^\mu, \quad \Pi_\mu \equiv \partial_\mu \phi - \frac{q}{\hbar} A_\mu.$$

The gauge-covariant phase strain Π_μ is the invariant object that carries the physical phase gradient.

The phase-time increment on the bundle is then

$$dt_\phi = \tau_C^{(\omega)} \chi e^{-i\phi} D\phi.$$

Equivalently,

$$dt_\phi = \tau_C^{(\omega)} \chi e^{-i\phi} \left[d\phi - \frac{q}{\hbar} A \right].$$

This is the bundle form of the UiT phase-time law. The factor χ determines the local phase-time capacity or fiber length, while $A = A_\mu dx^\mu$ is the connection that transports the internal phase-time coordinate between neighboring fibers.

The covariant phase increment is part of the physical phase-time line element. The mathematical structure is Kaluza–Klein type [94] [95]: a compact fiber coordinate appears together with a connection inside a metric contribution. In a standard compact-fiber construction one writes a fiber contribution of the form

$$dS^2 = g_{\mu\nu}dx^\mu dx^\nu + R^2(d\phi + \kappa A_\mu dx^\mu)^2.$$

In UiT the compact coordinate is the internal phase-time coordinate, and the corresponding contribution is

$$dS_{\text{UiT}}^2 = g_{\mu\nu}^{(I)}dx^\mu dx^\nu + c^2 \left(\tau_C^{(\omega)} \right)^2 \chi^2 (D\phi)^2.$$

The phase factor remains in the phase-time increment, but the physical fiber length is the Hermitian product $dt_\phi^* dt_\phi$. Therefore $e^{+i\phi}e^{-i\phi} = 1$, and the metric fiber term contains $(D\phi)^2$ rather than $e^{-2i\phi}(D\phi)^2$.

6.8 Electromagnetic Curvature

The electromagnetic potential appears as the connection required for comparing the coherent internal phase-time fiber across spacetime, matching the standard gauge-geometric reading of electromagnetism [91]. A connection is physically detected through its curvature. Electromagnetic curvature is therefore the curvature of transported Euler phase-time. The curvature of the phase-time connection is the exterior derivative of the connection [242]

$$F = dA,$$

or, in components,

$$F_{\mu\nu} = \partial_\mu A_\nu - \partial_\nu A_\mu.$$

The gauge transformation is the ordinary change of local fiber coordinate,

$$\phi \text{ to } \phi + \frac{q}{\hbar}\alpha(x), \quad A \text{ to } A + d\alpha,$$

under which $D\phi$ remains invariant:

$$D\phi \text{ to } D\phi.$$

For a phase-coupled field this same structure is expressed by the covariant derivative

$$D_\mu = \partial_\mu + i\frac{q}{\hbar}A_\mu.$$

Acting on $\Xi = \chi e^{-i\phi}$, one obtains

$$D_\mu \Xi = \left(\partial_\mu + i \frac{q}{\hbar} A_\mu \right) \Xi = e^{-i\phi} [\partial_\mu \chi - i \chi \Pi_\mu].$$

This single expression contains the clock-rate branch $\partial_\mu \chi$ and the fiber-connection branch Π_μ . The electromagnetic field is the curvature of this connection; the physical phase-gradient object is the gauge-covariant strain Π_μ .

The commutator of two covariant derivatives gives

$$[D_\mu, D_\nu] \psi = i \frac{q}{\hbar} (\partial_\mu A_\nu - \partial_\nu A_\mu) \psi = i \frac{q}{\hbar} F_{\mu\nu} \psi.$$

6.9 Maxwell Equations from Phase-Time Curvature

Since this curvature is an exterior derivative, the first Maxwell pair follows identically from $d^2 = 0$:

$$\boxed{dF = 0.}$$

In components this is the cyclic identity

$$\partial_\lambda F_{\mu\nu} + \partial_\mu F_{\nu\lambda} + \partial_\nu F_{\lambda\mu} = 0.$$

With the standard identifications

$$E_i = F_{i0}, \quad B_i = -\frac{1}{2} \epsilon_{ijk} F_{jk},$$

the cyclic identity gives the homogeneous Maxwell equations,

$$\nabla \cdot B = 0,$$

and

$$\nabla \times E + \frac{\partial B}{\partial t} = 0.$$

The remaining Maxwell pair follows from the lowest-order local curvature action coupled to the phase-writing current. The compact gauge equations are written in rationalized Heaviside–Lorentz units, with SI factors recovered by the usual rescaling of fields and sources [243]:

$$S_{\text{EM}} = \int d^4x \sqrt{-g^{(I)}} \left[-\frac{1}{4} F_{\mu\nu} F^{\mu\nu} - J^\mu A_\mu \right].$$

Varying the action with respect to A_μ gives

$$\boxed{\nabla_\nu F^{\nu\mu} = J^\mu.}$$

In flat spacetime this reduces to

$$\partial_\nu F^{\nu\mu} = J^\mu.$$

Thus the source J^μ is the current of matter modes coupled to the phase-time connection.

Writing the current as

$$J^\mu = (\rho, \mathbf{J}),$$

and separating temporal and spatial components gives the remaining Maxwell equations,

$$\nabla \cdot E = \rho,$$

and

$$\nabla \times B - \frac{\partial E}{\partial t} = \mathbf{J}.$$

6.10 Charge and Current as Phase-Writing Sources

The coupling q labels how strongly a matter carrier couples to the U(1) phase-time connection [243]. In the closed spherical phase-time matter model developed below, electric charge is the electromagnetic reading of the carrier's oriented phase projection or holonomy [242]. The current J^μ is therefore the macroscopic phase-writing current of charge-carrying matter. Later sections develop the closed spherical phase-time carrier and distinguish the U(1) charge sector from internal SU(3) color orientation.

$$Q_{\text{em}} = Q(\Phi_{\text{U}(1)}).$$

This identifies electric charge with the U(1) phase-time-holonomy reading of the matter carrier, while the later strong-sector discussion treats color as an internal SU(3) orientation.

6.11 The U(1) Phase Fiber on the Two-Sphere Interface

The coherent electromagnetic branch can now be placed back into the two-sphere geometry of the theory, using the standard fiber-bundle language of local phase transport [43]. The outer sphere represents potential information, the inner sphere represents the realized distinct-plus-dispersed domain, and the present is the interface across which potential distinctions become distinct records with dispersed thermodynamic cost. Denote this interface by

$$\Sigma_{\text{now}} = \partial(I_{\text{dist}} + I_{\text{disp}}) = \partial I_{\text{pot}}. \tag{435}$$

On this interface, coherent realization carries a phase coordinate, the local $U(1)$ freedom familiar from gauge geometry [44]. In the coherent branch this phase coordinate is the informational coordinate itself,

$$dI_\phi = d\phi. \quad (436)$$

Thus the present interface carries a compact internal phase-time fiber,

$$\phi : \Sigma_{\text{now}} \text{ to } S^1, \quad e^{-i\phi(x)} \in U(1). \quad (437)$$

Equivalently, the local relation between potential and realized amplitudes may be represented by a complex coordinate

$$z(x) = \frac{\psi_{\text{dist+disp}}(x)}{\psi_{\text{pot}}(x)} = \rho(x)e^{-i\phi(x)}, \quad (438)$$

with the compactified complex coordinate living on the Riemann sphere,

$$z \in \mathbb{C} \cup \{\infty\} \simeq \mathbb{CP}^1 \simeq S^2. \quad (439)$$

The electromagnetic $U(1)$ sector is the local phase freedom of this coherent interface coordinate,

$$z(x) \text{ to } e^{-i\alpha(x)}z(x). \quad (440)$$

Local comparison of this phase between neighboring points on Σ_{now} requires a connection. This connection is the electromagnetic potential,

$$D\phi = d\phi - \frac{q}{\hbar}A, \quad \Pi_\mu = \partial_\mu\phi - \frac{q}{\hbar}A_\mu. \quad (441)$$

The curvature of this phase connection is

$$F = dA, \quad F_{\mu\nu} = \partial_\mu A_\nu - \partial_\nu A_\mu. \quad (442)$$

The electromagnetic field is therefore the curvature of coherent phase transport on the present interface. The $U(1)$ sector is already contained in the two-sphere model as the local phase freedom of coherent realization across the interface between potential information and the realized sector $I_{\text{dist}} + I_{\text{disp}}$. The weak-sector discussion below extends the same interface geometry by treating the two signs of realized linear time as a local doublet: forward writing from I_{pot} into $I_{\text{dist}} + I_{\text{disp}}$, and negative-time unwriting from $I_{\text{dist}} + I_{\text{disp}}$ back into I_{pot} .

The derivation can now be read as one chain. Coherent informational change is represented by phase displacement, $dI_\phi = d\phi$. Local coherent phase requires a compact phase-time fiber. Comparing neighboring fibers requires a connection A_μ . The curvature of that connection is $F_{\mu\nu}$. The identity $dF = 0$ gives the homogeneous Maxwell equations, while variation of the quadratic curvature action coupled to J^μ gives $\nabla_\nu F^{\nu\mu} = J^\mu$. Electromagnetism is therefore the fiber-curvature dynamics of the coherent phase branch of the same complex time-load field whose clock-rate-amplitude branch yields inertia and gravitation through gradients of χ .

6.12 Metric Re-Derivation of the Electromagnetic Connection

The preceding derivation obtained electromagnetism directly from local phase-time transport, while the metric form parallels the Kaluza-Klein mechanism for reading gauge connection as mixed geometry [94] [95]. The same result can be written in metric language by inserting the full gauge-covariant phase-time increment into the spacetime line element. This gives a second reading of the same structure: the electromagnetic connection is the mixed metric connection between spacetime and the compact phase-time fiber, with the ordinary Maxwell field recovered as the curvature of that connection [243].

The direct phase-time force construction begins from

$$\Xi(x) = \chi(x)e^{-i\phi(x)}$$

and

$$U_\phi = mc^2\Xi.$$

The gradient force is

$$\mathbf{F} = -mc^2e^{-i\phi}\nabla\chi + imc^2\chi e^{-i\phi}\nabla\phi.$$

The $\nabla\chi$ branch is the clock-rate, inertial, and gravitational branch. The $\nabla\phi$ branch is the coherent phase branch, and it requires a local transport rule because ϕ lives on a compact fiber,

$$\phi \in S_\phi^1.$$

The already-derived covariant fiber increment is

$$D\phi = d\phi - \frac{q}{\hbar}A,$$

or, in components,

$$D\phi = \left(\partial_\mu\phi - \frac{q}{\hbar}A_\mu \right) dx^\mu \equiv \Pi_\mu dx^\mu.$$

The full phase-time increment is therefore

$$dt_\phi = \tau_C^{(\omega)}\chi e^{-i\phi}D\phi.$$

A purely naive substitution would insert $d\phi$ into the metric. The phase-time substitution fixed by the fiber derivation inserts the covariant increment,

$$dt_\phi = \tau_C^{(\omega)}\chi e^{-i\phi} \left(d\phi - \frac{q}{\hbar}A_\mu dx^\mu \right).$$

Starting from the local Minkowski form,

$$ds^2 = c^2dt^2 - d\mathbf{x}^2,$$

the physical phase-fiber interval is obtained from the Hermitian length $dt_\phi^*dt_\phi$:

$$dt_\phi^*dt_\phi = \left(\tau_C^{(\omega)} \right)^2 \chi^2 \left(e^{+i\phi} e^{-i\phi} \right) (D\phi)^2 = \left(\tau_C^{(\omega)} \right)^2 \chi^2 (D\phi)^2.$$

Thus

$$ds_\phi^2 = c^2 \left(\tau_C^{(\omega)} \right)^2 \chi^2 (D\phi)^2 - d\mathbf{x}^2.$$

This is the metric form of the phase-time fiber construction. Written over the informational space-time metric, the physical fiber contribution is

$$dS_\phi^2 = g_{\mu\nu}^{(I)} dx^\mu dx^\nu + c^2 \left(\tau_C^{(\omega)} \right)^2 \chi^2 (D\phi)^2.$$

The sign of the fiber term follows the metric convention. The structural object is the Hermitian covariant phase-time fiber length.

Define the local phase-fiber radius

$$R_\phi = c\tau_C^{(\omega)}\chi.$$

Since

$$c\tau_C^{(\omega)} = \frac{\hbar}{mc},$$

this becomes

$$R_\phi = \frac{\hbar}{mc}\chi = \lambda_C^{(\omega)}\chi.$$

The radius R_ϕ is the Compton-scaled phase-fiber radius of the matter carrier whose phase is transported. It is not a photon mass scale. The massless electromagnetic field is carried by the connection A_μ and its curvature $F_{\mu\nu}$.

The phase-time metric can then be written as

$$dS_\phi^2 = g_{\mu\nu}^{(I)} dx^\mu dx^\nu + R_\phi^2 \left(d\phi - \frac{q}{\hbar} A_\mu dx^\mu \right)^2.$$

Expanding the fiber square gives

$$(D\phi)^2 = d\phi^2 - 2\frac{q}{\hbar} d\phi A_\mu dx^\mu + \frac{q^2}{\hbar^2} A_\mu A_\nu dx^\mu dx^\nu.$$

Therefore

$$dS_\phi^2 = g_{\mu\nu}^{(I)} dx^\mu dx^\nu + R_\phi^2 \left[d\phi^2 - 2\frac{q}{\hbar} d\phi A_\mu dx^\mu + \frac{q^2}{\hbar^2} A_\mu A_\nu dx^\mu dx^\nu \right].$$

The mixed spacetime–fiber term identifies the gauge potential as a metric connection,

$$g_{\mu\phi} \propto -\frac{q}{\hbar} R_\phi^2 A_\mu.$$

Thus A_μ is the mixed connection between spacetime and the phase-time fiber. In the direct derivation A_μ was the transport rule for comparing neighboring phase-time fibers; in the metric reading the same object appears as the off-diagonal phase-fiber connection.

The curvature of this connection is

$$F = dA,$$

or

$$F_{\mu\nu} = \partial_\mu A_\nu - \partial_\nu A_\mu.$$

The same covariant phase increment is invariant under a local fiber-coordinate change,

$$\phi \text{ to } \phi + \frac{q}{\hbar}\alpha(x), \quad A \text{ to } A + d\alpha,$$

so that

$$D\phi \text{ to } D\phi.$$

The electromagnetic field is therefore the curvature of the same phase-time connection that appears as the mixed metric component of the fiber metric.

The Euler factor remains in the phase-time field and in the phase-time increment,

$$\Xi = \chi e^{-i\phi}, \quad dt_\phi = \tau_C^{(\omega)} \chi e^{-i\phi} D\phi.$$

The physical metric length is the Hermitian projection,

$$dt_\phi^* dt_\phi = \left(\tau_C^{(\omega)}\right)^2 \chi^2 (D\phi)^2,$$

so the phase cancels in the squared fiber length. The coherent phase projection is carried by the connection and its curvature, while the physical metric fiber length is carried by $R_\phi^2(D\phi)^2$.

The two electromagnetic derivations therefore meet at the same object:

$$\Xi = \chi e^{-i\phi} \quad \text{implies} \quad D\phi = d\phi - \frac{q}{\hbar}A \quad \text{implies} \quad F = dA.$$

In the direct derivation this appears as local phase transport and curvature. In the metric derivation it appears as the mixed spacetime–phase component of the phase-time fiber metric.

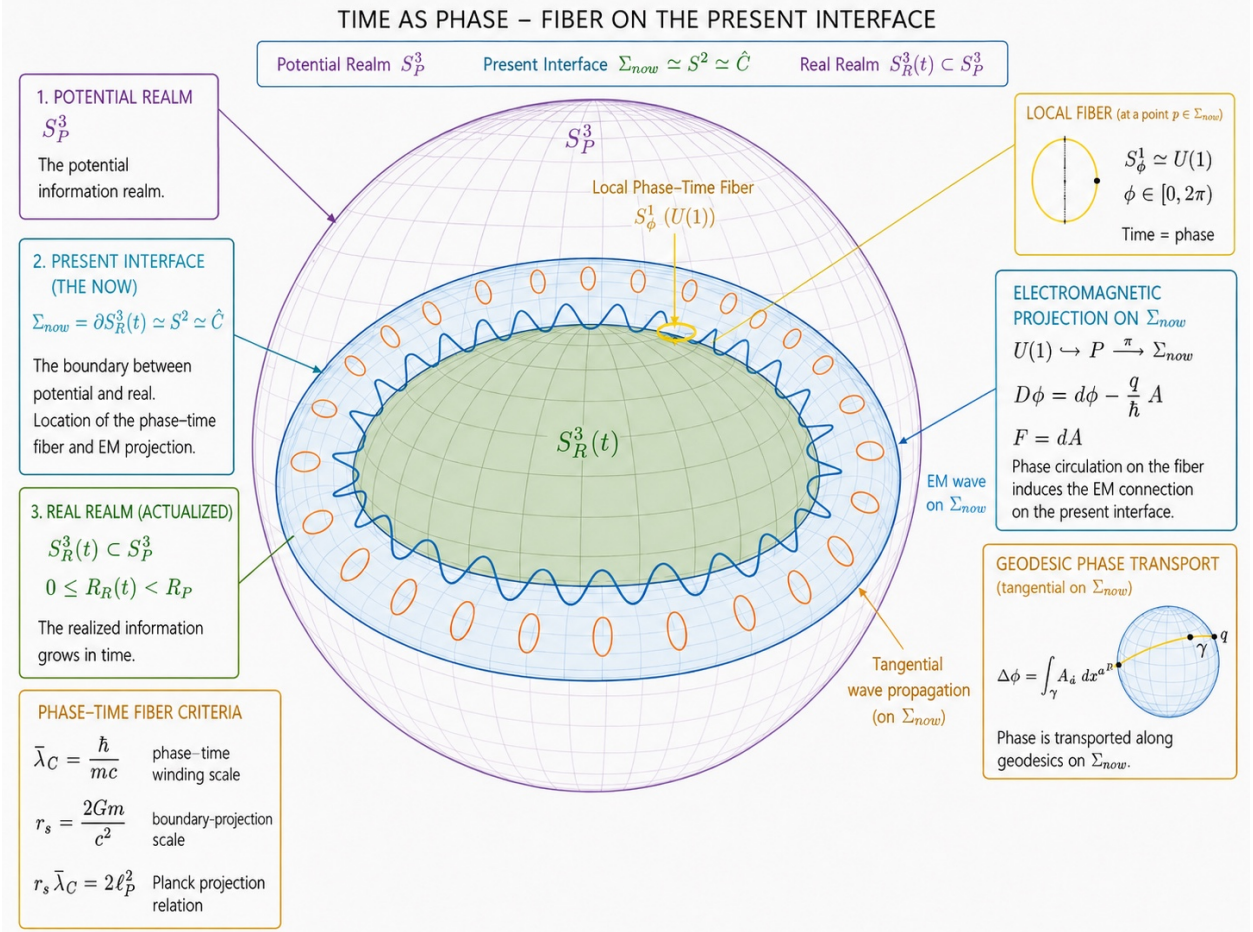


Figure 2: Time as phase: a local $U(1)$ phase-time fiber on the present interface Σ_{now} , with electromagnetic projection and geodesic phase transport represented on the two-sphere boundary between potential information and the realized sector $I_{\text{dist}} + I_{\text{disp}}$.

7 The Weak Interaction Sector

This section develops the weak sector as ordinary thermodynamics when the sign of realized linear time is negative. In forward realized time, potential information is consumed and written as distinct information together with dispersed information,

$$-dI_{\text{pot}} = dI_{\text{dist}} + dI_{\text{disp}}.$$

When the realized linear-time projection has negative sign, the same thermodynamic relation is read in the reverse direction,

$$-dI_{\text{dist}} - dI_{\text{disp}} = dI_{\text{pot}}.$$

Thus the weak interaction is the local channel in which a written distinct record and its dispersed thermodynamic component are returned to potential information, and then rewritten as another stable Compton phase-time resonance. The dispersed component is essential: in forward writing it is released as the thermodynamic cost of record formation; under negative linear time it returns from the environment as ordered erasure action that participates in removing the distinct record.

A weak event acts on the flavor-resonance sector of the closed spherical Compton phase-time carrier,

$$|f_i\rangle \text{ to } |f_j\rangle,$$

with

$$|f_i\rangle = |\omega_{C,i}\rangle, \quad |f_j\rangle = |\omega_{C,j}\rangle,$$

and

$$\omega_{C,f} = \frac{m_f c^2}{\hbar}.$$

The weak sector therefore rewrites one stable Compton phase-time writing resonance into another. Its rate is controlled by the number of bits that must be unwritten and rewritten; its gauge geometry is the usual electroweak $SU(2) \times U(1)$ interface; and its force form is the negative-linear-time projection of the same unified phase-time gradient structure.

7.1 Phase-Time Form of the Second Law

Ordinary irreversible thermodynamics on the forward record-forming branch begins from entropy generation,

$$dS_{\text{gen}} \geq 0,$$

and in rate form,

$$\dot{S}_{\text{gen}} = \frac{dS_{\text{gen}}}{dt} \geq 0.$$

In UiT, realized linear time is the real projection of phase-time. The full phase-time increment of a massive mode is

$$dt_\phi = \tau_C^{(\omega)} \chi e^{-i\phi} d\phi,$$

with the angular Compton time

$$\tau_C^{(\omega)} = \frac{1}{\omega_C} = \frac{\hbar}{mc^2},$$

where, in a weak rewrite event, m denotes the mass scale of the relevant parent or rewritten Compton mode. The local registration factor is

$$\chi = \frac{dI_{\text{dist}}}{dI_{\text{disp}}} = \frac{dI_{\text{dist}}}{dS/(k_B \ln 2)}.$$

The realized linear-time projection is

$$d\tau = \Re(dt_\phi) = \tau_C^{(\omega)} \chi \cos \phi d\phi.$$

The sign of $d\tau$ is therefore the sign of $\cos \phi$. For

$$\cos \phi > 0,$$

one has

$$d\tau > 0.$$

This is the forward-writing branch. Potential information is consumed and becomes distinct information plus dispersed information,

$$-dI_{\text{pot}} = dI_{\text{dist}} + dI_{\text{disp}}.$$

Here

$$dI_{\text{pot}} < 0, \quad dI_{\text{dist}} > 0, \quad dI_{\text{disp}} > 0.$$

The distinct term is the written record. The dispersed term is the thermodynamic cost of writing.

For

$$\cos \phi < 0,$$

one has

$$d\tau < 0.$$

The same thermodynamic bookkeeping is then read in the reverse direction,

$$-dI_{\text{dist}} - dI_{\text{disp}} = dI_{\text{pot}}.$$

Here

$$dI_{\text{dist}} < 0, \quad dI_{\text{disp}} < 0, \quad dI_{\text{pot}} > 0.$$

The distinct record is removed, and the dispersed component returns from the environment as ordered erasure action. Together they return the local realized record to the potential domain. This is the thermodynamic basis of the weak sector:

$$\boxed{\text{weak rewrite} = \text{ordinary thermodynamics evaluated at } d\tau < 0.}$$

Thus the weak interaction is the same thermodynamic writing law with the sign of realized linear time reversed.

7.2 Local Weak Rewrite Rate in Compton Time

The weak sector is selected by the negative sign of realized linear time:

$$d\tau = \tau_C^{(\omega)} \chi \cos \phi d\phi < 0, \quad \cos \phi < 0.$$

On this branch,

$$-dI_{\text{dist}} - dI_{\text{disp}} = dI_{\text{pot}}.$$

Define the weak rewrite-bit increment as the positive amount of distinct-plus-dispersed realized content returned to the potential domain,

$$dI_w = -(dI_{\text{dist}} + dI_{\text{disp}}) = dI_{\text{pot}} \quad (d\tau < 0).$$

The associated bit density along the phase coordinate is

$$J_w(\phi) = \frac{dI_w}{d\phi}.$$

Since ϕ is dimensionless,

$$[J_w] = 1.$$

The local weak rewrite rate is the rewrite-bit rate per Compton time on the negative linear-time part of the cycle. Since $-\cos \phi > 0$ on this branch,

$$\boxed{\lambda_{\text{weak}}^{\text{local}} \sim \frac{\ln 2}{\tau_C^{(\omega)} \chi} \frac{dI_w}{d\phi} (-\cos \phi), \quad \cos \phi < 0.}$$

The units are

$$[\tau_C^{(\omega)}] = s, \quad \left[\frac{dI_w}{d\phi} \right] = 1, \quad [-\cos \phi] = 1,$$

so

$$[\lambda_{\text{weak}}^{\text{local}}] = s^{-1}.$$

This local rate is the native weak-sector expression: rewrite bits per Compton time on the negative realized-time branch.

7.3 Integral Rewrite Barrier and Bit Suppression

The local rate describes where the weak channel is active. The transition probability is governed by the integrated rewrite-bit barrier.

Using

$$dI_w = -(dI_{\text{dist}} + dI_{\text{disp}}) = dI_{\text{pot}} \quad (d\tau < 0),$$

the total weak rewrite cost is

$$\Delta I_w = \int_{\cos \phi < 0} \frac{dI_w}{d\phi} (-\cos \phi) d\phi.$$

If the path variable $dI_w/d\phi$ is already defined only on the weak-accessible branch, the same barrier may be written simply as

$$\Delta I_w = \int_{\phi_i}^{\phi_f} \frac{dI_w}{d\phi} d\phi.$$

In entropy units, the same positive barrier is

$$\Delta S_{\text{rewrite}} = k_B \ln 2 \Delta I_w.$$

Therefore

$$B_{\text{eff}} = \frac{\Delta S_{\text{rewrite}}}{k_B} = \ln 2 \Delta I_w.$$

The transition weight is

$$p_{\text{weak}} = e^{-B_{\text{eff}}} = \exp[-\ln 2 \Delta I_w] = 2^{-\Delta I_w}.$$

The weak decay rate is the microscopic attempt rate multiplied by this rewrite weight:

$$\lambda_{\text{weak}} = \frac{1}{\tau_0} 2^{-\Delta I_w},$$

or equivalently,

$$\lambda_{\text{weak}} = \frac{1}{\tau_0} e^{-\Delta S_{\text{rewrite}}/k_B}.$$

The half-life is

$$T_{1/2} = \frac{\ln 2}{\lambda_{\text{weak}}} = \tau_0 \ln 2 2^{\Delta I_w}.$$

Thus

$$\Delta I_w = \log_2 \left(\frac{T_{1/2}}{\tau_0 \ln 2} \right).$$

The weak event can now be written as the information bookkeeping law

$$-dI_{\text{parent}}(\phi_\tau) = \sum_i dI_i^{\text{daughter}} + dI_\nu + dI_w,$$

where the daughter terms are the newly written stable closures, dI_ν is the coherent residual phase-time closure carried by the neutrino or antineutrino, and dI_w is the bit cost of returning the previous distinct-plus-dispersed record to the potential domain and rewriting it. Here $-dI_{\text{parent}}(\phi_\tau)$ denotes the parent closure content being opened, while dI_w denotes the positive rewrite-bit barrier of the return-to-potential and rewrite operation. This keeps the parent content and the rewrite cost distinct in the bookkeeping. This reconstruction remains aligned with parity violation [144] [145], the V–A weak-current formulation [146] [147], the electroweak structure of Glashow [148], Weinberg [149], and Salam [150], and irreversible thermodynamics [33].

7.4 The Rewrite Mechanism

In the two-sphere model, the outer sphere is potential information and the inner sphere contains the realized distinct-plus-dispersed record. Forward growth is described by

$$-dI_{\text{pot}} = dI_{\text{dist}} + dI_{\text{disp}}.$$

The weak event is the same thermodynamic bookkeeping under negative realized linear time,

$$d\tau < 0, \quad \cos \phi < 0.$$

Then the local record is unwritten according to

$$-dI_{\text{dist}} - dI_{\text{disp}} = dI_{\text{pot}}.$$

The dispersed term is not omitted. It is the thermodynamic component that was released during forward writing; in the negative-time part of the weak event it returns from the environment as ordered erasure action and participates in removing the distinct record.

A weak decay therefore has the information path

$$I_{\text{dist}}^{(i)} + I_{\text{disp}}^{(i)} \text{ to } I_{\text{pot}} \text{ to } I_{\text{dist}}^{(j)} + I_{\text{disp}}^{(j)}.$$

In flavor language,

$$|f_i\rangle \text{ to } |f_j\rangle.$$

In Compton language,

$$|\omega_{C,i}\rangle \text{ to } |\omega_{C,j}\rangle.$$

For a massive matter state, this means that the flavor resonance of the closed spherical Compton phase-time carrier is rewritten from one stable Compton phase-time writing eigenmode into another. The rewrite carries a bit cost and can produce unstable daughter products. This is the sense in which the weak interaction acts as a thermodynamic rewrite mechanism within the electroweak tradition of Glashow [148], Weinberg [149], and Salam [150].

7.5 The Neutrino as Residual Phase-Time Closure

The neutrino has a natural place in the rewrite mechanism. In standard weak-interaction physics, the neutrino enters beta decay as the neutral lepton required by the weak transition, with its modern role supported by Fermi's beta-decay theory, the direct detection of the neutrino, and neutrino oscillation experiments that establish nonzero mass differences. [151] [152] [153] [154] [155] [156] [157] [158] In the present framework, the same object is interpreted as the neutral residual phase-time closure of the parent particle's internal phase after a weak rewrite event.

In the information bookkeeping of the weak event, the parent record is not represented by a single undifferentiated realized quantity. It contains a distinct part and a dispersed part. The negative-time part of the weak process is

$$-dI_{\text{dist}} - dI_{\text{disp}} = dI_{\text{pot}}.$$

The dispersed term is therefore part of the closure: it is the thermodynamic component that returns from the environment and participates in erasing the distinct parent record before the daughter closure is written.

Radioactive decay is therefore a redistribution of a parent closed spherical Compton phase-time carrier. The parent structure is locally opened by the weak branch, its internal phase content is repartitioned, daughter closures are written, and the thermodynamic cost of the rewrite is paid. Total informational closure is preserved by assigning every part of the parent phase content to a realized daughter closure, a dispersive cost, or a coherent residual carrier.

In the closed spherical phase-time matter model, mass corresponds to closed internal Compton phase circulation. The internal phase is read as a phase-time quantum locked into spherical recurrence. For any massive carrier, the Compton frequency is

$$\omega_C = \frac{mc^2}{\hbar}, \quad (443)$$

and the corresponding mass-information writing rate is

$$\dot{I}_m = \frac{mc^2}{h}. \quad (444)$$

This is a normalized Compton writing rate measured in bit-equivalent internal Compton cycles per second, not entropy-produced thermodynamic bits per second.

Thus a particle with nonzero rest mass corresponds to a closed Compton phase recurrence. A small mass corresponds to a small Compton writing rate. The neutrino may therefore carry a complete neutral phase-time mass closure whose internal writing rate is small.

During a weak rewrite event, the internal phase locked in the parent closed spherical Compton phase-time carrier is partitioned into three contributions. The first contribution closes the daughter closed phase-time structures. The second contribution is dispersed as the thermodynamic cost of rewriting. The third contribution remains as a coherent residual phase-time closure. This residual neutral closure is identified with the neutrino or antineutrino.

The phase bookkeeping of the rewrite may be written schematically as

$$\Phi_{\text{parent}} = \sum_i \Phi_i^{\text{daughter}} + \Phi_\nu + \Phi_{\text{disp}}. \quad (445)$$

Equivalently, in energetic form,

$$E_{\text{parent}}^\phi = \sum_i E_i^\phi + E_\nu^\phi + E_{\text{disp}}. \quad (446)$$

Here E_{parent}^ϕ is the phase-energy content of the parent closed phase-time closure, E_i^ϕ are the phase-energy contributions used to close the daughter closed phase-time modes, E_{disp} is the thermodynamic dispersive cost, and E_ν^ϕ is the coherent residual phase-energy carried away by the neutrino.

If this residual phase closes into a massive neutral carrier, then

$$E_\nu^\phi = m_\nu c^2, \quad (447)$$

where m_ν denotes a neutrino mass eigencomponent; weak flavor neutrinos are coherent flavor states built from such components.

The corresponding Compton frequency is

$$\omega_{C,\nu} = \frac{m_\nu c^2}{\hbar}, \quad (448)$$

and mass-information writing rate

$$\dot{I}_{m,\nu} = \frac{m_\nu c^2}{h}. \quad (449)$$

This is likewise a normalized Compton recurrence rate, measured in bit-equivalent internal Compton cycles per second rather than entropy-produced thermodynamic bits per second.

The smallness of the neutrino mass is therefore interpreted as the smallness of the residual closed phase-energy after the daughter closures and thermodynamic dispersive cost have been accounted for. The neutrino is a complete neutral residual phase-time closure with a small Compton frequency.

For beta-minus decay,

$$n \text{ to } p + e^- + \bar{\nu}_e, \quad (450)$$

the parent neutron phase-time closure is redistributed into a proton closure, an electron closure, a dispersive rewrite cost, and an antineutrino residual closure:

$$\Phi_n = \Phi_p + \Phi_e + \Phi_{\bar{\nu}_e} + \Phi_{\text{disp}}. \quad (451)$$

For beta-plus decay,

$$p \text{ to } n + e^+ + \nu_e, \quad (452)$$

the residual phase-time closure appears with the opposite weak temporal orientation:

$$\Phi_p = \Phi_n + \Phi_{e^+} + \Phi_{\nu_e} + \Phi_{\text{disp}}. \quad (453)$$

The distinction between neutrino and antineutrino is therefore interpreted as the orientation of the residual weak phase-time closure. The weak interaction locally opens a previous closed phase-time configuration, performs a rewrite-like phase operation, and rejoins the forward record-forming branch by writing the daughter products. The residual phase-time closure carries the remaining orientation information required by the rewrite event.

This also explains why the neutrino is electrically neutral. Electric charge is read in this framework as a U(1) projection of internal phase-time orientation. For the neutrino, the residual phase-time closure has no net electromagnetic projection,

$$Q_\nu = 0, \quad (454)$$

while its weak rewrite projection remains nonzero,

$$\Pi_{\text{weak}}(\nu) \neq 0. \quad (455)$$

Thus the neutrino carries the weak-sector information required to complete the rewrite, while ordinary matter primarily reads electromagnetic charge, strong closure, and large metric load. The compact summary of the mechanism is

$$\nu = \Pi_{\text{weak}} \left(\Phi_{\text{parent}} - \sum_i \Phi_i^{\text{daughter}} - \Phi_{\text{disp}} \right). \quad (456)$$

In words, the neutrino is the weak projection of the coherent phase residue left after the parent closed phase-time closure has been redistributed into daughter closures and thermodynamic dispersal. It is the neutral phase-time carrier of the remaining phase information required for the weak rewrite event to preserve total informational closure.

7.6 Rewrite Barriers, Half-Life Scaling, and Environmental Shifts

At each microscopic step one may consider forward continuation and local negative-time rewrite. The weak bit barrier is defined by the positive number of bits returned from the distinct-plus-dispersed record to the potential domain,

$$\Delta I_w = \int_{\cos \phi < 0} - \left(\frac{dI_{\text{dist}}}{d\phi} + \frac{dI_{\text{disp}}}{d\phi} \right) (-\cos \phi) d\phi.$$

For continuity with the notation used in the decay-rate formulas below, define

$$\Delta I_{\text{disp}}^{\text{rewrite}} \equiv \Delta I_w.$$

Equivalently, in entropy units the same barrier is the rewrite barrier defined above [27] [33]:

$$B_{\text{eff}} = \frac{\Delta S_{\text{rewrite}}}{k_B} = \ln 2 \Delta I_{\text{disp}}^{\text{rewrite}}.$$

The local rewrite transition weight is

$$p_{\text{rewrite}} = e^{-B_{\text{eff}}} = 2^{-\Delta I_{\text{disp}}^{\text{rewrite}}}.$$

For the minimal one bit rewrite cost, $B_{\min} = \ln 2$, so

$$p_{\text{rewrite},\min} = \frac{1}{2}.$$

For N independent steps,

$$P_{\text{rewrite}}(N) = \left(\frac{1}{2}\right)^N = \exp[-(\ln 2)N].$$

Local reversal is therefore possible, but a fully reversed macroscopic history becomes exponentially suppressed.

The decay constant is the microscopic attempt rate multiplied by the rewrite weight. Thus [159]

$$\lambda = \frac{1}{\tau_0} e^{-B_{\text{eff}}} = \frac{1}{\tau_0} 2^{-\Delta I_{\text{disp}}^{\text{rewrite}}}.$$

The survival law becomes

$$P_{\text{surv}}(t) = e^{-\lambda t} = \exp\left[-\frac{t}{\tau_0} e^{-B_{\text{eff}}}\right].$$

The half life is therefore

$$T_{1/2} = \frac{\ln 2}{\lambda} = \tau_0 \ln 2 e^{B_{\text{eff}}}.$$

A microscopic energy bias may be defined through the transition weight,

$$\Delta E_{\text{bias}} = E_{\text{char}} e^{-B_{\text{eff}}} = E_{\text{char}} 2^{-\Delta I_{\text{disp}}^{\text{rewrite}}}.$$

The chain is therefore

$$B_{\text{eff}} \text{ to } e^{-B_{\text{eff}}} \text{ to } \lambda \text{ to } T_{1/2} \text{ to } \Delta E_{\text{bias}}.$$

For alpha decay, the Gamow exponent supplies the effective barrier,

$$B_G = 2\mathcal{G},$$

where \mathcal{G} is the WKB or Gamow exponent. The tunneling weight is therefore

$$p_{\alpha} = e^{-B_G} = e^{-2\mathcal{G}}.$$

The decay constant and half life become

$$\lambda_\alpha = \frac{1}{\tau_0} e^{-2\mathcal{G}}, \quad T_{1/2} = \tau_0 \ln 2 e^{2\mathcal{G}}.$$

Likewise,

$$\Delta E_{\text{bias}} = Q_\alpha e^{-2\mathcal{G}}.$$

The empirical Geiger–Nuttall relation follows,

$$\log_{10} T_{1/2} = a \frac{Z}{\sqrt{Q_\alpha}} + b.$$

In the present theory the Gamow exponent is read as the microscopic informational rewrite barrier, and $e^{-2\mathcal{G}}$ is the corresponding phase-time continuation weight. [159] [160]

For electron capture, the environment changes the local rewrite barrier. Write

$$B_{\text{eff}} = B_{\text{weak}} + \delta B_{\text{env}},$$

so that

$$\lambda_{EC} = \frac{1}{\tau_0} e^{-(B_{\text{weak}} + \delta B_{\text{env}})}.$$

For small environmental shifts,

$$\frac{\delta \lambda}{\lambda} \approx -\delta B_{\text{env}}.$$

In bit language,

$$\delta B_{\text{env}} = \ln 2 \delta I_{\text{env}},$$

so

$$\frac{\delta \lambda}{\lambda} \approx -\ln 2 \delta I_{\text{env}}.$$

Schematically, one may resolve the environmental barrier shift as

$$\delta B_{\text{env}} = \delta B_{\text{conf}} + \delta B_{\text{screen}} + \delta B_T + \delta B_{\text{affinity}}.$$

This is the theoretical place in which the ${}^7\text{Be}$ anomalies enter. Pressure, screening, lattice confinement, and local electronic structure shift the rewrite barrier of the realized branch. Lowering the

barrier increases the electron-capture rate; raising the barrier suppresses it. [161] [162] [163] [164] [165] The weak-sector background remains the electroweak theory of Glashow [148], Weinberg [149], and Salam [150].

7.7 SU(2), U(1), and Electroweak Decomposition of the Two-Sphere Interface

The two spheres model naturally defines a local doublet structure between the written distinct-plus-dispersed sector and the potential sector:

$$\Phi(x) = \begin{pmatrix} \phi_{\text{dist+disp}}(x) \\ \phi_{\text{pot}}(x) \end{pmatrix}.$$

The local patch has two orientations relative to the global realization flow: writing into the realized branch and erasure back toward the potential branch. These two local orientations form a two state complex space. All local norm preserving transformations of this space form U(2). Structurally,

$$\text{U}(2) \cong \frac{\text{SU}(2) \times \text{U}(1)}{\mathbb{Z}_2}.$$

The SU(2) factor rotates the local distinct-plus-dispersed/potential doublet orientation. The U(1) factor is the local phase-time fiber carried by the same patch. The physically projected state sphere is

$$\text{SU}(2)/\text{U}(1) \cong \mathbb{CP}^1 \cong S^2.$$

This is the precise sense in which the two spheres realization carries both sectors at once. The weak-sector geometry is the local two-state motion of a realized patch relative to the potential sphere, accompanied by a local phase-time fiber. In the present theory the electroweak hierarchy is therefore already implicit in the realization structure itself. [148] [149] [150] [166] [167]

The two-sphere interface carries the two ingredients of the electroweak gauge structure.

The first ingredient is the compact phase-time fiber of the present interface. In the complex representation of the interface, a local phase is written as

$$z(x) = \rho(x)e^{-i\phi(x)},$$

with local phase freedom

$$z(x) \text{ to } e^{-i\alpha(x)}z(x).$$

This local phase freedom defines the U(1) phase-time fiber of the interface. In the electromagnetic sector, this same local phase freedom is transported by the gauge connection A_μ .

The second ingredient is the two-state real-time projection of phase-time. The realized-time increment is

$$d\tau = \tau_C^{(\omega)} \chi \cos \phi d\phi.$$

The two signs of the real projection define a local doublet of temporal writing orientation,

$$\psi_+ \sim \cos \phi > 0, \quad \psi_- \sim \cos \phi < 0.$$

Equivalently, the doublet may be read as the two local directions of the two-sphere interface,

$$\psi_+ \sim -dI_{\text{pot}} = dI_{\text{dist}} + dI_{\text{disp}}, \quad \psi_- \sim -dI_{\text{dist}} - dI_{\text{disp}} = dI_{\text{pot}}.$$

Thus the local temporal doublet is

$$\Psi_\tau(x) = \begin{pmatrix} \psi_+(x) \\ \psi_-(x) \end{pmatrix}.$$

The norm-preserving local transformations of this doublet form $U(2)$,

$$\Psi_\tau(x) \text{ to } U(x)\Psi_\tau(x), \quad U(x) \in U(2).$$

The group $U(2)$ decomposes as

$$U(2) \simeq \frac{SU(2) \times U(1)}{\mathbb{Z}_2}.$$

In UiT this decomposition has a direct interface interpretation. The $SU(2)$ factor acts on the two-state temporal writing/unwriting doublet. The $U(1)$ factor acts on the compact phase-time fiber of the same interface. The quotient by \mathbb{Z}_2 identifies the shared central phase and prevents double-counting of the common sign structure.

The corresponding electroweak covariant derivative may therefore be written in the standard form

$$D_\mu \Psi_\tau = \left[\partial_\mu + igW_\mu^a \frac{\sigma_a}{2} + ig'B_\mu \frac{Y}{2} \right] \Psi_\tau.$$

Here W_μ^a is the local connection of the $SU(2)$ temporal doublet, B_μ is the local connection of the $U(1)_Y$ hypercharge phase-time fiber, σ_a are the Pauli generators, g is the $SU(2)$ coupling, g' is the $U(1)_Y$ coupling, and Y is the hypercharge assignment of the transported field. In this notation, B_μ denotes the pre-rotation hypercharge phase connection, while A_μ denotes the electromagnetic connection obtained after the Weinberg rotation.

Here Ψ_τ is the temporal-orientation substrate whose transport is read at low energy through the usual $SU(2)_L$ action on left-handed matter doublets.

The electric charge generator is then

$$Q = T_3 + \frac{Y}{2},$$

where

$$T_3 = \frac{\sigma_3}{2}.$$

The electromagnetic and neutral weak gauge fields are obtained by the usual electroweak rotation,

$$A_\mu = B_\mu \cos \theta_W + W_\mu^3 \sin \theta_W,$$

$$Z_\mu = -B_\mu \sin \theta_W + W_\mu^3 \cos \theta_W.$$

The electric coupling is

$$e = g \sin \theta_W = g' \cos \theta_W.$$

Thus the two-sphere interface supplies the local electroweak substrate: the $SU(2)$ connection transports the two-state temporal writing doublet, while the $U(1)$ connection transports the compact phase-time fiber. Electromagnetism appears as the unbroken phase-transport branch after the electroweak rotation, and the weak sector appears as the local rewrite dynamics of the temporal doublet.

In this reading, the electroweak structure is the gauge decomposition of the same phase-time interface that already produced the $U(1)$ electromagnetic fiber and the $SU(2)$ temporal doublet.

7.8 Weak Rewrite Scale, Electroweak Boson Masses, and the Metric Weinberg Angle

We now calibrate the weak rewrite scale using the measured strength of the weak interaction. Work in natural units,

$$\hbar = c = 1.$$

At low energies, the effective weak interaction is measured by the Fermi constant,

$$G_F = 1.1663787 \times 10^{-5} \text{ GeV}^{-2}.$$

The weak rewrite scale is defined by

$$E_{\text{rewrite}} \equiv v = \frac{1}{\sqrt{\sqrt{2} G_F}}.$$

Substituting the measured value of G_F ,

$$E_{\text{rewrite}} = v = \frac{1}{\sqrt{\sqrt{2} \cdot 1.1663787 \times 10^{-5}}} \simeq 246.22 \text{ GeV}.$$

The same scale has a bit-rate reading in UIT. Since a rewrite barrier is measured in bits, the electroweak rewrite scale can be written as

$$E_{\text{rewrite}} = \hbar \ln 2 \dot{I}_w^{\text{EW}}.$$

Equivalently,

$$\dot{I}_w^{\text{EW}} = \frac{E_{\text{rewrite}}}{\hbar \ln 2}.$$

In the natural units used in this subsection,

$$E_{\text{rewrite}} = \ln 2 \, I_w^{\text{EW}}.$$

This bit-rate reading interprets the calibrated electroweak rewrite scale from G_F in the native information language of UIT.

The weak rewrite interface carries the local doublet Ψ_τ . When the interface has a fixed rewrite norm, write

$$\langle \Psi_\tau \rangle = \frac{1}{\sqrt{2}} \begin{pmatrix} 0 \\ E_{\text{rewrite}} \end{pmatrix}.$$

The gauge-covariant metric energy of the doublet contains

$$(D_\mu \Psi_\tau)^\dagger (D^\mu \Psi_\tau).$$

Substituting the fixed rewrite norm gives the gauge-field mass terms

$$(D_\mu \Psi_\tau)^\dagger (D^\mu \Psi_\tau) \supset \frac{g^2 E_{\text{rewrite}}^2}{8} [(W_\mu^1)^2 + (W_\mu^2)^2] + \frac{E_{\text{rewrite}}^2}{8} (gW_\mu^3 - g'B_\mu)^2.$$

With

$$W_\mu^\pm = \frac{1}{\sqrt{2}} (W_\mu^1 \mp iW_\mu^2),$$

the charged sector gives

$$m_W^2 = \frac{g^2 E_{\text{rewrite}}^2}{4}, \quad m_W = \frac{g}{2} E_{\text{rewrite}}.$$

The neutral massive direction is

$$Z_\mu = \frac{gW_\mu^3 - g'B_\mu}{\sqrt{g^2 + g'^2}},$$

while the orthogonal phase-transport direction is the photon,

$$A_\mu = \frac{g'W_\mu^3 + gB_\mu}{\sqrt{g^2 + g'^2}}.$$

Hence

$$m_Z^2 = \frac{(g^2 + g'^2) E_{\text{rewrite}}^2}{4}, \quad m_Z = \frac{1}{2} \sqrt{g^2 + g'^2} E_{\text{rewrite}},$$

and

$$m_A = 0.$$

The neutral mixing angle is therefore determined by

$$\tan \theta_W = \frac{g'}{g},$$

so that

$$\frac{m_W}{m_Z} = \frac{g}{\sqrt{g^2 + g'^2}} = \cos \theta_W.$$

In UiT this angle is read geometrically. It is the projection angle between the compact $U(1)$ phase-time fiber and the neutral direction of the $SU(2)$ rewrite fiber on the two-sphere interface.

The electromagnetic phase-fiber radius has already been defined as

$$R_\phi = c\tau_C^{(\omega)}\chi = \lambda_C^{(\omega)}\chi.$$

For the weak rewrite interface, the corresponding rewrite-fiber scale is

$$R_\tau = \frac{\hbar}{E_{\text{rewrite}}}\chi_\tau.$$

Thus the electroweak interface contains two fiber scales,

$$R_\phi \quad \text{and} \quad R_\tau.$$

The $U(1)$ coupling measures phase transport on the compact phase-time fiber, while the $SU(2)$ coupling measures transport on the rewrite doublet fiber. Geometrically,

$$g'_{\text{eff}} \propto \frac{1}{R_\phi}, \quad g_{\text{eff}} \propto \frac{1}{R_\tau}.$$

Therefore the neutral mixing angle is the projection angle between the two fiber directions,

$$\tan \theta_{\text{UiT}} = \frac{g'_{\text{eff}}}{g_{\text{eff}}} \sim \frac{R_\tau}{R_\phi}.$$

In the flat-fiber approximation, the neutral electroweak fiber metric is diagonal,

$$G_{\text{EW}}^{(0)} = \begin{pmatrix} R_\tau^2 & 0 \\ 0 & R_\phi^2 \end{pmatrix}.$$

This gives the tree-level electroweak projection,

$$\frac{m_W}{m_Z} = \cos \theta_{\text{UiT}}.$$

The two-sphere interface contains a shared realization boundary between the $U(1)$ phase-time fiber and the $SU(2)$ rewrite doublet. Structurally,

$$U(2) \simeq \frac{SU(2) \times U(1)}{\mathbb{Z}_2},$$

so the phase-time fiber and the rewrite fiber share a common central phase identification. This shared interface allows a metric overlap between the neutral $SU(2)$ direction and the $U(1)$ phase direction.

The neutral electroweak fiber metric is therefore

$$G_{\text{EW}}^{(0)} = \begin{pmatrix} R_\tau^2 & C_{\phi\tau} \\ C_{\phi\tau} & R_\phi^2 \end{pmatrix}.$$

Equivalently,

$$C_{\phi\tau} = \Gamma_{\phi\tau} R_\tau R_\phi,$$

so that

$$G_{\text{EW}}^{(0)} = \begin{pmatrix} R_\tau^2 & \Gamma_{\phi\tau} R_\tau R_\phi \\ \Gamma_{\phi\tau} R_\tau R_\phi & R_\phi^2 \end{pmatrix}.$$

The physical photon and neutral weak boson are the two orthogonal directions of this metric interface. Orthogonality is the metric condition

$$\langle A, Z \rangle_{G_{\text{EW}}^{(0)}} = 0.$$

The flat-fiber limit is

$$\Gamma_{\phi\tau} = 0,$$

and the effective interface projection is

$$\Gamma_{\phi\tau} \neq 0.$$

Thus

$$\theta_W \quad \text{to} \quad \theta_{\text{eff}} = \theta\left(G_{\text{EW}}^{(0)}\right).$$

The distinction between the tree-level angle and the effective angle is the geometric distinction between a flat neutral fiber plane and the metric projection of the shared two-sphere interface.

In the flat-fiber numerical approximation,

$$e = g \sin \theta_W, \quad g' = \frac{e}{\cos \theta_W}.$$

Using

$$e \simeq 0.313, \quad \sin^2 \theta_W \simeq 0.231,$$

one obtains

$$\sin \theta_W \simeq 0.481, \quad \cos \theta_W \simeq \sqrt{1 - 0.231} \simeq 0.877.$$

Therefore

$$g \simeq \frac{0.313}{0.481} \simeq 0.652,$$

and

$$g' \simeq \frac{0.313}{0.877} \simeq 0.357.$$

The charged weak boson mass is then

$$m_W = \frac{0.652 \cdot 246.22}{2} \simeq 80.2 \text{ GeV}.$$

The neutral weak boson mass is

$$m_Z = \frac{246.22}{2} \sqrt{0.652^2 + 0.357^2} \simeq 91.5 \text{ GeV}.$$

Thus

$$\boxed{m_W \simeq 80.2 \text{ GeV}}$$

and

$$\boxed{m_Z \simeq 91.5 \text{ GeV}}.$$

The observed values are

$$m_W^{\text{obs}} \simeq 80.4 \text{ GeV}, \quad m_Z^{\text{obs}} \simeq 91.19 \text{ GeV}.$$

Thus, from the measured strength of the weak interaction, the weak rewrite scale gives the electroweak boson mass scale. The flat-fiber projection already recovers the correct scale and structure, while precision values require the effective interface angle determined by the full neutral fiber metric,

$$\boxed{\theta_W : \text{flat fiber projection}, \quad \theta_{\text{eff}} : \text{interface metric projection}.}$$

7.9 Metric Form of the Electroweak Interface

The electroweak decomposition obtained above can also be written in metric language, with the $SU(2)$ gauge structure following the Yang-Mills construction [166] and the $U(1)_Y$ branch matching the electroweak theory of Glashow [148]. It is the metric form of the same phase-time interface already described as a fiber geometry over the informational spacetime base.

The phase-time interval has the local form

$$dt_\phi = \tau_C^{(\omega)} \chi e^{-i\phi} D\phi.$$

The compact phase-time motion defines the $U(1)$ phase-time fiber. The realized linear-time projection,

$$d\tau = \tau_C^{(\omega)} \chi \cos \phi d\phi,$$

has two local orientations,

$$\cos \phi > 0, \quad \cos \phi < 0.$$

These two orientations define the temporal writing doublet

$$\Psi_\tau = \begin{pmatrix} \psi_+ \\ \psi_- \end{pmatrix},$$

where

$$\psi_+ \sim -dI_{\text{pot}} = dI_{\text{dist}} + dI_{\text{disp}},$$

and

$$\psi_- \sim -dI_{\text{dist}} - dI_{\text{disp}} = dI_{\text{pot}}.$$

Thus the electroweak interface is the geometric splitting of phase-time into its compact phase-time fiber and its two-state realized-time projection. The $U(1)$ sector transports the circular phase motion, while the $SU(2)$ sector transports the local forward-writing and backward-unwriting orientations of realized linear time.

The covariant transport of the doublet is therefore

$$D_\mu \Psi_\tau = \left[\partial_\mu + igW_\mu^a \frac{\sigma_a}{2} + ig' B_\mu \frac{Y}{2} \right] \Psi_\tau.$$

Here W_μ^a is the connection for local rotations of the temporal writing doublet, and B_μ is the pre-rotation hypercharge connection of the compact phase-time fiber, in the standard electroweak notation [149] [150]. The metric doublet is the temporal-orientation substrate; the Standard Model fermion doublets remain the low-energy matter fields on which $SU(2)_L$ acts.

The same structure may be written as a phase-time fiber metric,

$$dS_{\text{EW}}^2 = g_{\mu\nu}^{(I)} dx^\mu dx^\nu + R_\phi^2 (D_Y \phi)^2 + R_\tau^2 \langle D\Psi_\tau, D\Psi_\tau \rangle.$$

The first term is the informational spacetime base. The second term is the compact $U(1)_Y$ phase-fiber metric before electroweak rotation, with

$$D_Y \phi = d\phi - g' \frac{Y}{2} B_\mu dx^\mu.$$

The third term is the $SU(2)$ temporal-doublet fiber metric. After the Weinberg rotation the unbroken phase projection is $D_{\text{em}} \phi = d\phi - (q/\hbar) A_\mu dx^\mu$.

Expanding the pre-rotation $U(1)_Y$ fiber term gives the mixed hypercharge metric connection

$$g_{\mu Y} \propto B_\mu,$$

with Abelian curvature

$$B_{\mu\nu} = \partial_\mu B_\nu - \partial_\nu B_\mu.$$

Expanding the doublet fiber term gives the $SU(2)$ mixed connections

$$g_{\mu a} \propto W_\mu^a.$$

Their curvatures are the non-Abelian field strengths of the electroweak gauge fields [167]

$$W_{\mu\nu}^a = \partial_\mu W_\nu^a - \partial_\nu W_\mu^a + g\epsilon^{abc} W_\mu^b W_\nu^c.$$

This fixes the curvature convention used here; reversing the sign convention for the gauge connection reverses the commutator sign without changing the physical sector. Thus the same phase-time metric structure reproduces the electroweak gauge connections. The $U(1)_Y$ part is the pre-rotation hypercharge transport of the compact phase-time fiber, and the $SU(2)$ part is the transport of the two-state realized-time orientation doublet.

The physical electromagnetic and neutral weak fields are then obtained by the usual Weinberg rotation [149],

$$\begin{aligned} A_\mu &= B_\mu \cos \theta_W + W_\mu^3 \sin \theta_W, \\ Z_\mu &= -B_\mu \sin \theta_W + W_\mu^3 \cos \theta_W. \end{aligned}$$

The post-rotation electromagnetic metric direction is therefore

$$g_{\mu A} \propto A_\mu, \quad A_\mu = B_\mu \cos \theta_W + W_\mu^3 \sin \theta_W.$$

The charged weak fields are

$$W_\mu^\pm = \frac{1}{\sqrt{2}} (W_\mu^1 \mp iW_\mu^2).$$

Therefore the electroweak metric reading is the metric form of the same decomposition already obtained from the two-sphere phase-time interface,

$$U(2) \simeq \frac{SU(2) \times U(1)}{\mathbb{Z}_2}.$$

In this form, $U(1)_Y$ is the pre-rotation circular phase-time fiber, $SU(2)$ is the local doublet of forward-writing/backward-unwriting realized linear time, and the physical electromagnetic connection A_μ is the unbroken post-rotation direction selected by the Weinberg rotation.

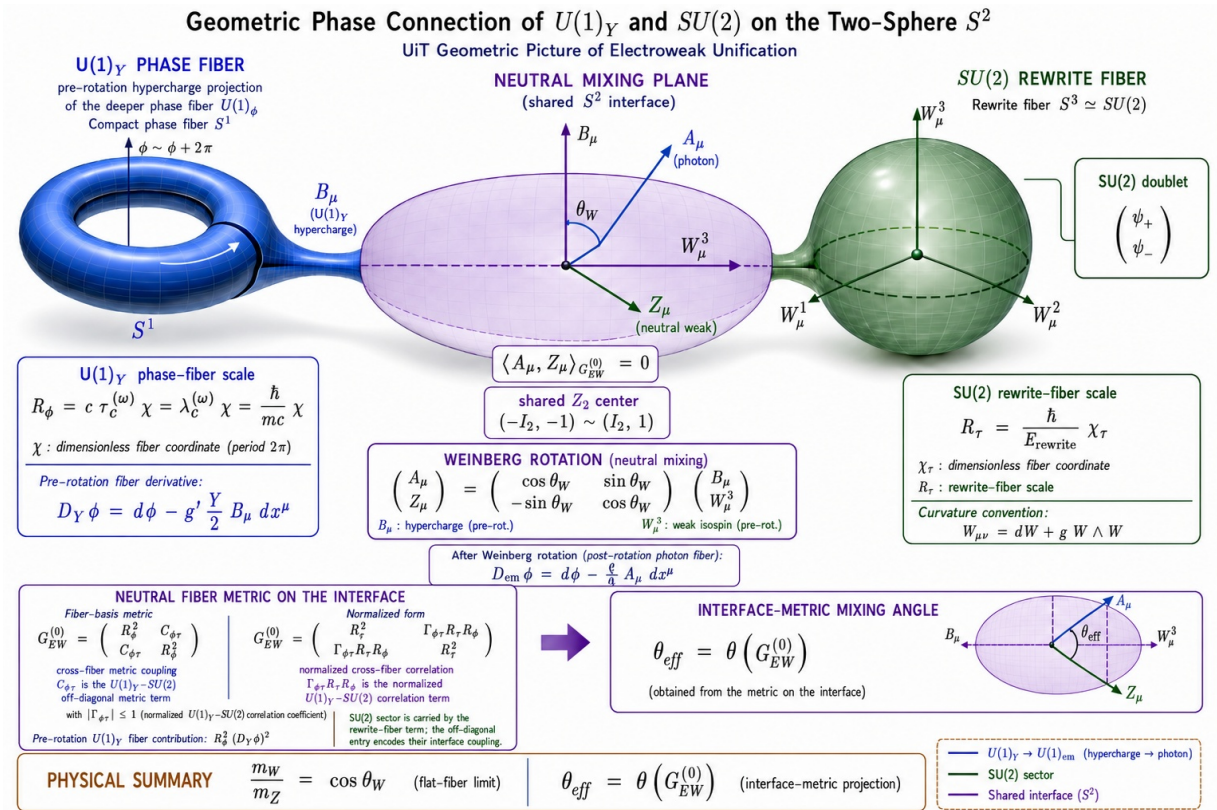


Figure 3: Geometric phase connection of the $U(1)_Y$ phase-time fiber and the $SU(2)$ rewrite fiber on the two-sphere interface. Circular fiber renderings are three-dimensional visual projections of compact phase structure; the physical construction is the complex phase geometry on the spherical present interface.

7.10 The Temporal Bit and the Symmetric Weak Doublet

The same structure returns the weak sector to the elementary definition of a bit. A single bit requires two possible orientations, with Shannon distinguishability providing the information-theoretic back-

ground [4] and physical bit erasure providing the thermodynamic background for the write/erase distinction [27]. Reversible computation supplies the symmetric write/erase limit used by the weak doublet [28]. If there were only one available orientation, no distinction could be written. In the present framework the elementary temporal bit is precisely the pair of real-time projection branches,

$$d\tau > 0, \quad d\tau < 0,$$

or equivalently,

$$\psi_+, \quad \psi_-.$$

Over a full phase cycle the two cosine domains have equal measure. Therefore, before thermodynamic bias or stable record selection is introduced,

$$P(\cos \phi > 0) = \frac{1}{2}, \quad P(\cos \phi < 0) = \frac{1}{2}.$$

Equivalently, for the weak temporal doublet,

$$P(\psi_+) = P(\psi_-) = \frac{1}{2}.$$

The unbiased weak doublet is therefore the elementary temporal bit: two symmetric orientations of the real-time projection, forward writing and backward erasure. Stable record selection then supplies the experienced arrow of time. In symbolic form,

$$(+, -), \quad (-dI_{\text{pot}} = dI_{\text{dist}} + dI_{\text{disp}}, \quad -dI_{\text{dist}} - dI_{\text{disp}} = dI_{\text{pot}}), \quad (\text{forward, backward}).$$

The weak interaction sits at the place where this symmetry can be locally mixed, biased, or realized as physical rewrite,

$$\psi_+ \text{ paired with } \psi_-.$$

Thus the weak doublet is not an added abstract label. It is the temporal bit itself: two symmetric orientations of the real projection of phase-time, each with the basic probability 1/2 before thermodynamic bias, environmental selection, or stable record formation. The arrow of time experienced by observers appears only along branches in which records survive and accumulate; at the level of the underlying temporal bit, the symmetric alternatives remain

$$P_+ = P_- = \frac{1}{2}.$$

This also closes the connection to Landauer. A bit is not only an abstract 0 or 1; in the present theory it is the physical alternative between writing and unwriting, realized as the two signs of the real-time projection.

7.11 CP Bias and the Weak Rewrite Force from Reverse Realized-Time Orientation

Because the weak sector is thermodynamic in this framework, its apparent directionality belongs to the negative linear-time branch. CP violating processes, connected to flavor mixing in the Cabibbo and Kobayashi–Maskawa framework [168] [169], are then read as small biases in the local negative-time unwriting-and-rewrite process. The available phase-time orientations remain symmetric at

the deeper level, while the realized record can weight one orientation slightly differently through the rewrite-bit barrier. [170] [107] [45]

The weak rewrite mechanism can be connected directly to the unified force law developed above. The phase-time field is

$$\Xi(x) = \chi(x)e^{-i\phi(x)}, \quad (457)$$

and the corresponding force law is

$$\mathbf{F}_\phi = -E_{\text{inv}} \nabla \Xi. \quad (458)$$

For a weak rewrite event, the relevant invariant energy scale is the parent phase-energy scale, denoted here by E_{parent} . The weak field is the same phase-time field evaluated on the negative-linear-time branch,

$$\Xi_{\text{weak}} = \chi_\tau e^{-i\phi_\tau}, \quad \cos \phi_\tau < 0. \quad (459)$$

The bit-weighted rewrite energy scale is

$$E_{\text{rewrite}} \equiv e^{-B_{\text{eff}}} E_{\text{parent}}. \quad (460)$$

The compact weak-force form is therefore

$$\mathbf{F}_{\text{weak}} = -E_{\text{rewrite}} \nabla \Xi_{\text{weak}}, \quad \cos \phi_\tau < 0. \quad (461)$$

Equivalently,

$$\boxed{\mathbf{F}_{\text{weak}} = -E_{\text{rewrite}} \nabla \left[\chi_\tau e^{-i\phi_\tau} \right], \quad \cos \phi_\tau < 0.} \quad (462)$$

Expanding the gradient gives

$$\mathbf{F}_{\text{weak}} = -E_{\text{rewrite}} e^{-i\phi_\tau} \nabla \chi_\tau + i E_{\text{rewrite}} \chi_\tau e^{-i\phi_\tau} \nabla \phi_\tau, \quad \cos \phi_\tau < 0. \quad (463)$$

Before the rewrite-bit weighting is applied, the local phase-time force at the rewrite boundary is

$$\mathbf{F}_{\text{weak}}^{(0)} = -E_{\text{parent}} \nabla \left(\chi_\tau e^{-i\phi_\tau} \right). \quad (464)$$

Expanding the gradient gives

$$\mathbf{F}_{\text{weak}}^{(0)} = -E_{\text{parent}} e^{-i\phi_\tau} \nabla \chi_\tau + i E_{\text{parent}} \chi_\tau e^{-i\phi_\tau} \nabla \phi_\tau. \quad (465)$$

The first term is the gradient of the local temporal-registration load. The second term is the gradient of the local temporal orientation. In the weak sector, a local region changes its realized-time orientation relative to the surrounding record-forming branch. The boundary between these regions carries a temporal-orientation gradient,

$$\nabla\phi_\tau \neq 0. \quad (466)$$

In the forward branch one may take $\phi_\tau \simeq 0$, giving $e^{-i\phi_\tau} \simeq 1$ and the usual clock-gradient form

$$\mathbf{F}_{\text{forward}} = -E_{\text{parent}} \nabla\chi_\tau. \quad (467)$$

For a fully reversed local patch, $\phi_\tau \simeq \pi$, so $e^{-i\phi_\tau} \simeq -1$. Inside such a patch, when the orientation is approximately constant, the clock-gradient contribution becomes

$$\mathbf{F}_{\text{backward}} = +E_{\text{parent}} \nabla\chi_\tau. \quad (468)$$

Thus a local negative-linear-time patch carries the opposite clock-gradient response. At the interface with the forward environment, the temporal-orientation term supplies the finite rewrite force generated by the mismatch between the negative-time patch and the forward record-forming branch.

The bit rewrite barrier weights the allowed transition. With

$$B_{\text{eff}} = \ln 2 \Delta I_w, \quad (469)$$

and

$$p_{\text{rewrite}} = e^{-B_{\text{eff}}}, \quad (470)$$

the effective weak force is

$$\boxed{\mathbf{F}_{\text{weak}}^{\text{eff}} = -e^{-B_{\text{eff}}} E_{\text{parent}} \nabla \left[\chi_\tau e^{-i\phi_\tau} \right] = -E_{\text{rewrite}} \nabla \Xi_{\text{weak}}, \quad \cos \phi_\tau < 0.} \quad (471)$$

or, equivalently,

$$\boxed{\mathbf{F}_{\text{weak}}^{\text{eff}} = e^{-B_{\text{eff}}} \left[-E_{\text{parent}} e^{-i\phi_\tau} \nabla \chi_\tau + i E_{\text{parent}} \chi_\tau e^{-i\phi_\tau} \nabla \phi_\tau \right], \quad \cos \phi_\tau < 0.} \quad (472)$$

This gives the weak interaction a direct force interpretation inside the same phase-time architecture used for gravity, inertia, diffusion, and gauge transport. The weak event is the rewrite force on the negative-linear-time component of the local phase-time field. Its small observed strength follows from the exponential rewrite weight, while its ability to change particle identity follows from the

local temporal-orientation gradient that opens and rewrites the parent closed spherical phase-time closure.

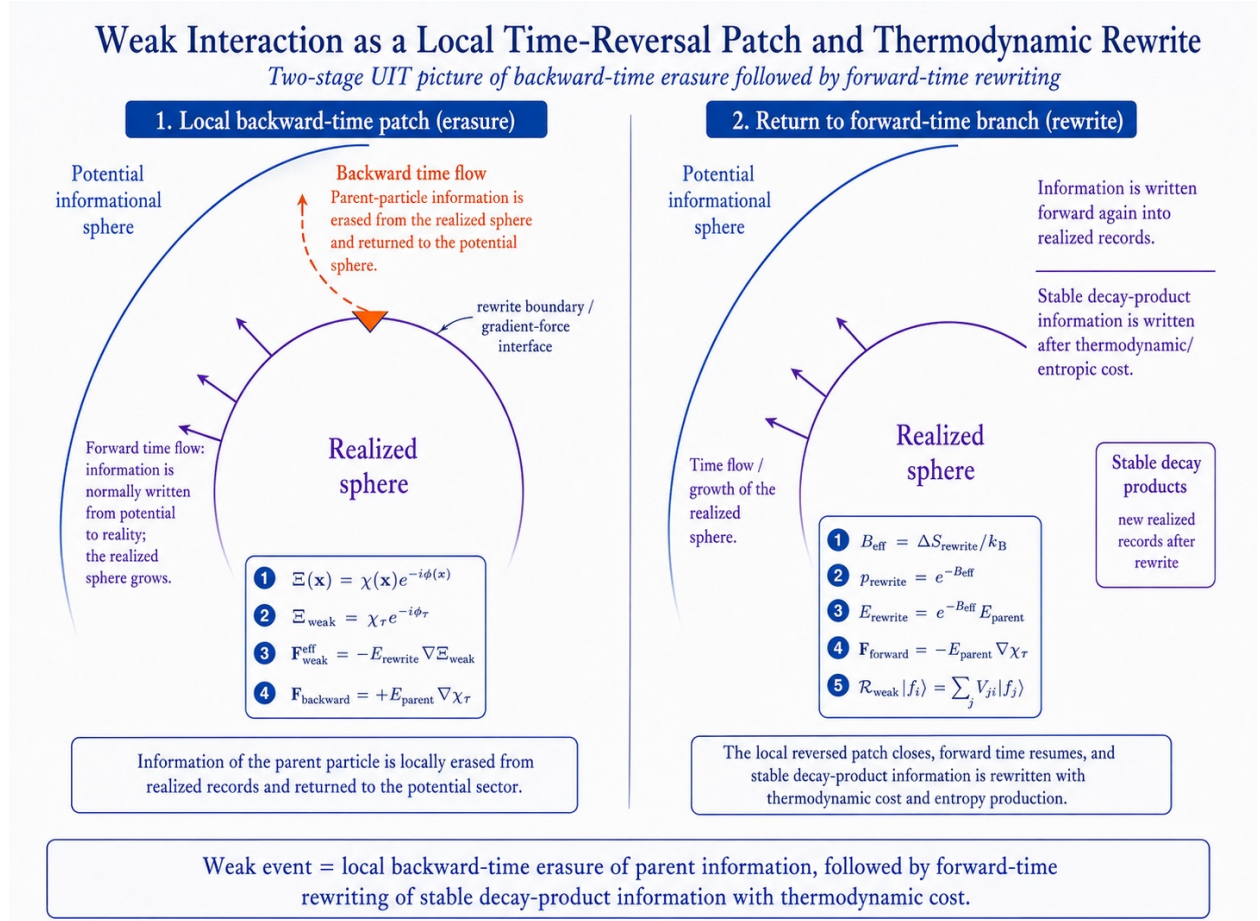


Figure 4: Weak interaction as a local phase-time rewrite: the distinct-plus-dispersed parent record is locally unwritten into the potential sector under negative realized linear time, then rewritten as stable daughter-product information with rewrite-bit cost.

8 The Strong Interaction Sector: Confined Phase-Time Circulation and SU(3)

This chapter develops the strong-sector expression of the same force principle developed earlier. If force is the response to gradients in phase-time load, then the strong sector admits an internal-gradient reading on the confined color manifold of the closed spherical Compton phase-time carrier. Color labels the carrier's internal three-state phase-time orientation. Gluons are exchange and tension modes of that internal closure space. Flavor is the carrier's stable Compton phase-time writing resonance. Confinement, color exchange, and the emergence of an SU(3) organization are therefore formulated as internal phase-time closure dynamics within the UiT architecture.

8.1 Three-State Phase-Time Closure: Mesons and Baryons

The strong interaction is reconstructed here as the internal phase-time closure sector of the closed spherical Compton phase-time carrier. In this reading, what QCD calls color becomes an effective label for internal orientation within a three-state phase-time manifold carried by the closed matter state. Introduce three internal basis states,

$$|1\rangle, |2\rangle, |3\rangle.$$

A general internal quark like state is

$$|\psi\rangle = a_1|1\rangle + a_2|2\rangle + a_3|3\rangle.$$

A single quark is interpreted as an unsaturated internal phase-time disturbance of the carrier's color space. Stable realized strong states are hadronic closures of this internal phase-time cycle. Confinement and asymptotic freedom are read as two limits of closure dynamics: stretching lowers closure capacity and strengthens the restoring tendency, while compression improves closure and weakens the additional restoring response. [171] [172] [173] [174]

A meson is a two-state closure in which an internal phase-time flow orientation is paired with its conjugate orientation. In schematic phase-time form,

$$\phi_1 = -\phi_2.$$

Its closure is therefore primarily pairwise cancellation. A baryon, by contrast, is a three-state circulating closure. The determinant-preserving phase condition is

$$\phi_1 + \phi_2 + \phi_3 = 0 \mod 2\pi.$$

A symmetric closed color-triangle representative is obtained when

$$e^{i\phi_1} + e^{i\phi_2} + e^{i\phi_3} = 0.$$

The intended interpretation is dynamical circulation,

$$\phi_1 \rightarrow \phi_2 \rightarrow \phi_3 \rightarrow \phi_1.$$

The symmetric baryonic point is

$$(\phi_1, \phi_2, \phi_3) = \left(0, \frac{2\pi}{3}, \frac{4\pi}{3}\right).$$

At this point the three phase-time orientations close into a perfect triangle in the complex plane. Mesons are therefore closer to tensioned pairwise cancellation, while baryons are self sustaining circulating closures. [171] [172]

8.2 Strong Load and Restoring Force

The strong sector is formulated as a gradient problem of temporal misclosure. The starting point is the same capacity closure used in the relativistic sectors,

$$\chi^2 + \Lambda_I = 1.$$

In the confined color branch this becomes

$$\boxed{\chi_{\text{strong}}^2 + \Lambda_{\text{color}} = 1},$$

where Λ_{color} is the local normalized color-closure load entering the clock-rate constraint, with

$$0 \leq \Lambda_{\text{color}}(x) \leq 1.$$

For local closure,

$$L \simeq 0,$$

the color load is small or balanced and the three internal phase-time orientations close as a local singlet. When color components are separated, the singlet condition must be preserved along an extended configurational path. The quantity that accumulates with separation is therefore not the normalized local variable Λ_{color} itself, but the energy cost required to maintain local color closure along the path.

Define the local closure-energy density by

$$\varepsilon_{\text{cl}}(s) = \frac{dV_{\text{conf}}}{ds}.$$

The connection between this density and the normalized local load follows from the differential form of

$$\chi_{\text{strong}}^2 + \Lambda_{\text{color}} = 1.$$

Differentiating along the color-separation path gives

$$2\chi_{\text{strong}} d\chi_{\text{strong}} + d\Lambda_{\text{color}} = 0,$$

and therefore

$$\left| \frac{d\chi_{\text{strong}}}{ds} \right| = \frac{1}{2\chi_{\text{strong}}(s)} \left| \frac{d\Lambda_{\text{color}}}{ds} \right|.$$

The local closure-energy density is then

$$\varepsilon_{\text{cl}}(s) = E_{\text{conf}} \left| \frac{d\chi_{\text{strong}}}{ds} \right| = \frac{E_{\text{conf}}}{2\chi_{\text{strong}}(s)} \left| \frac{d\Lambda_{\text{color}}}{ds} \right|.$$

Thus Λ_{color} remains a local normalized closure-load variable, while the long-distance confinement energy is the accumulated closure cost

$$V_{\text{conf}}(L) = \int_0^L \varepsilon_{\text{cl}}(s) ds.$$

In the effective confinement regime, the path-averaged closure-energy density is represented by the phenomenological string tension

$$\sigma_{\text{eff}}(L) = \frac{1}{L} \int_0^L \varepsilon_{\text{cl}}(s) ds,$$

so that, when the density is approximately constant,

$$V_{\text{conf}}(L) \simeq \sigma L, \quad \sigma \equiv \sigma_{\text{eff}}.$$

In this effective long-distance notation, the local factor $1/(2\chi_{\text{strong}})$ is absorbed into the phenomenological string tension σ . The resulting expression represents the accumulated closure cost per unit length, not an unbounded growth of the normalized variable Λ_{color} .

The effective strong closure potential is therefore

$$V_{\text{strong}} = \kappa \left| \sum_{i=1}^3 e^{i\phi_i} \right|^2 + \int_0^L \varepsilon_{\text{cl}}(s) ds,$$

or, for approximately constant closure-energy density,

$$V_{\text{strong}} = \kappa \left| \sum_{i=1}^3 e^{i\phi_i} \right|^2 + \sigma L.$$

This gives the direct chain

$$\boxed{\text{capacity closure to local } \chi_{\text{strong}}, \Lambda_{\text{color}} \text{ to } \varepsilon_{\text{cl}}(s) \text{ to } V_{\text{conf}}(L) \text{ to } \sigma L.}$$

The phase-completed internal strong field is

$$\Xi_{\text{strong}}(A) = \chi_{\text{strong}}(A)e^{-i\Phi_A},$$

where A collects the internal coordinates (L, ϕ_i, θ_a) and Φ_A denotes the internal phase-time circulation orientation on that coordinate space. The phase-completed closure-cost potential is

$$\boxed{u_{\text{conf}}^{(\phi)}(A) = E_{\text{conf}} [1 - \Xi_{\text{strong}}(A)].}$$

The phase-completed strong restoring force follows from the closure-cost potential,

$$\boxed{F_A^{(\text{strong})} = -\nabla_A u_{\text{conf}}^{(\phi)} = E_{\text{conf}} \nabla_A \Xi_{\text{strong}}.}$$

For the confinement branch, the local closure-cost projection may be written as

$$u_{\text{conf}}(s) = E_{\text{conf}}(1 - \chi_{\text{strong}}(s)).$$

The accumulated confinement potential is

$$V_{\text{conf}}(L) = \int_0^L \varepsilon_{\text{cl}}(s) ds,$$

so the restoring force along the elongation coordinate is

$$F_L^{\text{restore}} = -\frac{dV_{\text{conf}}}{dL} = -\varepsilon_{\text{cl}}(L) = E_{\text{conf}} \frac{\partial \chi_{\text{strong}}}{\partial L}.$$

Since $\partial \chi_{\text{strong}} / \partial L < 0$, this force is directed against elongation. Its magnitude is

$$\left| F_L^{\text{restore}} \right| = E_{\text{conf}} \left| \frac{\partial \chi_{\text{strong}}}{\partial L} \right| \simeq \sigma.$$

For internal phase-time coordinates, where the closure potential is represented by the phase-time circulation term, projection onto internal phases gives

$$F_{\phi_i}^{(\text{strong,cl})} = -\frac{\partial V_{\text{tri}}}{\partial \phi_i} = E_{\text{conf}} \frac{\partial \chi_{\text{strong}}}{\partial \phi_i} = 2\kappa \sum_{j \neq i} \sin(\phi_i - \phi_j).$$

These are internal generalized phase-time restoring forces, because the derivative is taken with respect to the dimensionless phase-time coordinates ϕ_i . Their units are therefore units of energy, not ordinary spatial force in newtons. They drive the system back toward closed circulation. [173] [174]

8.3 Stable Baryonic Closure and Emergent SU(3)

At the symmetric point,

$$F_{\phi_1}^{(\text{strong,cl})} = F_{\phi_2}^{(\text{strong,cl})} = F_{\phi_3}^{(\text{strong,cl})} = 0.$$

The baryon is therefore stable because the internal gradients vanish at a closed circulation point. Distorting one phase away from this point generates a restoring force by the previous equation. [171] [173] [174]

All norm preserving local transformations of the three state complex space form U(3). Removing the physically irrelevant global phase leaves

$$\text{SU}(3).$$

The present theory recovers SU(3) as the local mixing symmetry of a three state internal phase-time space, anchored in the color degree of freedom of quark models [175] [176] [177], with gauge-theoretic ancestry in Yang–Mills theory [166], quark structure in Gell-Mann [171], Zweig [172], and quark-parton treatments [178], and asymptotic-freedom physics in Gross–Wilczek [173] and Politzer [174].

Parameterize the internal strong configuration by eight coordinates θ_a on the traceless SU(3) sector:

$$\Phi = \theta_a \lambda_a, \quad a = 1, \dots, 8.$$

Then

$$F_a^{(\text{gluon,cl})} = E_{\text{conf}} \frac{\partial \chi_{\text{strong}}}{\partial \theta_a}, \quad a = 1, \dots, 8.$$

The six exchange generators correspond to transitions

$$1 \text{ paired with } 2, \quad 1 \text{ paired with } 3, \quad 2 \text{ paired with } 3,$$

each with cosine like and sine like modes. Explicitly, for the 1 paired with 2 pair one may write

$$\lambda_1 = |1\rangle\langle 2| + |2\rangle\langle 1|, \quad \lambda_2 = -i|1\rangle\langle 2| + i|2\rangle\langle 1|,$$

with analogous pairs (λ_4, λ_5) for 1 paired with 3 and (λ_6, λ_7) for 2 paired with 3. The two diagonal generators are tension modes,

$$\lambda_3 = \text{diag}(1, -1, 0), \quad \lambda_8 = \frac{1}{\sqrt{3}} \text{diag}(1, 1, -2),$$

which measure internal imbalance. In this reading the eight gluons are the six exchange modes and two internal tension modes of phase-time circulation.

8.4 Color Exchange and Internal Phase-Vector Closure

The preceding subsection reconstructed the eight gluon modes within the standard SU(3) color-language background [177] [179] [244] as the eight traceless generators of the internal three-state phase-time space. This subsection clarifies how color exchange, electric charge, and flavor occupy different levels of the same closed spherical phase-time structure.

The same closed spherical phase-time carrier contains three distinct phase readings:

$$\text{color orientation,} \quad \text{electric charge phase-time holonomy,} \quad \text{flavor resonance.}$$

Color describes the internal orientation of the confined strong cycle. Electric charge describes the global U(1) phase-time holonomy of the closed spherical phase-time matter carrier. Flavor describes the stable Compton phase-time writing resonance of that carrier.

The determinant-preserving phase condition was written as

$$\phi_1 + \phi_2 + \phi_3 = 0 \pmod{2\pi},$$

while the symmetric color-triangle closure is written in complex phase-vector form as

$$e^{i\phi_1} + e^{i\phi_2} + e^{i\phi_3} = 0.$$

Define the three internal color vectors

$$c_i \equiv e^{i\phi_i}, \quad i = 1, 2, 3.$$

For the symmetric color-triangle representative, the closure condition becomes

$$c_1 + c_2 + c_3 = 0.$$

A symmetric three-state closure is obtained by choosing

$$\phi_1 = 0, \quad \phi_2 = \frac{2\pi}{3}, \quad \phi_3 = \frac{4\pi}{3}.$$

Thus

$$c_1 = e^{i0} = 1,$$

$$c_2 = e^{2\pi i/3} = -\frac{1}{2} + i\frac{\sqrt{3}}{2},$$

and

$$c_3 = e^{4\pi i/3} = -\frac{1}{2} - i\frac{\sqrt{3}}{2}.$$

The real projections are therefore

$$\Re(c_1) = 1,$$

$$\Re(c_2) = -\frac{1}{2},$$

and

$$\Re(c_3) = -\frac{1}{2}.$$

The imaginary projections are

$$\Im(c_1) = 0,$$

$$\Im(c_2) = \frac{\sqrt{3}}{2},$$

and

$$\Im(c_3) = -\frac{\sqrt{3}}{2}.$$

The closure is visible separately in the real and imaginary projections:

$$\sum_{i=1}^3 \Re(c_i) = 1 - \frac{1}{2} - \frac{1}{2} = 0,$$

and

$$\sum_{i=1}^3 \Im(c_i) = 0 + \frac{\sqrt{3}}{2} - \frac{\sqrt{3}}{2} = 0.$$

Thus the strong color cycle is a closed internal triangle in the complex phase plane.

A color exchange changes which internal phase-time orientation is carried by a given quark line. For example, the transition

$$c_1 \text{ to } c_2$$

changes the real internal projection from

$$\Re(c_1) = 1$$

to

$$\Re(c_2) = -\frac{1}{2}.$$

The change in the real internal projection is

$$\Delta\Re(c)_{1 \text{ to } 2} = \Re(c_2) - \Re(c_1) = -\frac{1}{2} - 1 = -\frac{3}{2}.$$

Similarly,

$$\Delta\Re(c)_{1 \text{ to } 3} = \Re(c_3) - \Re(c_1) = -\frac{1}{2} - 1 = -\frac{3}{2}.$$

Conversely,

$$\Delta\Re(c)_{2 \text{ to } 1} = \Re(c_1) - \Re(c_2) = 1 - \left(-\frac{1}{2}\right) = \frac{3}{2},$$

and

$$\Delta\Re(c)_{3 \text{ to } 1} = \Re(c_1) - \Re(c_3) = 1 - \left(-\frac{1}{2}\right) = \frac{3}{2}.$$

Therefore a gluonic color exchange can reverse the sign of the local real projection of the internal color vector. This sign change belongs to the internal SU(3) phase-time circulation.

The strong exchange generators make this statement explicit. The six off-diagonal generators act as exchange modes between the three internal states,

$$1 \text{ paired with } 2, \quad 1 \text{ paired with } 3, \quad 2 \text{ paired with } 3.$$

For the 1 paired with 2 exchange pair,

$$\lambda_1 = |1\rangle\langle 2| + |2\rangle\langle 1|,$$

and

$$\lambda_2 = -i|1\rangle\langle 2| + i|2\rangle\langle 1|.$$

Analogously, λ_4, λ_5 generate the exchange 1 paired with 3, and λ_6, λ_7 generate the exchange 2 paired with 3. The remaining two generators,

$$\lambda_3 = \text{diag}(1, -1, 0),$$

and

$$\lambda_8 = \frac{1}{\sqrt{3}}\text{diag}(1, 1, -2),$$

measure diagonal internal imbalance. Together these eight traceless generators span the internal SU(3) color space.

The traceless property is central:

$$\text{Tr}(\lambda_a) = 0, \quad a = 1, \dots, 8.$$

The SU(3) generators redistribute internal phase-time orientation inside the color space while preserving the determinant-one condition. With

$$T_a = \frac{\lambda_a}{2},$$

the local strong transformation is written as

$$U_s = \exp(i\epsilon_a T_a) \in \text{SU}(3),$$

$$\det U_s = 1.$$

The determinant condition means that strong color exchange preserves the total internal phase volume of the three-state closure. It changes the distribution of internal phase-time orientation among the three color components while the closed color cycle remains a closed cycle.

THREE-STATE PHASE-TIME CLOSURE AND THE STRONG INTERACTION

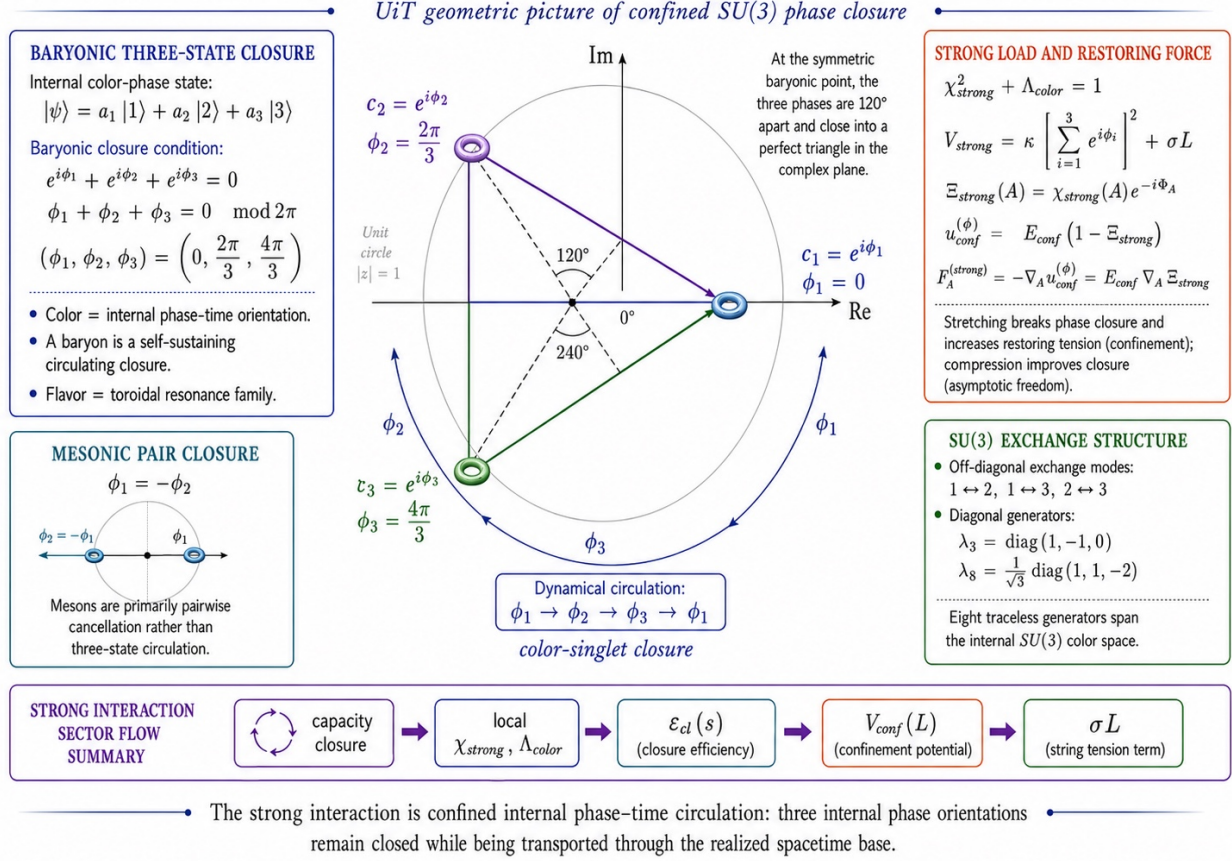


Figure 5: Three-state internal phase-time closure for the strong sector. The diagram visualizes the internal $SU(3)$ color-orientation closure carried by the closed spherical Compton phase-time mode; any circular circulation shown is a three-dimensional projection of the complex phase-time closure structure.

8.5 Electric Charge Holonomy and the Strong Commutation Structure

The electric charge is read from another layer, separating the electromagnetic $U(1)$ phase-time holonomy [91] [242] from the non-Abelian color sector [166] [177] of the same closed spherical phase-time carrier. In the electromagnetic sector, charge was associated with the global $U(1)$ phase-time holonomy. Denote this global phase reading by

$$\Phi_{U(1)}.$$

The electromagnetic charge is then represented schematically as

$$Q_{em} = Q(\Phi_{U(1)}).$$

By contrast, color is represented by the internal three-state phase-time coordinates

$$\phi_1, \phi_2, \phi_3,$$

or by the eight traceless $SU(3)$ coordinates

$$\theta_a, \quad a = 1, \dots, 8.$$

A quark-like closed phase-time carrier may therefore be written schematically as

$$|\Psi\rangle = |f\rangle \otimes |\psi_{\text{color}}\rangle \otimes |\Phi_{U(1)}\rangle.$$

Here f labels the flavor resonance, $|\psi_{\text{color}}\rangle$ labels the internal color state, and $|\Phi_{U(1)}\rangle$ labels the global electromagnetic phase-time holonomy.

A pure strong transformation acts as

$$|\Psi\rangle \mapsto |f\rangle \otimes U_s |\psi_{\text{color}}\rangle \otimes |\Phi_{U(1)}\rangle.$$

Thus the color state changes, while the global charge phase-time holonomy and the flavor resonance are preserved during pure strong exchange.

For a fixed flavor f , the electromagnetic charge operator acts on color space as a scalar multiple of the identity:

$$Q_{\text{em}}^{(f)} = q_f \mathbf{1}_3.$$

Therefore, for every strong generator λ_a ,

$$[Q_{\text{em}}^{(f)}, \lambda_a] = [q_f \mathbf{1}_3, \lambda_a].$$

Since

$$[\mathbf{1}_3, \lambda_a] = 0,$$

one obtains

$$[Q_{\text{em}}^{(f)}, \lambda_a] = 0.$$

Equivalently,

$$[Q_{\text{em}}^{(f)}, U_s] = 0.$$

This commutation relation expresses the separation between internal color orientation and global electric charge phase-time holonomy. A gluonic exchange moves the carrier inside the color triangle,

$$|i\rangle \text{ to } |j\rangle,$$

while the electromagnetic charge reading remains

$$Q_{\text{em}}^{(f)} = q_f.$$

In phase-time language, the local color projection

$$\Re(e^{i\phi_i})$$

may pass from positive to negative during color exchange, while the global charge phase-time holonomy

$$\Phi_{U(1)}$$

continues to encode the same electric charge branch.

This gives the precise internal meaning of color exchange in the present framework. A gluon changes the internal phase-time gradient orientation of the strong cycle. The electric charge is the global phase-time holonomy of the closed spherical phase-time matter mode. Charge conjugation acts on the global phase-time orientation of the carrier; color exchange acts inside the internal traceless phase manifold.

The two readings can be displayed as

$$\text{color:} \quad c_i = e^{i\phi_i},$$

and

$$\text{charge:} \quad Q_{\text{em}} = Q(\Phi_{\text{U}(1)}).$$

The first is an internal vertex of the confined strong circulation. The second is a global winding property of the closed phase-time carrier.

8.6 Flavor as a Closed Compton Phase-Time Resonance

This also provides the natural place to introduce flavor. In standard particle physics, quarks occur in six flavors, as organized in the quark model [171] [172] and in modern particle-data conventions [158].

$$u, d, c, s, t, b.$$

They are arranged into three up-type flavors,

$$u, c, t,$$

and three down-type flavors,

$$d, s, b.$$

The up-type flavors carry electric charge [183]

$$q_u = q_c = q_t = \frac{2}{3}e,$$

while the down-type flavors carry

$$q_d = q_s = q_b = -\frac{1}{3}e.$$

In the present framework, flavor is the stable Compton phase-time writing resonance of the closed spherical Compton phase-time carrier. Different flavors correspond to different stable resonance eigenmodes of the same closed mass-information architecture. For each flavor f , define its rest mass m_f , Compton angular frequency

$$\omega_{C,f} = \frac{m_f c^2}{\hbar},$$

ordinary Compton frequency

$$f_{C,f} = \frac{m_f c^2}{h},$$

and mass-information writing rate

$$\dot{I}_{m,f} = \frac{m_f c^2}{h}.$$

This is a normalized Compton writing rate, measured in bit-equivalent internal Compton cycles per second rather than entropy-produced thermodynamic bits per second.

Thus each flavor corresponds to a distinct stable internal writing rate:

$$f \quad \text{paired with} \quad \omega_{C,f}.$$

Equivalently,

$$|f\rangle = |\omega_{C,f}\rangle.$$

The flavor is therefore the resonance class of the closed spherical Compton phase-time carrier. The color index labels the carrier's internal strong-sector orientation. The charge labels the global U(1) phase-time holonomy.

A complete quark-like internal state can therefore be represented as

$$|q; f, i\rangle = |f\rangle \otimes |i\rangle \otimes |\Phi_{\text{U}(1)}^{(f)}\rangle,$$

where

$$f \in \{u, d, c, s, t, b\},$$

and

$$i \in \{1, 2, 3\}.$$

The mass operator reads the flavor resonance:

$$M|q; f, i\rangle = m_f|q; f, i\rangle.$$

The charge operator reads the global phase-time holonomy:

$$Q_{\text{em}}|q; f, i\rangle = q_f|q; f, i\rangle.$$

The strong transformation acts on the color index:

$$U_s|q; f, i\rangle = |f\rangle \otimes U_s|i\rangle \otimes |\Phi_{\text{U}(1)}^{(f)}\rangle.$$

Therefore,

$$M U_s|q; f, i\rangle = m_f U_s|q; f, i\rangle,$$

and

$$Q_{\text{em}} U_s|q; f, i\rangle = q_f U_s|q; f, i\rangle.$$

Equivalently,

$$[M, U_s] = 0,$$

and

$$[Q_{\text{em}}, U_s] = 0.$$

These relations express the UiT interpretation of pure strong exchange: the strong sector rotates internal color orientation while preserving the Compton phase-time resonance and electromagnetic phase-time holonomy of the closed spherical phase-time carrier.

8.7 Weak Rewrite and CKM-Like Flavor Mixing

A flavor transition has a different structure, compared here with the standard Cabibbo–Kobayashi–Maskawa flavor-mixing framework [168] [169] [158]. It changes the internal resonance itself:

$$|f_i\rangle \text{ to } |f_j\rangle.$$

In Compton-rate language,

$$\omega_{C,i} \text{ to } \omega_{C,j}.$$

Since

$$\omega_{C,f} = \frac{m_f c^2}{\hbar},$$

a flavor transition also changes the rest-mass resonance:

$$m_i \text{ to } m_j.$$

In the present framework, this is a rewrite event. The initial closed Compton phase-time resonance is locally opened, its phase-time content is redistributed, and a new stable Compton phase-time writing resonance is formed. This places flavor change in the weak sector developed above.

Let $\mathcal{R}_{\text{weak}}$ denote the weak rewrite operator acting on the flavor-resonance space. Then

$$\mathcal{R}_{\text{weak}}|f_i\rangle = \sum_j V_{ji}|f_j\rangle.$$

The coefficients V_{ji} measure the allowed rewrite amplitudes between stable Compton phase-time writing resonances. For quarks, they correspond to CKM mixing amplitudes. Thus the weak rewrite of a quark state is written as

$$\mathcal{R}_{\text{weak}}|q; f_i, i\rangle = \sum_j V_{ji}|q; f_j, i'\rangle \otimes |\text{rewrite products}\rangle.$$

The transition probability is

$$P_{i \text{ to } j} = |V_{ji}|^2.$$

The weak-sector chapter introduced a rewrite-bit barrier through

$$\lambda_{\text{weak}} = \frac{1}{\tau_0} e^{-B_{\text{eff}}}.$$

For flavor transitions, the same structure suggests that the transition amplitude carries an overlap factor between two closed Compton phase-time resonances and a rewrite-bit weight. A compact phenomenological form is

$$V_{ji} \sim \langle \omega_{C,j} | \mathcal{R}_{\text{weak}} | \omega_{C,i} \rangle.$$

With an effective rewrite barrier B_{ij} , the magnitude may be written schematically as

$$|V_{ji}| \sim \mathcal{O}_{ji} e^{-B_{ij}/2},$$

where

$$\mathcal{O}_{ji} = |\langle \omega_{C,j} | \omega_{C,i} \rangle_{\text{rewrite}}|$$

is the resonance-overlap factor between the initial and final closed Compton writing modes. Hence

$$P_{i \text{ to } j} = |V_{ji}|^2 \sim |\mathcal{O}_{ji}|^2 e^{-B_{ij}}.$$

This expresses CKM-like mixing as a weak rewrite map between stable Compton phase-time resonances. The mixing angles are interpreted as the geometry of overlap among stable Compton phase-time writing resonance modes of the closed spherical carrier, weighted by the rewrite-bit barrier for returning the previous distinct-plus-dispersed record to the potential sector and writing the new resonance.

8.8 Generations as Stable Flavor-Resonance Bands

The distinction among the three operations can now be summarized mathematically, with flavor mixing anchored to the Cabibbo angle [168] and its three-generation CKM extension [169]. A color exchange is

$$|f\rangle \otimes |i\rangle \otimes |\Phi_{\text{U}(1)}^{(f)}\rangle \text{ to } |f\rangle \otimes |j\rangle \otimes |\Phi_{\text{U}(1)}^{(f)}\rangle.$$

It changes

$$|i\rangle \text{ to } |j\rangle,$$

and preserves

$$f, \quad q_f, \quad \omega_{C,f}.$$

A charge conjugation reverses the global electromagnetic phase-time orientation:

$$|\Phi_{\text{U}(1)}^{(f)}\rangle \text{ to } |\Phi_{\text{U}(1)}^{(\bar{f})}\rangle,$$

with

$$q_f \text{ to } -q_f.$$

A flavor transition changes the Compton phase-time resonance:

$$|f_i\rangle \text{ to } |f_j\rangle,$$

with

$$\omega_{C,i} \text{ to } \omega_{C,j},$$

and

$$m_i \text{ to } m_j.$$

Thus the three readings are

color = internal SU(3) phase-time orientation

charge = global U(1) phase-time holonomy

and

flavor = stable Compton phase-time writing resonance

.

A generation is a stable resonance band in the Compton phase-time writing spectrum of the closed spherical Compton phase-time carrier. Each band contains an up-type and a down-type flavor resonance,

$$G_n = (f_{u,n}, f_{d,n}), \quad n = 1, 2, 3,$$

with

$$q(f_{u,n}) = \frac{2}{3}e, \quad q(f_{d,n}) = -\frac{1}{3}e.$$

The observed quark generations are therefore

$$G_1 = (u, d), \quad G_2 = (c, s), \quad G_3 = (t, b).$$

Each generation has a characteristic pair of Compton phase-time writing frequencies,

$$G_n \text{ paired with } (\omega_{C,u_n}, \omega_{C,d_n}).$$

The closed spherical carrier supports a discrete hierarchy of stable phase-time boundary eigenmodes. These eigenmodes are read by the mass operator as Compton frequencies,

$$\hat{M}|f\rangle = m_f|f\rangle, \quad \omega_{C,f} = \frac{m_f c^2}{\hbar}.$$

A physical generation is a stable pair of such eigenmodes that remains compatible with internal SU(3) color closure, global U(1) phase-time holonomy, and weak rewrite stability.

Define the color-closure defect by

$$\mathcal{C}_{\text{color}} = \left| e^{i\phi_1} + e^{i\phi_2} + e^{i\phi_3} \right|^2.$$

Exact color closure is therefore

$$\mathcal{C}_{\text{color}} = 0.$$

Equivalently, a generation band may be written as the stable spectral set

$$\mathcal{B}_n = \left\{ |f\rangle : \omega_{C,f} \in [\Omega_n^-, \Omega_n^+], \mathcal{C}_{\text{color}} = 0, \Phi_{\text{U}(1)} = q_f, \mathcal{R}_{\text{weak}} \text{ stable} \right\},$$

with

$$G_n = (f_{u,n}, f_{d,n}) \subset \mathcal{B}_n.$$

Here the band is a spectral phase-stability band of the closed spherical carrier. It is defined by Compton recurrence, color closure, charge phase-time holonomy, and weak-rewrite stability.

In the complex-plane projection of the spherical phase-time boundary, a single phase winding defines the U(1) phase-time orientation of the carrier. A two-state closure gives a pairwise cancellation structure. The first non-collinear closed phase cycle is

$$1 + e^{2\pi i/3} + e^{4\pi i/3} = 0.$$

This primitive threefold closure supplies the minimal phase template for the observed three-generation structure. Color reads this geometry as internal SU(3) phase-time orientation. Flavor

reads it as a hierarchy of stable Compton phase-time writing resonance bands. Charge reads the global U(1) phase-time holonomy of the same carrier.

The three-generation pattern is organized by the primitive threefold phase-time closure template

$$\left(0, \frac{2\pi}{3}, \frac{4\pi}{3}\right).$$

Color closure uses this primitive triangular phase geometry internally,

$$e^{i\phi_1} + e^{i\phi_2} + e^{i\phi_3} = 0,$$

while flavor generations appear as stable Compton phase-time writing resonance bands of the closed spherical phase-time carrier built on that same minimal closed phase-time closure structure.

The same primitive closure geometry is read in two sectors. The color sector reads internal SU(3) phase-time orientation. The flavor sector reads stable Compton phase-time writing resonance bands. The operators distinguish the readings:

λ_a reads color transitions,

Q_{em} reads charge phase-time holonomy,

and

M reads flavor resonance.

The strong force acts as the restoring dynamics of internal color closure. Electromagnetism reads the global phase-time holonomy of the carrier. The weak interaction rewrites one flavor resonance into another.

This yields the compact structural map

$\text{SU}(3)_{\text{color}} : i\rangle \text{ to } j\rangle,$	color changes, flavor and charge remain fixed,
$\text{U}(1)_{\text{em}} : \Phi_{\text{U}(1)} \text{ to } Q_{\text{em}},$	global phase-time holonomy gives charge,
$\text{Weak} : \omega_{C,i} \text{ to } \omega_{C,j},$	weak rewriting changes flavor.

and, in UiT language,

color is internal phase-time orientation; charge is global phase-time holonomy; flavor is Compton resonance; generation is a stable Compton phase-time resonance band.

The strong interaction is the restoring dynamics of internal phase-time closure. Flavor change is the weak-sector rewriting of the closed Compton phase-time resonance. Electric charge is the global electromagnetic reading of the same underlying carrier.

8.9 Color Singlets, Gluon Self-Coupling, and the QCD Limit

The strong-sector construction reconstructs the QCD structural limit: color, SU(3), the eight gluons, meson closure, baryon closure, confinement, asymptotic freedom, color exchange, charge phase-time holonomy, and flavor resonance. The bridge to standard QCD is expressed through the color-singlet condition, the non-Abelian self-coupling of gluons, the running of the strong coupling, and the QCD-limit action for color-triplet quark fields coupled to the gluon connection [173] [174] [158].

The central UiT statement is

$$\boxed{\text{the strong interaction is internal SU(3) phase-time closure}}.$$

Equivalently,

$$\boxed{\text{observable hadrons are closed phase-time color singlets}}.$$

In QCD, physically observed hadrons are color singlets [183] [244] [179]. In the present interpretation, a color singlet is a complete internal phase-time closure. For a meson, the color decomposition is

$$3 \otimes \bar{3} = 1 \oplus 8.$$

The physical closed meson state is the singlet

$$|M\rangle_{\text{singlet}} = \frac{1}{\sqrt{3}} \left(|r\bar{r}\rangle + |g\bar{g}\rangle + |b\bar{b}\rangle \right).$$

In UiT language this is the pair-closure condition

$$\phi_1 = -\phi_2,$$

read as

$$\boxed{\text{meson} = \text{pair cancellation}}.$$

For a baryon, the color decomposition is

$$3 \otimes 3 \otimes 3 = 1 \oplus 8 \oplus 8 \oplus 10.$$

The physical closed baryon state is the antisymmetric singlet

$$|B\rangle_{\text{singlet}} = \frac{1}{\sqrt{6}} \epsilon_{ijk} |i j k\rangle.$$

In UiT language this is the three-state circulation condition. The determinant-preserving phase representation is

$$\phi_1 + \phi_2 + \phi_3 = 0 \pmod{2\pi},$$

while the symmetric color-triangle representative is

$$e^{i\phi_1} + e^{i\phi_2} + e^{i\phi_3} = 0,$$

read as

$$\boxed{\text{baryon} = \text{three-state phase-time closure}}.$$

Thus

$$\boxed{\text{color singlet} = \text{complete internal phase-time closure}}.$$

This statement answers the basic observational question of why hadrons appear as color-neutral closed states.

The second basic QCD element is the self-interaction of the gluon field. In a non-Abelian gauge theory the field strength is

$$G_{\mu\nu}^a = \partial_\mu G_\nu^a - \partial_\nu G_\mu^a + g_s f^{abc} G_\mu^b G_\nu^c.$$

The specifically non-Abelian term is

$$g_s f^{abc} G_\mu^b G_\nu^c.$$

This term means that the strong field itself carries the internal color structure and can interact with itself. In the present framework this becomes

$$\boxed{\text{gluon self-interaction} = \text{self-coupling of internal phase-time circulation}}.$$

The difference between SU(3) and U(1) is therefore expressed geometrically: the electromagnetic phase-time holonomy is a global Abelian reading, while the strong sector is an internal non-Abelian circulation whose generators do not commute and whose gauge field carries its own internal phase-time orientation.

The standard QCD matter-field limit is obtained by reading each flavor as a color triplet,

$$q_f(x) = \begin{pmatrix} q_{f,r} \\ q_{f,g} \\ q_{f,b} \end{pmatrix}, \quad q_f(x) \text{ to } U(x)q_f(x), \quad U(x) \in \text{SU}(3).$$

The corresponding color-covariant derivative is

$$D_\mu q_f = \left(\partial_\mu + i g_s G_\mu^a T_a \right) q_f.$$

Thus the ordinary QCD action limit is

$$\boxed{\mathcal{L}_{\text{QCD}} = -\frac{1}{4} G_{\mu\nu}^a G^{a\mu\nu} + \sum_f \bar{q}_f (i \gamma^\mu D_\mu - m_f) q_f.}$$

In the present interpretation, the first term is the non-Abelian curvature energy of the internal closure field, while the Dirac term transports the flavor carriers as color triplets through that internal SU(3) phase-time closure connection.

The third basic QCD element is the running coupling [158]. At one-loop order, the strong coupling may be written as

$$\alpha_s(Q^2) \simeq \frac{12\pi}{(33 - 2n_f) \ln(Q^2/\Lambda_{\text{QCD}}^2)}.$$

When

$$Q^2 \text{ to } \infty,$$

one obtains

$$\alpha_s(Q^2) \text{ to } 0.$$

Thus, at short distances or high momentum transfer, quarks behave as nearly free degrees of freedom. In UiT language,

$$\boxed{\text{short distance} = \text{nearly closed local phase-time circulation}}.$$

At large separation, the closure potential already introduced above contains the integrated color-closure cost

$$V_{\text{strong}} = \kappa \left| \sum_{i=1}^3 e^{i\phi_i} \right|^2 + \int_0^L \varepsilon_{\text{cl}} ds.$$

For approximately constant closure-energy density, this becomes

$$V_{\text{strong}} = \kappa \left| \sum_{i=1}^3 e^{i\phi_i} \right|^2 + \sigma L, \quad \sigma = \varepsilon_{\text{cl}}.$$

In UiT variables the same coefficient is the color-closure gradient density,

$$\sigma = E_{\text{conf}} \left| \frac{d\chi_{\text{strong}}}{dL} \right| = \frac{E_{\text{conf}}}{2\chi_{\text{strong}}} \left| \frac{d\Lambda_{\text{color}}}{dL} \right|.$$

For static color sources, when

$$L \text{ to } \infty,$$

the integrated closure cost grows, so that

$$V_{\text{strong}} \text{ to large.}$$

In full QCD with dynamical quarks, this linear growth is eventually interrupted by string breaking through quark-antiquark pair creation.

The classical restoring force along the stretching coordinate has magnitude

$$\left| F_L^{(\text{strong,cl})} \right| \simeq \sigma.$$

Therefore the two limiting behaviors are

$$\boxed{L \rightarrow 0 \text{ implies asymptotic freedom}}$$

and

$$\boxed{L \rightarrow \infty \text{ implies confinement}}.$$

The strong-sector QCD-limit reconstruction is then

$$\text{color singlet} = \text{closed internal phase-time state,}$$

$$\text{gluon self-coupling} = \text{self-interaction of internal circulation,}$$

and

$$\text{running coupling} = \text{scale-dependent closure tension.}$$

Together these relations close the basic strong-sector QCD map:

$$\boxed{\text{color singlets} + \text{non-Abelian gluon self-coupling} + \text{running } \alpha_s}$$

The same strong-sector map is expressed below in the metric and action language of the internal SU(3) phase-time closure fiber.

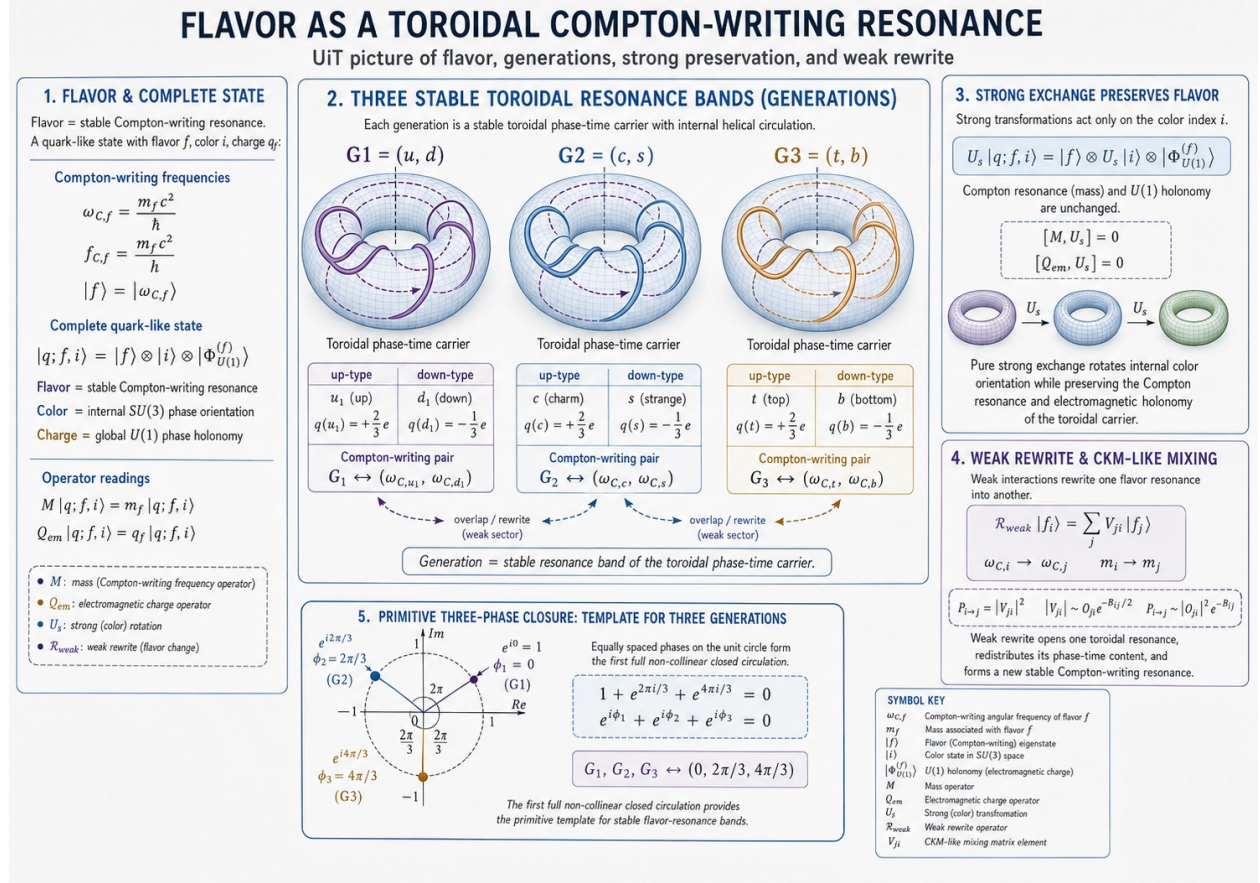


Figure 6: Flavor as a stable Compton phase-time writing resonance of the closed spherical carrier. The three-dimensional closed phase-time sphere renderings in the schematic are illustrative projections of the complex phase-time boundary structure, used to visualize resonance bands, phase-time circulation, and rewrite overlap. The physical definition used in the text is the closed complex spherical Compton phase-time carrier.

8.10 Phase-Time Bridge and Metric Form of Strong Phase Closure

The strong sector depends on the earlier phase-time derivation. The phase-time section identified the coherent branch as $dt_{\phi, \text{coh}} = \tau_C^{(\omega)} e^{-i\phi} d\phi$, which is the branch used here on the internal three-state phase space. The strong interaction uses this same temporal architecture on an internal three-state space. What remains the same is the phase-time gradient architecture; the strong sector uses the closure-cost potential on the internal three-state phase space.

The strong interaction sector can also be written in the same metric language used above for the electromagnetic and electroweak sectors. Confinement and strong-coupling behavior are expressed

through the QCD-limit fields and the internal $SU(3)$ phase-time closure geometry [180] [179]. The metric form expresses the already derived strong phase-time closure condition as a fiber geometry over the informational spacetime base.

In the two-sphere model, the strong sector corresponds to internal closure on the present interface. The realized interface preserves a closed triplet of internal phase-time orientations. We write this color phase-time triplet as

$$\Phi_c = \begin{pmatrix} e^{i\phi_1} \\ e^{i\phi_2} \\ e^{i\phi_3} \end{pmatrix}.$$

The symmetric color-triangle closure condition is

$$e^{i\phi_1} + e^{i\phi_2} + e^{i\phi_3} = 0.$$

The determinant-preserving phase-time representation is

$$\phi_1 + \phi_2 + \phi_3 = 0 \pmod{2\pi}.$$

These are two levels of closure. The phase-time sum condition expresses the special-unitary, determinant-preserving orientation constraint. The triangular condition

$$\sum_{i=1}^3 e^{i\phi_i} = 0$$

is the symmetric color-singlet representative of that internal phase-time closure.

Thus the strong sector is the local geometry of a closed three-orientation phase-time system. The interaction is the requirement that the three internal phase-time orientations remain closed on the two-sphere interface while they are transported through the realized spacetime base.

The natural gauge group of this closure is the color gauge group of QCD [177]

$$SU(3).$$

The special-unitary condition expresses the preservation of internal phase-time closure. Local transport of the color phase-time triplet is therefore written as the non-Abelian covariant transport of an internal triplet [244].

$$D_\mu \Phi_c = \left[\partial_\mu + ig_s G_\mu^a T_a \right] \Phi_c,$$

where

$$T_a = \frac{\lambda_a}{2},$$

and λ_a are the Gell-Mann generators. The fields G_μ^a are the local connections that preserve the three-orientation phase-time closure under spacetime transport. In the usual language, these are the gluon gauge fields.

The corresponding non-Abelian curvature is

$$G_{\mu\nu}^a = \partial_\mu G_\nu^a - \partial_\nu G_\mu^a + g_s f^{abc} G_\mu^b G_\nu^c.$$

The final term,

$$g_s f^{abc} G_\mu^b G_\nu^c,$$

is the metric expression of the fact that the strong connection transports a closed phase-time triplet rather than a single Abelian phase. In the electromagnetic sector, the $U(1)$ phase-time fiber has curvature

$$F = dA.$$

In compact notation, with the strong connection denoted by \mathcal{A}_s , the $SU(3)$ closure fiber has curvature

$$\mathcal{G} = d\mathcal{A}_s + \mathcal{A}_s \wedge \mathcal{A}_s.$$

Thus the gluon fields carry the closure structure they transport. In UiT language, the strong field is the curvature of internal phase-time closure preservation.

The same structure can be written as a phase-time closure fiber metric over the informational spacetime base:

$$dS_{\text{strong}}^2 = g_{\mu\nu}^{(I)} dx^\mu dx^\nu + R_s^2 \langle D\Phi_c, D\Phi_c \rangle.$$

Here $g_{\mu\nu}^{(I)}$ is the realized informational spacetime metric, while the second term is the metric of the internal $SU(3)$ phase-time closure fiber. Expanding the fiber term gives mixed metric connections of the form

$$g_{\mu a} \propto G_\mu^a.$$

Thus the gluon connection is the mixed metric connection between the spacetime base and the internal three-orientation phase-time closure fiber, exactly as A_μ appeared as the mixed connection

of the $U(1)$ phase-time fiber and W_μ^a appeared as the mixed connection of the $SU(2)$ temporal doublet.

The complete metric pattern is therefore

$$g_{\mu\phi} \propto A_\mu,$$

for the electromagnetic phase-time fiber,

$$g_{\mu a}^{(\text{weak})} \propto W_\mu^a,$$

for the weak temporal doublet, and

$$g_{\mu a}^{(\text{strong})} \propto G_\mu^a,$$

for the strong three-orientation phase-time closure fiber.

The physical meaning of confinement follows from the same closure condition. If the three phase-time components remain locally closed, the internal triangle

$$e^{i\phi_1} + e^{i\phi_2} + e^{i\phi_3} = 0$$

has no exposed color boundary. A color-neutral hadron is therefore a closed internal phase-time object on the two-sphere interface.

If the color components are separated through spacetime, the system must preserve phase-time closure along the separation path. This creates a closure-energy cost. The local phase-time closure contribution can be written as

$$V_{\text{cl}} = \kappa \left| \sum_{i=1}^3 e^{i\phi_i} \right|^2.$$

Spatial separation adds the metric cost of maintaining the closure channel along a path of length L :

$$V_{\text{string}} = \int_0^L \varepsilon_{\text{cl}}(s) ds.$$

In the long-distance limit, when the closure-energy density is approximately constant,

$$\varepsilon_{\text{cl}}(s) \text{ to } \sigma,$$

this becomes

$$V_{\text{string}} \text{ to } \sigma L.$$

Thus the strong potential takes the effective form

$$V_{\text{strong}} = \kappa \left| \sum_{i=1}^3 e^{i\phi_i} \right|^2 + \int_0^L \varepsilon_{\text{cl}}(s) ds,$$

with the confinement limit

$$V_{\text{strong}} \sim \sigma L.$$

The units are

$$[\kappa] = \text{energy}, \quad [\sigma] = \text{energy/length}.$$

This is the metric meaning of confinement in UiT. Color separation stretches the internal phase-time closure condition across realized spacetime. The energy grows because the two-sphere interface must preserve a closed $SU(3)$ phase-time relation over an increasing spatial separation.

Therefore the strong interaction is the metric geometry of three-orientation phase-time closure preservation. The gluon fields are the mixed metric connections of the $SU(3)$ closure fiber. Their non-Abelian curvature expresses the self-coupling of the closure transport, and the linear confinement term expresses the metric cost of preserving internal phase-time closure across distance.

In this form, the strong sector fits the same unified phase-time pattern as the previous sectors:

$$\text{gravity} \quad \text{to} \quad g_{\mu\nu}^{(I)}, \chi,$$

$$\text{electromagnetism} \quad \text{to} \quad U(1) \text{ phase-time fiber, } A_\mu, F_{\mu\nu},$$

$$\text{weak interaction} \quad \text{to} \quad SU(2) \text{ temporal writing doublet, } W_\mu^a,$$

$$\text{strong interaction} \quad \text{to} \quad SU(3) \text{ three-orientation phase-time closure fiber, } G_\mu^a, G_{\mu\nu}^a.$$

The strong interaction is represented here as the non-Abelian curvature and closure tension of the internal three-orientation phase-time sector of the same phase-time interface.

9 What Is Mass?

This section gives the internal matter carrier for the Compton writing channel. Mass is formulated as a closed complex spherical Compton phase-time mode. The same carrier supplies Compton

recurrence, the invariant energy scale mc^2 , the phase variable ϕ , the unified field $\Xi = \chi e^{-i\phi}$, spinorial closure, electromagnetic phase projection, the fine-structure fraction, CPT orientation, and the recurrence-fraction reading of observed particle masses.

The guiding identification is

$$\text{massive mode} = \text{closed complex spherical Compton phase-time mode.}$$

The real scalar projection of this mode is rest mass. The radial clock-rate projection is the closed Lorentzian gravitational reading. The oriented phase-gradient projection is the electromagnetic reading. The spinorial orientation of the phase-resolved spherical boundary supplies the spin structure.

9.1 Mass as a Closed Complex Spherical Phase-Time Mode

Mass-information I_m is the distinguished-information channel carried by a closed Compton phase-time recurrence. A massive system is a closed internal phase-time mode whose external scalar projection is the rest-energy scale

$$E_0 = mc^2.$$

The electromagnetic section above supplied the phase-time connection and curvature. The present section supplies the internal matter carrier whose phase-time orientation gives the real mass projection, whose radial registration projection gives the gravitational clock-load, and whose phase-gradient projection gives the electromagnetic reading.

In the informational notation of the theory,

$$I_m = \text{mass-information written by a closed Compton phase-time recurrence.}$$

The closure is spherical because the ordinary boundary direction of the rest state is a two-dimensional spherical direction space,

$$S_{R_B}^2,$$

where R_B denotes the boundary radius of the closed mode. The phase-resolved state over this spherical boundary is complex. The ordinary spatial boundary is spherical, and the full phase-resolved orientation is spinorial, as developed below.

The local internal momentum flow of the closed mode can remain directed at each point. Schematically,

$$\vec{p}_{\text{int}}(s)$$

denotes the internal momentum flow along an internal phase-time path or boundary parameter s . The observed rest state has zero net external linear momentum because the directed internal contributions close under the normalized closed-cycle average:

$$\vec{P}_{\text{net}}^{\text{ext}} = \langle \vec{p}_{\text{int}} \rangle_{\text{closed}} = 0.$$

Equivalently, when s is a path-length parameter over a closed path of length L_{closed} ,

$$\langle \vec{p}_{\text{int}} \rangle_{\text{closed}} = \frac{1}{L_{\text{closed}}} \oint \vec{p}_{\text{int}}(s) ds = 0.$$

The energy of the closed recurrence remains:

$$E_{\text{int}} = mc^2.$$

The scalar exterior reading is therefore

$$m = \frac{E_{\text{int}}}{c^2}.$$

This is the mass carrier used in the rest of the theory: internally directed phase-time activity closes into an externally scalar rest-energy reading and a radial Lorentzian clock-load.

9.2 Internal Phase Closure and Radial Lorentzian Distortion

The scalar equation

$$E_0 = mc^2$$

gives the rest-energy magnitude of a massive carrier. By itself, this scalar reading leaves the orientation question of mass open. Directed energy-momentum carries an orientation and produces directed Lorentzian time-distortion. A rest mass carries the same energy scale while having no surviving external net motion. The question is therefore why directed energy produces a directional Lorentzian distortion, while rest mass produces a radial clock distortion.

The Compton phase reading supplies the missing structure. The rest-energy magnitude also defines the Compton phase rate

$$E_0 = \hbar\omega_C,$$

so that

$$\omega_C = \frac{mc^2}{\hbar}.$$

Thus the rest energy is written as a closed internal phase-time recurrence,

$$\psi_C(t) = e^{-imc^2t/\hbar} = e^{-i\omega_C t}.$$

The scalar expression mc^2 gives the external rest-energy magnitude. The Compton phase expression gives the internal phase-time orientation through which that energy is closed.

Let $\hat{n}(s)$ denote the local internal orientation along the closed Compton phase-time cycle. The local internal momentum scale is

$$\vec{p}_{\text{int}}(s) = \frac{E_{\text{int}}}{c} \hat{n}(s).$$

Locally,

$$\vec{p}_{\text{int}}(s) \neq 0.$$

The closed spherical carrier cancels the surviving external vector direction through phase-time closure,

$$\langle \hat{n} \rangle_{\text{closed}} = 0,$$

and therefore

$$\langle \vec{p}_{\text{int}} \rangle_{\text{closed}} = 0.$$

Equivalently,

$$\vec{P}_{\text{net}}^{\text{ext}} = 0.$$

The scalar energy remains,

$$E_{\text{int}} = E_0 = mc^2.$$

The externally observed invariant mass follows from the closed energy-momentum system,

$$M_{\text{obs}}^2 c^4 = E_{\text{int}}^2 - \left| \vec{P}_{\text{net}}^{\text{ext}} \right|^2 c^2.$$

Since

$$\vec{P}_{\text{net}}^{\text{ext}} = 0,$$

one obtains

$$M_{\text{obs}} = \frac{E_{\text{int}}}{c^2}.$$

For the rest mode,

$$E_{\text{int}} = mc^2, \quad M_{\text{obs}} = m.$$

The closure cancels the first directional moment. The second directional moment remains. For an isotropic closed spherical phase-time projection,

$$\langle \hat{n}_i \hat{n}_j \rangle_{\text{closed}} = \frac{1}{3} \delta_{ij}.$$

Therefore,

$$\langle p_i p_j \rangle_{\text{closed}} = \left(\frac{E_{\text{int}}}{c} \right)^2 \langle \hat{n}_i \hat{n}_j \rangle_{\text{closed}} = \frac{1}{3} \left(\frac{E_{\text{int}}}{c} \right)^2 \delta_{ij}.$$

This is the mass-side mechanism. The local directed internal phase-time energy closes its external vector momentum, while the Lorentzian time-distortion carried by that energy remains as a radial scalar Lorentzian projection. Rest mass is closed Compton phase-time energy whose directed Lorentzian distortion appears externally as radial scalar Lorentzian distortion.

The relativistic capacity geometry developed earlier already identified the two readings of the same Lorentzian load. For directed motion,

$$\Lambda_v = \frac{v^2}{c^2},$$

and the Lorentzian clock factor is

$$\chi_v^2 = 1 - \Lambda_v = 1 - \frac{v^2}{c^2}.$$

For the static radial exterior of a closed mass carrier, the dimensionless radial load is the closed internal energy normalized by the gravitational coupling and the exterior radius:

$$\Lambda_g(r) = \frac{2GE_{\text{int}}}{rc^4}.$$

Using

$$E_{\text{int}} = M_{\text{obs}} c^2,$$

this becomes

$$\Lambda_g(r) = \frac{2GM_{\text{obs}} c^2}{rc^4} = \frac{2GM_{\text{obs}}}{rc^2} = \frac{r_s}{r}.$$

This is the normalized radial scalar Lorentzian load of the closed Compton phase-time carrier. The radial Lorentzian clock factor is

$$\chi_g^2(r) = 1 - \Lambda_g(r) = 1 - \frac{r_s}{r}.$$

Thus

$$\chi_g(r) = \sqrt{1 - \frac{r_s}{r}} = \sqrt{1 - \frac{2GM_{\text{obs}}}{rc^2}}.$$

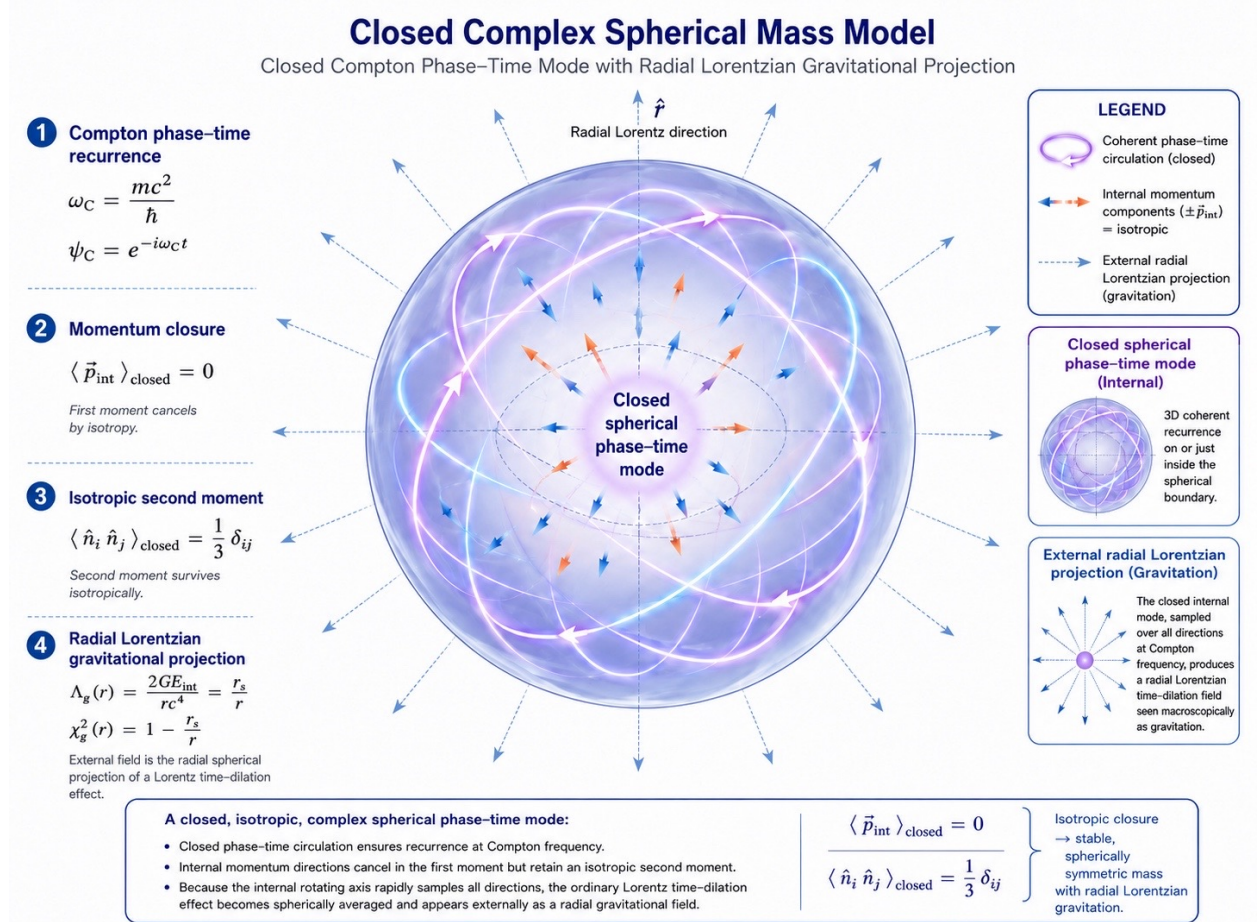
In the free-fall projection developed in the relativity section, the two loads coincide,

$$\frac{v(r)^2}{c^2} = \frac{r_s}{r},$$

so that

$$\chi_v(v(r)) = \chi_g(r).$$

The present mass section supplies the origin of the radial reading. The Schwarzschild clock factor is the radial closed phase-time projection of the same Lorentzian time-distortion that appears directionally in special relativity. Directed energy gives open Lorentzian load. Closed Compton phase-time energy gives radial Lorentzian load. [16] [97] [54] [48] [67] [68]



9.3 Compton Writing Rate and the Closed Mass-Information Channel

A closed massive mode carries the Compton angular frequency

$$\omega_C = \frac{mc^2}{\hbar}, \quad f_C = \frac{mc^2}{h}.$$

The corresponding angular and full-cycle times are

$$\tau_C^{(\omega)} = \frac{\hbar}{mc^2}, \quad T_C = \frac{h}{mc^2} = 2\pi\tau_C^{(\omega)}.$$

A one-radian phase step carries the action scale \hbar , while a full Compton recurrence carries the action scale h . This Compton recurrence supplies the mass-writing scale introduced at the beginning of the manuscript:

$$\dot{I}_m = \frac{dI_m}{dt} = f_C = \frac{mc^2}{h}.$$

Thus the mass channel is a closed internal writing rate. The invariant energy mc^2 and the Compton rate ω_C are two readings of the same closed recurrence:

$$E_0 = mc^2 = \hbar\omega_C.$$

The stationary phase form of the closed rest mode is

$$\psi_C(\tau) = \psi_0 e^{-imc^2\tau/\hbar} = \psi_0 e^{-i\omega_C\tau}.$$

Therefore

$$i\hbar \frac{\partial\psi_C}{\partial\tau} = mc^2\psi_C.$$

This is the stationary Schrödinger-form reading of the same closed Compton phase-time recurrence. The equation states that rest energy is the phase rate of the closed mass-information channel. [19] [90]

The reduced Compton wavelength is

$$\bar{\lambda}_C = \frac{\hbar}{mc},$$

and the full Compton wavelength is

$$\lambda_C = 2\pi\bar{\lambda}_C = \frac{h}{mc}.$$

The phase along a boundary path of length $s = c\tau$ is therefore

$$\phi_B(s) = \frac{s}{\bar{\lambda}_C}, \quad \omega_C\tau = \frac{s}{\bar{\lambda}_C}.$$

The Compton cycle is the phase-time recurrence of the closed spherical mode.

9.4 Fast Compton Carrier, Slow Envelope, and Free Schrödinger Dynamics

The same closed mass carrier also gives the quantum envelope structure. The internal Compton phase is

$$\psi_C(t) = e^{-i\omega_C t}, \quad \omega_C = \frac{mc^2}{\hbar}.$$

A freely propagating massive quantum state is written as a slow spatial envelope riding on this fast Compton carrier,

$$\Psi(\mathbf{x}, t) = \psi(\mathbf{x}, t)e^{-i\omega_C t}.$$

Equivalently,

$$\Psi(\mathbf{x}, t) = \psi(\mathbf{x}, t)e^{-imc^2 t/\hbar}.$$

The exponential factor is the fast internal mass clock. The envelope $\psi(\mathbf{x}, t)$ is the slow spatial update of the same carrier through external configuration space.

After the fast Compton phase has been factored out, the envelope carries the residual motional phase of the carrier. This is the same motion-information channel developed in the relativistic sector, now read after the Compton phase-time carrier has been separated from the slow external update. In the slow-envelope limit, the envelope generator is the kinetic update of that motion channel

$$E_{\text{env}} \simeq \frac{p^2}{2m}.$$

The envelope energy and momentum operators are

$$E_{\text{env}} \text{ to } i\hbar \frac{\partial}{\partial t},$$

and

$$\mathbf{p} \text{ to } -i\hbar \nabla.$$

Therefore,

$$i\hbar \frac{\partial \psi}{\partial t} = \frac{\hat{p}^2}{2m} \psi.$$

Since

$$\hat{p}^2 = (-i\hbar \nabla)^2 = -\hbar^2 \nabla^2,$$

the slow envelope obeys

$$i\hbar \frac{\partial \psi}{\partial t} = -\frac{\hbar^2}{2m} \nabla^2 \psi.$$

This is the free Schrödinger equation. In this reading, it is the slow-envelope dynamics of the closed Compton mass carrier. The fast phase is the internal mass clock; the slow envelope is the external spatial update of that carrier.

The same result can also be written in the phase-time transport notation used later. Define

$$D_q = \frac{\hbar}{2m}.$$

Then

$$-\frac{\hbar^2}{2m} \nabla^2 \psi = -\hbar D_q \nabla^2 \psi,$$

and therefore

$$i\hbar \frac{\partial \psi}{\partial t} = -\hbar D_q \nabla^2 \psi.$$

The transport notation is the coherent-flow reading of the same slow-envelope equation. The primary mass-sector result is the separation

$$\Psi(\mathbf{x}, t) = \psi(\mathbf{x}, t) e^{-i\omega_C t},$$

where the closed Compton phase supplies the fast carrier and the free Schrödinger equation describes the slow spatial envelope.

The closed mass carrier therefore has four projections:

$$\begin{aligned} \text{scalar rest-energy projection:} \quad & E_0 = mc^2, \\ \text{internal Compton phase projection:} \quad & \omega_C = \frac{mc^2}{\hbar}, \\ \text{radial Lorentzian gravitational projection:} \quad & \chi_g^2(r) = 1 - \frac{r_s}{r}, \\ \text{slow-envelope quantum projection:} \quad & i\hbar \frac{\partial \psi}{\partial t} = -\frac{\hbar^2}{2m} \nabla^2 \psi. \end{aligned}$$

Mass is the closed Compton phase-time carrier whose scalar, phase, radial, and slow-envelope projections give rest energy, Compton frequency, Schwarzschild clock-load, and free Schrödinger dynamics. [18] [19] [90]

9.5 Planck Closure, Compton Scale, and Gravitational Radius

The natural closure comparison uses the gravitational radius

$$r_g = \frac{Gm}{c^2},$$

and the reduced Compton wavelength

$$\bar{\lambda}_C = \frac{\hbar}{mc}.$$

Their ratio is

$$\frac{r_g}{\bar{\lambda}_C} = \frac{Gm^2}{\hbar c}.$$

Using the Planck mass

$$m_P = \sqrt{\frac{\hbar c}{G}},$$

this becomes

$$\frac{r_g}{\bar{\lambda}_C} = \left(\frac{m}{m_P} \right)^2.$$

At the Planck mass,

$$m = m_P,$$

the two scales coincide:

$$r_g = \bar{\lambda}_C.$$

The Schwarzschild radius is

$$r_s = 2r_g = \frac{2Gm}{c^2}.$$

The clean closure equality is therefore the equality between the reduced Compton scale and the gravitational radius, while the Schwarzschild boundary carries the conventional factor 2.

For $m = m_P$, one also has

$$\bar{\lambda}_C(m_P) = l_P,$$

where

$$l_P = \sqrt{\frac{\hbar G}{c^3}}.$$

Thus the Planck mass is the closure scale at which the Compton phase scale and the gravitational closure scale meet. Ordinary observed masses lie below this full closure scale, but their masses are still read by the same Compton recurrence law.

Thus the same object contains two standard scales: internally it carries the Compton phase recurrence, and externally it supplies the radial gravitational clock-rate boundary. This gives the matter carrier its Compton writing scale and its radial gravitational projection within one closed spherical phase-time structure. [97] [54] [19]

9.6 Spinorial Orientation on the Spherical Phase Boundary

Spin is the phase-resolved orientation law of the closed spherical Compton phase-time mode. The ordinary boundary direction is spherical, while the full phase-resolved orientation is spinorial.

Let Ψ_s be a normalized two-component spinor,

$$\Psi_s = \begin{pmatrix} z_1 \\ z_2 \end{pmatrix}, \quad z_1, z_2 \in \mathbb{C}, \quad |z_1|^2 + |z_2|^2 = 1.$$

The normalized spinor states form

$$S^3 \simeq SU(2).$$

The ordinary spatial direction is obtained by the Pauli projection

$$\hat{n} = \Psi_s^\dagger \boldsymbol{\sigma} \Psi_s, \quad \hat{n} \in S^2.$$

Thus the phase-resolved orientation has the structure

$$S^3 \simeq SU(2) \text{ to } S^2,$$

or, in group language,

$$SU(2) \text{ to } SO(3).$$

The spinorial closure law follows in the usual form. A rotation by angle θ acts on the internal orientation through

$$\Psi_s(\theta) = \exp\left(-\frac{i}{2}\theta \boldsymbol{\sigma} \cdot \hat{a}\right) \Psi_s(0),$$

where \hat{a} is the rotation axis. A single 2π spatial rotation returns the ordinary direction and reverses the spinor sign:

$$\Psi_s(2\pi) = -\Psi_s(0).$$

A second 2π rotation restores the full phase-resolved state:

$$\Psi_s(4\pi) = \Psi_s(0).$$

Equivalently,

$$U(2\pi) = -\mathbf{1}, \quad U(4\pi) = +\mathbf{1}.$$

Spin is therefore the orientation and closure law of the closed spherical Compton phase-time mode. The mass sector reads the recurrence rate. The spin sector reads the $SU(2)$ orientation law of the phase-resolved spherical boundary. [98] [99] [100]

9.7 Dirac Spinor as the Relativistic Completion of the Temporal Spinor Doublet

The previous subsection showed that the phase-resolved spherical boundary of the closed Compton mass mode carries a spinorial orientation law. The purpose of the present subsection is to make explicit how this two-component spinorial structure is completed into the standard relativistic Dirac spinor.

The unified phase-time field of the closed mass carrier is

$$\Xi = \chi e^{-i\phi}.$$

Here χ is the real clock-rate amplitude and ϕ is the internal phase-time angle. The phase factor $e^{-i\phi}$ is single-valued under a 2π phase recurrence. A spinor, however, is not a vectorial phase state. It is the square-root phase orientation of the closed boundary state. The natural spinorial lift of the phase-time factor is therefore

$$e^{-i\phi} \quad \text{to} \quad e^{-i\phi/2}.$$

Under a 2π phase rotation,

$$e^{-i(\phi+2\pi)/2} = -e^{-i\phi/2},$$

while under a 4π rotation,

$$e^{-i(\phi+4\pi)/2} = e^{-i\phi/2}.$$

Thus the half-phase lift already contains the spinorial closure law:

$$\Psi(2\pi) = -\Psi(0), \quad \Psi(4\pi) = \Psi(0).$$

In the present theory this spinorial half-phase is not introduced as an independent postulate. It is the local representation of the two temporal orientations of the closed phase-time carrier. Define the temporal spinor doublet

$$\Psi_\tau = \begin{pmatrix} \psi_+ \\ \psi_- \end{pmatrix},$$

where ψ_+ and ψ_- denote the forward and backward phase-time orientation amplitudes of the same closed carrier. In the simplest local phase representation,

$$\psi_+ \sim e^{-i\phi/2}, \quad \psi_- \sim e^{+i\phi/2}.$$

The normalized temporal spinor satisfies

$$\Psi_\tau^\dagger \Psi_\tau = |\psi_+|^2 + |\psi_-|^2 = 1.$$

Therefore the local temporal-orientation state lies on

$$S^3 \simeq SU(2).$$

The observable spatial spin direction is not the spinor itself. It is the Pauli projection of the temporal spinor doublet:

$$\hat{n} = \Psi_\tau^\dagger \boldsymbol{\sigma} \Psi_\tau, \quad \hat{n} \in S^2.$$

Thus the internal phase-time doublet supplies the spinorial orientation space,

$$S^3 \simeq SU(2),$$

while the ordinary spatial direction is the projected vector,

$$SU(2) \text{ to } SO(3), \quad \Psi_\tau \longmapsto \hat{n}.$$

This is the precise sense in which spin is the observable projection of a forward/backward phase-time doublet.

A local rotation by angle θ about axis \hat{a} acts on the temporal spinor by the standard $SU(2)$ operator

$$\Psi_\tau(\theta) = \exp\left(-\frac{i}{2}\theta \boldsymbol{\sigma} \cdot \hat{a}\right) \Psi_\tau(0).$$

Consequently,

$$\Psi_\tau(2\pi) = -\Psi_\tau(0), \quad \Psi_\tau(4\pi) = \Psi_\tau(0).$$

The closed spherical mass carrier is therefore vectorially closed in ordinary space but spinorially closed only after 4π in the phase-resolved orientation space.

The Dirac spinor is obtained when this temporal spinor structure is required to obey a local relativistic first-order wave equation. The closed Compton carrier satisfies the relativistic mass-shell relation

$$E^2 = p^2 c^2 + m^2 c^4.$$

Equivalently,

$$E^2 - c^2 \mathbf{p}^2 - m^2 c^4 = 0.$$

To write this as a first-order local evolution law, one seeks a Hamiltonian linear in \mathbf{p} ,

$$H_D = c \boldsymbol{\alpha} \cdot \mathbf{p} + \beta m c^2,$$

such that

$$H_D^2 = c^2 \mathbf{p}^2 + m^2 c^4.$$

This requires

$$\{\alpha_i, \alpha_j\} = 2\delta_{ij}\mathbf{1}, \quad \{\alpha_i, \beta\} = 0, \quad \beta^2 = \mathbf{1}.$$

The minimal matrices satisfying these relations are 4×4 matrices built from the Pauli matrices,

$$\alpha_i = \begin{pmatrix} 0 & \sigma_i \\ \sigma_i & 0 \end{pmatrix}, \quad \beta = \begin{pmatrix} \mathbf{1} & 0 \\ 0 & -\mathbf{1} \end{pmatrix}.$$

The four components are therefore not arbitrary. They are the minimal relativistic completion of two coupled two-component spinorial sectors.

In the notation of the present theory, write the Dirac field as

$$\Psi_D = \begin{pmatrix} \Phi_+ \\ \Phi_- \end{pmatrix}, \quad \Phi_+, \Phi_- \in \mathbb{C}^2.$$

The two sectors Φ_+ and Φ_- carry the two temporal orientations of the phase-time carrier, each with its Pauli spinorial boundary structure. The mass term couples the two temporal orientations through the invariant Compton recurrence scale mc^2 , while the momentum term transports the spinorial orientation through external space.

The first-order relativistic evolution equation is then

$$i\hbar \frac{\partial \Psi_D}{\partial t} = \left(-i\hbar c \boldsymbol{\alpha} \cdot \nabla + \beta mc^2 \right) \Psi_D.$$

Equivalently, in covariant notation,

$$\left(i\hbar c \gamma^\mu \partial_\mu - mc^2 \right) \Psi_D = 0.$$

This is the standard Dirac equation.

In the present interpretation, the Dirac spinor is not an added independent object. It is the relativistic completion of the temporal spinor doublet already contained in the closed complex spherical mass mode:

$$\Xi = \chi e^{-i\phi} \quad \text{to} \quad \Psi_\tau = \begin{pmatrix} \psi_+ \\ \psi_- \end{pmatrix} \quad \text{to} \quad \Psi_D = \begin{pmatrix} \Phi_+ \\ \Phi_- \end{pmatrix}.$$

The first relation is the spinorial half-phase lift of the closed phase-time field. The second relation is the relativistic completion required by the mass-shell relation. The Pauli matrices appear because the projected orientation of the temporal doublet is

$$\hat{n} = \Psi_\tau^\dagger \boldsymbol{\sigma} \Psi_\tau,$$

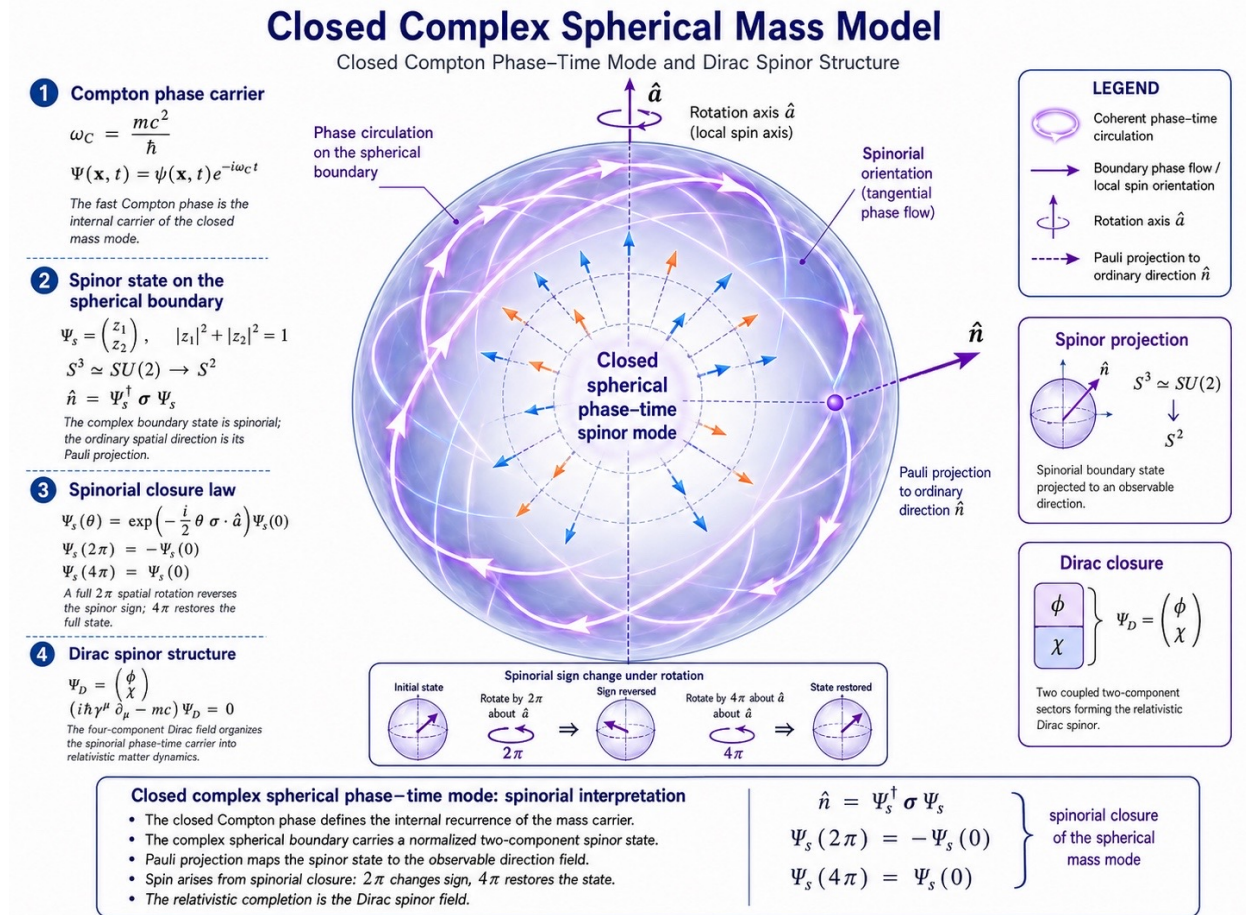
and the Dirac matrices appear because a first-order relativistic dynamics of such spinorial orientations requires the Clifford algebra.

Thus the chain is

closed Compton phase-time mode generates forward/backward temporal spinor doublet,
forward/backward temporal spinor doublet carries $SU(2)$ spinorial orientation,

$SU(2)$ spinorial orientation admits Dirac relativistic completion.

Spin is the Pauli projection of the normalized temporal doublet. The Dirac spinor is the four-component relativistic field obtained when the same closed phase-time carrier is required to propagate consistently with the relativistic energy-momentum relation.



9.8 Mass, Electromagnetic Phase, Fine Structure, and Observed Electron Mass

The phase-time energy of the closed Compton mass mode is written

$$E_\phi = mc^2 e^{-i\phi}.$$

This single complex phase-time mode has two projections. The real scalar projection gives rest mass, inertia, and the gravitational clock-load. The oriented phase-gradient projection gives the electromagnetic reading.

The real projection of this phase-time energy supplies the scalar mass and radial clock-load described above. The phase-gradient projection supplies the electromagnetic reading. For small phase,

$$e^{-i\phi} \approx 1 - i\phi,$$

so

$$E_\phi \approx mc^2(1 - i\phi).$$

The real sector is

$$E_{\text{real}} \approx mc^2,$$

and the phase sector is

$$E_{\text{phase}} \approx -imc^2\phi.$$

Therefore

$$\Re(E_\phi) \text{ to mass, inertia, and gravitational clock-load,}$$

while

$$\Im(E_\phi) \text{ to phase-gradient electromagnetic projection.}$$

Taking the phase-gradient contribution gives

$$-\nabla E_\phi = imc^2\nabla\phi$$

in the phase-force sector, so

$$F_{\text{phase}} \propto \nabla\phi.$$

This is the local route from the Compton phase-time mode to electromagnetic coupling. The U(1) language is the gauge representation of local phase transport.

The same statement is written more generally through the unified phase-time field

$$\Xi = \chi e^{-i\phi}.$$

For a massive carrier,

$$E_\Xi = mc^2\Xi = mc^2\chi e^{-i\phi}.$$

Its gradient is

$$\begin{aligned} F_\Xi &= -mc^2\nabla(\chi e^{-i\phi}) \\ &= -mc^2e^{-i\phi}\nabla\chi + imc^2\chi e^{-i\phi}\nabla\phi. \end{aligned}$$

The first term is the real clock-rate branch:

$$\nabla\chi \text{ to mass, inertia, gravity, and clock-rate loading.}$$

The second term is the phase branch:

$$\nabla\phi \text{ to charge and electromagnetism.}$$

Thus an electron is the charged electromagnetic projection of the same closed Compton phase-time mode: the real projection gives the electron rest mass, while the oriented phase-gradient projection

gives its charge and electromagnetic coupling. The U(1) fiber is the gauge-theoretic representation of this local phase transport.

The Planck energy of the closed Planck phase-time mode is

$$E_P = \sqrt{\frac{\hbar c^5}{G}} = \frac{\hbar c}{l_P}.$$

The maximal electrostatic interaction energy between two elementary charges at separation l_P is

$$U_{\text{el}}(l_P) = \frac{1}{4\pi\epsilon_0} \frac{e^2}{l_P}.$$

Using

$$\alpha = \frac{e^2}{4\pi\epsilon_0 \hbar c},$$

one obtains

$$U_{\text{el}}(l_P) = \alpha \frac{\hbar c}{l_P} = \alpha E_P.$$

Thus

$$\frac{U_{\text{el}}(l_P)}{E_P} = \alpha.$$

The fine structure constant, historically introduced in Sommerfeld's fine-structure analysis [102] and measured in modern constants tables [103], is therefore interpreted as the normalized electromagnetic phase projection of the Planck-scale closed phase-time capacity. [91] [101]

The Planck mass is the maximal closed phase-time registration capacity. The observed mass of a particle is read through its own Compton recurrence. From the recurrence relation,

$$m = \frac{h f_C}{c^2}.$$

Define the Planck frequency

$$f_P = \frac{m_P c^2}{h}.$$

Then

$$m = m_P \frac{f_C}{f_P}.$$

This relation is general. It holds for any observed rest mass. In energy units,

$$m c^2 = (m_P c^2) \frac{f_C}{f_P}.$$

For the electron specifically,

$$m_e = m_P \frac{f_{C,e}}{f_P},$$

or

$$m_e c^2 = (m_P c^2) \frac{f_{C,e}}{f_P}.$$

The Planck closed spherical phase-time mode provides the maximal internal registration capacity, while the observed electron mass is the realized recurrence of that mode at the electron's Compton

refresh rate. This closes the apparent gap between the Planck closure scale and the much smaller observed electron mass.

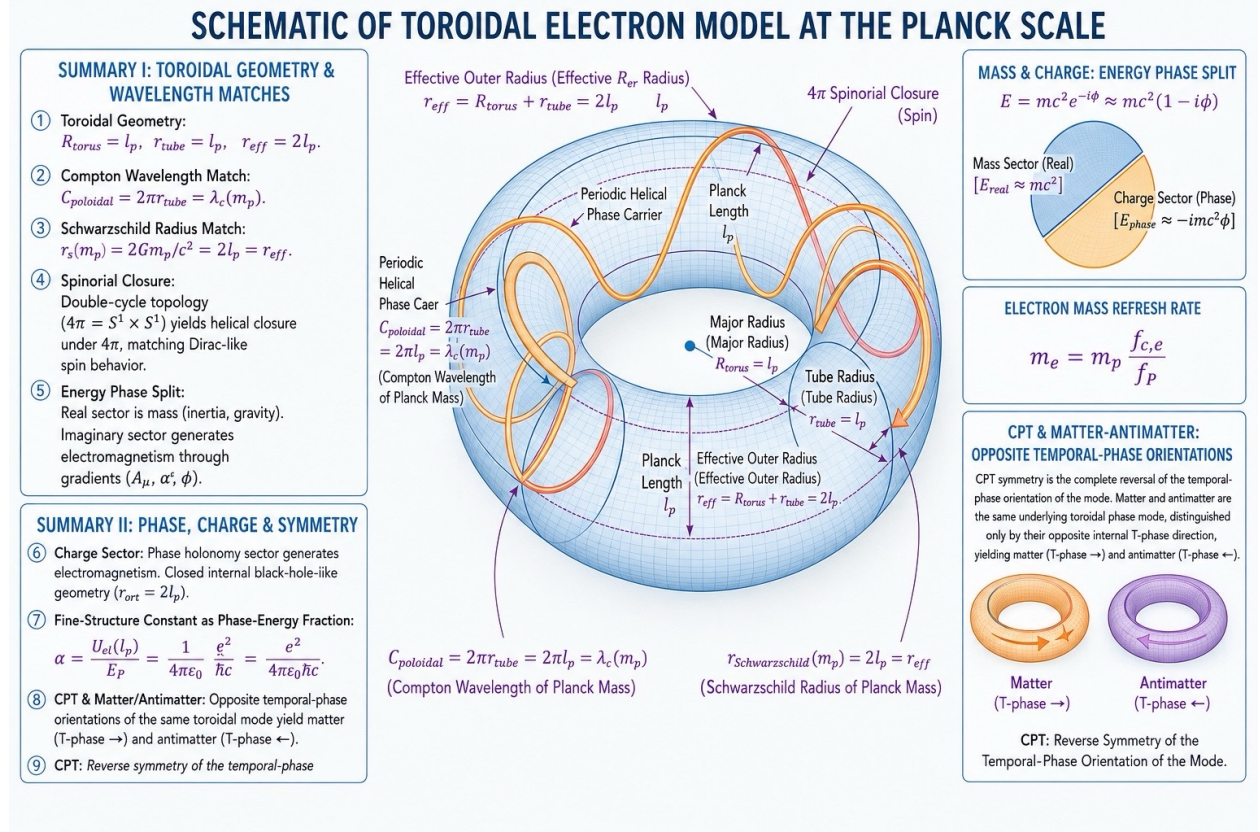


Figure 7: Three-dimensional visualization of the internal phase-circulation structure of the mass carrier. The physical carrier in the present formulation is the closed complex spherical Compton phase-time mode. The closed phase-time sphere rendering is an illustrative spatial projection of the complex phase-time boundary structure, used to visualize phase-time circulation, spinorial closure, electromagnetic phase-time holonomy, and CPT orientation.

9.9 CPT Orientation and Horizon Closure of the Closed Spherical Phase State

The same closed spherical phase-time structure admits opposite phase-time orientations. Matter and antimatter are interpreted as opposite orientations of one phase-time object, and CPT becomes the reversal symmetry of that geometric structure. [104] [105] [106] [101] [107] [45]

The experienced arrow remains tied to record formation. Inscribing distinct information requires thermodynamic dissipation, $dS > 0$, so a reversed temporal orientation erases the records that define the observer. Matter and antimatter are the same informational configuration read from opposite phase-time directions, while the apparent asymmetry belongs to the record-forming orientation of one underlying structure.

The orientation state may be represented schematically by

$$\Gamma_S = (m, \chi, \Phi_\phi, \sigma, \epsilon_t),$$

where m is the Compton recurrence mass, χ is the local clock-rate amplitude, Φ_ϕ is the electromagnetic phase-time holonomy or phase projection, σ is the spinorial orientation or handed phase-time orientation of the spherical phase state, and ϵ_t is the temporal orientation of the recurrence.

Charge conjugation reverses the electromagnetic phase reading,

$$C : \quad \Phi_\phi \text{ maps to } -\Phi_\phi, \quad q = Q(\Phi_\phi) \text{ maps to } -q = Q(-\Phi_\phi).$$

Parity reverses the spinorial handed orientation,

$$P : \quad \sigma \text{ maps to } -\sigma.$$

Time reversal reverses the orientation of the recurrence,

$$T : \quad \epsilon_t \text{ maps to } -\epsilon_t, \quad \omega_C \text{ maps to } -\omega_C,$$

while the invariant mass scale is preserved by the magnitude of the recurrence,

$$mc^2 = \hbar|\omega_C|.$$

The combined operation maps the matter carrier to the opposite phase-time orientation of the same closed spherical phase-time structure,

$$CPT : \quad (q, \sigma, \epsilon_t) \text{ maps to } (-q, -\sigma, -\epsilon_t), \quad |\Xi| = \chi, \quad |E_\phi| = mc^2.$$

Thus matter and antimatter are opposite readings of one closed phase-time carrier. The recurrence norm and the Compton mass scale are preserved, while charge, spinorial handed orientation, and temporal orientation are reversed together.

The horizon reading is also preserved. At the Planck closure scale the reduced Compton scale and the gravitational radius coincide, $\bar{\lambda}_C = r_g$, while the Schwarzschild radius is $r_s = 2r_g$. More generally, a closed Compton phase-time energy carrier supplies the radial Lorentzian clock-rate factor developed in the general-relativity sections. The horizon is therefore the limiting boundary of external distinguishable registration for the closed carrier, while the internal Compton recurrence remains the mass-writing scale of the mode.

9.10 The Higgs Excitation and the Information Fraction

The observed Higgs mass provides the empirical scale through the ATLAS [108] and CMS [109] discoveries, while the Higgs mechanism itself follows the original symmetry-breaking works [110] [111] [112] [113], and the electroweak–Planck hierarchy supplies the naturalness context developed by Susskind [114] and 't Hooft [115].

The same recurrence law extends beyond the electron. In the present reading, the measured mass is the realized recurrence fraction of the Planck-scale closed phase-time capacity. For the Higgs sector,

this means that the observed Higgs mass is read as the recurrence of the Higgs field excitation at its own realized Compton update rate.

From the general recurrence relation,

$$m = \frac{hf_C}{c^2},$$

one may write for the Higgs excitation

$$m_H = \frac{hf_H}{c^2},$$

where f_H is the realized Compton recurrence of the Higgs mode. Defining the Planck frequency by

$$f_P = \frac{m_P c^2}{h},$$

the same identity used for the electron gives

$$m_H = m_P \frac{f_H}{f_P}.$$

In the present theory, the ratio f_H/f_P is the information fraction of the Higgs excitation. It measures how much of the maximal Planck closed-mode bandwidth is actually realized by the Higgs mode. The Planck scale is the absolute bandwidth limit of closed spherical phase-time registration, whereas the Higgs mass is a local excitation of the Higgs field within that capacity. The hierarchy is therefore the statement that a local excitation can occupy a small recurrence fraction of the full internal capacity of the system.

Using the observed Higgs mass scale

$$m_H c^2 \approx 125.1 \text{ GeV}, \quad m_P c^2 \approx 1.2209 \times 10^{19} \text{ GeV},$$

the corresponding realized fraction is

$$\frac{f_H}{f_P} = \frac{m_H}{m_P} = \frac{m_H c^2}{m_P c^2} \approx \frac{125.1}{1.2209 \times 10^{19}} \approx 1.0247 \times 10^{-17}.$$

Substituting this fraction back into the recurrence formula returns the observed Higgs mass by construction,

$$m_H c^2 = (m_P c^2) \frac{f_H}{f_P} \approx 1.2209 \times 10^{19} \text{ GeV} \times 1.0247 \times 10^{-17} \approx 125.1 \text{ GeV}.$$

The significance is that the observed Higgs mass can be read as a realized recurrence fraction of the Planck-scale closed phase-time bandwidth. The point is conceptual as well as numerical. The Planck mass is the maximal internal capacity of the closed spherical Compton phase-time mode. The Higgs mass is the realized recurrence of a specific Higgs field excitation inside that deeper registration capacity. In that sense, the hierarchy problem is re-read as a bandwidth fraction problem. The Higgs is a local tension mode inside the structure, while the Planck limit is the total energy capacity of the closed mode.

10 Quantum Records and Schrödinger Dynamics

10.1 Quantum Records and Phase-Time Potential Information

In the present framework, time is not a background parameter that continues to flow independently of physical registration. Time appears only when distinguishable information is written relative to dispersive cost. The local time relation is therefore tied to informational realization itself.

For this reason, an entangled pair is described as one correlated potential structure before local records are written. Before measurement, the pair belongs to the potential informational sector. The correlated structure exists in the potential informational sector prior to distinct local records for the two subsystems.

When measurement occurs, the relevant distinguishable information is created at once as a physical record. In that act, the local realized time of the correlated outcome is generated for both members of the pair together. The observed anti correlation reflects one joint act of record formation inside one informational structure.

In this reading, the usual paradox is dissolved. The measured outcomes acquire independent realized-record status during measurement, so the usual faster-than-light reading is replaced by joint record formation. Measurement creates the observed spin value together with the local realized time in which that value becomes part of physical history.

Entanglement is therefore interpreted as synchronized realization, addressing the EPR tension [116] and Bohr's reply to it [117], Bell-type constraints [118], experimental violations of Bell inequalities [119], relative-branch readings [120], and time-symmetric quantum formulations [121]. The two outcomes appear together because the record is written together. The correlation is immediate because realized time is generated with the act of informational distinction itself.

The same resolution applies to Schrödinger's cat, the standard paradox of unrealized quantum alternatives [122]. Until the box is opened, no realized local time has yet been written for that outcome, because no distinguishable measurement record has been formed. The system remains in unrealized potential before a classical history is registered. When the box is opened and a record is created, the local realized time of the outcome is generated, and the cat appears as one definite result within physical history. The paradox is therefore dissolved in the same way as entanglement: realized time appears with informational registration.

In this reading the wave function is the compact mathematical representation of potential information before record formation. A quantum state describes a coherent phase-time potential whose distinguishable outcome becomes physical record only when registration occurs.

Write the state schematically as

$$\Psi(x) = \psi(x)e^{-i\phi(x)}.$$

The amplitude carries the available potential density and the phase carries coherent temporal orientation. Measurement is then the conversion of a component of this phase-time potential into a distinct record with dispersed thermodynamic cost,

$$-dI_{\text{pot}} = dI_{\text{dist}} + dI_{\text{disp}}.$$

The Born weight is read as the registration weight of distinguishable outcomes within the potential structure,

$$P(x) = |\Psi(x)|^2.$$

Thus the wave function is the phase-time bookkeeping of unrealized distinguishability before a stable record is written.

10.2 Informational Wormhole Interpretation

Before measurement, an entangled pair belongs to one common potential informational state,

$$|\Psi\rangle \in \mathcal{H}_{\text{pot}}^{(AB)},$$

This state belongs to the shared potential sector of the pair before two independent realized space-time histories are written. In the present theory, realized local time exists only when distinguishable information is written into record,

$$d\tau(x) = \chi(x) dt, \quad \chi(x) = \frac{dI_{\text{dist}}(x)}{dI_{\text{disp}}(x)}.$$

Thus, prior to record formation, the correlated outcome is not yet assigned separate realized times for A and B . The pair remains one unresolved informational structure in the potential sector.

This motivates an informational notion of wormhole connectivity: two regions may be far apart in the realized metric, with

$$d_g(A, B) \gg 1,$$

while remaining adjacent in the deeper informational structure, with

$$d_I(A, B) \ll d_g(A, B).$$

Accordingly, a wormhole in the present theory is the realized geometric projection of a nontrivial informational connection in the potential phase sector,

$$\text{wormhole} = \Pi_{\text{real}}(\mathcal{W}(A, B)).$$

Measurement then generates the correlated record jointly,

$$-dI_{\text{pot}}^{(AB)} = dI_{\text{dist}}^{(AB)} + dI_{\text{disp}}^{(AB)},$$

so the correlation reflects a shared informational relation rather than a later signal passing between two fully realized distant events. Entanglement and wormhole like connectivity, beginning with the Einstein–Rosen bridge [123], are therefore interpreted as two projections of the same deeper informational relation [124].

10.3 Black-Hole Information Paradox and White-Hole Projection

The phase-time law contains the information-paradox mechanism and is formulated in direct contact with Hawking's information-loss formulation [125], Page's entropy analysis [126], and later firewall and review literature [127] [128]. The complex time increment is

$$\boxed{dt_\phi = \tau_C^{(\omega)} \chi e^{-i\phi} d\phi,} \quad (473)$$

and the realized linear-time projection is

$$\boxed{d\tau = \Re(dt_\phi) = \tau_C^{(\omega)} \chi \cos \phi d\phi.} \quad (474)$$

The sign of the realized projection is controlled by $\cos \phi$. The positive branch, $\cos \phi > 0$, is the forward realized-time orientation. The negative branch, $\cos \phi < 0$, is the reverse realized-time orientation.

A black-hole horizon is the saturation surface of the forward realized branch. Information falling through the forward branch reaches the horizon capacity boundary. The same phase-time structure contains the reverse branch, in which the realized projection changes sign. Information that enters the horizon in the forward orientation appears as outward informational release in the reverse orientation, echoing black-hole information recovery scenarios [129].

The paradox is resolved by the cosine projection of phase-time. Forward linear time carries information inward toward horizon saturation. Reverse linear time carries the same informational content outward from the same horizon structure. Conservation belongs to the full phase-time process, while each observer samples one realized projection.

White-Hole Projection. White holes are the reverse-time projection of the same horizon mechanism. A black hole is the $\cos \phi > 0$ projection, where the distinct-plus-dispersed horizon record is driven inward toward saturation. A white hole is the $\cos \phi < 0$ projection, where the same horizon structure releases the distinct-plus-dispersed record outward. The black-hole and white-hole descriptions are complementary linear-time projections of one phase-time boundary.

This section derives diffusion from the clock-rate force branch and recovers Schrodinger dynamics through the coherent phase-time branch. The dissipative and coherent descriptions are treated as projections of one temporal structure.

10.4 Informational Diffusion and Schrödinger Dynamics from the Clock-Rate Force Branch

Diffusion is another realization of the same clock-rate force branch already obtained from the mismatch energy. Whenever the concentration of distinguishable matter or structure varies from one region to another, the entropic or dispersive load also varies, and therefore the local linear-time factor varies as well. A spatial gradient of concentration is thus also a spatial gradient of local time load.

Write the dissipative branch in terms of the mismatch load energy associated with the local clock-rate factor, connecting Einstein's relativistic dynamics [96], gravitational field theory [97], and thermodynamic or entropic readings of gravity [130] [131]:

$$E_{\text{diff}} = mc^2(1 - \chi).$$

This sign belongs to the dissipative-relaxation projection of the same clock-rate field. The static configuration branch uses the configuration potential

$$U_\chi = mc^2\chi, \quad \mathbf{F}_\chi = -\nabla U_\chi = -mc^2\nabla\chi,$$

while diffusion uses the load energy

$$E_{\text{diff}} = mc^2(1 - \chi).$$

Thus the same χ -field has two complementary projections: configuration response and dissipative relaxation. These two energies are not reciprocal to one another. They are complementary energy readings of the same clock-rate field:

$$E_{\text{diff}} = mc^2(1 - \chi) = mc^2 - U_\chi.$$

The configuration branch follows gradients of the available clock-rate capacity, while the diffusion branch relaxes gradients of the missing or consumed clock-rate capacity. This is the mathematical distinction between gravitational/configurational response and diffusion: gravity follows the load in the configuration potential, while diffusion and osmosis relax the dispersive load created by concentration differences.

The reciprocal variable appears only when the same load is written as the thermodynamic/Lorentz cost

$$\gamma = \frac{1}{\chi}, \quad E_\gamma = mc^2(\gamma - 1) = mc^2\left(\frac{1}{\chi} - 1\right).$$

This gives

$$-\nabla E_\gamma = -mc^2\nabla\gamma = +mc^2\frac{1}{\chi^2}\nabla\chi.$$

Thus the γ -load form points in the same relaxation direction as $E_{\text{diff}} = mc^2(1 - \chi)$. In the weak-load limit $\chi \approx 1$, the two load energies agree to first order:

$$mc^2(1 - \chi) \simeq mc^2\left(\frac{1}{\chi} - 1\right).$$

The diffusion force is the negative gradient of this dissipative-load energy,

$$F_{\text{diff}} = -\nabla E_{\text{diff}} = -\nabla [mc^2(1 - \chi)] = +mc^2\nabla\chi.$$

Now consider a medium whose local state is characterized by a concentration or dispersive-load field $C(x)$. If different concentrations correspond to different local dispersive loads, then the local time factor becomes a function of concentration,

$$\chi = \chi(C).$$

Applying the chain rule gives

$$\nabla\chi = \frac{d\chi}{dC}\nabla C.$$

The force law therefore becomes

$$F_{\text{diff}} = mc^2 \frac{d\chi}{dC} \nabla C.$$

This is the real dissipative diffusion force. It is not introduced independently. It appears because different concentrations correspond to different local informational and entropic loads, which means different local rates of linear-time realization. Wherever the local time field varies, the clock-rate branch generates a dissipative-load force.

To obtain the transport law, balance this force against viscous drag in the standard overdamped limit. If the mobility is μ , then the drift velocity is

$$v = \mu F_{\text{diff}} = \mu mc^2 \frac{d\chi}{dC} \nabla C.$$

The corresponding flux is

$$J = Cv = \mu mc^2 C \frac{d\chi}{dC} \nabla C.$$

In the load variable used here, increasing concentration increases the local dispersive load and therefore decreases the available time factor, so

$$\frac{d\chi}{dC} < 0.$$

The positive dissipative diffusion coefficient is therefore

$$D_{\text{diss}} \equiv -\mu mc^2 C \frac{d\chi}{dC} > 0.$$

With this sign convention, the transport law takes the standard Fick form

$$J = -D_{\text{diss}} \nabla C.$$

This is Fick's law in its classical transport form [132], placed here in contact with Einstein's Brownian-motion treatment of diffusion [133]. In the present framework it arises because concentration differences imply different local informational loads, different local time rates, and therefore a real force that drives transport down the gradient. Real dissipative diffusion is therefore the transport limit of the same clock-rate mismatch mechanism, evaluated through the dissipative-load projection $F_{\text{diff}} = +mc^2 \nabla\chi$.

For the ideal dilute case used in Section 3.8, one may set $C = n$ and $\mu = M$. The Section 3.8 chemical-potential gradient requires

$$mc^2 \frac{d\chi}{dn} \nabla n = -k_B T \nabla \ln n = -\frac{k_B T}{n} \nabla n,$$

so that

$$\frac{d\chi}{dn} = -\frac{k_B T}{mc^2 n}.$$

Substitution into the dissipative coefficient gives

$$D_{\text{diss}} = -\mu mc^2 n \frac{d\chi}{dn} = M k_B T,$$

which recovers the same Einstein mobility-diffusion relation obtained in Section 3.8.

10.5 Phase-Time Diffusion and Complex Schrödinger Transport

The Schrödinger bridge uses a different projection of the same architecture: the coherent phase-time branch. The dissipative coefficient D_{diss} above belongs to real Fick transport. The coherent quantum coefficient belongs to the phase branch and is fixed by the Compton scale of the massive carrier,

$$D_q = \frac{\hbar}{2m}.$$

Using the phase-time law developed above, the elementary coherent Compton branch is obtained by taking the coherent normalized branch of the registration ratio.

On the elementary coherent Compton branch this becomes

$$dt_{\phi, \text{coh}} = \tau_C^{(\omega)} e^{-i\phi} d\phi.$$

The coherent Schrödinger projection is obtained on the pure phase-time orientation

$$\phi = -\frac{\pi}{2},$$

for which

$$e^{-i\phi} = e^{-i(-\pi/2)} = e^{i\pi/2} = i.$$

Thus the coherent phase-time increment is

$$dt_{\phi} = i dt_{\text{linear}},$$

where t_{linear} denotes the magnitude of the realized linear-time parameter. Equivalently,

$$\frac{\partial}{\partial t_\phi} = -i \frac{\partial}{\partial t_{\text{linear}}}.$$

The coherent phase-time diffusion equation is then

$$\frac{\partial \psi}{\partial t_\phi} = D_q \nabla^2 \psi.$$

Substituting $dt_\phi = i dt_{\text{linear}}$ gives

$$-i \frac{\partial \psi}{\partial t_{\text{linear}}} = D_q \nabla^2 \psi.$$

Multiplication by $-\hbar$ yields

$$i\hbar \frac{\partial \psi}{\partial t_{\text{linear}}} = -\hbar D_q \nabla^2 \psi.$$

Using the coherent quantum diffusion coefficient $D_q = \hbar/(2m)$ gives

$$i\hbar \frac{\partial \psi}{\partial t_{\text{linear}}} = -\frac{\hbar^2}{2m} \nabla^2 \psi.$$

This is the free Schrödinger equation [90], connected here with Madelung’s hydrodynamic form [134] and Bohm’s pilot-wave reconstruction [135], Nelson’s stochastic reconstruction [136] and related stochastic mechanics [137], and Feynman’s path-integral perspective [138] and the Feynman–Kac bridge between diffusion and quantum amplitudes [139]. The result is not a formal Wick rotation [140] imposed from outside. It is the coherent phase-time projection of diffusion under the UiT time law. Ordinary Fick diffusion, described by the standard Fokker–Planck and stochastic-process treatments [141] [142], remains the real dissipative projection, while Schrödinger evolution is the coherent phase projection of the same informational-time structure.

The same result can be stated in compact form. Diffusion and Schrödinger evolution are not two unrelated laws. They are the same transport architecture evaluated on two different temporal projections. In the realized branch, time is real and the equation remains dissipative transport with coefficient D_{diss} . In the coherent branch, the realized projection vanishes, $\phi = -\pi/2$, and the same architecture is evaluated on the purely imaginary temporal increment

$$dt_\phi = i dt_{\text{linear}}.$$

The coherent branch uses

$$D_q = \frac{\hbar}{2m},$$

and therefore becomes

$$i\hbar \frac{\partial \psi}{\partial t_{\text{linear}}} = -\frac{\hbar^2}{2m} \nabla^2 \psi,$$

which is exactly the free Schrödinger equation. The coherent quantum branch is therefore not added to diffusion from outside. It emerges directly from the phase-time law.

The thermodynamic direction of records is read here through Boltzmann's statistical irreversibility [\[32\]](#) and modern information-theoretic accounts of the arrow of time [\[143\]](#).

11 Unified Action, Cosmology, and Metric Residues

This section collects the action-level formulation, the cosmological time-action terms, and the metric-residue construction associated with the real projection of electromagnetic phase-time structure.

11.1 The Unified Informational Action

The preceding sections developed the writing channels, relativistic capacity metric, phase connection, diffusion branch, and internal interaction sectors within the action-based language of field theory [68]. These structures combine in a single effective action whose geometric core is the informational metric $g_{\mu\nu}^{(I)}$ derived above. The local clock-rate-capacity field χ is the scalar projection of this metric in the sector under consideration. In the static gravitational sector,

$$g_{tt}^{(I)} = -c^2 \chi^2.$$

In kinematics the same symbol denotes the surviving temporal writing fraction $\chi_v = \sqrt{1 - v^2/c^2}$. In the action language, the metric $g_{\mu\nu}^{(I)}$ carries the gravitational degree of freedom, while χ is used as the local projection that generates the force laws and transport limits.

Using the same metric and normalization conventions as the tensor completion, the unified effective action is written as an effective-field-theory action [184] [185] [186] [244] [187]

$$\mathcal{A}_{\text{unified}} = \int d^4x \sqrt{-g^{(I)}} \left[\frac{c^3}{16\pi G} \left(R[g^{(I)}] - 2\Lambda_\tau \right) + \mathcal{L}_{\text{src}}^{(I)} + \mathcal{L}_{\text{EW}} + \mathcal{L}_{\text{diff}} + \mathcal{L}_{\text{flavor}} + \mathcal{L}_{\text{strong}} + \mathcal{L}_{\Xi} + \mathcal{L}_{\text{int}} \right].$$

This expression collects the previously derived sectors in one variational framework. The electroweak interface sector is represented by \mathcal{L}_{EW} , built from the $SU(2)$ temporal-doublet connection W_μ^a , the $U(1)_Y$ phase-fiber connection B_μ , the rewrite doublet Ψ_τ , the weak rewrite scale E_{rewrite} , and the neutral fiber metric $G_{\text{EW}}^{(0)}$. The electroweak part contains the covariant doublet term $(D_\mu \Psi_\tau)^\dagger (D^\mu \Psi_\tau)$, whose fixed rewrite norm

$$\langle \Psi_\tau \rangle = \frac{1}{\sqrt{2}} \begin{pmatrix} 0 \\ E_{\text{rewrite}} \end{pmatrix}$$

gives the charged and neutral weak-boson mass projections described above. After the electroweak rotation, this sector separates into the electromagnetic transport branch and the weak temporal-rewrite branch. The effective neutral mixing angle is determined by the neutral interface metric

$$G_{\text{EW}}^{(0)} = \begin{pmatrix} R_\tau^2 & C_{\phi\tau} \\ C_{\phi\tau} & R_\phi^2 \end{pmatrix}.$$

The curvature term is the same capacity action introduced in the tensor completion. Its variation gives

$$G_{\mu\nu}[g^{(I)}] + \Lambda_\tau g_{\mu\nu}^{(I)} = \frac{8\pi G}{c^4} T_{\mu\nu}^{(I)}.$$

The source term $\mathcal{L}_{\text{src}}^{(I)}$ generates the informational stress-energy tensor,

$$T_{\mu\nu}^{(I)} = -\frac{2c}{\sqrt{-g^{(I)}}} \frac{\delta \mathcal{A}_{\text{src}}^{(I)}}{\delta g_{(I)}^{\mu\nu}},$$

in the $x^0 = t$ convention used throughout this manuscript. It contains the mass-writing, motion-writing, temporal-registration, dispersive-cost, pressure, flux, and anisotropic-stress contributions defined in the tensorial reconstruction.

The Bianchi identity fixes the conservation structure. For a variable homogeneous temporal-writing term,

$$\nabla^\mu \left(T_{\mu\nu}^{(I)} - \frac{c^4}{8\pi G} \Lambda_\tau g_{\mu\nu}^{(I)} \right) = 0,$$

or equivalently

$$\nabla^\mu T_{\mu\nu}^{(I)} = \frac{c^4}{8\pi G} \partial_\nu \Lambda_\tau.$$

Thus the unified action uses the same conservation law already obtained from the covariant metric reconstruction.

The electromagnetic term is the post-rotation action-level component obtained from \mathcal{L}_{EW} after the Weinberg rotation. In the boxed unified action, \mathcal{L}_{EW} denotes the pre-rotation electroweak fiber sector; the expression below is its electromagnetic projection, not an additional independently counted sector.

The electromagnetic branch is encoded by [188]

$$\mathcal{L}_{\text{EM}} = -\frac{1}{4} F_{\mu\nu} F^{\mu\nu} - J^\mu A_\mu, \quad F_{\mu\nu} = \partial_\mu A_\nu - \partial_\nu A_\mu.$$

The electromagnetic field term is written in rationalized natural/Heaviside–Lorentz normalization; SI factors such as μ_0 are restored by the standard rescaling of $F_{\mu\nu}$, A_μ , and J^μ . Here A_μ is the full dynamical phase-time connection. This is the field-theoretic completion of the coherent phase branch. Variation with respect to A_μ gives

$$\nabla_\nu F^{\nu\mu} = J^\mu,$$

while the definition of $F_{\mu\nu}$ gives the homogeneous Maxwell identity. The connection A_μ is the transport rule for comparing the phase-time fiber over neighboring spacetime points.

The diffusion branch is written in terms of a concentration field $C(x)$ and the same metric capacity map:

$$\mathcal{L}_{\text{diff}} = -\frac{D_0}{2} g^{(I)\mu\nu} \partial_\mu C \partial_\nu C - \mathcal{U}_{\text{diff}}(C, \chi).$$

D_0 is the phenomenological informational transport stiffness of the diffusive branch. It sets the action-level cost of maintaining gradients in the concentration or distinguishability field C , and in the hydrodynamic limit it corresponds to the macroscopic diffusion response of the medium.

The force-level diffusive load is the per-carrier quantity

$$u_{\text{diff}}(C) = mc^2 [1 - \chi(C)].$$

The action-level potential is the corresponding energy density,

$$\mathcal{U}_{\text{diff}}(C) = C u_{\text{diff}}(C) = C m c^2 [1 - \chi(C)].$$

This separates the units of the action density from the per-carrier force law. The clock-rate projection gives the common field, while the sign is set by the physical branch. The configuration branch uses

$$U_\chi = m c^2 \chi, \quad \mathbf{F}_\chi = -\nabla U_\chi = -m c^2 \nabla \chi,$$

whereas the dissipative-load branch uses

$$u_{\text{diff}} = m c^2 (1 - \chi), \quad \mathbf{F}_{\text{diff}} = -\nabla u_{\text{diff}} = +m c^2 \nabla \chi.$$

Thus the action keeps the same χ -field while separating configuration response from dissipative relaxation. The two per-carrier projections are related by

$$u_{\text{diff}} = m c^2 - U_\chi,$$

so the opposite sign is the relaxation projection of the same field. If the same local load is expressed by $\gamma = 1/\chi$, then

$$-m c^2 \nabla \gamma = +m c^2 \frac{1}{\chi^2} \nabla \chi,$$

which has the same relaxation direction and reduces to $+m c^2 \nabla \chi$ in the weak-load limit. The $\nabla \chi$ projection therefore supplies the common clock-rate branch: inertia and gravitation use the configuration projection $U_\chi = m c^2 \chi$, while diffusion and osmosis use the complementary dissipative-load projection $u_{\text{diff}} = m c^2 (1 - \chi)$.

The corresponding per-carrier derivative is

$$\frac{\partial u_{\text{diff}}}{\partial C} = -m c^2 \frac{d\chi}{dC}.$$

The relaxation force is therefore

$$\mathbf{F}_{\text{diff}} = -\nabla u_{\text{diff}} = +m c^2 \nabla \chi = m c^2 \frac{d\chi}{dC} \nabla C.$$

Since increasing concentration increases dispersive load and decreases χ , one has $d\chi/dC < 0$. Balancing this force against the effective transport resistance gives the diffusive flux law $J = -D \nabla C$ on the clock-rate branch, while the Schrödinger branch is obtained when the same transport structure is evaluated on coherent phase-time.

The complex time-load sector is encoded by

$$\mathcal{L}_\Xi = \mathcal{L}_\Xi \left(\Xi, D_\mu \Xi; g_{\mu\nu}^{(I)} \right), \quad \Xi(x) = \chi(x) e^{-i\phi(x)}.$$

The local phase-completed energy carrier is

$$U_\phi(x) = E_0 \Xi(x),$$

with E_0 supplied by the sector under consideration. Its gradient gives the configuration-potential force expression

$$\boxed{\mathbf{F}_\phi = -E_0 \nabla \Xi.}$$

The complementary closure-cost or dissipative-load form is

$$\boxed{u_\phi(x) = E_0 [1 - \Xi(x)], \quad \mathbf{F}_\phi = -\nabla u_\phi = E_0 \nabla \Xi.}$$

Sectors written as capacity potentials use $U_\phi = E_0 \Xi$, while closure-cost or dissipative-load sectors use $u_\phi = E_0(1 - \Xi)$. The strong confinement branch is written in the closure-cost form. For massive matter, the configuration-potential expression becomes

$$\mathbf{F}_\phi = -mc^2 \nabla (\chi e^{-i\phi}) = -mc^2 e^{-i\phi} \nabla \chi + imc^2 \chi e^{-i\phi} \nabla \phi.$$

The $\nabla \chi$ projection gives the common clock-rate-capacity branch. Inertia and gravitation use the configuration projection $U_\chi = mc^2 \chi$, whereas diffusion and osmosis use the complementary dissipative-load projection $u_{\text{diff}} = mc^2(1 - \chi)$. The $\nabla \phi$ projection gives the coherent phase branch: gauge connection, electromagnetic curvature, and phase-coherent transport.

The weak and strong effective sectors use the same action language. The weak projection of \mathcal{L}_{EW} , denoted $\mathcal{L}_{\text{weak}}$ in the sector discussion, represents negative-linear-time thermodynamic unwriting and rewrite. It acts on the branch

$$d\tau = \tau_C^{(\omega)} \chi \cos \phi d\phi < 0, \quad \cos \phi < 0,$$

where the forward writing law

$$-dI_{\text{pot}} = dI_{\text{dist}} + dI_{\text{disp}}$$

is read as

$$-dI_{\text{dist}} - dI_{\text{disp}} = dI_{\text{pot}}.$$

The rewrite barrier is

$$B_{\text{eff}} = \ln 2 \Delta I_w, \quad dI_w = -(dI_{\text{dist}} + dI_{\text{disp}}) = dI_{\text{pot}}, \quad d\tau < 0,$$

and the corresponding transition weight is

$$p_{\text{rewrite}} = e^{-B_{\text{eff}}} = 2^{-\Delta I_w}.$$

It weights flavor-changing transitions by the rewrite-bit barrier for returning the previous distinct-plus-dispersed record to the potential sector and writing the new closed Compton phase-time resonance. The flavor-resonance notation is recorded by

$$\mathcal{L}_{\text{flavor}} = \mathcal{L}_{\text{flavor}}(|\omega_{C,f}\rangle, \mathcal{R}_{\text{weak}}, V_{ij}),$$

with

$$|f\rangle = |\omega_{C,f}\rangle, \quad \mathcal{R}_{\text{weak}}|f_i\rangle = \sum_j V_{ji}|f_j\rangle.$$

The strong term $\mathcal{L}_{\text{strong}}$ represents confined internal phase-time circulation and its QCD-limit notation,

$$\mathcal{L}_{\text{strong}} = \mathcal{L}_{\text{cl}} + \mathcal{L}_{\text{SU}(3),\text{lim}},$$

where

$$\mathcal{L}_{\text{cl}} = \mathcal{L}_{\text{cl}}(\phi_{\text{cl}}, V_{\text{strong}}, \Xi_{\text{strong}}, u_{\text{conf}}^{(\phi)}),$$

with

$$u_{\text{conf}}^{(\phi)} = E_{\text{conf}} (1 - \Xi_{\text{strong}}).$$

The QCD-limit term is the standard gluon-plus-quark action limit,

$$\mathcal{L}_{\text{SU}(3),\text{lim}} \sim -\frac{1}{4} G_{\mu\nu}^a G^{a\mu\nu} + \sum_f \bar{q}_f (i\gamma^\mu D_\mu - m_f) q_f.$$

Here

$$D_\mu q_f = \left(\partial_\mu + ig_s G_\mu^a T_a \right) q_f, \quad q_f \in \mathbf{3}.$$

The non-Abelian field-strength notation is

$$G_{\mu\nu}^a = \partial_\mu G_\nu^a - \partial_\nu G_\mu^a + g_s f^{abc} G_\mu^b G_\nu^c.$$

Its closure potential is

$$V_{\text{strong}} = \kappa \left| \sum_{i=1}^3 e^{i\phi_i} \right|^2 + \int_0^L \varepsilon_{\text{cl}} ds,$$

where the closure-energy density is related to the local normalized color load by

$$\varepsilon_{\text{cl}}(s) = E_{\text{conf}} \left| \frac{d\chi_{\text{strong}}}{ds} \right| = \frac{E_{\text{conf}}}{2\chi_{\text{strong}}(s)} \left| \frac{d\Lambda_{\text{color}}}{ds} \right|, \quad \chi_{\text{strong}}^2 + \Lambda_{\text{color}} = 1.$$

The constant-density confinement limit is

$$\int_0^L \varepsilon_{\text{cl}}(s) ds \simeq \sigma L, \quad \sigma = \frac{1}{L} \int_0^L \varepsilon_{\text{cl}}(s) ds.$$

Thus Λ_{color} is the local normalized closure-load variable, while σL is the accumulated closure energy. In the effective long-distance notation, the factor $1/(2\chi_{\text{strong}})$ is absorbed into the phenomenological string tension σ . The phase-completed internal load is

$$\Xi_{\text{strong}}(A) = \chi_{\text{strong}}(A) e^{-i\Phi_A},$$

where A denotes the internal elongation and phase coordinates and Φ_A denotes the internal phase-time circulation orientation. The phase-completed closure-cost potential is

$$u_{\text{conf}}^{(\phi)}(A) = E_{\text{conf}} [1 - \Xi_{\text{strong}}(A)].$$

The strong restoring force is

$$F_A^{(\text{strong})} = -\nabla_A u_{\text{conf}}^{(\phi)} = E_{\text{conf}} \nabla_A \Xi_{\text{strong}}.$$

For confinement along the elongation coordinate, the local closure-cost projection is

$$u_{\text{conf}}(s) = E_{\text{conf}} (1 - \chi_{\text{strong}}(s)),$$

while the accumulated confinement potential is

$$V_{\text{conf}}(L) = \int_0^L \varepsilon_{\text{cl}}(s) ds.$$

Thus the restoring force is

$$F_L^{\text{restore}} = -\frac{dV_{\text{conf}}}{dL} = -\varepsilon_{\text{cl}}(L) = E_{\text{conf}} \frac{\partial \chi_{\text{strong}}}{\partial L}, \quad \frac{\partial \chi_{\text{strong}}}{\partial L} < 0,$$

with magnitude $|F_L^{\text{restore}}| \simeq \sigma$ in the approximately constant-density limit. These terms express the closure-cost branch of the internal strong sector: the restoring force is the negative gradient of the closure-cost potential, equivalently the gradient of the remaining closure capacity.

The interaction term \mathcal{L}_{int} collects the couplings among matter currents, phase connection, concentration fields, and internal phase variables. In the metric sector the gravitational response is carried by $g_{\mu\nu}^{(I)}$; in transport and material sectors the scalar χ remains the local projection that converts metric capacity gradients into ordinary force laws. The unified action therefore matches the tensorial relativistic reconstruction and the later phase, weak, strong, diffusion, and superconducting branches with one metric representation of the gravitational degree of freedom.

11.2 Metric Fiber Form of the Unified Action

The preceding action can also be read directly from the metric fiber form developed in the electromagnetic, electroweak, and strong sectors, using the standard differential-geometric language of bundles and connections [43] [44]. The unified action is therefore the effective four-dimensional action of one informational spacetime base together with the phase-time fibers transported over that base.

The compact summary of the fiber geometry is the base-plus-fiber form of the unified gauge structure [92].

$$\boxed{dS_{\text{UIT}}^2 = g_{\mu\nu}^{(I)} dx^\mu dx^\nu + R_\phi^2 (D\phi)^2 + R_\tau^2 \langle D\Psi_\tau, D\Psi_\tau \rangle + R_s^2 \langle D\Phi_c, D\Phi_c \rangle.}$$

The first term is the realized informational spacetime base, whose curvature term is the general-relativistic action structure [68]. Its scalar curvature gives the Einstein-Hilbert capacity action and its local clock-rate projection is the field χ . In this sector inertia and gravitation use the configuration potential

$$U_\chi = mc^2 \chi, \quad \mathbf{F}_\chi = -mc^2 \nabla \chi.$$

The same χ -field also supplies the complementary dissipative-load projection used by diffusion and osmosis,

$$u_{\text{diff}} = mc^2 (1 - \chi), \quad \mathbf{F}_{\text{diff}} = +mc^2 \nabla \chi.$$

Thus the sign difference between gravitation and diffusion expresses the difference between the configuration projection and the relaxation projection of the same clock-rate-capacity field.

The second term is the compact phase-time fiber, whose connection term matches the gauge-field action language used in quantum field theory [244]. Its covariant increment is

$$D\phi = d\phi - \frac{q}{\hbar} A_\mu dx^\mu.$$

Expansion of this fiber term gives the mixed metric connection

$$g_{\mu\phi} \propto A_\mu,$$

and the curvature of this connection is

$$F_{\mu\nu} = \partial_\mu A_\nu - \partial_\nu A_\mu.$$

The electromagnetic action term \mathcal{L}_{EM} is the four-dimensional field-action expression of this phase-fiber curvature.

The third term is the temporal-doublet fiber. The doublet

$$\Psi_\tau = \begin{pmatrix} \psi_+ \\ \psi_- \end{pmatrix}$$

represents the two local orientations of realized-time writing, corresponding to the two signs of the real projection $\cos\phi$. This is the temporal-orientation substrate; the Standard Model fermion doublets remain the low-energy matter doublets on which the weak connection acts. Its covariant transport is

$$D_\mu \Psi_\tau = \left[\partial_\mu + igW_\mu^a \frac{\sigma_a}{2} + ig'B_\mu \frac{Y}{2} \right] \Psi_\tau.$$

Expansion of the doublet fiber term gives the electroweak mixed metric connections

$$g_{\mu a}^{(\text{weak})} \propto W_\mu^a, \quad g_{\mu Y} \propto B_\mu.$$

The corresponding curvatures are

$$W_{\mu\nu}^a = \partial_\mu W_\nu^a - \partial_\nu W_\mu^a + g\epsilon^{abc}W_\mu^b W_\nu^c,$$

and

$$B_{\mu\nu} = \partial_\mu B_\nu - \partial_\nu B_\mu.$$

After the Weinberg rotation these fields separate into the electromagnetic transport branch and the neutral and charged weak branches already described in the electroweak sector. Thus \mathcal{L}_{EW} is the action-level expression of the temporal-doublet fiber metric.

The compact diagonal form above is the separated fiber expression. In the neutral electroweak plane, the phase-time fiber and rewrite fiber share the same two-sphere realization interface, so the effective neutral fiber metric is

$$G_{\text{EW}}^{(0)} = \begin{pmatrix} R_\tau^2 & C_{\phi\tau} \\ C_{\phi\tau} & R_\phi^2 \end{pmatrix}.$$

The effective mixing angle is therefore the metric projection angle of this neutral interface,

$$\theta_{\text{eff}} = \theta(G_{\text{EW}}^{(0)}).$$

In the flat-fiber limit $C_{\phi\tau} = 0$, this reduces to the tree-level Weinberg projection; with interface overlap, the neutral projection uses the full metric angle.

The fourth term is the strong phase-time closure fiber. The color phase-time triplet

$$\Phi_c = \begin{pmatrix} e^{i\phi_1} \\ e^{i\phi_2} \\ e^{i\phi_3} \end{pmatrix}$$

obeys the symmetric color-triangle closure condition

$$e^{i\phi_1} + e^{i\phi_2} + e^{i\phi_3} = 0.$$

The associated determinant-preserving phase representation is

$$\phi_1 + \phi_2 + \phi_3 = 0 \pmod{2\pi}.$$

Its covariant transport is

$$D_\mu \Phi_c = \left[\partial_\mu + ig_s G_\mu^a T_a \right] \Phi_c, \quad T_a = \frac{\lambda_a}{2}.$$

Expansion of the strong fiber term gives the mixed color connections

$$g_{\mu a}^{(\text{strong})} \propto G_\mu^a,$$

with non-Abelian curvature

$$G_{\mu\nu}^a = \partial_\mu G_\nu^a - \partial_\nu G_\mu^a + g_s f^{abc} G_\mu^b G_\nu^c.$$

The self-coupling term is the metric expression of transporting a closed three-orientation phase-time system whose connection carries the closure structure itself. The closure-tension part of the strong sector is the metric cost of preserving the same $SU(3)$ phase-time closure over spatial separation,

$$V_{\text{strong}} = \kappa \left| \sum_{i=1}^3 e^{i\phi_i} \right|^2 + \int_0^L \varepsilon_{\text{cl}}(s) ds,$$

with the confinement limit for static color sources

$$\int_0^L \varepsilon_{\text{cl}}(s) ds \text{ to } \sigma L.$$

The corresponding phase-completed closure-cost potential is

$$\boxed{u_{\text{conf}}^{(\phi)} = E_{\text{conf}} (1 - \Xi_{\text{strong}})}.$$

In full QCD with dynamical quarks, the same long-distance linear growth is eventually interrupted by string breaking through quark-antiquark pair creation.

In this metric-fiber reading, the action terms are the variational expressions of one geometric structure:

$\mathcal{L}_{\text{grav}}$ paired with $g_{\mu\nu}^{(I)}, \chi$,

\mathcal{L}_{EM} paired with $U(1)$ post-rotation phase-fiber projection, $A_\mu, F_{\mu\nu}$,

\mathcal{L}_{EW} paired with $SU(2) \times U(1)_Y$ pre-rotation temporal-doublet fiber, W_μ^a, B_μ ,

$\mathcal{L}_{\text{strong}}$ paired with $SU(3)$ three-orientation phase-time closure fiber, $G_\mu^a, G_{\mu\nu}^a, \Xi_{\text{strong}}, u_{\text{conf}}^{(\phi)}$,

$\mathcal{L}_{\text{diff}}$ paired with $u_{\text{diff}} = mc^2(1 - \chi)$.

The unified action is therefore the action-level form of the same base-plus-fiber geometry. The base metric gives the gravitational and inertial clock-rate structure; the electroweak temporal-doublet fiber contains the post-rotation electromagnetic phase-time fiber and the weak rewrite structure; the three-orientation phase-time closure fiber gives the strong interaction; and the complementary $1 - \chi$ projection gives diffusion and osmosis.

11.3 Cosmic Inflation, Self-Braking, and Dark Energy from the Time Action

The same informational action supplies the cosmological regime. The gravitational contribution is the capacity action already defined above,

$$\mathcal{A}_{\text{cap}} = \frac{c^3}{16\pi G} \int d^4x \sqrt{-g^{(I)}} \left(R[g^{(I)}] - 2\Lambda_\tau \right),$$

with local sources contained in $\mathcal{A}_{\text{src}}^{(I)}$. In a homogeneous cosmological branch, the informational metric is written as

$$ds^2 = -c^2 \Theta_\tau(t)^2 dt^2 + a(t)^2 \bar{g}_{ij} dx^i dx^j,$$

where $\Theta_\tau(t)$ is the homogeneous temporal-writing metric factor. The local load factor χ used in the inertial and static gravitational sectors remains the normalized surviving temporal-writing fraction satisfying $\chi^2 + \Lambda_I = 1$. The cosmological opening variable is the homogeneous source ratio

$$\mathcal{R}_\tau(t) = dt^* = \frac{dI_{\text{dist}}}{dI_{\text{disp}}} = (k_B \ln 2) \frac{dI_{\text{dist}}}{dS}.$$

The cosmological sector uses \mathcal{R}_τ as the homogeneous temporal-writing source ratio. The local dissipative sector uses η_{th} as the bounded registration efficiency. The metric factor $\Theta_\tau(t)$ is the geometric response of the homogeneous capacity map to this source ratio and to the vacuum-writing term $\Lambda_\tau(t)$. This notation keeps the local load variable χ distinct from the cosmological metric-opening response.

The cosmological field equation is the homogeneous projection of the same tensor equation,

$$G_{\mu\nu}[g^{(I)}] + \Lambda_\tau(t) g_{\mu\nu}^{(I)} = \frac{8\pi G}{c^4} T_{\mu\nu}^{(I)}.$$

For an isotropic informational source this gives the Friedmann-type capacity equation

$$H^2 = \frac{8\pi G}{3} \rho_I + \frac{c^2}{3} \Lambda_\tau - \frac{kc^2}{a^2},$$

where ρ_I is the homogeneous mass-equivalent information-source density written by the source sector, defined from the information-energy density ε_I by

$$\rho_I \equiv \frac{\varepsilon_I}{c^2}.$$

With this definition, the Friedmann source term has the standard mass-density form $8\pi G \rho_I/3$. The Bianchi identity imposes the exchange law

$$\nabla^\mu T_{\mu\nu}^{(I)} = \frac{c^4}{8\pi G} \partial_\nu \Lambda_\tau,$$

so the homogeneous temporal-writing term and the ordinary informational source form one conserved total source.

The cosmological interpretation is then immediate. [189] [190] In the early universe, before the full differentiated structure of matter had stabilized, symmetry breaking generated a rapid surge of physically distinct structure. [191] [192] [193] [194] Mass sectors, charge sectors, interaction

channels, and distinguishable particle content appeared in a short interval while the entropy budget was still comparatively low. In the notation of the theory,

$$dI_{\text{dist}} \text{ strongly increases,} \quad dI_{\text{disp}} \text{ small}$$

implies

$$\mathcal{R}_\tau(t) = \frac{dI_{\text{dist}}}{dI_{\text{disp}}} \text{ large.}$$

This is the inflationary regime of the theory: the homogeneous temporal-writing source becomes large, and the metric opens accordingly through $\Theta_\tau(t)$ and $\Lambda_\tau(t)$. Here metric opening means an increase in distinguishable configuration-writing capacity, represented geometrically by the effective metric. Since temporal writing and spatial scale are components of the same informational metric, a sharp rise in the homogeneous temporal-writing source appears geometrically as rapid metric opening.

The same mechanism explains why inflation slows. As the universe evolves, entropy grows and the dispersed informational sector accumulates. The denominator in the ratio defining \mathcal{R}_τ therefore increases, so the homogeneous temporal-writing drive is reduced. In the language of the action, the growth of thermodynamic load suppresses the same temporal-writing source that initially drove rapid opening. The expansion is self-braking because the entropic sector catches up with the informational burst that originally opened the metric.

One may summarize the mechanism in the following sequence:

$$\text{early symmetry breaking implies } dI_{\text{dist}} \text{ strongly increases,} \quad dI_{\text{disp}} \text{ small}$$

$$\text{implies } \mathcal{R}_\tau = \frac{dI_{\text{dist}}}{dI_{\text{disp}}} \text{ large}$$

$$\text{implies rapid metric opening.}$$

followed by

$$dI_{\text{disp}} \text{ increases implies } \mathcal{R}_\tau \text{ decreases}$$

$$\text{implies self-braking of inflation.}$$

The late universe is then understood as the residual tail of the same process. Inflation is no longer in its violent early regime because the entropic denominator has grown substantially, yet the homogeneous temporal-writing term need not relax all the way to zero. If a small residual temporal-writing source remains, or equivalently if the potential leaves a weak effective vacuum contribution, then the metric continues to open slightly at late times.

This can be written in the standard effective fluid form associated with the homogeneous temporal-writing sector:

$$\rho_\tau = \frac{\kappa_\tau}{2} \dot{\Theta}_\tau^2 + V(\Theta_\tau), \quad p_\tau = \frac{\kappa_\tau}{2} \dot{\Theta}_\tau^2 - V(\Theta_\tau).$$

Whenever the potential term dominates, in the observational dark-energy setting opened by Riess et al. [195], Perlmutter et al. [196], and the cosmological review tradition of Peebles [197],

$$V(\Theta_\tau) \gg \frac{\kappa_\tau}{2} \dot{\Theta}_\tau^2,$$

one obtains the effective negative-pressure regime

$$p_\tau \approx -\rho_\tau,$$

which is the structure associated with dark energy in the supernova evidence [195] [196] and modern cosmological interpretation [197]. In the present framework, this is the weak residual continuation of the same time-load dynamics that opened the metric violently in the early universe and was later braked by the growth of the dispersed sector.

The result is that inflation, its natural braking, and the present weak accelerated expansion, measured through supernova evidence [195] [196] and summarized in modern cosmological-parameter fits [198] [199] [200], arise from one and the same informational structure. In the early universe, symmetry breaking under low-entropy conditions drives a large homogeneous temporal-writing source and produces a burst of metric opening. As entropy accumulates, that opening is damped automatically. What remains at late times is the weak residual tail of the same field, observed cosmologically as dark energy.

11.4 Osmosis as the Membrane Limit of Local Capacity Opening

Section 3.8 showed that ordinary diffusion follows when the already identified equality

$$\gamma_{\text{th}} = \gamma_I$$

is applied locally, with the local Lorentz load branch written as

$$mc^2[\gamma(x) - 1] = \Delta\mu_{\text{load}}(x), \quad \gamma = \frac{1}{\chi}.$$

The same construction gives the osmotic case once transport is constrained by a semipermeable membrane, the classical setting of osmotic pressure [87]. Osmosis is therefore the membrane-limited expression of the same local time-capacity gradient that appears as diffusion in an unconstrained medium.

This is why osmosis is naturally read as local capacity opening. A gravitational load reduces available clock-rate capacity through the configuration projection $U_\chi = mc^2\chi$, producing the response $-mc^2\nabla\chi$. A concentration load reduces available clock-rate capacity through the per-carrier dissipative projection $u_{\text{diff}} = mc^2(1 - \chi)$, producing the relaxation response $+mc^2\nabla\chi$. Across a semipermeable membrane, the blocked distinctions maintain a concentration difference, and the system responds by opening the allowed transport channel until the dispersive-load gradient is relaxed. The standard osmotic pressure is therefore the macroscopic pressure form of the same sign structure that gives Fick transport.

The important point is that this local construction is not separate from the time action used in the cosmological sector. The capacity action has the schematic form

$$S_\chi = \int d^4x \sqrt{-g} \left[\frac{K_\chi}{2} \partial_\mu \chi \partial^\mu \chi - V(\chi) \right].$$

A membrane imposes boundary conditions on the allowed flow of the density field, matching the thermodynamic membrane-transport formulation of Kedem and Katchalsky [88]. The resulting concentration gradient opens a local capacity/time-load difference across the boundary. In the ideal dilute limit this recovers the standard osmotic pressure relation [87]

$$\Pi = k_B T \Delta n,$$

or, in molar form,

$$\Pi = cRT.$$

In UiT language, the membrane selects which distinctions can cross and which remain blocked. The osmotic pressure is the macroscopic expression of that constrained information-flow gradient.

11.5 Dark Matter as Metric Residue: Realized Time as the Linear Projection of Phase-Time

The empirical dark-matter background includes cluster dynamics [201], galactic rotation curves [202] [203] and MOND/radial-acceleration phenomenology [204] [205], halo profiles [206] [207], and particle-dark-matter reviews [208] [209]. The starting point is the phase-time differential

$$dt_\phi = \tau_C^{(\omega)} \chi e^{-i\phi} d\phi,$$

where $\tau_C^{(\omega)}$ is the angular Compton time scale of the relevant mode, χ is the local clock-rate or time-writing field, and ϕ is the internal phase coordinate.

Using

$$e^{-i\phi} = \cos \phi - i \sin \phi,$$

the linearly recorded component of time is the real projection:

$$d\tau = \Re(dt_\phi) = \tau_C^{(\omega)} \chi \cos \phi d\phi.$$

Thus the realized-time branch is governed by the cosine projection of the deeper phase-time structure.

The Taylor expansion is

$$\cos \phi = 1 - \frac{\phi^2}{2!} + \frac{\phi^4}{4!} - \frac{\phi^6}{6!} + \frac{\phi^8}{8!} - \dots.$$

Therefore,

$$d\tau = \tau_C^{(\omega)} \chi \left(1 - \frac{\phi^2}{2} + \frac{\phi^4}{24} - \frac{\phi^6}{720} + \frac{\phi^8}{40320} - \dots \right) d\phi.$$

This expansion gives the hierarchy of real clock-rate contributions generated by phase-time. The fourth-order coefficient later compared with the electromagnetic residue is read together with the fine-structure constant introduced by Sommerfeld [102] and measured in modern constants tables [103]. Since force in the theory arises from gradients of the clock-rate field,

$$F = -mc^2 \nabla \chi,$$

the Taylor coefficients first define dimensionless clock-rate or metric-load contributions. Dynamical forces appear when these contributions acquire spatial dependence through the physical distribution of matter, phase, records, or boundary structure.

11.6 Quadratic Gravity and the Fourth-Order Electromagnetic Residue

The first nontrivial term in the realized-time projection is

$$-\frac{\phi^2}{2}.$$

In the exterior Schwarzschild field, the gravitational clock-rate factor is [54]

$$\chi_g = \sqrt{1 - \frac{r_s}{r}},$$

where

$$r_s = \frac{2GM}{c^2}.$$

In the weak-field limit,

$$\chi_g \simeq 1 - \frac{1}{2} \frac{r_s}{r}.$$

The phase-time projection gives, to second order,

$$\cos \phi \simeq 1 - \frac{\phi^2}{2}.$$

Matching the real phase-time projection to the weak-field gravitational clock-rate gives

$$1 - \frac{\phi_g^2}{2} \simeq 1 - \frac{1}{2} \frac{r_s}{r},$$

and therefore

$$\phi_g^2 \simeq \frac{r_s}{r}.$$

Thus the second-order real phase-time term reproduces the ordinary Schwarzschild clock-rate load:

$$-\frac{\phi_g^2}{2} = -\frac{1}{2} \frac{r_s}{r}.$$

This identifies ordinary gravity with the quadratic loss of realized time-writing capacity in the real branch of phase-time.

The same clock-rate factor gives the Schwarzschild metric when the temporal and radial components are written as

$$g_{tt} = -c^2 \chi_g^2, \quad g_{rr} = \chi_g^{-2}.$$

Therefore,

$$ds^2 = -c^2 \chi_g^2 dt^2 + \chi_g^{-2} dr^2 + r^2 d\Omega^2.$$

With

$$\chi_g^2 = 1 - \frac{r_s}{r},$$

this becomes

$$ds^2 = -c^2 \left(1 - \frac{r_s}{r}\right) dt^2 + \left(1 - \frac{r_s}{r}\right)^{-1} dr^2 + r^2 d\Omega^2.$$

The second-order term therefore anchors the expansion: the real projection of phase-time contains the standard gravitational clock-rate structure as its quadratic contribution.

After the ordinary gravitational contribution, the next positive real term in the phase-time projection is

$$+\frac{\phi^4}{4!} = +\frac{\phi^4}{24}.$$

This term has a different role from the second-order gravitational term. The second-order term identifies the radial gravitational phase load. The fourth-order term gives the first positive residual contribution in the realized-time branch.

The natural question is therefore: which physically defined phase should enter this fourth-order real residue?

Within the theory, the relevant phase is the electromagnetic phase fraction of the internal mass mode. This phase is measured by the fine-structure constant α .

The use of α is fixed by the internal phase-energy interpretation of charge.

At the Planck scale, the Planck energy is

$$E_P = \frac{\hbar c}{\ell_P}.$$

The electrostatic energy of two elementary charges separated by one Planck length is

$$U_{\text{el}}(\ell_P) = \frac{1}{4\pi\epsilon_0} \frac{e^2}{\ell_P}.$$

Using the definition

$$\alpha = \frac{1}{4\pi\epsilon_0} \frac{e^2}{\hbar c},$$

we obtain

$$U_{\text{el}}(\ell_P) = \alpha \frac{\hbar c}{\ell_P} = \alpha E_P.$$

Therefore,

$$\frac{U_{\text{el}}(\ell_P)}{E_P} = \alpha.$$

In this formulation, α is the electromagnetic phase-energy fraction of the internal Planck-scale mass mode. It measures the fraction of the total internal phase-energy that appears through the electromagnetic sector.

Thus,

$$\phi_{\text{EM}} \sim \alpha$$

is not introduced as a numerical choice. It is the theory's own electromagnetic phase scale.

In informational terms,

$$\alpha = \text{electromagnetic phase-energy fraction of the internal mass mode.}$$

Equivalently, α measures how much of the internal phase structure of mass is expressed as charge and electromagnetic phase relation.

Substituting the electromagnetic phase scale into the fourth-order real term gives

$$\chi_{\text{EM,res}} \sim \frac{\phi_{\text{EM}}^4}{24}.$$

With

$$\phi_{\text{EM}} = \alpha,$$

this becomes

$$\chi_{\text{EM,res}} \sim \frac{\alpha^4}{24}.$$

Using

$$\alpha \simeq \frac{1}{137},$$

one obtains

$$\frac{\alpha^4}{24} = \frac{1}{24 \cdot 137^4} \approx 1.18 \times 10^{-10}.$$

This is a dimensionless clock-rate residue. It is a real projection of electromagnetic phase into the metric/time-writing branch.

The important structural point is that ordinary electromagnetism appears through the phase/gauge branch, while the residual metric term appears through the realized linear projection of phase-time into the clock-rate geometry. The same electromagnetic phase therefore has two readings:

phase/gauge projection to ordinary electromagnetism,

and

realized linear projection into clock-rate geometry to residual metric load.

The fourth-order term is the first positive real residue of the electromagnetic phase.

11.7 Effective Dark-Matter Clock-Rate Residue and Structural Significance

The proposed dark-matter-like contribution is therefore written as a residual clock-rate field

$$\chi_{\text{DM}}(x) = \frac{\alpha^4}{24} \mathcal{F}(x),$$

where $\mathcal{F}(x)$ is a dimensionless spatial profile encoding the large-scale distribution of the electromagnetic metric residue. It encodes the spatial organization of the baryonic matter, electromagnetic phase structure, record density, boundary conditions, or coherent phase distribution of the system.

The corresponding acceleration follows from the time-gradient law:

$$a_{\text{DM}} = -c^2 \nabla \chi_{\text{DM}}.$$

Therefore,

$$a_{\text{DM}} = -\frac{c^2 \alpha^4}{24} \nabla \mathcal{F}(x).$$

The factor

$$\frac{\alpha^4}{24}$$

sets the natural dimensionless strength of the dark-matter-like metric residue. The spatial function $\mathcal{F}(x)$ determines how this residue is distributed in a galaxy or gravitational system.

This gives the compact interpretation, anchored to the cluster-dynamics [201] and rotation-curve [202] [203] evidence:

dark matter is the real metric residue
of electromagnetic phase.

More explicitly,

dark matter is a fourth-order real phase-time projection
of the electromagnetic phase fraction of matter.

In this reading, the dark component is tied to baryonic matter because the electromagnetic phase fraction is carried by the charged internal structure of matter. It appears gravitationally because part of that phase contributes to the real clock-rate geometry.

The effective clock-rate projection can be written schematically as

$$\chi_{\text{eff}} \simeq 1 - \frac{1}{2} \frac{r_s}{r} + \frac{\alpha^4}{24} \mathcal{F}(r) + \dots$$

The second term is the ordinary gravitational clock-rate load:

$$\chi_g \simeq 1 - \frac{1}{2} \frac{r_s}{r}.$$

The third term is the proposed electromagnetic residual load:

$$\chi_{\text{DM}} \simeq \frac{\alpha^4}{24} \mathcal{F}(r).$$

The total acceleration is generated by

$$a = -c^2 \nabla \chi_{\text{eff}}.$$

Thus,

$$a = a_g + a_{\text{DM}} + \dots,$$

with

$$a_g = -c^2 \nabla \left(-\frac{1}{2} \frac{r_s}{r} \right),$$

and

$$a_{\text{DM}} = -c^2 \nabla \left(\frac{\alpha^4}{24} \mathcal{F}(r) \right).$$

This keeps the distinction clear: the Taylor term gives a dimensionless time-load scale; the physical acceleration is obtained only after applying the spatial gradient.

The appearance of the scale

$$\frac{\alpha^4}{24} \approx 1.18 \times 10^{-10}$$

follows from three internal elements of the theory.

First, realized time is the real projection of phase-time:

$$d\tau = \tau_C^{(\omega)} \chi \cos \phi d\phi.$$

Second, the second-order term of the same projection reproduces ordinary gravitational clock-rate structure:

$$-\frac{\phi_g^2}{2} = -\frac{1}{2} \frac{r_s}{r}.$$

Third, the electromagnetic phase scale is independently fixed by the Planck-scale phase-energy ratio:

$$\frac{U_{\text{el}}(\ell_P)}{E_P} = \alpha.$$

The fourth-order real term therefore gives

$$\frac{\phi_{\text{EM}}^4}{24} = \frac{\alpha^4}{24}.$$

This is a structurally determined residual scale. It arises from the overlap of realized time, electromagnetic phase, and metric clock-rate geometry.

The proposed physical reading is therefore:

ordinary gravity is the second-order real time-load of radial mass phase,

dark matter is the fourth-order real time-load residue of electromagnetic phase.

The phase-time expansion naturally separates the ordinary gravitational contribution from a possible dark-matter-like residual contribution.

The second-order real term,

$$-\frac{\phi^2}{2},$$

reproduces the weak-field Schwarzschild clock-rate load when

$$\phi_g^2 = \frac{r_s}{r}.$$

This identifies ordinary gravity as the quadratic real-time loss generated by radial mass phase.

The next positive real term,

$$+\frac{\phi^4}{24},$$

receives a natural electromagnetic interpretation when the phase is taken to be the fine-structure phase fraction

$$\phi_{\text{EM}} = \alpha.$$

Since

$$\frac{U_{\text{el}}(\ell_P)}{E_P} = \alpha,$$

α is the electromagnetic phase-energy fraction of the internal mass mode. Substitution gives

$$\chi_{\text{DM}} \sim \frac{\alpha^4}{24} \approx 1.18 \times 10^{-10}.$$

This quantity is a dimensionless residual clock-rate load. With a spatial distribution $\mathcal{F}(x)$, it produces an additional acceleration through

$$a_{\text{DM}} = -c^2 \nabla \left[\frac{\alpha^4}{24} \mathcal{F}(x) \right].$$

Thus the dark-matter-like sector appears as the gravitational shadow of electromagnetism: the real metric residue of electromagnetic phase inside the linear projection of phase-time.

12 Empirical Test: Driven Coherent Transport Above the Critical Temperature

This section states the coherent-transport prediction in operational form. It begins from the phase-ordered registration law, derives the complex transport field, separates dissipative power from coherent phase response, and then maps the criterion onto optical, thermal-gradient, pressure, phonon, and isotope-tuned experiments.

12.1 General Registration Law for Coherent Transport

Coherent transport is a registration process in which phase-ordered potential information is written into a collective transport state while a dispersed thermodynamic cost is produced. The governing registration law is

$$-dI_{\text{pot}}(\phi) = dI_{\text{dist}}^{\text{coh}} + \frac{dS}{k_B \ln 2}.$$

Here $dI_{\text{dist}}^{\text{coh}}$ is the distinguishable coherent writing of the collective transport state, and $dS/(k_B \ln 2)$ is the dispersed thermodynamic cost in entropy bits, using the standard thermodynamic and physical-bit relation between entropy and information [27, 34]. The corresponding transport registration ratio is

$$\chi_{\text{tr}} = \frac{dI_{\text{dist}}^{\text{coh}}}{dS/(k_B \ln 2)}.$$

Combining the conservation law with this ratio gives the explicit split of each phase-ordered potential increment:

$$dI_{\text{dist}}^{\text{coh}} = \frac{-\chi_{\text{tr}}}{1 + \chi_{\text{tr}}} dI_{\text{pot}}(\phi),$$

and

$$\frac{dS}{k_B \ln 2} = \frac{-1}{1 + \chi_{\text{tr}}} dI_{\text{pot}}(\phi).$$

Thus χ_{tr} measures the coherent registration channel relative to entropy-producing dispersion. The fractions of the consumed phase-ordered potential increment are

$$\frac{dI_{\text{dist}}^{\text{coh}}}{-dI_{\text{pot}}(\phi)} = \frac{\chi_{\text{tr}}}{1 + \chi_{\text{tr}}},$$

and

$$\frac{dS/(k_B \ln 2)}{-dI_{\text{pot}}(\phi)} = \frac{1}{1 + \chi_{\text{tr}}}.$$

These relations provide the source equation for the rest of the section. Optical conductivity, Josephson plasma response, Nernst transport, pressure tuning, phonon driving, and isotope substitution are different experimental readings of the same split between coherent distinguishable writing and dispersed entropy production.

12.2 Empirical Transport Arena and Complex Force Projections

Superconducting transport provides a direct empirical arena for separating real dissipative power from coherent phase response: BCS pairing supplies the equilibrium reference [212], Josephson physics supplies the phase-sensitive channel [213], standard superconductivity phenomenology fixes the transport language [214], and driven materials provide the nonequilibrium [245] empirical arena [215]. The UiT test signature is a high coherent-to-dissipative response: coherent phase transport increases while dissipative spectral weight remains suppressed.

Using the complex-force decomposition derived in the coherent electromagnetic branch, the same informational force law yields a direct transport criterion for superconducting and coherent transport, compared below with BCS theory [212]. The transport field is the local coherent registration ratio. Throughout the transport equations we write $\chi \equiv \chi_{\text{tr}}$. In structurally tuned systems the same ratio is denoted χ_{conf} to emphasize that pressure and lattice configuration tune the coherent registration channel.

The phase-completed transport field is

$$\Xi(\mathbf{x}) = \chi(\mathbf{x})e^{-i\phi(\mathbf{x})}.$$

The transport potential is

$$U_\phi(\mathbf{x}) = mc^2\Xi(\mathbf{x}),$$

and the corresponding complex force is

$$\mathbf{F}_\phi = -mc^2\nabla\Xi = -mc^2e^{-i\phi}\nabla\chi + imc^2\chi e^{-i\phi}\nabla\phi.$$

The first gradient, $\nabla\chi$, is the realized clock-rate or mismatch-gradient channel. The second gradient, $\nabla\phi$, is the coherent phase-transport channel. Transport therefore depends on the full complex projection combining the clock-rate gradient and the coherent phase-gradient channel.

Using

$$e^{-i\phi} = \cos\phi - i\sin\phi,$$

the force expands as

$$\mathbf{F}_\phi = -mc^2(\cos\phi - i\sin\phi)\nabla\chi + imc^2\chi(\cos\phi - i\sin\phi)\nabla\phi.$$

Term by term this gives

$$\mathbf{F}_\phi = -mc^2 \cos \phi \nabla \chi + imc^2 \sin \phi \nabla \chi + imc^2 \chi \cos \phi \nabla \phi + mc^2 \chi \sin \phi \nabla \phi.$$

Thus the real and imaginary projections are

$$\Re(\mathbf{F}_\phi) = -mc^2 \cos \phi \nabla \chi + mc^2 \chi \sin \phi \nabla \phi$$

and

$$\Im(\mathbf{F}_\phi) = mc^2 \sin \phi \nabla \chi + mc^2 \chi \cos \phi \nabla \phi.$$

This is the projected transport form. The real-imaginary separation is the Euler separation of the transported phase-time factor. Since

$$e^{-i\phi} = \cos \phi - i \sin \phi,$$

the complex force has two orthogonal projections. The real projection is the work-producing channel measured as dissipative transport. The imaginary projection is the reactive phase-orthogonal channel measured as inductive or stiffness-like response [214]. In electromagnetic language, the phase branch supplies the local $U(1)$ transport structure and the corresponding connection; in transport language, it supplies the channel through which a phase-ordered current can persist.

12.3 Dissipative Projection and Effective Resistance

Let q be the charge of the phase-coupled carrier and let \mathbf{J} be the macroscopic current density, as in standard transport descriptions of superconductors [214]. The real projection defines an effective dissipative electric field,

$$\mathbf{E}_{\text{diss}} \equiv \frac{1}{q} \Re(\mathbf{F}_\phi).$$

The local dissipative power density is then

$$\mathcal{D} \equiv \mathbf{J} \cdot \mathbf{E}_{\text{diss}} = \frac{1}{q} \mathbf{J} \cdot \Re(\mathbf{F}_\phi).$$

For carrier density n and drift velocity \mathbf{v} , $\mathbf{J} = nq\mathbf{v}$, so equivalently

$$\mathcal{D} = n \mathbf{v} \cdot \Re(\mathbf{F}_\phi).$$

The corresponding local Euler-projection ratio is

$$\eta_{\text{Euler}}(\mathbf{x}, t) := \frac{|\mathbf{J} \cdot \Im(\mathbf{F}_\phi)|}{|\mathbf{J} \cdot \Re(\mathbf{F}_\phi)| + \epsilon}.$$

This ratio measures the reactive phase-orthogonal channel relative to the work-producing dissipative channel. The optical diagnostic introduced below, $\eta_{\text{coh}} = S_{\text{coh}}/S_{\text{diss}}$, is the experimentally accessible spectral version of this local Euler projection ratio.

Substituting the real projection gives

$$\boxed{\mathcal{D} = nmc^2 \mathbf{v} \cdot (-\cos \phi \nabla \chi + \chi \sin \phi \nabla \phi)}.$$

This expression is the transport criterion. Resistance is the macroscopic manifestation of a positive real projected power,

$$\mathcal{D} > 0.$$

For a uniform one-dimensional sample, an effective resistivity may be defined directly from the same projection,

$$\rho_{\text{eff}} = \frac{\mathbf{J} \cdot \mathbf{E}_{\text{diss}}}{|\mathbf{J}|^2} = \frac{\mathbf{J} \cdot \Re(\mathbf{F}_\phi)}{q|\mathbf{J}|^2},$$

and hence $R = \rho_{\text{eff}} L/A$ for length L and cross-sectional area A . This recovers the ordinary circuit meaning of resistance as real power loss per current squared, while identifying the microscopic origin of that loss with the real projection of the complex phase-time force.

12.4 Criterion for Coherent Dissipationless Transport

The criterion for dissipationless transport, compared with phase-coherent superconducting transport [212], is

$$\boxed{\mathcal{D} = \mathbf{J} \cdot \mathbf{E}_{\text{diss}} = \frac{1}{q} \mathbf{J} \cdot \Re(\mathbf{F}_\phi) \approx 0}$$

with nonzero current and nontrivial phase transport,

$$\boxed{\mathbf{J} \neq 0, \quad \Im(\mathbf{F}_\phi) \neq 0.}$$

Equivalently,

$$\boxed{\mathbf{v} \cdot (-\cos \phi \nabla \chi + \chi \sin \phi \nabla \phi) \approx 0}$$

while the coherent phase projection remains active,

$$mc^2 \sin \phi \nabla \chi + mc^2 \chi \cos \phi \nabla \phi \neq 0.$$

Thus dissipationless transport requires the vanishing of the real power projection along the current. A nonzero phase-gradient channel can persist as a coherent reactive channel while the real dissipative projection averages to zero or becomes orthogonal to the macroscopic current.

This supplies the central superconducting interpretation of the complex force law:

resistive transport: $\mathbf{J} \cdot \Re(\mathbf{F}_\phi) > 0$

coherent dissipationless transport: $\mathbf{J} \cdot \Re(\mathbf{F}_\phi) = 0, \quad \Im(\mathbf{F}_\phi) \neq 0.$

The phase channel then carries transport without ordinary Ohmic heating, as in the superconducting distinction between dissipative and reactive response [214]. Superconducting behavior is the phase-dominated transport limit of the same complex force law that also contains the realized clock-rate branch.

12.5 Cooper-Pair Phase-Time Closure and the Vanishing Real Projection

The coherent carrier of superconducting transport is the Cooper-pair condensate. In the present notation, a Cooper pair is a shared phase-time closure of two closed spherical electron phase-time carriers. The single-electron closed spherical phase-time carrier supplies mass, charge, spinorial closure, and internal phase. Pairing forms a collective state in which the two electron carriers share one macroscopic phase variable while their momenta and spins close into a coherent pair channel, as in the standard BCS condensate description [212, 214]. The pair field is written as

$$\Psi_{\text{CP}} = |\Psi_{\text{CP}}| e^{i\Theta},$$

with collective pair phase

$$\Theta = \phi_1 + \phi_2,$$

and pair charge

$$q_{\text{pair}} = -2e.$$

The pair therefore carries a collective phase-time transport field,

$$\Xi_{\text{CP}} = \chi_{\text{CP}} e^{-i\Theta},$$

where

$$\chi_{\text{CP}} = \frac{dI_{\text{dist}}^{\text{coh,CP}}}{dS/(k_B \ln 2)}.$$

The pair registration law is the Cooper-pair version of the transport source equation,

$$-dI_{\text{pot}}^{\text{pair}}(\Theta) = dI_{\text{dist}}^{\text{coh,CP}} + \frac{dS}{k_B \ln 2}.$$

The electromagnetic coupling of the pair is governed by the gauge-covariant phase differential

$$D\Theta = d\Theta - \frac{q_{\text{pair}}}{\hbar} A.$$

In spatial form this gives the familiar phase-gauge combination

$$\mathbf{\Pi}_{\Theta} = \nabla\Theta - \frac{q_{\text{pair}}}{\hbar} \mathbf{A}.$$

The supercurrent is therefore

$$\mathbf{J}_s = \frac{n_s q_{\text{pair}}}{m_{\text{pair}}} (\hbar \nabla\Theta - q_{\text{pair}} \mathbf{A}),$$

where n_s is the coherent pair density and m_{pair} is the effective pair mass. The Meissner–London condition is the bulk phase-time closure condition

$$D\Theta \approx 0,$$

or spatially,

$$\nabla\Theta \approx \frac{q_{\text{pair}}}{\hbar} \mathbf{A}.$$

This condition states that the condensate adjusts its collective phase so that the gauge-covariant phase strain remains cancelled in the coherent bulk. Taking the curl gives the London–Meissner response [210, 211, 214],

$$\nabla \times \mathbf{J}_s = -\frac{n_s q_{\text{pair}}^2}{m_{\text{pair}}} \mathbf{B},$$

and hence

$$\nabla^2 \mathbf{B} = \frac{1}{\lambda_L^2} \mathbf{B},$$

with London penetration length

$$\lambda_L^2 = \frac{m_{\text{pair}}}{\mu_0 n_s q_{\text{pair}}^2}.$$

In the force notation of this section, the Cooper-pair dissipative projection is

$$\mathcal{D}_{\text{CP}} = \frac{1}{q_{\text{pair}}} \mathbf{J}_s \cdot \Re \left[-E_{\text{CP}} \nabla (\chi_{\text{CP}} e^{-i\Theta}) \right].$$

The superconducting branch satisfies

$$\boxed{\mathcal{D}_{\text{CP}} \rightarrow 0}$$

while the phase projection remains active,

$$\boxed{\Im \left[-E_{\text{CP}} \nabla (\chi_{\text{CP}} e^{-i\Theta}) \right] \neq 0.}$$

In the ideal phase-branch limit,

$$\cos \Theta \rightarrow 0,$$

so that

$$\Re(\Xi_{\text{CP}}) = \chi_{\text{CP}} \cos \Theta \rightarrow 0,$$

and

$$|\Im(\Xi_{\text{CP}})| = \chi_{\text{CP}} |\sin \Theta| \rightarrow \chi_{\text{CP}}.$$

This is the phase-time representation of superconducting transport. The pair current occupies the coherent phase branch, while the real work-producing projection along the current vanishes. The Meissner effect is the gauge expression of the same condition: the condensate creates a current whose phase response cancels the internal covariant phase strain produced by the external vector potential.

The analogy with free fall is structural. In the gravitational case, a body in free fall develops a Lorentz time-space response that matches the local gravitational time factor, $\chi_v = \chi_g$, producing local force cancellation. In the superconducting case, the condensate develops a phase current that matches the electromagnetic gauge connection,

$$\nabla \Theta \approx \frac{q_{\text{pair}}}{\hbar} \mathbf{A},$$

producing bulk covariant phase cancellation. In both cases, a field distortion is absorbed into an internal kinematic or phase response, and the coherent branch carries the resulting motion without local dissipative work.

This subsection supplies the physical carrier behind the criteria that follow. Optical conductivity, resonant driving, chemical-potential gradients, Nernst response, pressure tuning, phonon driving, and isotope substitution are operational probes of how the Cooper-pair phase-time channel increases $dI_{\text{dist}}^{\text{coh,CP}}$ relative to $dS/(k_B \ln 2)$.

12.6 Driven Coherent Transport Above the Equilibrium Critical Temperature

The same criterion gives a direct nonequilibrium prediction. A coherent external drive changes the effective fields,

$$\chi \text{ maps to } \chi_{\text{driven}}(\mathbf{x}, t), \quad \phi \text{ maps to } \phi_{\text{driven}}(\mathbf{x}, t),$$

and therefore changes the real and imaginary force projections. The driven dissipative power density is

$$\mathcal{D}_{\text{driven}} = nmc^2 \mathbf{v} \cdot (-\cos \phi_{\text{driven}} \nabla \chi_{\text{driven}} + \chi_{\text{driven}} \sin \phi_{\text{driven}} \nabla \phi_{\text{driven}}).$$

A drive that couples primarily to the coherent phase sector can reduce the real projected power while preserving or increasing the imaginary phase response. The predicted transient transport regime is therefore

$$\boxed{\mathcal{D}_{\text{driven}} \rightarrow 0, \quad \Im(\mathbf{F}_{\phi, \text{driven}}) \neq 0, \quad \mathbf{J} \neq 0.}$$

This is the mathematical form of driven coherent transport above the equilibrium critical temperature, a regime explored in light-induced superconducting-like experiments [216]. The drive supplies energy, and the relevant question is the projection of that energy in the complex force plane. Energy placed into a coherent phase channel can enhance the reactive response with limited growth of the real dissipative projection. Dynamically, the cancellation condition requires phase locking or resonant entrainment between the driven coherent mode and the phase-gradient channel along the current direction, consistent with resonant pump-frequency effects reported in driven cuprates [217]. In a material system this locking may be supplied by a resonantly driven phonon, Josephson plasma mode, charge-order mode, or another collective coordinate that couples selectively to $\nabla \phi$ while keeping the thermal load $\nabla \chi$ small.

If the driven state is maintained by continuously correcting thermally generated mismatch events, the pump must still pay a stabilization cost. By Landauer's principle, the minimal energy per corrected bit is $k_B T \ln 2$. If \dot{N}_{corr} is the correction rate, then

$$P_{\text{pump}} \geq k_B T \ln 2 \dot{N}_{\text{corr}}.$$

If the correction rate is written in terms of an effective thermal scattering or decoherence rate Γ_{th} , then

$$P_{\text{pump}} \gtrsim N_{\text{eff}} k_B T \ln 2 \Gamma_{\text{th}},$$

where N_{eff} is the effective number of thermally corrected informational degrees of freedom participating in the driven coherent transport process. The coherent regime is therefore constrained by both the phase-projection condition and the thermodynamic cost of maintaining that condition against thermal mismatch.

12.7 Minimal Driven-Phase Toy Model

The preceding criterion can be made more explicit by separating a coherent resonant drive from ordinary heating, as in nonlinear lattice-dynamics interpretations of driven superconductivity [218]. The purpose of this subsection is to state the smallest mathematical model required to connect the complex-force criterion to pump-probe experiments. The essential physical ingredient is resonant phase locking: the pump must entrain a collective mode that modifies the phase-gradient projection along the current more efficiently than it increases the ordinary dissipative clock-load projection.

Let the equilibrium fields be $\chi_0(\mathbf{x})$ and $\phi_0(\mathbf{x})$. A pump pulse produces perturbations

$$\chi_{\text{driven}} = \chi_0 + \delta\chi_{\text{th}} + \delta\chi_{\text{coh}}, \quad \phi_{\text{driven}} = \phi_0 + \delta\phi_{\text{coh}} + \delta\phi_{\text{th}}.$$

Here $\delta\chi_{\text{th}}$ denotes the ordinary thermal or scattering load produced by absorption and decoherence, while $\delta\phi_{\text{coh}}$ denotes the coherent phase-ordering response produced when the drive is resonant with a lattice, charge-order, Josephson-plasma, or other phase-selective mode. A nonresonant thermal drive is characterized schematically by

$$|\nabla\delta\chi_{\text{th}}| \gtrsim |\chi_0 \nabla\delta\phi_{\text{coh}}|,$$

whereas a phase-selective coherent drive is characterized by

$$|\chi_0 \nabla\delta\phi_{\text{coh}}| \gg |\nabla\delta\chi_{\text{th}}|.$$

The real dissipative projection along the direction of the macroscopic current $\hat{\mathbf{J}} = \mathbf{J}/|\mathbf{J}|$ is

$$\hat{\mathbf{J}} \cdot \Re(\mathbf{F}_\phi) = mc^2 \hat{\mathbf{J}} \cdot (-\cos\phi \nabla\chi + \chi \sin\phi \nabla\phi).$$

Thus the minimal cancellation condition for coherent transport is

$$\hat{\mathbf{J}} \cdot \chi \sin\phi \nabla\phi \approx \hat{\mathbf{J}} \cdot \cos\phi \nabla\chi.$$

This condition gives a dimensionless threshold parameter,

$$\Theta_{\text{coh}} = \frac{|\hat{\mathbf{J}} \cdot \chi \sin \phi \nabla \phi|}{|\hat{\mathbf{J}} \cdot \cos \phi \nabla \chi| + \theta_0},$$

where θ_0 is a small regularizing scale set by experimental resolution or by the residual background load. The transport regimes are then

$$\Theta_{\text{coh}} < 1 \quad \text{implies} \quad \text{dissipative transport,}$$

$$\Theta_{\text{coh}} = 1 \quad \text{implies} \quad \text{near-cancellation of the real power projection,}$$

and

$$\Theta_{\text{coh}} > 1 \quad \text{implies} \quad \text{phase-dominated reactive response.}$$

The observable optical diagnostic introduced below is the experimental proxy for this threshold. In a phase-selective driven state one expects

$$\Theta_{\text{coh}} \gtrsim 1 \quad \text{implies} \quad \eta_{\text{coh}} \gg 1,$$

because the real dissipative projection is suppressed while the imaginary or inductive response remains large. A thermal broadband drive increases $\nabla \chi$, broadens scattering, raises σ_1 , and gives a much smaller η_{coh} . The toy model therefore supplies a direct order-of-magnitude test: the relevant experimental question is the size of the pump-induced phase-gradient correction relative to the thermal time-load gradient along the transport direction.

12.8 Microscopic Phonon Closure of the Driven-Phase Criterion

The toy model becomes directly testable once the coherent drive is tied to the microscopic collective coordinates of the material. Let $Q_\lambda(t)$ denote a phonon or molecular vibrational coordinate, with λ labeling branch, wave vector, polarization, and symmetry. In frequency space the driven coordinate is written as

$$Q_\lambda(\omega) = D_\lambda(\omega) f_\lambda(\omega),$$

with the damped mode response

$$D_\lambda(\omega) = \frac{1}{\Omega_\lambda^2 - \omega^2 - i\Gamma_\lambda \omega}.$$

Here Ω_λ is the eigenfrequency of the driven mode, Γ_λ is its damping rate, and $f_\lambda(\omega)$ is the optical driving force. For an infrared-active phonon, f_λ is set by the Born effective charge and the pump

electric field. For Raman-active or nonlinear phonon processes, f_λ is set by the corresponding Raman or nonlinear lattice force. This is the microscopic material coordinate behind the phase-locking language used above: the pump drives a selected lattice or molecular mode, and that mode changes the local writing-capacity geometry experienced by the transport carriers.

To first order in the driven coordinate, the material response can be written as

$$\delta\chi(\mathbf{x}, \omega) = \sum_{\lambda} a_{\chi}^{(\lambda)}(\mathbf{x}) Q_{\lambda}(\omega) + O(Q^2),$$

$$\delta\phi(\mathbf{x}, \omega) = \sum_{\lambda} a_{\phi}^{(\lambda)}(\mathbf{x}) Q_{\lambda}(\omega) + O(Q^2).$$

The coefficient $a_{\chi}^{(\lambda)}$ measures how strongly the driven mode increases the dissipative load channel: absorption, scattering, quasiparticle production, thermal mismatch, or entropy production. The coefficient $a_{\phi}^{(\lambda)}$ measures how strongly the same mode increases the coherent phase channel: phase alignment, interlayer tunneling, Josephson coupling, orbital overlap, or phase stiffness. In this language a driven lattice coordinate is a material update of the local informational capacity map. It changes the electronic geometry and transport couplings through deformation potentials, electron-phonon coupling, Born effective charges, Raman tensors, and Josephson or interlayer tunneling terms. In UiT notation these material changes appear as mode-dependent corrections to χ and ϕ .

The corresponding corrections to the gradients entering the real projection are

$$\delta(\nabla\chi) = \sum_{\lambda} \nabla \left[a_{\chi}^{(\lambda)}(\mathbf{x}) Q_{\lambda}(\omega) \right] + O(Q^2),$$

$$\delta(\nabla\phi) = \sum_{\lambda} \nabla \left[a_{\phi}^{(\lambda)}(\mathbf{x}) Q_{\lambda}(\omega) \right] + O(Q^2).$$

Substitution into the real force projection gives the driven correction along the current direction:

$$\delta \left[\hat{\mathbf{J}} \cdot \Re(\mathbf{F}_{\phi}) \right] = mc^2 \hat{\mathbf{J}} \cdot (-\cos \phi \delta(\nabla\chi) + \chi \sin \phi \delta(\nabla\phi)).$$

This equation supplies the microscopic closure of the criterion stated above. The selected pump is the frequency that gives the largest coherent phase-writing response relative to the added dissipative load. Equivalently, the optimal pump maximizes conversion into the Euler-orthogonal phase channel: it increases inductive or stiffness-like response more strongly than absorptive response. A useful frequency-domain diagnostic is therefore

$$\eta_{\text{ph}}(\omega) = \frac{\left| \chi \sin \phi \sum_{\lambda} \hat{\mathbf{J}} \cdot \nabla \left[a_{\phi}^{(\lambda)} Q_{\lambda}(\omega) \right] \right|}{\left| \cos \phi \sum_{\lambda} \hat{\mathbf{J}} \cdot \nabla \left[a_{\chi}^{(\lambda)} Q_{\lambda}(\omega) \right] \right| + \Lambda_{\text{heat}}(\omega) + \Lambda_{\text{qp}}(\omega) + \epsilon},$$

where Λ_{heat} collects ordinary heating and broadband absorptive load and Λ_{qp} collects quasiparticle-generating or pair-breaking load. These two quantities are not bare scattering rates. They are

effective projected load terms expressed in the same units as the current-projected gradient terms in the denominator. If the experimentally extracted inputs are rates, for example Γ_{heat} or Γ_{qp} , they must first be converted into projected load gradients by the appropriate material conversion scale, such as an effective transport length, group velocity, or calibrated response coefficient. Equivalently one may write $\Lambda_{\text{heat}} = C_{\text{heat}}\Gamma_{\text{heat}}$ and $\Lambda_{\text{qp}} = C_{\text{qp}}\Gamma_{\text{qp}}$, with C_{heat} and C_{qp} carrying the units needed to match the gradient terms. The small quantity ϵ is an experimental regularizer in the same projected-load units. The predicted pump frequency is

$$\omega_{\text{opt}} = \arg \max_{\omega} \eta_{\text{ph}}(\omega).$$

The prediction is mode-selective. A useful driven mode increases $a_{\phi}^{(\lambda)}Q_{\lambda}$ along the transport direction while keeping the load terms small over the measured time window. In optical language the same condition appears as increased reactive spectral weight, enhanced σ_2 , or superfluid-stiffness-like response with limited added σ_1 absorption. The optimum is the resonance at which $\Delta\sigma_2$, or superfluid-stiffness-like spectral weight, is maximized relative to positive added $\Delta\sigma_1$. Resonant pump-frequency effects in driven cuprates and fullerenes therefore become a quantitative test of phase-selective lattice coupling with limited broadband dissipative absorption [219] [218] [217] [220] [221].

In UiT language, the experimentally relevant phonon is the mode that converts pump energy most efficiently into coherent phase-writing capacity before that energy is dispersed into entropy. This microscopic closure connects the abstract threshold Θ_{coh} to measurable pump frequency, phonon linewidth, optical conductivity [222], and transient phase stiffness.

12.9 Observable Optical and Transport Signatures

The preceding criterion can be compared directly with optical and THz experiments, the same experimental language used to identify transient coherent transport signatures [219]. In a conventional optical-conductivity notation,

$$\sigma(\omega, t) = \sigma_1(\omega, t) + i\sigma_2(\omega, t),$$

σ_1 measures the dissipative absorptive response, while σ_2 measures the reactive inductive response. This is the experimental optical reading of the same Euler projection used in the complex force: σ_1 is the empirical proxy for the real dissipative projection, and σ_2 is the empirical proxy for the coherent phase-orthogonal projection. In compact form,

$$\sigma_1 + i\sigma_2 \quad \text{paired with} \quad \Re(\mathbf{F}_{\phi}) + i\Im(\mathbf{F}_{\phi}).$$

This coherence criterion predicts that a coherent phase-selective drive should produce a large gain in reactive spectral weight relative to dissipative spectral weight. A simple local diagnostic is

$$\mathcal{R}_{\text{coh}}(\omega, t) = \frac{|\Delta\sigma_2(\omega, t)|}{|\Delta\sigma_1(\omega, t)| + \epsilon_0},$$

where ϵ_0 is a small regularizing scale set by the experimental noise floor. A more integrated diagnostic is

$$\eta_{\text{coh}}(t) = \frac{S_{\text{coh}}(t)}{S_{\text{diss}}(t)},$$

with

$$S_{\text{coh}}(t) = \lim_{\omega \rightarrow 0} \omega \Delta\sigma_2(\omega, t),$$

and

$$S_{\text{diss}}(t) = \int_{\omega_1}^{\omega_2} [\Delta\sigma_1(\omega, t)]_+ d\omega.$$

Here $[x]_+ = \max(x, 0)$ counts added dissipative spectral weight in the measured window. The predicted signature of phase-selective coherent transport is

$$\boxed{\eta_{\text{coh}} \gg 1}$$

near a resonant coherent drive, together with the appearance of Josephson-plasma-like response, plasma-edge formation, enhanced inductive response, or transient low-frequency divergence of σ_2 . A primarily thermal or nonresonant drive gives a much smaller ratio,

$$\eta_{\text{coh}} = 1 \quad \text{or} \quad \eta_{\text{coh}} < 1,$$

because the injected energy appears mainly as added absorption and scattering.

12.10 Integral Spectral-Weight Test of Coherent Transport

The preceding subsection identified the optical signatures. This subsection turns the same signatures into an integral spectral-weight protocol. The optical conductivity [222] data provide a direct integral spectral-weight test [223] [224] of the coherent-transport criterion. The measured transient conductivity is written as

$$\sigma(\omega, t) = \sigma_1(\omega, t) + i\sigma_2(\omega, t),$$

where the absorptive component in the Mattis–Bardeen optical-response tradition [225] σ_1 measures real dissipative spectral weight and the reactive component σ_2 measures inductive phase response. The UiT criterion can therefore be evaluated by comparing the coherent low-frequency spectral weight to the added dissipative spectral weight over the same transient window.

Define

$$\eta_{\text{coh}}(t) = \frac{S_{\text{coh}}(t)}{S_{\text{diss}}(t)},$$

with

$$S_{\text{coh}}(t) = \lim_{\omega \rightarrow 0} \omega \Delta\sigma_2(\omega, t),$$

and

$$S_{\text{diss}}(t) = \int_{\omega_1}^{\omega_2} [\Delta\sigma_1(\omega, t)]_+ d\omega.$$

Here

$$[x]_+ = \max(x, 0)$$

counts added dissipative spectral weight. This positive-part prescription implements the physical distinction used throughout the transport section: entropy-producing absorption and scattering contribute to the dissipative denominator, and depletion of low-frequency σ_1 inside a transient gap contributes to the coherent reorganization of spectral weight. The superconducting test is therefore an Euler-projection test: a successful drive transfers spectral weight from the real dissipative projection into the phase-orthogonal reactive projection. Experimentally this appears as suppressed or limited $\Delta\sigma_1$, enhanced $\Delta\sigma_2$, and, in the strongest case, magnetic-field expulsion.

The same condition can be written directly in the force language. A phase-selective coherent transport state satisfies

$$\mathcal{D} = \mathbf{J} \cdot \mathbf{E}_{\text{diss}} \rightarrow 0, \quad \Im(\mathbf{F}_\phi) \neq 0.$$

The spectral integral is the experimental version of this statement. The numerator S_{coh} measures the inductive or superfluid-stiffness-like response associated with the imaginary/reactive channel, while the denominator S_{diss} measures the added real absorptive load associated with the dissipative projection. A driven coherent state is therefore characterized by

$$S_{\text{coh}} \gg S_{\text{diss}}, \quad \eta_{\text{coh}} \gg 1.$$

This formulation gives a quantitative protocol for existing pump-probe data. In optically driven K_3C_{60} , Mitrano *et al.* reported a nonequilibrium optical state above the equilibrium transition temperature with a gap-like suppression in σ_1 and a low-frequency inductive response in σ_2 resembling superconducting optical behavior. [220] In the present notation this corresponds to a large S_{coh} and a small positive added S_{diss} over the measured low-frequency window, giving

$$\eta_{\text{coh}} \gg 1.$$

The same integral criterion also applies to pump-frequency scans in cuprates. In $\text{YBa}_2\text{Cu}_3\text{O}_{6.5}$, resonant excitation of apical-oxygen modes in the far infrared produces a strong transient coherent response, and pump-frequency dependence identifies the modes that most efficiently generate the superconducting-like optical signature. [219] [218] [217] Within the present framework the selected frequency is the one that maximizes coherent phase writing relative to dissipative load,

$$\omega_{\text{opt}} = \arg \max_{\omega} \eta_{\text{ph}}(\omega),$$

and the optical integral test is

$$\eta_{\text{coh}}(\omega_{\text{pump}}, t) = \frac{\lim_{\omega \rightarrow 0} \omega \Delta\sigma_2(\omega, t)}{\int_{\omega_1}^{\omega_2} [\Delta\sigma_1(\omega, t)]_+ d\omega}.$$

A pump that addresses the coherent phase channel gives a large numerator and a small positive dissipative denominator. A pump dominated by absorptive load gives a small coherent numerator and a larger dissipative denominator. Thus the measured frequency dependence of η_{coh} supplies a direct empirical map of phase-selective coherent transport.

The existing data therefore already contain the principal ingredients needed for this test: the inductive spectral weight is extracted from $\omega\sigma_2$, and the added dissipative spectral weight is extracted from the positive part of $\Delta\sigma_1$. Applying the same integral prescription uniformly to digitized or raw transient spectra would turn the UiT coherent-transport criterion into a quantitative comparison across fullerenes, cuprates, and other driven superconducting-like systems.

12.11 Thermodynamic Phase Driving: Chemical Potential, Phase-Time, and Coherent Registration

The coherent transport criterion developed above separates transport into a dissipative real projection and a coherent phase projection. This separation can be written experimentally through optical conductivity, and its thermodynamic source is more general. Temperature gradients, pressure, strain, gating, and phonon driving all act by changing the thermodynamic landscape in which phase-time evolves.

The central thermodynamic variable is the chemical potential. For a material degree of freedom, the local differential form may be written in the standard thermodynamic notation [31, 34] as

$$d\mu = -s dT + v dP + \sum_a X_a d\lambda_a.$$

Here s is the entropy per relevant carrier or collective excitation, v is the conjugate volume, and λ_a denotes additional controllable material coordinates such as strain, lattice distortion, carrier density, phonon displacement, orbital configuration, or interface geometry.

Taking a spatial gradient gives

$$\nabla\mu = -s\nabla T + v\nabla P + \sum_a X_a \nabla\lambda_a.$$

This equation gives the common thermodynamic source for several experimental regimes. A temperature gradient contributes through $-s\nabla T$. Pressure contributes through $v\nabla P$. A driven phonon or structural distortion contributes through $X_a \nabla\lambda_a$. Each term changes the local chemical-potential landscape.

The chemical potential controls phase evolution through the gauge-invariant phase equation, the same phase-voltage structure used in Josephson superconducting dynamics [213,214],

$$\hbar\partial_t\theta + \mu + q\Phi = 0.$$

Equivalently,

$$\partial_t\theta = -\frac{\mu + q\Phi}{\hbar}.$$

Thus a change in chemical potential produces a change in the local phase-writing rate. Taking a gradient,

$$\hbar\nabla\partial_t\theta + \nabla\mu + q\nabla\Phi = 0.$$

Using

$$\mathbf{E} = -\nabla\Phi - \partial_t\mathbf{A},$$

the electric response is tied to the combined evolution of chemical potential, electromagnetic phase transport, and gauge potential.

In UiT this phase evolution is embedded in phase-time. The local phase-time increment is

$$dt_\phi = \tau_C^{(\omega)} \chi e^{-i\phi} d\phi,$$

with realized linear projection

$$d\tau = \tau_C^{(\omega)} \chi \cos\phi d\phi.$$

The registration efficiency is

$$\chi = \frac{dI_{\text{dist}}^{\text{coh}}}{dS/(k_B \ln 2)}.$$

The chemical potential therefore acts as a thermodynamic handle on phase-time registration. It changes the rate and orientation with which coherent phase information can become distinguishable physical transport.

The same statement can be written as the sequence

$$d\mu \text{ to } d(\partial_t \theta) \text{ to } d\phi \text{ to } dt_\phi \text{ to } dI_{\text{dist}}^{\text{coh}}.$$

When the thermodynamic drive feeds the coherent phase channel, the response is governed by the imaginary or reactive projection of the phase-time force. When the drive feeds incoherent scattering or heating, the response appears in the dissipative real projection.

The phase-time force is

$$\mathbf{F}_\phi = -mc^2 \nabla(\chi e^{-i\phi}).$$

Its real and imaginary projections are

$$\Re(\mathbf{F}_\phi) = -mc^2 \cos \phi \nabla \chi + mc^2 \chi \sin \phi \nabla \phi,$$

and

$$\Im(\mathbf{F}_\phi) = mc^2 \sin \phi \nabla \chi + mc^2 \chi \cos \phi \nabla \phi.$$

The dissipative power is

$$\mathcal{D} = \frac{1}{q} \mathbf{J} \cdot \Re(\mathbf{F}_\phi).$$

Coherent transport is favored when

$$\mathcal{D} \text{ to } 0, \quad \mathbf{J} \neq 0, \quad \Im(\mathbf{F}_\phi) \neq 0.$$

This condition is the common UiT reading of several experimental situations.

For thermal-gradient experiments, such as the Nernst regime,

$$\nabla T \text{ to } \nabla \mu \text{ to } \nabla \partial_t \theta \text{ to transverse electromagnetic phase response.}$$

For pressure-tuned superconductors,

$$P \text{ to } \mu(P) \text{ to } \theta(P) \text{ to } \chi_{\text{conf}}(P) \text{ to } T_c.$$

For driven phonon systems,

$$Q_\lambda(\omega) \text{ to } \mu[Q_\lambda] \text{ to } \phi_\lambda \text{ to } \eta_{\text{coh}}.$$

The same thermodynamic phase equation therefore organizes Nernst transport, pressure-enhanced superconductivity, isotope tuning, phonon driving, and coherent optical response. These are different experimental handles on one phase-time registration channel.

The informational registration law remains

$$-dI_{\text{pot}}(\phi) = dI_{\text{dist}}^{\text{coh}} + \frac{dS}{k_B \ln 2}.$$

The thermodynamic drive determines how much of the available phase-ordered potential information enters the coherent distinguishable channel and how much appears as dispersed entropy. In this notation, the coherent-registration ratio is

$$\eta_{\text{coh}} = \frac{S_{\text{coh}}}{S_{\text{diss}}},$$

where the experimental proxy for S_{coh} depends on the measurement: optical σ_2 , Josephson plasma weight, phase stiffness, Nernst phase signal, or pressure-enhanced coherent pairing. The dissipative denominator is supplied by σ_1 , relaxation rate, incoherent broadening, vortex drag, or structural disorder.

This subsection establishes the shared notation for the two regimes developed below. The Nernst effect is the thermal-gradient branch, where $-s\nabla T$ drives phase motion through $\nabla\mu$. Pressure and phonon tuning are the structural branch, where $v\nabla P$ and $X_a\nabla\lambda_a$ tune the same phase-time registration channel through the material configuration capacity.

12.12 Nernst Response as Thermal Phase-Time Registration

The thermodynamic phase-driving equation gives a direct route to the Nernst regime, whose superconducting and quasiparticle contributions are widely used as probes of phase fluctuations and entropy transport [233, 234]. A thermal gradient contributes to the chemical-potential landscape through

$$\nabla\mu = -s\nabla T$$

when the pressure and structural coordinates are held fixed. The gauge-invariant phase equation

$$\hbar\partial_t\theta + \mu + q\Phi = 0$$

then converts this thermal chemical-potential gradient into a phase-evolution gradient:

$$\hbar \nabla \partial_t \theta + \nabla \mu + q \nabla \Phi = 0.$$

Using

$$\mathbf{E} = -\nabla \Phi - \partial_t \mathbf{A},$$

the electromagnetic response is determined by the coupled chemical-potential gradient, phase evolution, and gauge field. In a Nernst geometry, a temperature gradient is applied along one direction, a magnetic field is applied transverse to the plane, and the measured electric field is transverse to both. The magnetic field converts phase motion into a transverse electromagnetic response.

For phase objects such as vortices or short-lived Cooper-pair correlations, the transverse electric field may be written schematically as in vortex and superconducting-fluctuation readings of the Nernst response [235, 236],

$$\mathbf{E} = -\mathbf{v}_{\text{phase}} \times \mathbf{B}.$$

If the thermal force on the phase object is

$$\mathbf{F}_T = -S_{\text{phase}} \nabla T,$$

and the dissipative drag is

$$\eta_{\text{diss}} \mathbf{v}_{\text{phase}} = \mathbf{F}_T,$$

then

$$\mathbf{v}_{\text{phase}} = -\frac{S_{\text{phase}}}{\eta_{\text{diss}}} \nabla T,$$

and therefore

$$\mathbf{E} = \frac{S_{\text{phase}}}{\eta_{\text{diss}}} \nabla T \times \mathbf{B}.$$

The Nernst coefficient is then

$$\nu = \frac{E_y}{B_z(-\nabla_x T)} \sim \frac{S_{\text{phase}}}{\eta_{\text{diss}}}.$$

This is the thermal-gradient reading of the same coherent-registration structure. Optical conductivity measures the coherent phase channel through σ_2 and the dissipative channel through σ_1 . The

Nernst branch is not an optical σ_2/σ_1 test. It is the thermal-gradient version of the same phase-time registration structure, with the coherent phase object carrying entropy transversely under a magnetic field. The Nernst response therefore measures entropy carried by phase objects divided by the dissipative drag that relaxes their motion. The experimental signal is a phase-electromagnetic response of entropy-carrying coherent objects above the temperature where global zero-resistance transport is stabilized.

In UiT notation, the Nernst regime probes partial phase-time registration:

$$-dI_{\text{pot}}(\phi) \text{ to } dI_{\text{dist}}^{\text{phase}} + \frac{dS_{\text{carried}}}{k_B \ln 2}.$$

The superconducting fluctuation or vortex-like object carries entropy through a phase-ordered channel. The transverse electromagnetic field records the motion of that channel under the combined action of ∇T , $\nabla\mu$, and \mathbf{B} . This is the empirical structure reported, for example, in above- T_c Nernst measurements of K_3C_{60} [237]. The Nernst branch is therefore the thermal-gradient branch of the general phase-driving equation, while the pressure and phonon branch below is the structural branch of the same equation.

12.13 Pressure, Phonon Phase-Time, and Isotope Tuning of Coherent Registration

The optical conductivity criterion developed above separates charge transport into a dissipative real channel and a coherent phase channel. The same distinction also applies to superconductivity generated or enhanced by structural tuning. In this case the external control parameter is the configuration-writing capacity of the material itself.

The basic informational registration law is

$$-dI_{\text{pot}}(\phi) = dI_{\text{dist}}^{\text{coh}} + \frac{dS}{k_B \ln 2}.$$

The corresponding registration efficiency is

$$\chi = \frac{dI_{\text{dist}}^{\text{coh}}}{dS/(k_B \ln 2)}.$$

In the transport setting, $dI_{\text{dist}}^{\text{coh}}$ represents coherent distinguishable writing of a collective electronic state, while $dS/(k_B \ln 2)$ represents the dispersed thermodynamic cost associated with incoherent scattering, structural disorder, and absorption into non-coherent degrees of freedom.

The coherent transport condition can therefore be written as

$$\eta_{\text{coh}} = \frac{S_{\text{coh}}}{S_{\text{diss}}} \gg 1.$$

For optical conductivity,

$$S_{\text{coh}} = \lim_{\omega \rightarrow 0} \omega \Delta \sigma_2(\omega, t),$$

and

$$S_{\text{diss}} = \int_{\omega_1}^{\omega_2} [\Delta \sigma_1(\omega, t)]_+ d\omega.$$

In pressure-driven superconductors, the same ratio is expressed through structural and phononic quantities. Pressure changes the accessible configuration-writing capacity of the lattice. Phonons provide the phase-time oscillatory channel through which this capacity is written coherently into the electronic state, as illustrated by high-pressure hydride superconductors and their structural phases [239–241].

A minimal UiT proxy for the coherent-registration efficiency is

$$\eta_{\text{UiT}}(P, M) \sim \frac{\omega_{\text{ph}}(P, M) \lambda(P)}{\Gamma_{\text{diss}}(P) + \Gamma_{\text{struct}}(P)}.$$

Here P is pressure, M is the isotope mass, ω_{ph} is the relevant phonon frequency, λ is the electron-phonon coupling strength, and the denominator represents dissipative and structural broadening channels.

This expression is the pressure-phonon analogue of the optical criterion. The numerator measures the strength of coherent phase writing. The denominator measures the dispersed cost of maintaining that coherent state.

In this language, pressure acts on the configuration capacity:

$$P \text{ to } \chi_{\text{conf}}(P).$$

A structural transition can therefore produce a sharp change in

$$\frac{d\chi_{\text{conf}}}{dP}.$$

When this change increases the coherent channel relative to the dispersed channel, the superconducting transition temperature rises:

$$\chi_{\text{conf}}(P) \text{ increases} \quad \text{implies} \quad T_c \text{ increases}.$$

The phonon contribution enters through phase-time. A phonon is a coherent oscillatory mode of the lattice configuration. Its characteristic phase-time scale is

$$dt_{\phi}^{\text{ph}} \sim \frac{1}{\omega_{\text{ph}}} e^{-i\phi_{\text{ph}}} d\phi_{\text{ph}}.$$

High-frequency phonons provide a faster coherent writing channel. In hydrogen-rich superconductors, the light mass of hydrogen gives high phonon frequencies, allowing a strong coherent-registration channel, consistent with the conventional electron-phonon interpretation of high-pressure sulfur hydride superconductivity [239].

The isotope effect follows immediately. Replacing hydrogen by deuterium changes the oscillator mass and lowers the phonon frequency approximately as

$$\omega_D \approx \frac{\omega_H}{\sqrt{2}}.$$

Therefore the coherent phase-writing channel is reduced:

$$\omega_{\text{ph}} \text{ decreases} \quad \text{implies} \quad \eta_{\text{UiT}} \text{ decreases} \quad \text{implies} \quad T_c \text{ decreases.}$$

This gives the UiT interpretation of isotope tuning. The isotope changes the phase-time rate of the lattice writing channel.

For high-pressure hydrides such as H_3S , where high transition temperatures, isotope shifts, and pressure-sensitive structural phases are observed [239–241], the empirical structure is therefore read as follows:

$$P \text{ increases} \quad \text{implies} \quad \chi_{\text{conf}}(P) \text{ increases}$$

near the optimal structural phase, while

$$H \text{ to } D \quad \text{implies} \quad \omega_{\text{ph}} \text{ decreases} \quad \text{implies} \quad \eta_{\text{UiT}} \text{ decreases.}$$

The observed rise of T_c under pressure and its reduction under isotope substitution are then two sides of the same registration law. Pressure tunes the configuration-writing capacity. Phonons supply the coherent phase-time channel. Isotope mass changes the rate of that channel. Superconductivity appears when coherent distinguishable writing dominates over dispersed thermodynamic cost.

The pressure-phonon criterion may therefore be summarized as

$$\frac{T_c(P, M)}{T_0} \sim \eta_{\text{UiT}}(P, M) \sim \frac{\omega_{\text{ph}}(P, M)\lambda(P)}{\Gamma_{\text{diss}}(P) + \Gamma_{\text{struct}}(P)}.$$

Here T_0 is the material temperature scale set by the relevant coherent energy. This dimensionless relation gives the UiT-level interpretation of why high pressure, light ions, strong phonon coupling, and reduced incoherent broadening all favor the same physical outcome: coherent transport with suppressed dispersive cost.

The same phase-time registration structure therefore appears in two experimentally distinct regimes. In optical pump experiments, the control parameter is the external phase drive. In high-pressure

hydrides, the control parameters are lattice configuration, phonon phase-time, and isotope mass. In both cases the measured effect is an increase in coherent registration relative to entropy-producing dispersion:

$$-dI_{\text{pot}}(\phi) \text{ to } dI_{\text{dist}}^{\text{coh}} + \frac{dS}{k_B \ln 2},$$

with superconductivity favored when

$$dI_{\text{dist}}^{\text{coh}} \gg \frac{dS}{k_B \ln 2}.$$

12.14 Existing Experiments and the Final Empirical Prediction

The transport criterion above is directly testable because a coherent drive should reduce the real dissipative projection while preserving or strengthening phase-ordered transport. Light-driven or phonon-driven superconducting-like transport above the equilibrium critical temperature has already been reported in several material families. The mechanism remains open across these systems, with different studies emphasizing different microscopic channels. The present framework proposes a specific organizing principle for them: externally injected phase order can temporarily reduce informational dispersion and restore coherent transport above the equilibrium thermal threshold. Ultrafast and microwave experiments already provide several relevant material families.

In the stripe-ordered cuprate $\text{La}_{1.675}\text{Eu}_{0.2}\text{Sr}_{0.125}\text{CuO}_4$, Fausti *et al.* reported that mid-infrared excitation produced a transient three-dimensional superconducting-like state, indicated by the prompt appearance of a Josephson plasma resonance in the *c*-axis response. [216] Hunt *et al.* later observed distinct relaxation regimes and a light-induced coherent state extending over a wider temperature window, with an upper scale of roughly 70–80 K. [226] These observations match the projected-force criterion qualitatively: the drive creates an inductive phase-ordered response while suppressing the ordinary resistive state.

In $\text{YBa}_2\text{Cu}_3\text{O}_{6.5}$, Hu *et al.* observed optically enhanced coherent interlayer transport after resonant mid-infrared excitation of apical-oxygen motion. [219] Mankowsky *et al.* connected this effect to nonlinear lattice dynamics, and Liu *et al.* then measured pump-frequency resonances for light-induced incipient superconductivity in the same compound. [218] [217] This last experiment is especially useful for the present criterion because it compares response strength as a function of pump frequency and can test whether the coherent response peaks when the drive addresses the phase-selective lattice channel with limited broadband heating.

In fullerenes, Mitranó *et al.* reported superconducting-like optical properties in K_3C_{60} after mid-infrared excitation, including optical signatures resembling an equilibrium superconducting state above the ordinary transition temperature. [220] Budden *et al.* later found metastable photo-induced superconducting-like optical properties with lifetimes exceeding 10 ns under sustained optical driving. [227] Rowe *et al.* further reported resonant enhancement of photo-induced superconductivity in K_3C_{60} . [221] These fullerene results are consistent with the expectation that resonant coherent driving can increase the imaginary/reactive channel relative to real dissipation.

Recent magnetic measurements strengthen the empirical comparison because they move beyond optical conductivity alone. Fava *et al.* probed optically driven $\text{YBa}_2\text{Cu}_3\text{O}_{6.48}$ and reported transient magnetic-field expulsion under the same driving conditions associated with superconducting-like optical properties. [228] This is important for the present criterion because a Meissner-like diamagnetic response is a macroscopic phase-coherence signature and a strong reactive/coherent-channel measurement.

In the Euler-projection language this magnetic observation has a special role. The pump field supplies an external electromagnetic drive, often through the electric coupling of an infrared-active lattice mode. The superconducting-like signature is read most sharply in the reactive magnetic response: inductive spectral weight, phase stiffness, and Meissner-like field expulsion. The experiment separates the input channel from the successful coherent output channel. The electric component injects energy into the material coordinate, while the magnetic or inductive response measures conversion into the phase-orthogonal coherent projection.

Other families provide additional tests. In FeSe, Suzuki *et al.* reported a possible photoinduced superconducting state with long-lived disproportionate band filling and transient behavior favorable to superconductivity above the equilibrium transition temperature. [229] Nishida *et al.* performed a broad study of light-induced superconducting-like responses in La-based cuprates emerging from charge-density-wave states. [230] Microwave-enhanced superconductivity, including enhanced critical current and critical-temperature effects in thin superconducting structures, provides an older nonequilibrium setting in which external electromagnetic driving changes the balance between dissipative and coherent response. [231] [232]

Across these systems the recurring empirical pattern is the same: selective coherent driving can enhance inductive, Josephson-like, gap-like, or superconducting-like response at temperatures where the undriven equilibrium state is resistive. In the present framework these observations are the expected qualitative signatures of

$$\mathbf{J} \cdot \Re(\mathbf{F}_\phi) \text{ decreases} \quad \text{with} \quad \Im(\mathbf{F}_\phi) \text{ active or enhanced.}$$

A quantitative test requires digitized or raw optical-conductivity data. The most direct test is to compute

$$\eta_{\text{coh}}(\omega_{\text{pump}}, t) = \frac{S_{\text{coh}}(\omega_{\text{pump}}, t)}{S_{\text{diss}}(\omega_{\text{pump}}, t)}$$

from the same transient spectra and determine whether η_{coh} peaks at the experimentally identified coherent phonon or phase resonance. The theory predicts that resonant phase-channel pumping gives a large η_{coh} , while nonresonant heating gives a much smaller value.

The final empirical prediction is therefore broader than an optical-pump criterion. The controlling quantity is the coherent registration ratio

$$\chi_{\text{tr}} = \frac{dI_{\text{dist}}^{\text{coh}}}{dS/(k_B \ln 2)}.$$

Any experimental control parameter that increases this ratio should enhance coherent transport. Optical driving does so by coupling selectively to phase or phonon modes. Thermal-gradient experiments probe the same structure through

$$\nabla\mu = -s\nabla T.$$

Pressure and structural tuning probe it through

$$\nabla\mu = v\nabla P + \sum_a X_a \nabla\lambda_a.$$

Isotope substitution changes the phase-time rate of the phonon channel through

$$\omega_{\text{ph}} \propto M^{-1/2}.$$

Thus optical conductivity, Nernst response, pressure tuning, and isotope shifts are different operational probes of the same registration law,

$$-dI_{\text{pot}}(\phi) = dI_{\text{dist}}^{\text{coh}} + \frac{dS}{k_B \ln 2}.$$

The theory predicts that coherent transport is favored whenever the experimental control increases $dI_{\text{dist}}^{\text{coh}}$ relative to the entropy-producing channel $dS/(k_B \ln 2)$. In optical probes this appears as enhanced σ_2 or superfluid spectral weight with limited σ_1 growth. In thermal-gradient probes it appears as a phase-dominated Nernst response. In pressure and phonon systems it appears as increased T_c/T_0 , stronger phase stiffness, or reduced incoherent broadening under the structural condition that maximizes η_{UIT} .

13 Final Structural Map of the Theory

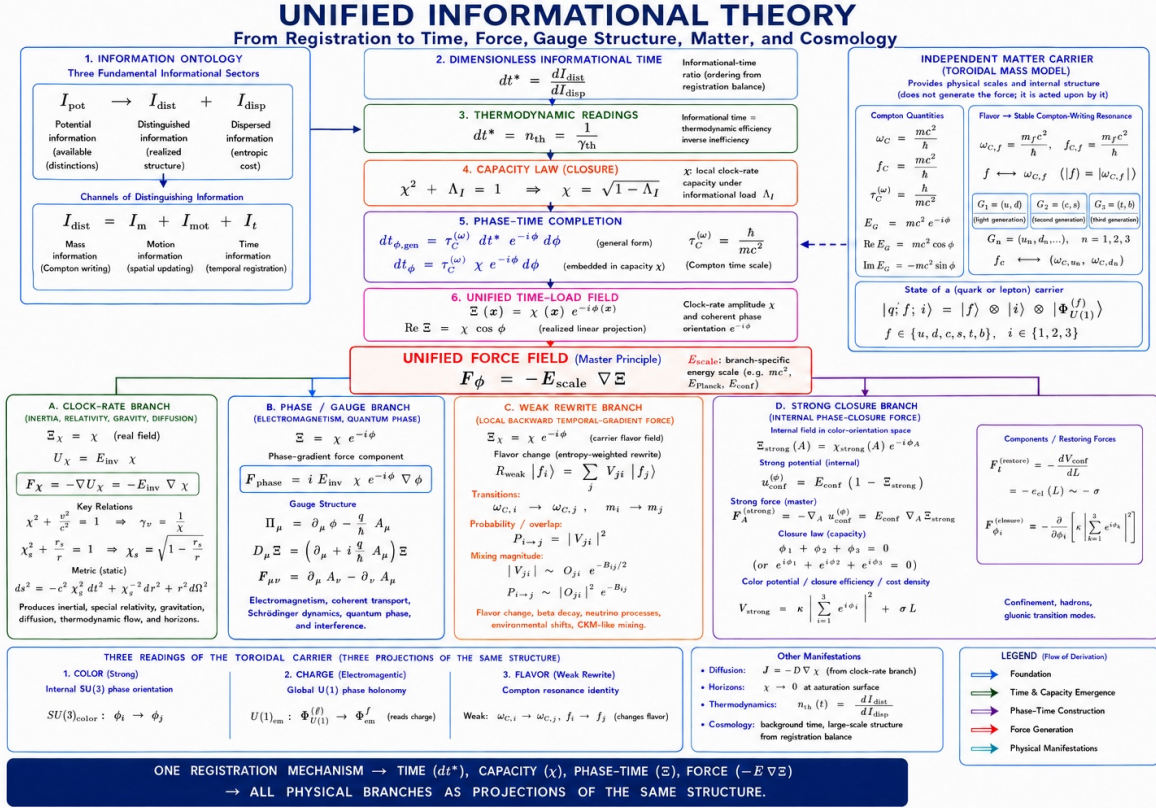


Figure 8: Final structural map of the theory. The figure is used as a schematic overview of the branch structure. In the present formulation, matter is described by the closed complex spherical Compton phase-time mode. The circular carrier rendering is read as a three-dimensional projection of the complex-plane phase-time boundary structure, used to visualize phase-time circulation, phase-time holonomy, and closure.

Funding

No external funding was received for this work.

Conflict of Interest

The author declares that there are no financial, institutional, or personal conflicts of interest related to this work.

Data Availability

No datasets were generated or analyzed for this theoretical study.

Acknowledgments

The author thanks readers and colleagues who engaged with earlier versions of these ideas and whose questions helped sharpen the present exposition.

References

- [1] Kolmogorov, A. N. (1965). Three approaches to the quantitative definition of information. *Problems of Information Transmission*, **1**(1), 1–7.
- [2] Chaitin, G. J. (1966). On the length of programs for computing finite binary sequences. *Journal of the ACM*, **13**(4), 547–569.
- [3] Solomonoff, R. J. (1964). A formal theory of inductive inference. Part I. *Information and Control*, **7**(1), 1–22.
- [4] Shannon, C. E. (1948). A Mathematical Theory of Communication. *Bell System Technical Journal*, **27**(3), 379–423.
- [5] Cover, T. M., & Thomas, J. A. (2006). *Elements of Information Theory* (2nd ed.). Wiley.
- [6] Brillouin, L. (1962). *Science and Information Theory*. Academic Press.
- [7] Wheeler, J. A. (1990). Information, Physics, Quantum: The Search for Links. In *Complexity, Entropy, and the Physics of Information*.
- [8] Zeilinger, A. (1999). A Foundational Principle for Quantum Mechanics. *Foundations of Physics*.
- [9] Landauer, R. (1996). The physical nature of information. *Physics Letters A*, **217**(4–5), 188–193.
- [10] Jaynes, E. T. (1957). Information Theory and Statistical Mechanics. *Physical Review*, **106**(4), 620–630.
- [11] Lloyd, S. (2000). Ultimate physical limits to computation. *Nature*, **406**, 1047–1054.
- [12] Deutsch, D. (2013). Constructor theory. *Synthese*, **190**, 4331–4359.
- [13] L. Szilard, “Über die Entropieverminderung in einem thermodynamischen System bei Eingriffen intelligenter Wesen,” *Zeitschrift für Physik* **53**, 840–856 (1929).
- [14] Landauer, R. (1957). Spatial Variation of Currents and Fields Due to Localized Scatterers in Metallic Conduction. *IBM Journal of Research and Development*, **1**(3), 223–231.
- [15] Bekenstein, J. D. (1981). Universal upper bound on the entropy-to-energy ratio for bounded systems. *Physical Review D*, **23**(2), 287–298.
- [16] A. Einstein, “Zur Elektrodynamik bewegter Körper,” *Annalen der Physik* **17**, 891–921 (1905).
- [17] H. Minkowski, “Raum und Zeit,” *Physikalische Zeitschrift* **10**, 104–111 (1909).
- [18] L. de Broglie, *Recherches sur la théorie des quanta*, doctoral thesis, University of Paris (1924).
- [19] A. H. Compton, “A Quantum Theory of the Scattering of X-rays by Light Elements,” *Physical Review* **21**, 483–502 (1923).
- [20] M. Planck, “Über irreversible Strahlungsvorgänge,” *Sitzungsberichte der Königlich Preussis-*

- chen Akademie der Wissenschaften* 440–480 (1899).
- [21] Connes, A., & Rovelli, C. (1994). Von Neumann algebra automorphisms and time-thermodynamics relation in generally covariant quantum theories. *Classical and Quantum Gravity*, **11**(12), 2899.
 - [22] von Neumann, J. (1932). *Mathematische Grundlagen der Quantenmechanik*. Springer.
 - [23] Zurek, W. H. (1981). Pointer basis of quantum apparatus: Into what mixture does the wave packet collapse? *Physical Review D*, **24**(6), 1516–1525.
 - [24] Zurek, W. H. (1982). Environment-induced superselection rules. *Physical Review D*, **26**(8), 1862–1880.
 - [25] Zurek, W. H. (2003). Decoherence, einselection, and the quantum origins of the classical. *Reviews of Modern Physics*, **75**(3), 715–775.
 - [26] Rovelli, C. (1996). Relational Quantum Mechanics. *International Journal of Theoretical Physics*.
 - [27] Landauer, R. (1961). Irreversibility and Heat Generation in the Computing Process. *IBM Journal of Research and Development*, **5**(3), 183–191.
 - [28] Bennett, C. H. (1973). Logical Reversibility of Computation. *IBM Journal of Research and Development*, **17**(6), 525–532.
 - [29] Bennett, C. H. (1982). The thermodynamics of computation—a review. *International Journal of Theoretical Physics*, **21**(12), 905–940.
 - [30] Clausius, R. (1865). *The Mechanical Theory of Heat*. Vieweg.
 - [31] Gibbs, J. W. (1902). *Elementary Principles in Statistical Mechanics*. Charles Scribner’s Sons.
 - [32] Boltzmann, L. (1896). *Vorlesungen "uber Gastheorie*.
 - [33] Prigogine, I. (1967). *Thermodynamics of Irreversible Processes*. Interscience Publishers.
 - [34] Callen, H. B. (1985). *Thermodynamics and an Introduction to Thermostatistics* (2nd ed.). Wiley.
 - [35] Reif, F. (1965). *Fundamentals of Statistical and Thermal Physics*. McGraw-Hill.
 - [36] Pathria, R. K., & Beale, P. D. (2011). *Statistical Mechanics* (3rd ed.). Academic Press.
 - [37] Riemann, B. (1851). *Grundlagen für eine allgemeine Theorie der Functionen einer veränderlichen complexen Grösse*. Doctoral dissertation, University of Göttingen.
 - [38] Ahlfors, L. V. (1979). *Complex Analysis* (3rd ed.). McGraw-Hill.
 - [39] Forster, O. (1981). *Lectures on Riemann Surfaces*. Springer.
 - [40] ’t Hooft, G. (1993). Dimensional Reduction in Quantum Gravity. In *Salamfestschrift*.
 - [41] Susskind, L. (1995). The World as a Hologram. *Journal of Mathematical Physics*, **36**(11),

6377–6396.

- [42] Maldacena, J. (1999). The Large N Limit of Superconformal Field Theories and Supergravity. *International Journal of Theoretical Physics*, **38**(4), 1113–1133.
- [43] Nakahara, M. (2003). *Geometry, Topology and Physics* (2nd ed.). Taylor & Francis.
- [44] Frankel, T. (2011). *The Geometry of Physics: An Introduction* (3rd ed.). Cambridge University Press.
- [45] Zeh, H. D. (2001). *The Physical Basis of The Direction of Time*. Springer.
- [46] Joos, E., Zeh, H. D., Kiefer, C., Giulini, D., Kupsch, J., & Stamatescu, I.-O. (2003). *Decoherence and the Appearance of a Classical World in Quantum Theory* (2nd ed.). Springer.
- [47] Schlosshauer, M. (2007). *Decoherence and the Quantum-to-Classical Transition*. Springer.
- [48] Rindler, W. (2006). *Relativity: Special, General, and Cosmological* (2nd ed.). Oxford University Press.
- [49] Taylor, E. F., & Wheeler, J. A. (1992). *Spacetime Physics* (2nd ed.). W. H. Freeman.
- [50] H. A. Lorentz, “Electromagnetic Phenomena in a System Moving with Any Velocity Smaller than That of Light,” *Proceedings of the Royal Netherlands Academy of Arts and Sciences* **6**, 809–831 (1904).
- [51] Pauli, W. (1921). *Relativitätstheorie*. In *Encyklopädie der mathematischen Wissenschaften*.
- [52] L. D. Landau and E. M. Lifshitz, *The Classical Theory of Fields*, 4th ed., Pergamon Press, Oxford (1975).
- [53] E. Mach, *Die Mechanik in ihrer Entwicklung historisch-kritisch dargestellt*, Brockhaus, Leipzig (1883).
- [54] Schwarzschild, K. (1916). "Über das Gravitationsfeld eines Massenpunktes nach der Einsteinschen Theorie. *Sitzungsberichte der Königlich Preussischen Akademie der Wissenschaften*, 189–196.
- [55] Einstein, A. (1907). Über das Relativitätsprinzip und die aus demselben gezogenen Folgerungen. *Jahrbuch der Radioaktivität und Elektronik*, **4**, 411–462.
- [56] Einstein, A. (1911). Über den Einfluss der Schwerkraft auf die Ausbreitung des Lichtes. *Annalen der Physik*, **35**, 898–908.
- [57] R. V. Pound and G. A. Rebka, Jr., “Apparent Weight of Photons,” *Physical Review Letters* **4**, 337–341 (1960).
- [58] Hafele, J. C., & Keating, R. E. (1972). Around-the-world atomic clocks: Predicted relativistic time gains. *Science*, **177**(4044), 166–168.
- [59] R. Penrose, “Gravitational Collapse: The Role of General Relativity,” *Rivista del Nuovo Cimento* **1**, 252–276 (1969/1970).

- [60] P. C. W. Davies, “The Thermodynamic Theory of Black Holes,” *Proceedings of the Royal Society of London A* **353**, 499–521 (1977).
- [61] Unruh, W. G. (1976). Notes on black-hole evaporation. *Physical Review D*, **14**(4), 870–892.
- [62] Birrell, N. D., & Davies, P. C. W. (1982). *Quantum Fields in Curved Space*. Cambridge University Press.
- [63] Bekenstein, J. D. (1973). Black Holes and Entropy. *Physical Review D*, **7**(8), 2333–2346.
- [64] Hawking, S. W. (1975). Particle Creation by Black Holes. *Communications in Mathematical Physics*, **43**(3), 199–220.
- [65] R. Bousso, “The Holographic Principle,” *Reviews of Modern Physics* **74**, 825–874 (2002).
- [66] Cartan, E. (1923). Sur les variétés à connexion affine et la théorie de la relativité généralisée. *Annales Scientifiques de l’École Normale Supérieure*, **40**, 325–412.
- [67] C. W. Misner, K. S. Thorne, and J. A. Wheeler, *Gravitation*, W. H. Freeman, San Francisco (1973).
- [68] R. M. Wald, *General Relativity*, University of Chicago Press, Chicago (1984).
- [69] D. Lovelock, “The Einstein tensor and its generalizations,” *Journal of Mathematical Physics* **12**, 498–501 (1971).
- [70] A. Einstein, “Die Feldgleichungen der Gravitation,” *Sitzungsberichte der Königlich Preussischen Akademie der Wissenschaften* 844–847 (1915).
- [71] Padmanabhan, T. (2010). Thermodynamical Aspects of Gravity: New insights. *Reports on Progress in Physics*, **73**(4), 046901.
- [72] R. v. Eötvös, D. Pekár, and E. Fekete, “Beiträge zum Gesetze der Proportionalität von Trägheit und Gravität,” *Annalen der Physik* **68**, 11–66 (1922).
- [73] Dicke, R. H. (1964). The theoretical significance of experimental relativity. Gordon and Breach.
- [74] Will, C. M. (2014). The confrontation between general relativity and experiment. *Living Reviews in Relativity*, **17**, 4.
- [75] Schlaminger, S., Choi, K.-Y., Wagner, T. A., Gundlach, J. H., & Adelberger, E. G. (2008). Test of the equivalence principle using a rotating torsion balance. *Physical Review Letters*, **100**, 041101.
- [76] R. P. Kerr, “Gravitational Field of a Spinning Mass as an Example of Algebraically Special Metrics,” *Physical Review Letters* **11**, 237–238 (1963).
- [77] J. Lense and H. Thirring, “Über den Einfluss der Eigenrotation der Zentralkörper auf die Bewegung der Planeten und Monde nach der Einsteinschen Gravitationstheorie,” *Physikalische Zeitschrift* **19**, 156–163 (1918).
- [78] Fierz, M., & Pauli, W. (1939). On relativistic wave equations for particles of arbitrary spin

- in an electromagnetic field. *Proceedings of the Royal Society A*, **173**, 211–232.
- [79] Weinberg, S. (1965). Infrared photons and gravitons. *Physical Review*, **140**(2B), B516–B524.
 - [80] J. F. Donoghue, “General Relativity as an Effective Field Theory: The Leading Quantum Corrections,” *Physical Review D* **50**, 3874–3888 (1994).
 - [81] Maggiore, M. (2008). *Gravitational Waves, Volume 1: Theory and Experiments*. Oxford University Press.
 - [82] Abbott, B. P., et al. (LIGO Scientific Collaboration and Virgo Collaboration). (2016). Observation of gravitational waves from a binary black hole merger. *Physical Review Letters*, **116**, 061102.
 - [83] I. Newton, *Philosophiæ Naturalis Principia Mathematica*, London (1687).
 - [84] de Groot, S. R., & Mazur, P. (1962). *Non-Equilibrium Thermodynamics*. North-Holland.
 - [85] Onsager, L. (1931). Reciprocal Relations in Irreversible Processes. I. *Physical Review*, **37**(4), 405–426.
 - [86] Onsager, L. (1931). Reciprocal Relations in Irreversible Processes. II. *Physical Review*, **38**(12), 2265–2279.
 - [87] van ’t Hoff, J. H. (1887). Die Rolle des osmotischen Druckes in der Analogie zwischen Lösungen und Gasen. *Zeitschrift für physikalische Chemie*, **1**, 481–508.
 - [88] Kedem, O., & Katchalsky, A. (1958). Thermodynamic analysis of the permeability of biological membranes to non-electrolytes. *Biochimica et Biophysica Acta*, **27**, 229–246.
 - [89] F. W. Dyson, A. S. Eddington, and C. Davidson, “A Determination of the Deflection of Light by the Sun’s Gravitational Field,” *Philosophical Transactions of the Royal Society A* **220**, 291–333 (1920).
 - [90] Schrödinger, E. (1926). Quantisierung als Eigenwertproblem. *Annalen der Physik*, **79**, 361–376.
 - [91] Weyl, H. (1918). Gravitation und Elektrizität. *Sitzungsberichte der Preussischen Akademie*, 465–480.
 - [92] Baez, J. C., & Muniain, J. P. (1994). *Gauge Fields, Knots and Gravity*. World Scientific.
 - [93] Aitchison, I. J. R., & Hey, A. J. G. (2003). *Gauge Theories in Particle Physics* (3rd ed.). Institute of Physics Publishing.
 - [94] Kaluza, T. (1921). Zum Unitätsproblem der Physik. *Sitzungsberichte der Preussischen Akademie der Wissenschaften*, 966–972.
 - [95] Klein, O. (1926). Quantentheorie und fünfdimensionale Relativitätstheorie. *Zeitschrift für Physik*, **37**, 895–906.
 - [96] Einstein, A. (1905). Zur Elektrodynamik bewegter Körper. *Annalen der Physik*, **17**, 891–921.

- [97] Einstein, A. (1915). Die Feldgleichungen der Gravitation. *Sitzungsberichte der Preussischen Akademie*, 844–847.
- [98] Pauli, W. (1927). Zur Quantenmechanik des magnetischen Elektrons. *Zeitschrift für Physik*, **43**, 601–623.
- [99] Dirac, P. A. M. (1928). The quantum theory of the electron. *Proceedings of the Royal Society A*, **117**, 610–624.
- [100] Penrose, R., & Rindler, W. (1984). *Spinors and Space-Time, Volume 1*. Cambridge University Press.
- [101] Dirac, P. A. M. (1931). Quantised Singularities in the Electromagnetic Field. *Proceedings of the Royal Society A*, **133**(821), 60–72.
- [102] Sommerfeld, A. (1916). Zur Quantentheorie der Spektrallinien. *Annalen der Physik*, **51**, 1–94.
- [103] Tiesinga, E., Mohr, P. J., Newell, D. B., & Taylor, B. N. (2022). CODATA recommended values of the fundamental physical constants: 2018. *Reviews of Modern Physics*, **93**, 025010.
- [104] Lüders, G. (1954). On the equivalence of invariance under time reversal and under particle-antiparticle conjugation for relativistic field theories. *Kongelige Danske Videnskabernes Selskab, Matematisk-fysiske Meddelelser*, **28**(5), 1–17.
- [105] Pauli, W. (1955). Exclusion principle, Lorentz group and reflection of space-time and charge. In W. Pauli (Ed.), *Niels Bohr and the Development of Physics*. Pergamon.
- [106] Jost, R. (1957). Eine Bemerkung zum CTP Theorem. *Helvetica Physica Acta*, **30**, 409–416.
- [107] Penrose, R. (1979). Singularities and Time-Asymmetry. In *General Relativity: An Einstein Centenary Survey*.
- [108] ATLAS Collaboration, “Observation of a New Particle in the Search for the Standard Model Higgs Boson with the ATLAS Detector at the LHC,” *Physics Letters B* **716**, 1–29 (2012).
- [109] CMS Collaboration, “Observation of a New Boson at a Mass of 125 GeV with the CMS Experiment at the LHC,” *Physics Letters B* **716**, 30–61 (2012).
- [110] Higgs, P. W. (1964). Broken symmetries and the masses of gauge bosons. *Physical Review Letters*, **13**, 508–509.
- [111] Englert, F., & Brout, R. (1964). Broken symmetry and the mass of gauge vector mesons. *Physical Review Letters*, **13**, 321–323.
- [112] Guralnik, G. S., Hagen, C. R., & Kibble, T. W. B. (1964). Global conservation laws and massless particles. *Physical Review Letters*, **13**, 585–587.
- [113] Kibble, T. W. B. (1967). Symmetry breaking in non-Abelian gauge theories. *Physical Review*, **155**, 1554–1561.
- [114] L. Susskind, “Dynamics of Spontaneous Symmetry Breaking in the Weinberg-Salam Theory,” *Physical Review D* **20**, 2619–2625 (1979).

- [115] G. 't Hooft, “Naturalness, Chiral Symmetry, and Spontaneous Chiral Symmetry Breaking,” in *Recent Developments in Gauge Theories*, NATO Advanced Study Institutes Series B, Vol. 59, Plenum Press, New York, pp. 135–157 (1980).
- [116] Einstein, A., Podolsky, B., & Rosen, N. (1935). Can Quantum-Mechanical Description of Physical Reality Be Considered Complete? *Physical Review*, **47**(10), 777–780.
- [117] Bohr, N. (1935). Can quantum-mechanical description of physical reality be considered complete? *Physical Review*, **48**(8), 696–702.
- [118] Bell, J. S. (1964). On the Einstein Podolsky Rosen Paradox. *Physics Physique Fizika*, **1**(3), 195–200.
- [119] Aspect, A., Dalibard, J., & Roger, G. (1982). Experimental Test of Bell’s Inequalities Using Time-Varying Analyzers. *Physical Review Letters*, **49**(25), 1804–1807.
- [120] Everett, H. (1957). Relative State Formulation of Quantum Mechanics. *Reviews of Modern Physics*, **29**(3), 454–462.
- [121] Aharonov, Y., & Bohm, D. (1959). Significance of Electromagnetic Potentials in the Quantum Theory. *Physical Review*.
- [122] Schrödinger, E. (1935). Die gegenwärtige Situation in der Quantenmechanik. *Naturwissenschaften*, **23**, 807–812, 823–828, 844–849.
- [123] Einstein, A., & Rosen, N. (1935). The particle problem in the general theory of relativity. *Physical Review*, **48**, 73–77.
- [124] Maldacena, J., & Susskind, L. (2013). Cool horizons for entangled black holes. *Fortschritte der Physik*, **61**(9), 781–811.
- [125] Hawking, S. W. (1976). Breakdown of predictability in gravitational collapse. *Physical Review D*, **14**, 2460–2473.
- [126] Page, D. N. (1993). Information in black hole radiation. *Physical Review Letters*, **71**, 3743–3746.
- [127] Almheiri, A., Marolf, D., Polchinski, J., & Sully, J. (2013). Black holes: Complementarity or firewalls? *Journal of High Energy Physics*, **2013**(2), 62.
- [128] Harlow, D. (2016). Jerusalem lectures on black holes and quantum information. *Reviews of Modern Physics*, **88**, 015002.
- [129] Hayden, P., & Preskill, J. (2007). Black holes as mirrors: Quantum information in random subsystems. *Journal of High Energy Physics*, **2007**(09), 120.
- [130] Jacobson, T. (1995). Thermodynamics of Spacetime: The Einstein Equation of State. *Physical Review Letters*, **75**(7), 1260–1263.
- [131] Verlinde, E. (2011). On the Origin of Gravity and the Laws of Newton. *Journal of High Energy Physics*, **2011**(4), 29.

- [132] Fick, A. (1855). Ueber Diffusion. *Annalen der Physik*, **170**(1), 59–86.
- [133] Einstein, A. (1905). "Über die von der molekularkinetischen Theorie der Wärme geforderte Bewegung. *Annalen der Physik*, **17**, 549–560.
- [134] Madelung, E. (1927). Quantentheorie in hydrodynamischer Form. *Zeitschrift für Physik*, **40**, 322–326.
- [135] Bohm, D. (1952). A suggested interpretation of the quantum theory in terms of hidden variables. I. *Physical Review*, **85**, 166–179.
- [136] Nelson, E. (1966). Derivation of the Schrödinger Equation from Newtonian Mechanics. *Physical Review*, **150**(4), 1079–1085.
- [137] Guerra, F., & Ruggiero, P. (1978). New interpretation of the Euclidean-Markov field in the framework of physical Minkowski space. *Physical Review Letters*, **41**, 1022–1025.
- [138] Feynman, R. P. (1948). Space-Time Approach to Non-Relativistic Quantum Mechanics. *Reviews of Modern Physics*, **20**(2), 367–387.
- [139] Kac, M. (1949). On distributions of certain Wiener functionals. *Transactions of the American Mathematical Society*, **65**, 1–13.
- [140] Wick, G. C. (1954). Properties of Bethe-Salpeter wave functions. *Physical Review*, **96**, 1124–1134.
- [141] Risken, H. (1989). *The Fokker-Planck Equation* (2nd ed.). Springer.
- [142] Gardiner, C. W. (2009). *Stochastic Methods* (4th ed.). Springer.
- [143] Maccone, L. (2009). Quantum Solution to the Arrow-of-Time Dilemma. *Physical Review Letters*, **103**(8), 080401.
- [144] Lee, T. D., & Yang, C. N. (1956). Question of parity conservation in weak interactions. *Physical Review*, **104**, 254–258.
- [145] Wu, C. S., Ambler, E., Hayward, R. W., Hoppes, D. D., & Hudson, R. P. (1957). Experimental test of parity conservation in beta decay. *Physical Review*, **105**, 1413–1415.
- [146] Feynman, R. P., & Gell-Mann, M. (1958). Theory of the Fermi interaction. *Physical Review*, **109**, 193–198.
- [147] Sudarshan, E. C. G., & Marshak, R. E. (1958). Chirality invariance and the universal Fermi interaction. *Physical Review*, **109**, 1860–1862.
- [148] Glashow, S. L. (1961). Partial-symmetries of weak interactions. *Nuclear Physics*, **22**(4), 579–588.
- [149] Weinberg, S. (1967). A Model of Leptons. *Physical Review Letters*, **19**(21), 1264–1266.
- [150] Salam, A. (1968). Weak and Electromagnetic Interactions. In *Elementary Particle Theory*.
- [151] Fermi, E. (1934). Versuch einer Theorie der β -Strahlen. I. *Zeitschrift für Physik*, **88**, 161–177.

- [152] Cowan, C. L., Reines, F., Harrison, F. B., Kruse, H. W., & McGuire, A. D. (1956). Detection of the Free Neutrino: A Confirmation. *Science*, **124**(3212), 103–104.
- [153] Pontecorvo, B. (1957). Mesonium and antimesonium. *Soviet Physics JETP*, **6**, 429.
- [154] Pontecorvo, B. (1958). Inverse beta processes and nonconservation of lepton charge. *Soviet Physics JETP*, **7**, 172–173.
- [155] Maki, Z., Nakagawa, M., & Sakata, S. (1962). Remarks on the unified model of elementary particles. *Progress of Theoretical Physics*, **28**, 870–880.
- [156] Super-Kamiokande Collaboration. (1998). Evidence for Oscillation of Atmospheric Neutrinos. *Physical Review Letters*, **81**(8), 1562–1567.
- [157] SNO Collaboration. (2002). Direct Evidence for Neutrino Flavor Transformation from Neutral-Current Interactions in the Sudbury Neutrino Observatory. *Physical Review Letters*, **89**(1), 011301.
- [158] Particle Data Group. (2024). Review of Particle Physics. *Physical Review D*, **110**, 030001.
- [159] Gamow, G. (1928). Zur Quantentheorie des Atomkernes. *Zeitschrift f"ur Physik*, **51**(3–4), 204–212.
- [160] Geiger, H., & Nuttall, J. M. (1911). The ranges of the α particles from various radioactive substances. *Philosophical Magazine*, **22**(130), 613–621.
- [161] Ohtsuki, T., et al. (2004). Enhanced electron-capture decay rate of ^7Be encapsulated in C_{60} cages. *Physical Review Letters*, **93**, 112501.
- [162] Norman, E. B., et al. (2001). Influence of physical and chemical environments on the decay rates of ^7Be and ^{40}K . *Physics Letters B*, **519**, 15–22.
- [163] Nir-El, Y., Haquin, G., Lavi, N., Halfon, S., & German, U. (2007). Half-life of ^7Be in different chemical forms. *Physical Review C*, **75**, 012801.
- [164] Ohtsuki, T., et al. (2007). Radioactive decay rate of ^7Be in C_{60} at low temperature. *Physical Review C*, **75**, 045801.
- [165] Morisato, T., et al. (2008). First-principles calculation of electron density at the ^7Be nucleus in endohedral C_{60} . *Physical Review C*, **78**, 015801.
- [166] Yang, C. N., & Mills, R. L. (1954). Conservation of Isotopic Spin and Isotopic Gauge Invariance. *Physical Review*, **96**(1), 191–195.
- [167] Utiyama, R. (1956). Invariant Theoretical Interpretation of Interaction. *Physical Review*, **101**(5), 1597–1607.
- [168] Cabibbo, N. (1963). Unitary symmetry and leptonic decays. *Physical Review Letters*, **10**, 531–533.
- [169] Kobayashi, M., & Maskawa, T. (1973). CP-violation in the renormalizable theory of weak interaction. *Progress of Theoretical Physics*, **49**, 652–657.

- [170] Christenson, J. H., Cronin, J. W., Fitch, V. L., & Turlay, R. (1964). Evidence for the 2π Decay of the K_2^0 Meson (CP Violation). *Physical Review Letters*, **13**(4), 138–140.
- [171] Gell-Mann, M. (1964). A Schematic Model of Baryons and Mesons. *Physics Letters*, **8**(3), 214–215.
- [172] Zweig, G. (1964). An SU(3) model for strong interaction symmetry and its breaking. *CERN Reports*.
- [173] Gross, D. J., & Wilczek, F. (1973). Ultraviolet Behavior of Non-Abelian Gauge Theories. *Physical Review Letters*, **30**(26), 1343–1346.
- [174] Politzer, H. D. (1973). Reliable Perturbative Results for Strong Interactions? *Physical Review Letters*, **30**(26), 1346–1349.
- [175] Greenberg, O. W. (1964). Spin and unitary-spin independence in a paraquark model of baryons and mesons. *Physical Review Letters*, **13**, 598–602.
- [176] Han, M. Y., & Nambu, Y. (1965). Three-triplet model with double SU(3) symmetry. *Physical Review*, **139**, B1006–B1010.
- [177] Fritzsch, H., Gell-Mann, M., & Leutwyler, H. (1973). Advantages of the color octet gluon picture. *Physics Letters B*, **47**, 365–368.
- [178] Close, F. E. (1979). *An Introduction to Quarks and Partons*. Academic Press.
- [179] Georgi, H. (1999). *Lie Algebras in Particle Physics* (2nd ed.). Westview Press.
- [180] Wilson, K. G. (1974). Confinement of quarks. *Physical Review D*, **10**, 2445–2459.
- [181] Kogut, J., & Susskind, L. (1975). Hamiltonian formulation of Wilson’s lattice gauge theories. *Physical Review D*, **11**, 395–408.
- [182] Creutz, M. (1980). Monte Carlo study of quantized SU(2) gauge theory. *Physical Review D*, **21**, 2308–2315.
- [183] Griffiths, D. (2008). *Introduction to Elementary Particles* (2nd ed.). Wiley-VCH.
- [184] Weinberg, S. (1995). *The Quantum Theory of Fields, Volume I*. Cambridge University Press.
- [185] Srednicki, M. (2007). *Quantum Field Theory*. Cambridge University Press.
- [186] Zee, A. (2010). *Quantum Field Theory in a Nutshell* (2nd ed.). Princeton University Press.
- [187] Ryder, L. H. (1996). *Quantum Field Theory* (2nd ed.). Cambridge University Press.
- [188] Maxwell, J. C. (1865). A Dynamical Theory of the Electromagnetic Field. *Philosophical Transactions of the Royal Society of London*, **155**, 459–512.
- [189] A. Friedmann, “"Über die Kr"ummung des Raumes,” *Zeitschrift f"ur Physik* **10**, 377–386 (1922).
- [190] P. J. E. Peebles and B. Ratra, “The Cosmological Constant and Dark Energy,” *Reviews of Modern Physics* **75**, 559–606 (2003).

- [191] Guth, A. H. (1981). Inflationary universe: A possible solution to the horizon and flatness problems. *Physical Review D*, **23**(2), 347–356.
- [192] Linde, A. D. (1982). A new inflationary universe scenario. *Physics Letters B*, **108**(6), 389–393.
- [193] Starobinsky, A. A. (1980). A new type of isotropic cosmological models without singularity. *Physics Letters B*, **91**(1), 99–102.
- [194] Lloyd, S. (2002). Computational capacity of the universe. *Physical Review Letters*, **88**(23), 237901.
- [195] Riess, A. G., et al. (1998). Observational evidence from supernovae for an accelerating universe and a cosmological constant. *The Astronomical Journal*, **116**(3), 1009–1038.
- [196] Perlmutter, S., et al. (1999). Measurements of Omega and Lambda from 42 high-redshift supernovae. *The Astrophysical Journal*, **517**(2), 565–586.
- [197] Peebles, P. J. E., & Ratra, B. (2003). The cosmological constant and dark energy. *Reviews of Modern Physics*, **75**(2), 559–606.
- [198] Planck Collaboration. (2020). Planck 2018 results. VI. Cosmological parameters. *Astronomy & Astrophysics*, **641**, A6.
- [199] Dodelson, S. (2003). *Modern Cosmology*. Academic Press.
- [200] Weinberg, S. (2008). *Cosmology*. Oxford University Press.
- [201] Zwicky, F. (1933). Die Rotverschiebung von extragalaktischen Nebeln. *Helvetica Physica Acta*, **6**, 110–127.
- [202] Rubin, V. C., & Ford, W. K. (1970). Rotation of the Andromeda nebula from a spectroscopic survey of emission regions. *The Astrophysical Journal*, **159**, 379–403.
- [203] Rubin, V. C., Ford, W. K., & Thonnard, N. (1980). Rotational properties of 21 Sc galaxies with a large range of luminosities and radii. *The Astrophysical Journal*, **238**, 471–487.
- [204] Milgrom, M. (1983). A modification of the Newtonian dynamics as a possible alternative to the hidden mass hypothesis. *The Astrophysical Journal*, **270**, 365–370.
- [205] McGaugh, S. S., Lelli, F., & Schombert, J. M. (2016). Radial acceleration relation in rotationally supported galaxies. *Physical Review Letters*, **117**, 201101.
- [206] Navarro, J. F., Frenk, C. S., & White, S. D. M. (1996). The structure of cold dark matter halos. *The Astrophysical Journal*, **462**, 563–575.
- [207] Navarro, J. F., Frenk, C. S., & White, S. D. M. (1997). A universal density profile from hierarchical clustering. *The Astrophysical Journal*, **490**, 493–508.
- [208] Bertone, G., Hooper, D., & Silk, J. (2005). Particle dark matter: Evidence, candidates and constraints. *Physics Reports*, **405**, 279–390.
- [209] Bullock, J. S., & Boylan-Kolchin, M. (2017). Small-scale challenges to the Λ CDM paradigm. *Annual Review of Astronomy and Astrophysics*, **55**, 343–387.

- [210] Meissner, W., & Ochsenfeld, R. (1933). Ein neuer Effekt bei Eintritt der Supraleitfähigkeit. *Naturwissenschaften*, **21**, 787–788.
- [211] London, F., & London, H. (1935). The electromagnetic equations of the supraconductor. *Proceedings of the Royal Society A*, **149**(866), 71–88.
- [212] Bardeen, J., Cooper, L. N., & Schrieffer, J. R. (1957). Theory of Superconductivity. *Physical Review*, **108**(5), 1175–1204.
- [213] Josephson, B. D. (1962). Possible new effects in superconductive tunnelling. *Physics Letters*, **1**(7), 251–253.
- [214] Tinkham, M. (1996). *Introduction to Superconductivity*. McGraw-Hill.
- [215] Cavalleri, A. (2018). Photo-induced superconductivity. *Contemporary Physics*, **59**(1), 31–46.
- [216] Fausti, D., et al. (2011). Light-Induced Superconductivity in a Stripe-Ordered Cuprate. *Science*, **331**(6014), 189–191.
- [217] Liu, B., Först, M., Fechner, M., Nicoletti, D., Porras, J., Loew, T., Keimer, B., & Cavalleri, A. (2020). Pump frequency resonances for light-induced incipient superconductivity in $\text{YBa}_2\text{Cu}_3\text{O}_{6.5}$. *Physical Review X*, **10**(1), 011053.
- [218] Mankowsky, R., et al. (2014). Nonlinear lattice dynamics as a basis for enhanced superconductivity in $\text{YBa}_2\text{Cu}_3\text{O}_{6.5}$. *Nature*, **516**, 71–73.
- [219] Hu, W., et al. (2014). Optically enhanced coherent transport in $\text{YBa}_2\text{Cu}_3\text{O}_{6.5}$. *Nature Materials*, **13**(7), 705–711.
- [220] Mittrano, M., et al. (2016). Possible light-induced superconductivity in K_3C_{60} at high temperature. *Nature*, **530**(7591), 461–464.
- [221] Rowe, E., et al. (2023). Resonant enhancement of photo-induced superconductivity in K_3C_{60} . *Nature Physics*, **19**, 1821–1826.
- [222] Basov, D. N., & Timusk, T. (2005). Electrodynamics of high- T_c superconductors. *Reviews of Modern Physics*, **77**, 721–779.
- [223] Ferrell, R. A., & Glover, R. E. (1958). Conductivity of superconducting films: A sum rule. *Physical Review*, **109**, 1398–1399.
- [224] Homes, C. C., et al. (2004). A universal scaling relation in high-temperature superconductors. *Nature*, **430**, 539–541.
- [225] Mattis, D. C., & Bardeen, J. (1958). Theory of the anomalous skin effect in normal and superconducting metals. *Physical Review*, **111**, 412–417.
- [226] Hunt, C. R., et al. (2015). Two distinct kinetic regimes for the relaxation of light-induced superconductivity. *Physical Review B*, **91**(2), 020505.
- [227] Budden, M., et al. (2021). Evidence for metastable photo-induced superconductivity in K_3C_{60} . *Nature Physics*, **17**, 611–618.

- [228] Fava, S., De Vecchi, G., Jotzu, G., Buzzi, M., Gebert, T., Liu, Y., Keimer, B., & Cavalleri, A. (2024). Magnetic field expulsion in optically driven $\text{YBa}_2\text{Cu}_3\text{O}_{6.48}$. *Nature*, **632**, 75–80.
- [229] Suzuki, T., et al. (2019). Photoinduced possible superconducting state with long-lived disproportionate band filling in FeSe. *Communications Physics*, **2**(1), 39.
- [230] Nishida, M., Song, D., Hallas, A. M., Eisaki, H., & Shimano, R. (2024). Emergence of light-induced superconducting-like state from the charge density wave state in high- T_c cuprate superconductors. *Physical Review B*, **110**, 224515.
- [231] Wyatt, A. F. G., Dmitriev, V. M., Moore, W. S., & Sheard, F. W. (1966). Microwave-enhanced critical supercurrents in superconducting constricted tin films. *Physical Review Letters*, **16**, 1166–1169.
- [232] Pals, J. A., & Dobben, J. (1979). Measurements of microwave-enhanced superconductivity in aluminum strips. *Physical Review B*, **20**, 935–943.
- [233] Behnia, K. (2009). The Nernst effect and the boundaries of the Fermi liquid picture. *Journal of Physics: Condensed Matter*, **21**, 113101.
- [234] Behnia, K., & Aubin, H. (2016). Nernst effect in metals and superconductors: A review of concepts and experiments. *Reports on Progress in Physics*, **79**, 046502.
- [235] Ussishkin, I., Sondhi, S. L., & Huse, D. A. (2002). Gaussian superconducting fluctuations, thermal transport, and the Nernst effect. *Physical Review Letters*, **89**, 287001.
- [236] Wang, Y., Li, L., & Ong, N. P. (2006). Nernst effect in high- T_c superconductors. *Physical Review B*, **73**, 024510.
- [237] Jotzu, G., Meier, G., Cantaluppi, A., Cavalleri, A., Pontiroli, D., Ricco, M., Ardavan, A., & Nam, M.-S. (2023). Superconducting fluctuations observed far above T_c in the isotropic superconductor K_3C_{60} . *Physical Review X*, **13**, 021008.
- [238] Nicoletti, D., Fu, D., Mehio, O., Moore, S., Disa, A. S., Gu, G. D., & Cavalleri, A. (2018). Magnetic-field tuning of light-induced superconductivity in striped $\text{La}_{2-x}\text{Ba}_x\text{CuO}_4$. *Physical Review Letters*, **121**, 267003.
- [239] Drozdov, A. P., Erements, M. I., Troyan, I. A., Ksenofontov, V., & Shylin, S. I. (2015). Conventional superconductivity at 203 kelvin at high pressures in the sulfur hydride system. *Nature*, **525**, 73–76.
- [240] Einaga, M., Sakata, M., Ishikawa, T., Shimizu, K., Erements, M. I., Drozdov, A. P., Troyan, I. A., Hirao, N., & Ohishi, Y. (2016). Crystal structure of the superconducting phase of sulfur hydride. *Nature Physics*, **12**, 835–838.
- [241] Gor'kov, L. P., & Kresin, V. Z. (2016). Pressure and high- T_c superconductivity in sulfur hydrides. *Scientific Reports*, **6**, 25608.
- [242] Wu, T. T., & Yang, C. N. (1975). Concept of nonintegrable phase factors and global formulation of gauge fields. *Physical Review D*, **12**(12), 3845–3857.

- [243] Jackson, J. D. (1999). *Classical Electrodynamics* (3rd ed.). Wiley.
- [244] Peskin, M. E., & Schroeder, D. V. (1995). *An Introduction to Quantum Field Theory*. Addison-Wesley.
- [245] Eliashberg, G. M. (1970). Film superconductivity stimulated by a high-frequency field. *JETP Letters*, **11**, 114–116.